Fault detection techniques based on set-membership state estimation for uncertain systems

Sofiane Ben Chabane

NNT : 2015SACLC007

THESE DE DOCTORAT
DE
L'UNIVERSITE PARIS-SACLAY
PREPAREE A
CENTRALESUPELEC

ECOLE DOCTORALE N°580
Sciences et technologies de l'information et de la communication

Spécialité de doctorat : Automatique

Par

M. Sofiane Ben Chabane

Techniques de détection de défauts à base d'estimation d'état ensembliste pour systèmes incertains

Thèse présentée et soutenue à Gif-sur-Yvette, le 13 Octobre 2015 :

Composition du Jury :

Mme Dorothée Normand-Cyrot	Directeur de recherche, L2S	Président
M. Vicenç Puig Cayuela	Professeur, Universitat Politècnica de Catalunya	Rapporteur
M. Didier Theilliol	Professeur, Université de Lorraine	Rapporteur
Mme Hélène Piet-Lahanier	Conseiller scientifique, ONERA	Examinateur
M. Christophe Combastel	Maître de Conférences, Université Bordeaux 1	Examinateur
M. Morten Hovd	Professeur, NTNU	Examinateur
M. Teodoro Alamo	Professeur, Universidad de Sevilla	Co-encadrant
M. Didier Dumur	Professeur, CentraleSupélec/L2S	Directeur de thèse
M. Eduardo F. Camacho	Professeur, Universidad de Sevilla	Invité, co-encadrant
Mme Cristina Stoica Maniu	Professeur Adjoint, CentraleSupélec/L2S	Invité, co-encadrant

Remerciements

Le travail présenté dans ce mémoire a été mené à CentraleSupélec/Laboratoire des Signaux et Système (L2S) en collaboration avec l'Université de Séville.

Je tiens à remercier vivement mes encadrants Cristina Stoica Maniu, Didier Dumur, Teodoro Alamo et Eduardo F. Camacho. Je leurs exprime toute ma reconnaissance et ma gratitude pour leur soutien, la confiance qu'ils m'ont donnée, leurs conseils judicieux et leur suivi régulier qui ont permis l'acconplissement de ce travail.

Mes remerciement vont aussi à tous les membres du jury pour avoir accepté d'examiner mon travail et spécialement aux rapporteurs qui ont fourni de grands efforts pour lire mon rapport.

Enfin, je remercie tout le personnel du département Automatique de CentraleSupélec et toutes les personnes qui ont contribué de près ou loin à l'aboutissement de ce travail.

Dédicaces

Je dédie ce modeste travail :

A mes chers parents, qui par leurs sacrifices, leur amour, leur patience et leurs encouragements m'ont permis de toujours persévérer, de viser haut et de donner le meilleur de moi-même

A ma soeur Taous et mon frère Hachimi ainsi qu'à son épouse et sa petite fille Nora

A ma copine qui m'a soutenu tout au long de ces années

A mes cousins, mes cousines, mes oncles et mes tantes

A tous mes amis et spécialement à Seif, Djawad, Djamal, Zaki, Imad, Mircea et Tri

Contents

List of Figures

List of Tables

List of symbols

$\mathbb{R}$	Set of real numbers
$\mathbb{R}_+$	Set of positive real numbers
$\mathbb{R}_+^*$	Set of strictly positive real numbers
$\mathbb{R}^n$	Set of n-dimensional real vector
$\mathbb{N}^*$	Set of non-zero natural numbers
$\mathbf{B}^n$	Unitary box in $\mathbb{R}^n$
A	General notation for a matrix
I_n	Identity matrix in $\mathbb{R}^{n\times n}$
$[A]$	General notation for an interval matrix
$\mathcal{V}_{[A]}$	Vertices of interval matrix A
$mid[A]$	Center of interval matrix A
$rad[A]$	Radius of interval matrix A
$A^\top$	Transpose of matrix A
A^{-1}	Inverse of matrix A
$det(A)$	Determinant of matrix A
$Tr(A)$	Trace of matrix A
$Im(A)$	Image of matrix A
$diag(\sigma_1, \ldots, \sigma_n)$	Diagonal matrix of dimension n
$A \succ 0$	General notation for strictly positive definite matrix A
$A \succeq 0$	General notation for positive definite matrix A
$A \prec 0$	General notation for strictly negative definite matrix A
$A \preceq 0$	General notation for negative definite matrix A
$\mathbb{0}_{n,m}$	Zeros matrix of dimensions $n \times m$
$\mathbb{1}_{n,m}$	Matrix of dimensions $n \times m$ having all elements equal to 1
$\mathcal{X}$	General notation for a set
$Vol(\mathcal{X})$	Volume of the set $\mathcal{X}$
$\mathcal{V}_\mathcal{X}$	Vertices of the set $\mathcal{X}$
$\in$	It belongs to
$\subset$	Subset
$\cap$	Intersection

$conv(\cdot)$	Convex hull
$\oplus$	Minkowski sum
$\mathcal{Z} = \mathcal{Z}(p; H) = p \oplus H\mathbf{B}^m$	General notation of a m-zonotope
$rs(H)$	"Row sum" of matrix H
$box(\mathcal{Z})$	Approximation of zonotope Z by a box
$\mathcal{E}(P, \bar{x}, \rho)$	General notation of an ellipsoid
$M(\mathcal{S})$	Image of a set S
$d(\mathcal{X}, \mathcal{Y})$	Distance between $\mathcal{X}$ and $\mathcal{Y}$ (also called "normal" distance)
$d_H(\mathcal{X}, \mathcal{Y})$	Hausdorff distance between $\mathcal{X}$ and $\mathcal{Y}$
$\binom{n}{m}$	n combination of m elements
$n!$	Factorial of n
$\langle x, y \rangle$	Dot product of the vectors x and y
$\lvert \cdot \rvert$	Absolute value
$\lVert \cdot \rVert_\infty$	Infinity norm
$\lVert \cdot \rVert_P$	P-norm
$\lVert \cdot \rVert_1$	1-norm
$\lVert \cdot \rVert_F$	Frobenius norm
$*$	Term required for the matrix symmetry
$\triangleq$	equal by definition

Acronyms

BMI	Bilinear Matrix Inequality
ESO	Equivalent Single-Output
ESOCE	Equivalent Single-Output with Coupling Effect
FD	Fault Detection
FTC	Fault Tolerant Control
LMI	Linear Matrix Inequality
LPV	Linear Parametric Varying
LQ	Linear Quadratic control
LTI	Linear Time Invariant
LTV	Linear Time Variant
MIMO	Multi Input Multi Output
MM	Multiple Model
MPC	Model Predictive Control
OBE	Outer Bounding Ellipsoid
PAZI	Polytope and Zonotope Intersection
PMI	Polynomial Matrix Inequality
PWA	Piecewise Affine
QP	Quadratic Programming
SISO	Single Input Single Output
SVD	Singular Value Decomposition

Chapitre 1

Résumé

L'automatisation des processus prend de plus en plus d'importance aux yeux des industriels. Ceci amène les ingénieurs à générer des lois de commande pour automatiser ces processus. Généralement, ces processus sont représentés par des modèles mathématiques. Par conséquent, il est impératif de développer des modèles mathématiques reproduisant le mieux possible le comportement du système à commander. Malheureusement, le développement d'une loi de commande devient de plus en plus difficile de par la complexité croissante du modèle mathématique. C'est pour cette raison que les modèles linéaires ont été choisis dans cette thèse, de façon à conserver une complexité raisonable.
Un autre aspect, très important, se mêlant à l'automatisation des processus, est la maintenance qui tend à augmenter la durée de vie des machines / composants. Cependant, malgré les opérations de maintenance, les machines restent soumises à des défauts, qui peuvent altérer le bon fonctionnement du système.
Avec l'augmentation de la demande en termes de disponibilité, efficacité, qualité, fiabilité et sécurité, les approches de détection de défauts sont devenues cruciales à des fins de commande (automatisation des processus). Ceci s'avère fondamental pour la commande tolérante aux défauts (FTC). La commande tolérante aux défauts a pour but de traiter les défauts de sorte que le système puisse fonctionner d'une manière acceptable, quand ces défauts se produisent. Pour palier à ces défauts, des algorithmes de détection de défauts fondés sur des modèles mathématiques sont présents, dans la littérature. Dans la plupart des cas, ces algorithmes comparent le comportement du système avec celui du modèle quand ces deux derniers sont alimentés par la même entrée. Trois types de défauts sont à considérer : défauts actionneur, défauts composant et défauts capteur. Généralement, la détection de défauts et la commande tolérante aux défauts sont fondées sur l'observation/estimation de

l'état/paramètres du système, de sorte qu'une bonne estimation est requise. Dans cet esprit, les contributions de cette thèse peuvent être divisées en trois parties :

- La première partie propose une méthode d'estimation d'état ensembliste améliorée combinant l'estimation d'état à base de zonotopes (qui offre une bonne précision) et l'estimation d'état se basant sur des ellipsoïdes (qui offre une complexité réduite, i.e. temps de calcul réduit).

- Dans la deuxième partie, une nouvelle approche d'estimation d'état ellipsoïdale se basant sur la minimisation du rayon de l'ellipsoïde est développée. Dans cet esprit, quatre méthodes conduisant à la résolution de problèmes d'optimisation sous la forme d'Inégalités Matricielles Linéaires (LMI) ont été proposées.

- Reprenant les techniques précédemment développées, deux techniques de détection de défauts ont été proposées dans la troisième partie. La première technique permet de détecter des défauts capteur en testant la cohérence entre le modèle et les mesures. La deuxième technique traite les défauts actionneur/composant/capteur simultanément. Elle est fondée sur la notion de modèles multiples pour les systèmes linéaires.

Cette thèse est structurée comme suit. Le Chapitre 2, non repris et résumé ci-après, propose une introduction portant sur le contexte, les motivations, les contributions et les publications issues des résultats obtenus pendant ces travaux. Le Chapitre 3 présente les outils usuels et nécessaires pour représenter généralement les incertitudes dans le contexte des systèmes linéaires. Dans le Chapitre 4, plusieurs méthodes d'estimation ensembliste d'état fondées sur les zonotopes et les ellipsoïdes ont été résumées. Une méthode proposant une amélioration de ces stratégies combinant les avantages des zonotopes (précision) et des ellipsoïdes (complexité réduite) est développée. Par la suite, une nouvelle approche d'estimation ensembliste fondée sur les ellipsoïdes est proposée dans le Chapitre 5. Elle se base sur la minimisation du rayon de l'ellipsoïde d'estimation. Quatre méthodes ont été développées pour cette approche. Les *Méthodes 1*, *2* et *3* s'appliquent pour les systèmes linéaires invariants dans le temps. La *Méthode 3* a été étendue au cas des systèmes linéaires incertains invariant dans le temps. La *Méthode 4* est dédiée aux systèmes linéaires variant dans le temps. Le Chapitre 6 propose deux techniques de détection de défauts. La première technique détecte les défauts capteur tandis que la deuxième (fondée sur les modèles multiples) permet de détecter les défauts capteur/actionneur/composant simultanément. Une commande prédictive Min-Max a été développée afin de déterminer la commande optimale et le meilleur modèle à utiliser pour le système malgré la présence de

défauts. Enfin, le Chapitre 7 reprend et résume le contenu du manuscrit ainsi que les perspectives proposées dans le but d'améliorer et d'utiliser ce travail pour d'autres problèmes d'automatique. Le résumé de chaque chapitre est proposé ci-dessous.

1.1 Chapitre 3 : Outils nécessaires pour les systèmes linéaires incertains

Généralement, le modèle mathématique choisi pour décrire un système ne représente pas exactement le comportement du système réel. Dans ce cas, les modèles mathématiques présentent des incertitudes et sont soumis à des perturbations et des bruits de mesure. Dans la littérature, il existe deux approches pour modéliser les incertitudes : stochastique et déterministe. Dans la première approche, les propriétés statistiques (moyenne, covariance, etc.) des incertitudes, des perturbations et des bruits de mesure sont supposées connues. Mais en pratique, il s'avère très difficile de connaître la distribution statistique des incertitudes et des perturbations. Dans la plupart des cas, seules les bornes de ces incertitudes peuvent être connues. D'où l'utilisation de l'approche déterministe qui est plus adaptée dans ce cas. Dans cette approche, les incertitudes, les perturbations et les bruits de mesure sont inconnus, mais bornés. Dans la plupart des cas, ces bornes peuvent être représentées par des ensembles convexes (intervalles, ellipsoïdes, polytopes, zonotopes, etc.).

Le Chapitre 3 est décomposé en deux grandes parties : plusieurs définitions et propriétés utilisées et nécessaires à la compréhension des travaux développés dans cette thèse sont tout d'abord rappelées, certains ensembles les plus utilisés pour décrire des incertitudes sont ensuite présentés. Un résumé de ces parties est donné ci-dessous.

1.1.1 Définitions et propriétés

Plusieurs définitions et propriétés sont décrites dans le Chapitre 3 concernant des opérations matricielles. Voici les plus importantes à retenir.

***Définition* 1.1.** Une *Inégalité Matricielle Linéaire* (LMI) possède la forme :

$$F(x) \triangleq F_0 + \sum_{i=1}^{m} x_i F_i \succ 0 \tag{1.1}$$

où $x = \begin{bmatrix} x_1 & x_2 & \dots & x_m \end{bmatrix}^\top \in \mathbb{R}^m$ est le vecteur de variables de décision et les matrices $F_i = F_i^\top \in \mathbb{R}^{n \times n}$, avec $i = 0, \dots, m$, sont connues.

L'Inégalité Matricielle Linéaire (1.1) est donnée sous une formulation *stricte*. Une forme *non-stricte* s'écrivait sous la forme :

$$F(x) \succeq 0.$$

En général, les problèmes d'Inégalité Matricielle Linéaire sont formulés en utilisant les variables de décision comme suit :

$$A^\top P + PA \prec 0, \tag{1.2}$$

avec $A \in \mathbb{R}^{n\times n}$ une matrice connue et $P = P^\top \in \mathbb{R}^{n\times n}$ la variable matricielle de décision.

***Définition* 1.2.** Une *Inégalité Matricielle Bilinéaire* est définie par l'expression suivante :

$$F(x) = F_0 + \sum_{i=1}^{n} x_i F_i + \sum_{i=1}^{n}\sum_{j=1}^{m} x_i x_j F_{ij} \succ 0, \tag{1.3}$$

où

$$x = \begin{cases} \begin{bmatrix} x_1 & x_2 & \dots & x_n \end{bmatrix}^\top \in \mathbb{R}^n \text{ si } n \geq m \\ \begin{bmatrix} x_1 & x_2 & \dots & x_m \end{bmatrix}^\top \in \mathbb{R}^m \text{ sinon} \end{cases} \tag{1.4}$$

est le vecteur de variables de décision et F_0, F_i, F_{ij}, avec $i = 1, \dots, n$ et $j = 1, \dots, m$, sont des matrices symétriques connues.

***Définition* 1.3.** *Complément de Schur.* [19], [93] Soit l'Inégalité Matricielle Linéaire suivante :

$$\begin{bmatrix} Q(x) & S(x) \\ S^\top(x) & R(x) \end{bmatrix} \succ 0, \tag{1.5}$$

où $Q(x)$, $R(x)$ sont des matrices symétriques et $Q(x)$, $R(x)$ et $S(x)$ sont affines en x. Cette Inégalité Matricielle Linéaire est équivalente à :

$$\begin{cases} Q(x) \succ 0, \\ Q(x) - S(x)R^{-1}(x)S^\top(x) \succ 0, \end{cases} \tag{1.6}$$

ou

$$\begin{cases} R(x) \succ 0, \\ R(x) - S^\top(x)Q^{-1}(x)S(x) \succ 0. \end{cases} \tag{1.7}$$

Avec cette définition, les inégalités matricielles non-linéaires (1.6) et (1.7) peuvent être transformées en un problème d'Inégalité Matricielle Linéaire de la forme du problème (1.5). Il est donc possible de transformer une Inégalité Matricielle Bilinéaire en une Inégalité Matricielle Linéaire et vice versa.

1.1.2 Ensembles convexes décrivant des incertitudes bornées

L'estimation d'état ensembliste concerne la majeure partie de cette thèse. Il est donc nécessaire de définir les ensembles les plus utilisés dans la littérature. Plusieurs ensembles convexes sont utilisés dans le domaine de l'estimation ensembliste : les intervalles [76], [55], les polytopes [105], [63], [111], les parallèlotopes [26], les zonotopes [27], [2], [67] et les ellipsoïdes [61], [36], [80]. Les définitions essentielles permettant de se familiariser avec ces ensembles sont drappelées ci-dessous.

1.1.2.1 Intervalle

La façon la plus simple pour représenter des incertitudes est d'utiliser l'ensemble intervalle.

***Définition* 1.4.** Un *intervalle* $[a, b]$ est défini par l'ensemble borné $\{x \in \mathbb{R} : a \leq x \leq b\}$.

***Définition* 1.5.** Un *intervalle unitaire* est décrit par $\mathbf{B} = [-1, 1]$.

***Définition* 1.6.** Une *boîte* $([a_1, b_1], \ldots, [a_n, b_n])^\top$, avec $a_i \leq b_i$ pour $i = 1, \ldots, n$, est un vecteur intervalle.

***Définition* 1.7.** Une *boîte unitaire* $\mathbf{B}^n$ est composée de n intervalles unitaires donnés par $\{x \in ([a_1, b_1], \ldots, [a_n, b_n])^\top : a_i = -1, b_i = 1, i = 1, \ldots, n\} \subset \mathbb{R}^n$.

***Définition* 1.8.** Une *matrice intervalle* est définie par $[M] \subset \mathbb{I}^{n \times m}$, avec $a_{ij} \leq m_{ij} \leq b_{ij}$, $i = 1, ..., n$, et $j = 1, ..., m$. Dans ce cas $mid[M]_{ij} = \frac{a_{ij}+b_{ij}}{2}$ et $rad[M]_{ij} = \frac{a_{ij}-b_{ij}}{2}$ définissent le centre et le rayon de la matrice intervalle $[M]$, respectivement, pour $i = 1, \ldots, n$ et $j = 1, \ldots, m$.

1.1.2.2 Polytope

Le polytope est très répandu dans les problèmes de commande pour décrire les incertitudes. Il permet d'approcher avec une très grande précision tout ensemble convexe. Il peut être défini par deux formes équivalentes. Ceci permet de choisir la forme la plus adaptée au problème considéré. Ces deux formes sont données dans ce qui suit.

***Définition* 1.9.** *Représentation par demi-espaces.* Un *polyhèdre* $\mathcal{P} \in \mathbb{R}^n$ dans un espace euclidien de dimension finie est l'intersection d'un nombre fini de demi-espaces fermés comme suit :

$$\mathcal{P} = \{x \in \mathbb{R}^n : Ax \leq b\}, \tag{1.8}$$

avec $A \in \mathbb{R}^{m \times n}$ et $b \in \mathbb{R}^n$. Si $\mathcal{P}$ est borné, alors $\mathcal{P}$ est un *polytope*.

***Définition* 1.10.** *Représentation par sommets* ou *V-polytope.* Pour un ensemble fini de points $\mathcal{V} = \{v_1, v_2, \ldots, v_m\} \in \mathbb{R}^n$, un polytope $\mathcal{P}$ peut être défini comme étant l'enveloppe convexe de l'ensemble $\mathcal{V}$:

$$\mathcal{P} = conv(\mathcal{V}) = \{\alpha_1 v_1 + \alpha_2 v_2 + \ldots + \alpha_m v_m : \alpha_i \in \mathbb{R}^+, \sum_{i=1}^{m} \alpha_i = 1\}. \tag{1.9}$$

Les deux représentations sont équivalentes. L'inconvénient majeur du polytope est la complexité des calculs qui augmente exponentiellement avec le nombre de ses sommets.

1.1.2.3 Zonotope

Le zonotope est un polytope symétrique. Comme pour un polytope, un zonotope peut être représenté par des demi-espaces et par ses sommets. En revanche, pour le zonotope, deux définitions supplémentaires sont données ici : la représentation par les générateurs et la représentation par une transformation linéaire d'un hypercube (application linéaire). La dernière représentation est la plus utilisée dans le domaine de l'estimation ensembliste fondée sur les zonotopes pour sa simplicité.

***Définition* 1.11.** *Représentation par les générateurs.* Soit un vecteur $p \in \mathbb{R}^n$ et un ensemble de vecteurs $\mathcal{G} = \{g_1, g_2, ..., g_m\} \subset \mathbb{R}^n$, avec $m \geq n$. Un *zonotope* $\mathcal{Z}$ d'ordre m est défini comme suit :

$$\mathcal{Z} = (p; g_1, g_2, ..., g_m) = \{x \in \mathbb{R}^n : x = p + \sum_{i=1}^{m} \alpha_i g_i; |\alpha_i| \leq 1\}. \tag{1.10}$$

Le vecteur p est appelé le *centre* du zonotope $\mathcal{Z}$. Les vecteurs g_1, ..., g_m sont appelés les *générateurs* de $\mathcal{Z}$. L'*ordre* du zonotope est défini par le nombre de générateurs (m dans ce cas). Dans le cas où $m < n$, l'ensemble $\mathcal{Z}$ est dit zonotope dégénéré. Les segments du zonotope $\mathcal{Z}$ sont les segments de droite entre deux sommets du zonotope. Cette définition est équivalente

à la définition d'un zonotope par la somme de Minkovski d'un nombre fini de segments :

$$Z = (p; g_1, g_2, ..., g_m) = p \oplus g_1\mathbf{B}^1 \oplus \ldots \oplus g_m\mathbf{B}^1. \tag{1.11}$$

La complexité du zonotope $\mathcal{Z}$ est proportionnelle au nombre de ses générateurs m et à la dimension de son espace n.

***Définition* 1.12.** *Projection linéaire d'un hypercube.* Un zonotope d'ordre m dans $\mathbb{R}^n$ ($m \geq n$) est la translation de centre $p \in \mathbb{R}^n$ de l'image d'un hypercube unitaire de dimension m dans $\mathbb{R}^n$ par le biais d'une application linéaire. Soit une matrice $H \in \mathbb{R}^{n\times m}$ représentant l'application linéaire. Le zonotope $\mathcal{Z}$ est défini par :

$$\mathcal{Z} = (p; H) = p \oplus H\mathbf{B}^m. \tag{1.12}$$

Les deux définitions (1.11) et (1.12) sont équivalentes si on considère la matrice $H = \begin{bmatrix} g_1 & g_2 & ... & g_m \end{bmatrix}$.

***Définition* 1.13.** [64] Le *P-rayon* du zonotope $\mathcal{Z} = p \oplus H\mathbf{B}^m$ est défini par l'expression suivante :

$$r = \max_{z\in\mathcal{Z}}(\|z - p\|_P^2) \tag{1.13}$$

où P est une matrice symétrique définie positive ($P = P^T \succeq 0$).

Cette définition nous donne un critère pour évaluer la taille du zonotope. En effet, une valeur faible de ce P-rayon entraîne une taille faible du zonotope.

1.1.2.4 Ellipsoïdes

Les ellipsoïdes occupent une large place dans le domaine de l'estimation ensembliste. Effectivement, ils sont utilisés dans plusieurs domaines de l'automatique [36], [24], [80], [62] (estimation, identification, diagnostic, etc.).

***Définition* 1.14.** *Ensemble ellipsoïdal.* Soit une matrice symétrique définie positive $P = P^\top \succ 0$, un vecteur $\bar{x} \in \mathbb{R}^n$ et un scalaire réel strictement positif $\rho \in \mathbb{R}_+^*$. L'*ellipsoïde* borné $\mathcal{E}(P, \bar{x}, \rho)$ est défini par l'ensemble :

$$\mathcal{E}(P, \bar{x}, \rho) = \{x \in \mathbb{R}^n : (x - \bar{x})^\top P(x - \bar{x}) \leq \rho\}, \tag{1.14}$$

où $P = P^\top \succ 0$ est la *matrice d'orientation* de l'ellipsoïde, $\bar{x}$ est son *centre* et ρ est son *rayon*.

***Remarque* 1.1.** *L'ellipsoïde normalisé* est défini par :

$$\mathcal{E}(P, \bar{x}, 1) = \mathcal{E}(P, \bar{x}) = \{x \in \mathbb{R}^n : (x - \bar{x})^\top P(x - \bar{x}) \leq 1\}, \tag{1.15}$$

où $\bar{x}$ est son centre et la matrice $P = P^\top \succ 0$ caractérise son orientation et sa taille.

***Remarque* 1.2.** La notion de P-rayon définie par (1.13) donne lieu à l'ellipsoïde lié au P-rayon d'un zonotope. Cet ellipsoïde est défini par la relation :

$$(z - p)^\top P(z - p) \leq r. \tag{1.16}$$

1.2 Chapitre 4 : Estimation d'état ensembliste fondée sur les zonotopes et les ellipsoïdes

Ce chapitre traite de la problématique de l'estimation ensembliste d'état pour des systèmes linéaires soumis à des incertitudes, des perturbations et des bruits de mesures bornés, en utilisant les zonotopes et les ellipsoïdes. Les zonotopes offrent une estimation avec une meilleure précision, mais avec une complexité élevée par rapport aux ellipsoïdes. Une nouvelle méthode combinant les avantages de l'estimation zonotopique (précision) et de l'estimation ellipsoïdale (complexité réduite) est proposée.

La formulation du problème général de l'estimation ellipsoïdale est présentée ci-dessous.

1.2.1 Formulation du problème d'estimation

Soit le système linéaire suivant :

$$\begin{cases} x_{k+1} = Ax_k + \omega_k \\ y_k = Cx_k + v_k \end{cases} \tag{1.17}$$

où $x_k \in \mathbb{R}^{n_x}$ est l'état du système, $y_k \in \mathbb{R}^{n_y}$ est la mesure à l'instant k, les matrices A et C ont les dimensions appropriées ($A \in \mathbb{R}^{n_x \times n_x}$, $C \in \mathbb{R}^{n_y \times n_x}$) et le couple ($A$,$C$) est détectable. Le vecteur $\omega_k \in \mathbb{R}^{n_x}$ représente le vecteur de perturbations sur l'état et $v_k \in \mathbb{R}^{n_y}$ est la perturbation sur la mesure. On suppose que l'état initial est dans un ensemble compact $x_0 \in \mathcal{X}_0$ et que les perturbations et les bruits de mesure sont bornées par des ensembles compacts : $\omega_k \in \mathcal{W}, v_k \in \mathcal{V}$.

Soit l'ensemble d'état initial $\mathcal{X}_0$ (avec $x_0 \in \mathcal{X}_0$) et considérons qu'à l'instant k l'ensemble d'estimation d'état est noté $\hat{\mathcal{X}}_k$ (avec $x_k \in \hat{\mathcal{X}}_k$). L'objectif est de trouver l'ensemble d'estimation d'état $\hat{\mathcal{X}}_{k+1}$ qui contient l'état x_{k+1} du système (1.17) à l'instant $k+1$.

Dans la littérature, ce problème est résolu en général en suivant trois étapes :

- *Étape de prédiction* : L'ensemble de prédiction $\bar{\mathcal{X}}_{k+1}$ contenant l'état est donné par :
$$\bar{\mathcal{X}}_{k+1} \subseteq A\hat{\mathcal{X}}_k \cup \mathcal{W}. \tag{1.18}$$
Cet ensemble offre des bornes pour la trajectoire incertaine du système (1.17).

- *Étape de mesure* : Calculer l'ensemble des états cohérents avec les mesures $\mathcal{X}_{y_{k+1}}$. Il est donné par :
$$\mathcal{X}_{y_{k+1}} = \{x_{k+1} \in \mathbb{R}^{n_x} : (y_{k+1} - Cx_{k+1}) \in \mathcal{V}\}. \tag{1.19}$$

- *Étape de correction* : Calculer l'ensemble d'estimation d'état garanti $\hat{\mathcal{X}}_{k+1}$ à l'instant k. Il est donné par :
$$\hat{\mathcal{X}}_{k+1} = \bar{\mathcal{X}}_{k+1} \cap \mathcal{X}_{y_{k+1}}. \tag{1.20}$$

La Figure 4.1 illustre les trois étapes nécessaires au calcul de l'ensemble d'estimation garanti d'état $\hat{\mathcal{X}}_{k+1}$ pour le système (1.17). A l'instant k, l'en-

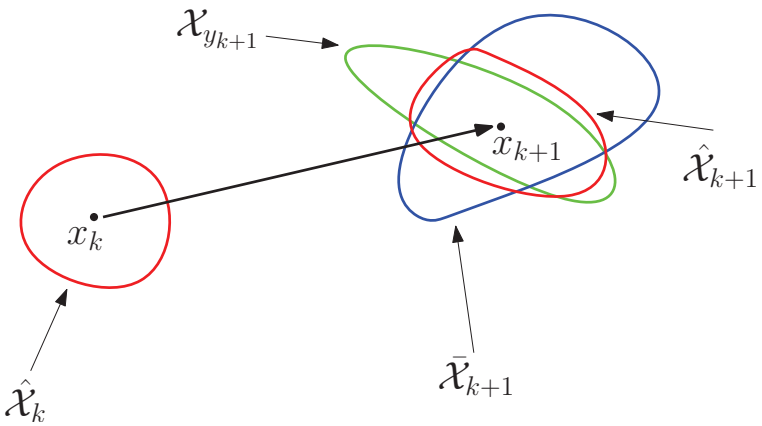

FIGURE 1.1 – Illustration des étapes d'estimation ensembliste

semble bleu $\hat{\mathcal{X}}_k$ contient l'état x_k. L'ensemble rouge représente l'ensemble de

prédiction $\bar{X}_{k+1}$ contenant l'état en utilisant (1.18). L'ensemble vert représente l'ensemble des états $\mathcal{X}_{y_{k+1}}$ cohérents avec les mesures y_{k+1}. Cet ensemble est intersecté avec l'ensemble de prédiction contenant les états en utilisant (1.20) pour construire l'ensemble rouge $\hat{\mathcal{X}}_{k+1}$.

Généralement, l'ensemble contenant l'état possède une forme géométrique particulière (zonotope, ellipsoïde, etc.). Cependant, l'ensemble d'estimation d'état exact $\hat{\mathcal{X}}_{k+1}$ contenant x_{k+1} à l'instant $k+1$, qui est l'intersection entre $\bar{\mathcal{X}}_{k+1}$ et $\mathcal{X}_{y_{k+1}}$, n'a pas cette forme particulière et doit être approché (extérieurement pour garantir l'estimation) par un ensemble ayant la même forme particulière que l'ensemble d'estimation d'état précédent. L'objectif est de trouver l'ensemble le plus petit (en termes de précision et de complexité) $\hat{\mathcal{X}}_{k+1}$ qui approxime extérieurement $\bar{\mathcal{X}}_{k+1} \cap \mathcal{X}_{y_{k+1}}$ en terme de précision et de complexité.

1.2.2 Estimations zonotopique et ellipsoïdale dans la littérature

Dans la littérature, plusieurs ensembles (formes particulières) ont été utilisés pour l'estimation ensembliste (intervalles, polytopes, zonotopes, ellipsoïdes). Dans ce chapitre, quelques méthodes ensemblistes d'estimation d'état fondées sur les zonotopes et les ellipsoïdes sont présentées.

D'un côté, les ellipsoïdes sont largement utilisés pour la simplicité de leur formulation. Les premiers travaux tournaient sur la somme et la différence géométrique d'ellipsoïdes. Par la suite, d'autres travaux ont été réalisés pour étudier des opérations importantes comme l'union et l'intersection d'ellipsoïdes, ainsi que l'approximation extérieure et intérieure d'intersections d'ellipsoïdes [61], [24]. Ceci a joué un rôle important pour résoudre un grand nombre de problèmes en automatique avec des contraintes ellipsoïdales, parmi lesquels on trouve le problème d'estimation ensembliste fondé sur les ellipsoïdes. Afin de minimiser la taille de l'ensemble d'estimation ellipsoïdal, deux méthodes sont classiquement rencontrées. Dans la première méthode, le critère du déterminant est traité [36]. Il consiste à minimiser le logarithme de la matrice d'orientation d'un ellipsoïde normalisé. Ceci est équivalent à la minimisation du volume de l'ellipsoïde. Dans la deuxième méthode, le critère de la trace est présenté [36]. Il s'agit de minimiser la trace de la matrice d'orientation de l'ellipsoïde d'estimation, ce qui revient à minimiser la somme des carrés des semi-axes de l'ellipsoïde d'estimation. Ces deux méthodes offrent une complexité réduite (temps de calcul réduit) mais avec une précision moins bonne que celle considérant des polytopes.

D'un autre côté, les zonotopes ont été proposés afin d'obtenir un compro-

mis entre la grande précision des polytopes et la complexité réduite des ellipsoïdes. Plusieurs méthodes d'estimation zonotopiques sont présentées dans ce chapitre. Dans ces méthodes, la taille du zonotope d'estimation est minimisée. La méthode fondée sur la minimisation des segments d'un zonotope permet d'avoir un calcul simple mais une précision d'estimation limitée [2]. Les méthodes fondées sur la Décomposition en Valeurs Singulières [27] et celle de la minimisation du volume du zonotope d'estimation [2] offrent une meilleure précision d'estimation, mais les calculs sont complexes. Enfin, la minimisation du P-rayon du zonotope d'estimation [67] est un compromis entre la rapidité de la méthode minimisant les segments et la bonne précision de la minimisation du volume du zonotope d'estimation.

1.2.3 Estimation combinant les zonotopes et les ellipsoïdes

Dans cette partie, une méthode combinant la bonne précision de l'estimation zonotopique et la complexité réduite des ellipsoïdes est proposée. Ceci est la première contribution de la thèse. La méthode de minimisation du P-rayon utilisant les zonotopes est choisie pour le fait qu'un zonotope possède un ellipsoïde lié à son P-rayon (voir Remarque 1.2). Pour l'estimation ellipsoïdale, le critère de la trace est choisi pour sa simplicité (i.e. solution explicite) avec une précision acceptable pour l'estimation. Cette méthode est initialisée par l'estimation zonotopique. Quand la décroissance du P-rayon du zonotope d'estimation est très faible, le zonotope d'estimation est approximé extérieurement par un ellipsoïde possédant le même centre et la même orientation que l'ellipsoïde lié au P-rayon du zonotope en question. Par la suite, la méthode d'estimation ellipsoïdale fondée sur la minimisation de la trace est appliquée. La Figure 1.2 illustre la philosophie de cette méthode. Ceci est fait dans le but de gagner en rapidité tout en gardant une précision acceptable. L'algorithme suivant résume cette méthode.

Algorithme :

Entrées :
N : Horizon d'estimation ;
ϵ : précision désirée pour le P-rayon ;
x_0 : état initial ;
$\hat{\mathcal{Z}}_0$: ensemble d'état initial ;
l : horizon d'une faible variation du P-rayon ;

Sorties :
$test = 1$;

Pour $k = 1 : N$
  Si $(|r_k - r_{k-l}| \geq \epsilon$ et $test = 1)$ or $(k \leq l)$ alors
    Calculer le zonotope d'estimation $\hat{\mathcal{Z}}_k$ et son P-rayon
    $test = 1$;
  Sinon si $|r_k - r_{k-l}| \leq \epsilon$ et $test = 1$ alors
    Calculer l'ellipsoïde $\hat{\mathcal{E}}_k$ approchant extérieurement le zonotope d'estimation ;
    $test = 0$;
  sinon
    Calculer l'ellipsoïde d'estimation $\hat{\mathcal{E}}_k$ via la minimisation de la trace
    $test = 0$;
  fin
  Enregistrer la mesure y_k ;
fin

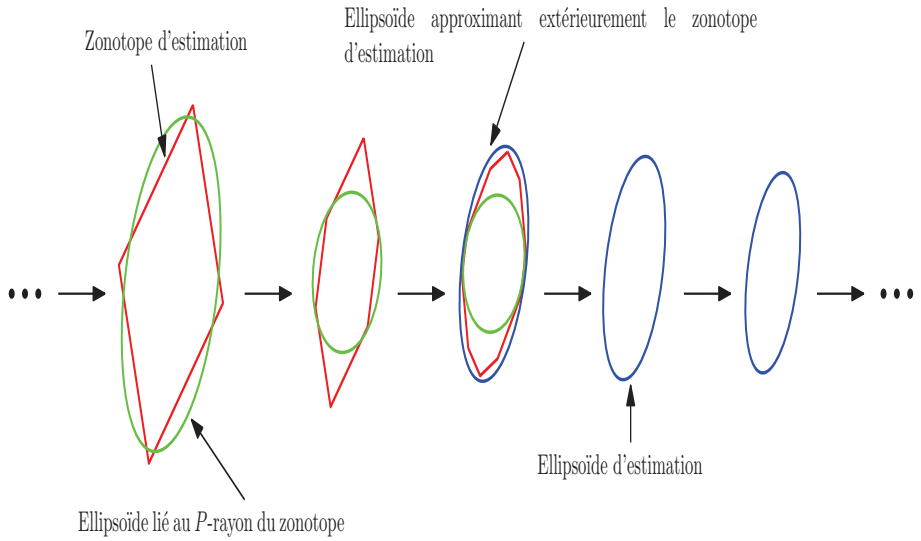

FIGURE 1.2 – Estimation combinant les zonotopes et les ellipsoïdes

1.3 Chapitre 5 : Estimation ellipsoïdale d'état fondée sur la minimisation du rayon

Dans ce chapitre, une nouvelle approche d'estimation d'état ellipsoïdale pour les systèmes linéaires multivariables (MIMO) est proposée. Elle est fondée sur la minimisation du rayon de l'ellipsoïde contenant l'estimation de l'état du système. Dans ce contexte, quatre méthodes ont été développées (comme

le montre la Figure 1.3). La *Méthode 1* considère une matrice constante pour le gain de l'observateur. La *méthode 2* considère une matrice variable pour le gain de l'observateur. La *Méthode 3* considère une matrice variable pour le gain de l'observateur avec une technique de modulation vectorielle et la *Méthode 4* considère en plus une matrice d'orientation variable pour l'ensemble ellipsoïdal d'estimation.

Les *Méthodes 1*, *2* et *3* sont appliquées dans le cadre des systèmes linéaires multi-variables invariants dans le temps soumis à des perturbations et des bruits de mesure bornés. Dans la *Méthode 1*, une matrice constante pour le gain de l'observateur liée au centre de l'ellipsoïde est obtenue en résolvant un problème d'Inégalités Matricielles Linéaires. Ce résultat est fondé sur la S-procédure pour les fonctions quadratiques [19]. Afin d'améliorer l'estimation, le gain de l'observateur est mis à jour en résolvant un problème LMI à chaque itération dans la *Méthode 2*. Ceci donne une estimation plus précise que celle obtenue avec la *Méthode 1*, mais avec une augmentation significative du temps de calcul. Dans le but de réduire ce temps de calcul tout en gardant une bonne précision de l'estimation, la *Méthode 3* propose une nouvelle technique de modulation (*scaling technique*) pour éviter de résoudre le problème LMI pour tous les sommets de la boîte contenant les perturbations et les bruits de mesure. Cette méthode est étendue aux systèmes linéaires incertains invariant dans le temps, pour lesquels les matrices d'évolution et d'observation sont des matrices intervalles.

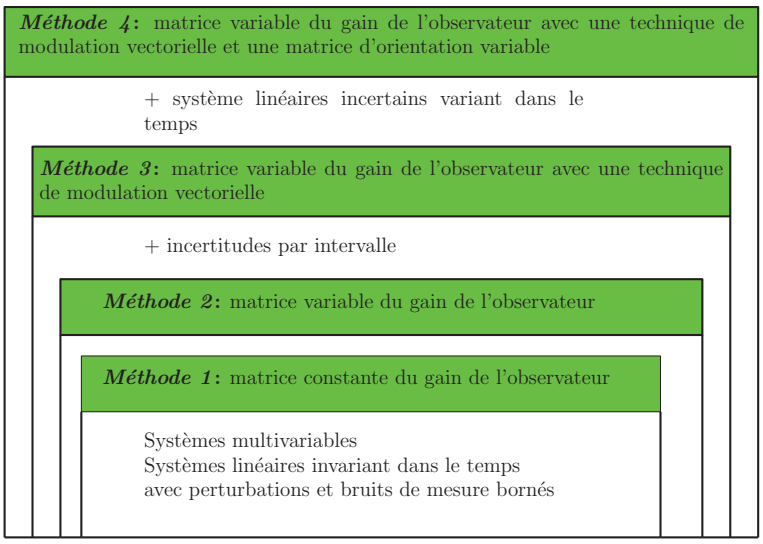

FIGURE 1.3 – Les quatre méthodes proposées pour une nouvelle approche d'estimation ellipsoïdale

Elle consiste à minimiser à chaque instant le rayon de l'ensemble d'estimation ellipsoïdal en résolvant un problème LMI. Elle offre une meilleure estimation par rapport à celle obtenue avec la méthode d'estimation zonotopique fondée sur la minimisation du P-rayon [67]. Pour ces méthodes appliquées aux systèmes linéaires invariant dans le temps avec ou sans incertitudes par intervalle (notamment les Méthodes *1*, *2* et *3*), l'orientation de l'ellipsoïde d'estimation est initialement fixée et ne change pas dans l'horizon d'estimation, ce qui pourrait être une source de conservatisme. Afin d'éviter cet inconvénient, la *Méthode 4* a été développée. Elle propose une extension pour le cas des systèmes linéaires incertains variants dans le temps en utilisant une matrice d'orientation variable pour l'ellipsoïde d'estimation. La nouveauté de cette méthode réside dans la minimisation de la taille de l'ellipsoïde d'estimation tout en ajustant son orientation. Ceci permet de diminuer le conservatisme de l'estimation par rapport aux méthodes précédentes. De plus, des contraintes quadratiques sur les mesures ont été ajoutées pour réduire encore plus la taille de l'ensemble ellipsoïdal d'estimation.

1.3.1 Formulation du problème général

Soit le système linéaire à temps discret :

$$\begin{cases} x_{k+1} = Ax_k + Bu_k + E\omega_k, \\ y_k = Cx_k + Du_k + F\omega_k, \end{cases} \tag{1.21}$$

où $x_k \in \mathbb{R}^{n_x}$ est l'état du système, $u_k \in \mathbb{R}^{n_u}$ est le vecteur des entrées et $y_k \in \mathbb{R}^{n_y}$ est le vecteur de mesures à l'instant k. Le vecteur $\omega_k \in \mathbb{R}^{n_x+n_y}$ contient les perturbations sur l'état et les bruits de mesures simultanément. Les matrices A, B, C, D, E, et F ont les dimensions appropriées, avec la paire (C, A) détectable et la paire (A, B) stabilisable. On suppose que les perturbations ω_k sont bornées par la boîte unitaire $\mathbf{B}^{n_x+n_y}$ et que l'état initial x_0 appartient à l'ellipsoïde $\mathcal{E}(P_0, \bar{x}_0, \rho_0) = \{x \in \mathbb{R}^{n_x} : (x - \bar{x}_0)^\top P_0 (x - \bar{x}_0) \leq \rho_0\}$, avec $\bar{x}_0$ l'état nominal initial. Les matrices E et F représentent les poids (pondérations) sur les perturbations normalisées $\omega_k \in \mathbf{B}^{n_x+n_y}$.

En supposant qu'à l'instatnt k l'ellipsoïde contenant x_k est donné par $\mathcal{E}(P, \bar{x}_k, \rho_k)$, avec $\bar{x}_k$ l'estimation nominale, l'objectif est de trouver un ellipsoïde de la forme $\mathcal{E}(P, \bar{x}_{k+1}, \rho_{k+1})$ contenant l'état x_{k+1} à l'instant $k + 1$.

Dans ce qui suit, un résumé des résultats obtenus en appliquant les quatre méthodes décrites ci-dessus est proposé.

1.3.2 Systèmes linéaires invariant dans le temps

Ici, les matrices A, B, C, D, E et F dans (1.21) sont supposées constantes.

1.3.2.1 *Méthode 1*

L'ellipsoïde contenant l'état du système à chaque instant est donné par le théorème qui suit.

***Théorème* 1.1.** Soit l'état initial x_0 et considérons que $x_k \in \mathcal{E}(P, \bar{x}_k, \rho_k)$ à l'instant k. Étant donné un scalaire $\beta \in (0,1)$, s'il existe une matrice symétrique définie positive $P = P^\top \succ 0$ dans $\mathbb{R}^{n_x \times n_x}$, une matrice $Y \in \mathbb{R}^{n_x \times n_y}$ et un scalaire $\sigma > 0$ pour lesquels la LMI est vérifiée pour chaque $\omega_k \in \mathcal{V}_{\mathbf{B}^{n_x+n_y}}$ (où $\mathcal{V}_{\mathbf{B}^{n_x+n_y}}$ représente les sommets de $\mathbf{B}^{n_x+n_y}$) :

$$\begin{bmatrix} \beta P & 0 & A^\top P - C^\top Y^\top \\ 0 & \sigma & \omega_k^\top (E^\top P - F^\top Y^\top) \\ PA - YC & (PE - YF)\omega_k & P \end{bmatrix} \succ 0, \tag{1.22}$$

alors l'état x_{k+1} à l'instant $k+1$ est contenu dans l'ellipsoïde $\mathcal{E}(P, \bar{x}_{k+1}, \rho_{k+1})$, pour tout $\omega_k \in \mathbf{B}^{n_x+n_y}$, avec :

$$Y = PL, \tag{1.23}$$
$$\bar{x}_{k+1} = A\bar{x}_k + Bu_k + L(y_k - C\bar{x}_k - Du_k), \tag{1.24}$$
$$\rho_{k+1} \leq \beta\rho_k + \sigma. \tag{1.25}$$

Le problème d'optimisation (1.22) est résolu hors ligne. Il est possible de prendre en compte la connaissance de la matrice P pour obtenir un gain adaptatif L_k à chaque instant k. Ceci améliore la rapidité de la convergence de l'estimation. La solution à ce problème est donnée par la *Méthode 2*.

1.3.2.2 *Méthode 2*

Cette méthode propose une amélioration de la convergence du rayon de l'ellipsoïde d'estimation par rapport à la *Méthode 1*. L'idée est de calculer un gain variable L_k à chaque instant. L'existence de P, L et β (calculés avec la *Méthode 1*) garantit l'existence de L_k vérifiant les contraintes considérées. Cette méthode minimise le rayon de l'ellipsoïde d'estimation ρ_{k+1} à chaque instant. Le théorème suivant explique la *Méthode 2*.

***Théorème* 1.2.** Considérons qu'à l'instant k le vecteur d'état x_k appartient à l'ellipsoïde $\mathcal{E}(P, \bar{x}_k, \rho_k)$, avec la matrice P, le rayon ρ_k et le scalaire σ calculés à partir des résultats obtenus avec le *Théorème* 1.1. S'il existe une matrice $Y_k \in \mathbb{R}^{n_x \times n_y}$, un scalaire $\beta \in (0,1)$ et un rayon ρ_{k+1} vérifiant le problème d'optimisation suivant pour tout $\omega_k \in \mathcal{V}_{\mathbf{B}^{n_x+n_y}}$:

$\min_{\beta, Y_k, \rho_{k+1}} \rho_{k+1}$
tel que

$$\begin{cases} \begin{bmatrix} \beta P & 0 & A^\top P - C^\top Y_k^\top \\ 0 & \rho_{k+1} - \beta\rho_k & \omega_k^\top (E^\top P - F^\top Y_k^\top) \\ PA - Y_k C & (PE - Y_k F)\omega_k & P \end{bmatrix} \succ 0, \\ \rho_{k+1} \leq \beta\rho_k + \sigma, \end{cases} \tag{1.26}$$

alors le vecteur d'état x_{k+1} à l'instant $k+1$ est contenu dans l'ellipsoïde $\mathcal{E}(P, \bar{x}_{k+1}, \rho_{k+1})$, pour tout $\omega_k \in \mathbf{B}^{n_x+n_y}$, avec :

$$PL_k = Y_k, \tag{1.27}$$
$$\bar{x}_{k+1} = A\bar{x}_k + Bu_k + L_k(y_k - C\bar{x}_k - Du_k). \tag{1.28}$$

***Remarque* 1.3.** La vérification en ligne du problème LMI (1.26), pour tous les sommets de la boîte unitaire $\mathbf{B}^{n_x+n_y}$, requiert un important temps de calcul.

1.3.2.3 *Méthode 3*

Pour éviter la résolution du problème (1.26) pour tous les sommets de $\mathbf{B}^{n_x+n_y}$ et réduire le temps de calcul, une nouvelle technique de modulation (*scaling technique*) est proposée et appliquée au problème (1.26) conduisant à la *Méthode 3*. Le résultat est donné par la proposition suivante.

***Proposition* 1.1.** Si la contrainte LMI du problème d'optimisation (1.26) :

$$\begin{bmatrix} \beta P & 0 & A^\top P - C^\top Y_k^\top \\ 0 & \rho_{k+1} - \beta\rho_k & \omega_k^\top (E^\top P - F^\top Y_k^\top) \\ PA - Y_k C & (PE - Y_k F)\omega_k & P \end{bmatrix} \succ 0, \quad \forall \omega_k \in \mathcal{V}_{\mathbf{B}^{n_x+n_y}}, \tag{1.29}$$

est vérifiée, alors il existe un scalaire $\beta > 0$ et une matrice $S = S^\top \succ 0 \in \mathbb{R}^{(n_x+n_y)\times(n_x+n_y)}$ tels que :

$$\begin{cases} \begin{bmatrix} \beta P & A^\top P - C^\top Y_k^\top & 0 \\ PA - Y_k C & P & PE - Y_k F \\ 0 & E^\top P - F^\top Y_k^\top & S \end{bmatrix} \succ 0, \\ \rho_{k+1} - \beta\rho_k > 0. \end{cases} \tag{1.30}$$

La *Méthode 3* offre une meilleure précision d'estimation comparée à la *Méthode 1* avec un gain en terme de temps de calcul par rapport à la *Méthode 2*.

***Remarque* 1.4.** La *Méthode 3* a été étendue au cas des systèmes linéaires incertains invariant dans le temps (les matrices A et C sont des matrices intervalles pour le système (1.21)). La solution est donnée dans le théorème suivant.

***Théorème* 1.3.** Soit le vecteur d'état initial x_0 et à l'instant k, $x_k \in \mathcal{E}(P, \bar{x}_k, \rho_k)$, avec $P = P^\top \succ 0$ et $\rho_k > 0$. S'il existe une matrice $Y_k \in \mathbb{R}^{n_x \times n_y}$, une matrice $S = S^\top \succ 0$ dans $\mathbb{R}^{(n_x+n_y+n_\delta)\times(n_x+n_y+n_\delta)}$ et les scalaires $\rho_{k+1} > 0$ et $\beta \in (0,1)$ tels que le problème suivant est vérifié pour tout $A_\delta \in \mathcal{V}_{[A]}$ and $C_\delta \in \mathcal{V}_{[C]}$:

$$\min_{\beta, Y_k, S, \rho_{k+1}} \rho_{k+1}$$

tel que

$$\begin{cases} \begin{bmatrix} \beta P & * & * \\ PA_\delta - Y_k C_\delta & P & * \\ 0 & \begin{bmatrix} E^\top P - F^\top Y_k^\top \\ \mathcal{A}_k^\top \\ -\mathcal{C}_k^\top Y_k^\top \end{bmatrix} & S \end{bmatrix} \succ 0, \\ \rho_{k+1} - \beta\rho_k > 0, \\ \beta < 1, \end{cases} \tag{1.31}$$

avec $\mathcal{A}_k = \begin{bmatrix} PA_{\delta_1}\bar{x}_k & \dots & PA_{\delta_{n_{A_\delta}}}\bar{x}_k \end{bmatrix}$ et $\mathcal{C} = \begin{bmatrix} C_{\delta_1}\bar{x}_k & \dots & C_{\delta_{n_{C_\delta}}}\bar{x}_k \end{bmatrix}$, alors l'état x_{k+1} à l'instant $k+1$ est contenu dans l'ellipsoïde $\mathcal{E}(P, \bar{x}_{k+1}, \rho_{k+1}), \forall \omega_k \in \mathbf{B}^{n_x+n_y+n_\delta}$, $\forall A_\delta \in [A]$ et $\forall C_\delta \in [C]$, où :

$$Y_k = PL_k, \tag{1.32}$$

$$\bar{x}_{k+1} = mid[A]\bar{x}_k + L_k(y_k - mid[C]\bar{x}_k) \tag{1.33}$$

1.3.3 Systèmes linéaires variant dans le temps

L'approche d'estimation ellipsoïdale est étendue au cas des systèmes variant dans le temps (avec des matrices d'évolution A_k et d'observation C_k variables) soumis à des incertitudes par intervalles, des perturbations et des bruits de mesure bornés. La nouveauté est que la matrice d'orientation de l'ellipsoïde d'estimation est variable dans le but d'améliorer la précision.

1.3.3.1 *Méthode 4*

La solution à ce problème (pour un système linéaire variant dans le temps avec une matrice d'orientation variable de l'ellipsoïde d'estimation) est donnée par le théorème suivant.

***Théorème* 1.4.** Soit le système (1.21) avec des matrices intervalles variables dans le temps $A_k \in [A]$ et $C_k \in [C]$. Si les hypothèses suivantes sont vérifiées :

(i) À l'instant k, le vecteur d'état x_k appartient à l'ellipsoïde $\mathcal{E}(P_k, \bar{x}_k, \rho_k)$;

(ii) À l'instant k, les incertitudes considérées (incertitudes par intervalles présentes dans A_k et C_k, perturbations et bruits de mesure) sont bornées dans un ensemble convexe Ω_k, avec $\mathcal{V}_{\Omega_k}$ l'ensemble des sommets de Ω_k ;

(iii) Il existe des matrices $P_{k+1} = P_{k+1}^\top \succ 0$, avec $P_{k+1} \in \mathbb{R}^{n_x \times n_x}$, $Y_{k+1} \in \mathbb{R}^{n_x \times n_y}$, $G_{k+1} \in \mathbb{R}^{n_x \times n_x}$, un vecteur $g_{k+1} \in \mathbb{R}^{n_x}$ et des scalaires positifs $\beta_{k+1}, \rho_{k+1} > 0$ tels que l'Inégalité Matricielle Linéaire suivante est satisfaite pour tout $(\omega_k, A_k, C_k) \in \mathcal{V}_{\Omega_k}$:

$$\begin{bmatrix} \beta_{k+1}P_k & * & * \\ 0 & \rho_{k+1} - \beta_{k+1}\rho_k & * \\ P_{k+1}A_k - Y_{k+1}C_k & \tau_{k+1} & P_{k+1} \end{bmatrix} \succ 0, \tag{1.34}$$

avec $\tau_{k+1} = (P_{k+1}A_k - Y_{k+1}C_k - G_{k+1})\bar{x}_k + (P_{k+1}E - Y_{k+1}F)\omega_k - g_{k+1}$;

alors, à l'instant $k+1$, le vecteur d'état x_{k+1} appartient à l'ellipsoïde : $\mathcal{E}(P_{k+1}, \bar{x}_{k+1}, \rho_{k+1})$, avec $\bar{x}_{k+1} = P_{k+1}^{-1}(G_{k+1}\bar{x}_k + Y_{k+1}y_k + g_{k+1})$.

***Remarque* 1.5.** Des contraintes sur P_{k+1} et ρ_{k+1} peuvent être ajoutées au problème de faisabilité (1.34) dans le but de réduire la taille de l'ellipsoïde d'estimation. Le problème d'optimisation à résoudre est alors le suivant :

$$\min_{\beta_{k+1}, Y_{k+1}, P_{k+1}, \rho_{k+1}, G_{k+1}, g_{k+1}, \alpha, \gamma} \alpha$$

tel que

$$\begin{cases} \begin{bmatrix} \beta_{k+1}P_k & * & * \\ 0 & \rho_{k+1} - \beta_{k+1}\rho_k & * \\ P_{k+1}A_k - Y_{k+1}C_k & \tau_{k+1} & P_{k+1} \end{bmatrix} \succ 0, \\ P_{k+1} \geq P_k, \\ \rho_{k+1} \leq \alpha\rho_k + \gamma, \\ 0 < \alpha < 1, \\ \gamma > 0, \end{cases} \tag{1.35}$$

où $\tau_{k+1} = (P_{k+1}A_k - Y_{k+1}C_k - G_{k+1})\bar{x}_k + (P_{k+1}E - Y_{k+1}F)\omega_k - g_{k+1}$, $\forall(\omega_k, A_k, C_k) \in \Omega_k$ et $\bar{x}_{k+1} = P_{k+1}^{-1}(G_{k+1}\bar{x}_k + Y_{k+1}y_k + g_{k+1})$.

1.3.3.2 Amélioration de la *Méthode 4*

L'estimation d'état (1.35) calcule l'ensemble ellipsoïdal $\mathcal{E}(P_{k+1}, \bar{x}_{k+1}, \rho_{k+1})$ en utilisant la mesure y_k. Il peut être judicieux et intéressant d'utiliser la mesure y_{k+1} pour améliorer (i.e. diminuer) la taille de l'ellipsoïde d'estimation. Pour ce faire, des contraintes quadratiques sur la mesure et sur les perturbations à l'instant $k+1$ ont été ajoutées. En partant de l'ellipsoïde d'estimation calculé à partir de (1.35), l'idée est de considérer des contraintes quadratiques en y_{k+1} et ω_{k+1} afin de calculer un nouvel ellipsoïde qui contient l'état x_{k+1}. Ceci est similaire à une étape de correction fondée sur la mesure à l'instant $k+1$. La solution est donnée ci-dessous.

***Proposition* 1.2.** Soit $\mathcal{E}(P_{k+1}, \bar{x}_{k+1}, \rho_{k+1})$ obtenus en solvant le problème (1.35) pour le système (1.21) à l'instant $k+1$, fondé sur les informations disponible à l'instant k. S'il existe une matrice $P'_{k+1} = P'^{\top}_{k+1} \succ 0$ dans $\mathbb{R}^{n_x \times n_x}$, une matrice $H = H^{\top} \succ 0$ dans $\mathbb{R}^{n_y \times n_y}$, un vecteur $\bar{x}'_{k+1} \in \mathbb{R}^{n_x}$ et un scalaire réel positif $\rho'_{k+1} > 0$ tels que le problème suivant est vérifié pour tout $C_{k+1} \in \mathcal{V}_{[C]}$:

$$\begin{cases} \begin{bmatrix} \eta_1 & * & * \\ \eta_2 & \eta_3 - \sum_{i=1}^{n_x+n_y} \mu_i & * \\ P'_{k+1} & -b_{k+1} & P'_{k+1} \end{bmatrix} \succ 0, \\ F^{\top} H F < \sum_{i=1}^{n_x+n_y} \mu_i T_i, \\ \mu_i \geq 0, \;\; i = 1, ..., n_x + n_y, \\ \theta \geq 0, \;\; \theta < 1, \\ \rho'_{k+1} > \theta \rho_{k+1}, \end{cases} \tag{1.36}$$

avec :

$$\begin{aligned} b_{k+1} &= P'_{k+1} \bar{x}'_{k+1} \\ \eta_1 &= \theta P_{k+1} + C_{k+1}^{\top} H C_{k+1} \\ \eta_2 &= -\theta \bar{x}_{k+1}^{\top} P_{k+1} - y_{k+1}^{\top} H C_{k+1} \\ \eta_3 &= \rho'_{k+1} - \theta \rho_{k+1} + \theta \|\bar{x}_{k+1}\|^2_{P_{k+1}} + \|y_{k+1}\|^2_H \end{aligned} \tag{1.37}$$

alors l'ellipsoïde d'estimation contenant l'état est is $\mathcal{E}'(P'_{k+1}, \bar{x}'_{k+1}, \rho'_{k+1})$.

Cette méthode offre une meilleure précision par rapport à la *Méthode 4* mais avec une grande complexité. Afin de réduire le temps de calcul, des approches de type "scaling technique" peuvent être utilisées [4].

1.4 Chapitre 6 : Détection de défauts fondée sur l'estimation ensembliste

Les méthodes d'estimation ensembliste présentées dans les deux chapitres précédents vont être utilisées à des fins de détection de défauts. Dans ce chapitre, la détection de défauts sur des systèmes linéaires a été traitée. Pour ce faire, les approches d'estimation ensembliste sont utilisées. L'estimation zonotopique fondée sur la minimisation du P-rayon est tout d'abord appliquée pour la détection de défauts capteur. Dans une deuxième étape, un nouvel algorithme de détection de défauts fondé sur la notion des modèles multiples et sur l'approche d'estimation ellipsoïdale proposée dans le chapitre précédent a été développé.

1.4.1 Détection de défauts capteur fondée sur l'estimation zonotopique

Une approche de détection de défauts capteur dans l'espace d'état est proposée. Elle est basée sur l'estimation ensembliste. Cette approche de détection de défauts capteur peut être appliquée en utilisant toutes les méthodes d'estimation citées dans cette thèse (zonotopiques, ellipsoïdales ou une combinaison de ces approches). Toutefois, et afin de donner une vision élargie, la méthode d'estimation zonotopique fondée sur la minimisation du P-rayon est considérée. Cette méthode d'estimation présente trois étapes importantes : prédiction, mesure et correction.

Avant l'étape de correction, le zonotope de prédiction et l'ensemble d'état cohérent avec les mesures sont construits. Deux configurations peuvent alors se produire : intersection non-vide et intersection vide entre ces deux ensembles. Le premier cas nous renseigne sur la présence de défaut, tandis que pour le deuxième cas, on peut dire qu'il n'y a pas de défaut. La Figure 1.4 illustre ces deux cas pour un système à deux dimensions avec une seule sortie.

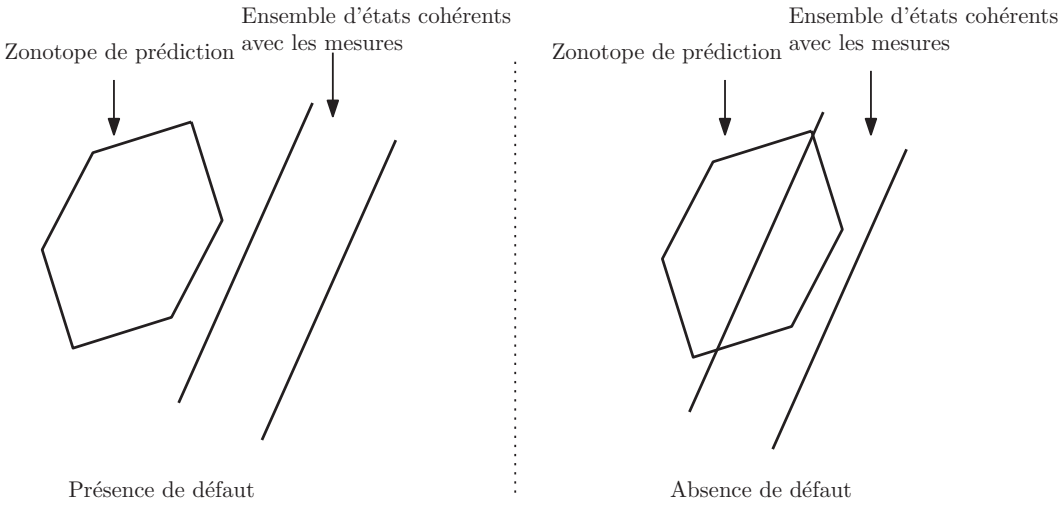

FIGURE 1.4 – Les deux situations possibles avant l'étape de correction : présence ou absence de défaut

L'application directe de la méthode d'estimation zonotopique fondée sur la minimisation du P-rayon pour des systèmes présentant des défauts capteur ne garantit pas l'estimation quand le défaut existe. Pour palier cet inconvénient, un nouvel algorithme de détection de défauts utilisant cette méthode d'estimation zonotopique est proposé. Cet algorithme permet de garantir l'estimation malgré la présence de défauts. L'idée est que durant la présence du défaut, seule l'estimation obtenue par l'étape de prédiction est prise en compte. En l'absence de défauts, les trois étapes (prédiction, mesure et correction) sont appliquées. Pour cela, l'intersection entre le zonotope de prédiction et l'ensemble d'états cohérent avec la mesure est faite en utilisant la méthode du P-rayon. Cette méthode conduit à une estimation garantie, mais avec une mauvaise précision quand les défauts sont présents. Pour remédier à cet inconvénient, une technique de calibration de la mesure est proposée. Elle consiste à centrer la mesure sur le zonotope de prédiction quand les défauts capteur sont présents (voir Figure 1.5). Après la calibration, on obtient une nouvelle mesure calibrée et ensuite la méthode d'estimation zonotopique fondée sur la minimisation du P-rayon est appliquée. Ceci permet de décroitre le conservatisme de la méthode proposée en terme d'estimation quand les défauts sont présents. Ce peut être bénéfique à des fins de commande (commande tolérante aux défauts).

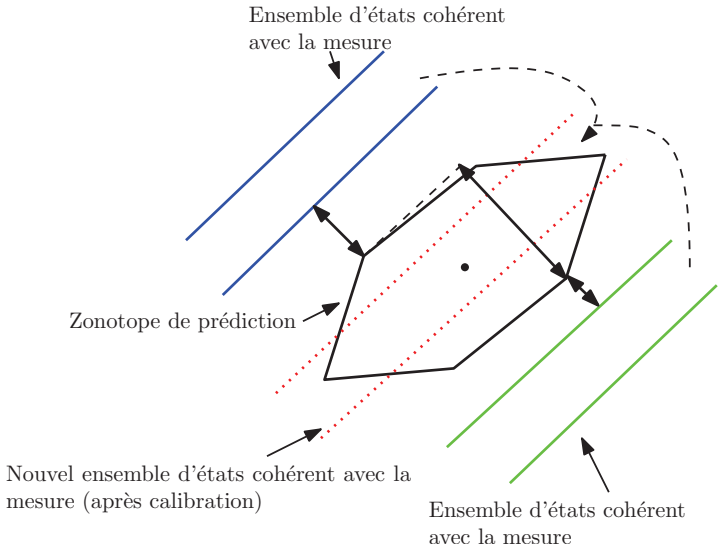

FIGURE 1.5 – Calibration de la mesure

1.4.2 Détection de défauts fondée sur des modèles multiples

Dans cette approche, une large classe de défauts (actionneur, capteur et composant) peut être détectée. Pour ce faire, une nouvelle approche de détection de défauts utilisant l'estimation ensembliste et fondée sur la technique de modèles multiples a été développée. Ces modèles sont construits en se référant au système original (sans défauts), tels que chaque modèle est adéquat à un type de défaut. En général, dans une représentation d'état pour un système linéaire, les défauts composant peuvent être modélisés par une modification de la matrice d'évolution (A), les défauts actionneur sont modélisés par une modification sur la matrice de commande (B) et les défauts capteur sont représentés par une modification dans la matrice d'observation (C).

Cette approche de détection de défauts consiste, dans une première étape, à la vérification de la cohérence de chaque modèle avec les mesures. Cette vérification est fondée sur l'utilisation de l'estimation ellipsoïdale proposée dans le chapitre précédent. À noter aussi que les autres méthodes d'estimation ensembliste peuvent être utilisées.

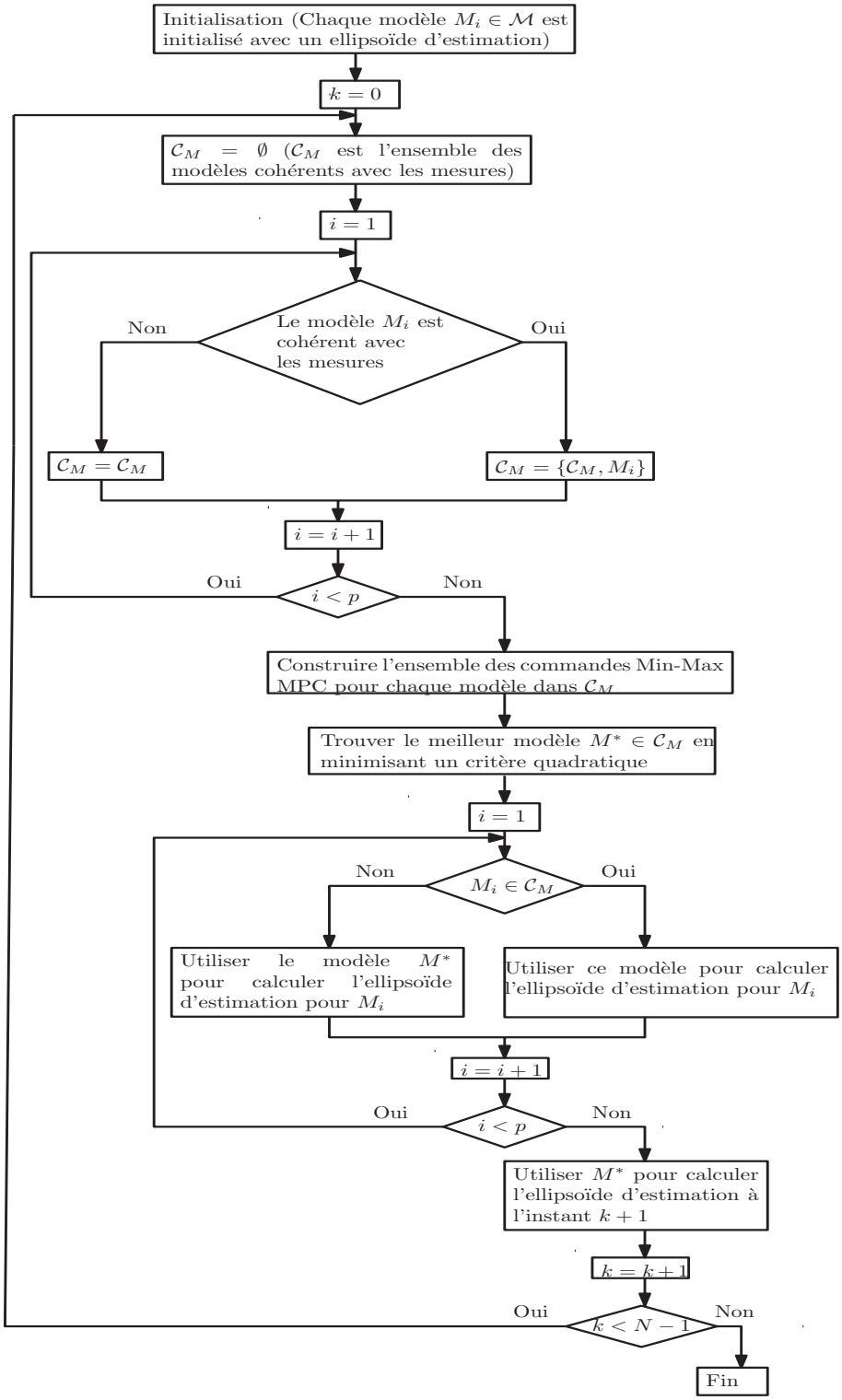

FIGURE 1.6 – Organigramme de la méthode de détection de défauts fondée sur les modèles multiples

Dans une deuxième étape, l'ensemble des modèles cohérents avec les mesures est formé. La troisième étape consiste à développer une commande prédictive de type Min-Max pour chaque modèle compatible avec les mesures dans le but de choisir le meilleur modèle pour l'estimation. Finalement, un critère quadratique classique est minimisé dans le but de choisir :

- La meilleure commande à appliquer pour le système original ;
- Le meilleur modèle pour l'estimation.

Ce processus est répété à chaque instant k sur l'horizon d'estimation N. L'algorithme développé pour cette approche est résumé sur la Figure 1.6. À noter ici que l'ensemble des modèles est noté $\mathcal{M}$ et que chaque modèle est noté M_i, pour $i = 0, \ldots, p$ (où p est le nombre de modèles), $\mathcal{C}_M$ représente l'ensemble des modèles cohérents avec les mesures et M^* représente le meilleur modèle pour l'estimation.

La nouveauté ici est l'utilisation de l'estimation ensembliste couplée avec une commande prédictive de type Min-Max pour estimer l'état d'un système linéaire soumis à des perturbations et des bruits de mesure bornés malgré la présence concomitante de défauts composant, actionneur et capteur.

1.5 Conclusion

Dans cette thèse, des algorithmes de détection de défauts fondés sur l'estimation ensembliste d'état pour des systèmes linéaires incertains soumis à des perturbations et des bruits de mesure bornés ont été proposés. Les principales contributions de cette thèse peuvent être divisées en trois parties :

- La première partie propose une méthode d'estimation ensembliste qui combine les avantages de l'estimation zonotopique (bonne précision) et de l'estimation ellipsoïdale (complexité réduite) ;
- Dans la deuxième partie, une nouvelle approche d'estimation ellipsoïdale fondée sur la minimisation du rayon de l'ellipsoïde est développée. Quatre méthodes ont été présentées dans cette approche. Les méthodes *1*, *2* et *3* sont appliquées pour les systèmes linéaires invariant dans le temps. Par la suite, la *Méthode 3* a été étendue au cas des systèmes linéaires incertains invariant dans le temps avec des incertitudes par intervalles dans les matrices d'évolution et d'observation. Finalement, la *Méthode 4* a été développée pour les systèmes linéaires variant dans le temps ;

- Deux techniques de détection de défauts ont été proposées dans la troisième partie. La première technique permet de détecter les défauts capteur en vérifiant la cohérence entre le modèle et les mesures. La deuxième technique est fondée sur les modèles multiples pour les systèmes linéaires soumis à des incertitudes et des bruits de mesure bornés. Il traite les défauts composant, actionneur et capteur.

Cette thèse peut être étendue en considérant les points suivants :

- Étendre l'approche d'estimation ellipsoïdale proposée (fondée sur la minimisation du rayon) pour le cas des systèmes à retard et des systèmes affines par morceaux ;
- Utilisation des algorithmes de détection de défauts proposés pour la commande tolérante aux défauts ;
- Valider les méthodes d'estimation et les algorithmes de détection de défauts expérimentalement.

Chapter 2

Introduction

2.1 Context and motivations

In the last decades, the automation of industrial processes reached a high level. The number of tasks performed by computers is increasing every day whether in the fields of aerospace, biomedical applications, automotive, electronics and robotics. Maintenance operations are regularly scheduled in order to increase the life-time of the machines/components. Despite these maintenance operations, machines are still subject to faults (i.e. malfunctions in system components). However, in most applications, the faults are not taken into account, and often a small fault can have an important impact on the evolution of a system. With the increasing demand for availability, efficiency, quality, reliability and safety, the Fault Detection (FD) approaches have become a crucial issue for control purposes. These approaches are known under the name of Fault Tolerant Control (FTC) systems. The goal is to treat the faults in such a way that the system can operate in an acceptable way, when malfunctions occur. This aims at developing model based Fault Detection algorithms, usually developed by comparing the behavior of the process and its model when both are fed with the same inputs. With respect to the closed-loop system elements, there are three types of faults: actuator faults, component faults and sensor faults. Generally, FD and FTC techniques are based on an observation/estimation of the state/parameters of the system. Thus, a good estimation is required.

In literature, there are two main classes for the estimation: stochastic approaches and deterministic approaches. In the first approach, some characteristics (average, covariance, etc.) of noises and perturbations are assumed to be known [57]. However, sometimes the probabilistic assumptions are difficult to verify. Thus, the deterministic approach (i.e. considering that noises

and perturbations belong to bounded compact sets) seems more realistic. In this way, interval state observers [86], [37] and set-membership estimation approaches have been developed [95], [106], where perturbations are considered unknown but bounded. In these approaches, the evolution of system states at each time instant is not described by a point in the state-space but by a set. In the context of interval state observers, the exact state estimation set is approximated by its interval hull. Interval state observers algorithms can be classified into two categories: approximations of estimated states using one step-ahead iteration based on the previous approximated sets [1] or a set of point-wise trajectories generated by selecting particular values of parameters of the system using trajectory-based optimization approaches [84]. The set-membership estimation approaches compute at each time instant the estimated set containing all the possible states consistent with the measurements, the possible perturbations and uncertainties. Several sets are used to implement set-membership estimation methods: parallelotopes [105], [26], ellipsoids [39], [24], [61], [22], zonotopes [83], [27], [2], etc.

In this thesis, the set-membership state estimation is chosen because of its ability to deal with uncertainties and disturbances. A combined method between zonotopes and ellipsoids is firstly proposed. Then, the ellipsoidal set is privileged for its simplicity. A new approach based on the minimization of the ellipsoidal radius will be presented in this thesis. Moreover, the zonotopic set-membership estimation method proposed in [64] is applied for sensor Fault Detection. Finally, a new Fault Detection algorithm based on linear Multiple Model systems with bounded perturbations and bounded measurement noises and using the proposed ellipsoidal set-membership state estimation will be further detailed.

2.2 Contributions and organization of the thesis

In this section, a short description of the next chapters is given with highlights on the main contributions.

- **Chapter 3:** This chapter presents useful tools for representing uncertainties in the context of linear systems. It starts with basic definitions and properties necessary to manipulate matrix and important operations for sets. Finally, the most used sets (and their main properties) to represent uncertainties (interval, polytope, zonotope and ellipsoid) are analyzed. Due to the simplicity of zonotopes and ellipsoids, these two sets will be used in this thesis.

- **Chapter 4:** In this chapter, several existing set-membership state estimation techniques based on zonotopes or ellipsoids are summarized.

  - To minimize the size of the ellipsoidal estimation set, two methods are mainly considered. Firstly, the determinant-based criterion is minimized [36], which is equivalent to minimize the volume of the ellipsoidal set. Secondly, the minimization of the trace criterion, which is equivalent to minimize the sum of squares of the half length of the axes of the ellipsoid, is considered in the literature [36].
  - For zonotopes, four methods are outlined: the Singular Value Decomposition-based method [27], the minimization of the zonotope segments [2], the minimization of the zonotope volume [2] and the P-radius of the zonotope methods. In [67], the minimization of the P-radius of the zonotope leads to a trade-off between the rapidity of the segments minimization and the estimation accuracy of the volume minimization of a zonotope.
    The main contribution of this chapter consists in proposing an improved method which combines the advantages of the zonotopic set-membership state estimation (i.e. accuracy) and of the ellipsoidal set-membership estimation (i.e. reduced complexity). This is formulated as an optimization problem which starts with the zonotopic estimation and continues with the ellipsoidal estimation (once the estimation set is small enough). A new criterion based on the P-radius of the zonotopic estimation is used to make the transition between the use of zonotopic sets and ellipsoidal sets.

- **Chapter 5:** A new guaranteed ellipsoidal state estimation approach for multivariable Linear Time Invariant (LTI) systems with bounded perturbations and measurement noises has been proposed in this chapter. For this, four methods are given. *Method 1* is applied for Linear Time Invariant (LTI) systems and consists in solving a LMI (Linear Matrix Inequality) problem by considering a constant observer gain. In *Method 2*, the radius of the ellipsoidal set is minimized at each iteration by online solving an LMI problem. It considers an updated observer gain. In *Method 3*, a new vector scaling technique is applied. The computation time is significantly reduced in *Method 3*, while keeping an acceptable level of the estimation accuracy. This method is also extended for uncertain LTI systems, with interval uncertainties both in the evolution and the observation matrices. *Method 4* is ap-

plied for Linear Time Variant (LTV) systems. It is based on the online minimization of the size of the ellipsoidal state estimation set by considering an updated observer gain and a flexible shape matrix for this ellipsoidal estimation set (which is another important contribution of this thesis). An improvement of the accuracy of this ellipsoidal estimation method is further presented in *Improved Method 4* by adding quadratic constraints on both measurements and perturbations. This allows us to reduce the bounds of the estimation domain, offering a better estimation accuracy.

- **Chapter 6:** This chapter proposes two Fault Detection approaches:
  - The first approach allows the sensor FD using the consistency test. In this context, three algorithms based on the zonotopic P-radius minimization method are proposed. The first algorithm checks the consistency between the model and the measurement in the fault-free case. The second one gives a guaranteed but conservative estimation in the presence of sensor faults without considering the measurement for the estimation when sensor fault occurs. The last algorithm gives and estimation with reduced conservativeness when sensor faults occur by updating the set of measurements. This algorithm is suitable for control perspectives.
  - In order to simultaneously consider all types of faults (i.e. actuator, component and sensor faults), a new Fault Detection algorithm based on Multiple Models for linear systems with bounded perturbations and measurement noises is developed. This algorithm allows to estimate the state of the system despite the presence of different faults. A Min-Max Model Predictive Control is developed in order to find the optimal control and the best model to use for the system in spite of the presence of these faults.
- **Chapter 7:** The last chapter summarizes the developed work in this PhD thesis and proposes some future directions.

2.3 Publications

The work in this thesis has resulted in several accepted/submitted publications to prestigious international conferences and journals.

Journal paper:

- **S. Ben Chabane**, C. Stoica Maniu, T. Alamo, E. F. Camacho and D. Dumur. Ellipsoidal guaranteed state estimation for uncertain linear time-variant systems. *2nd submission to Automatica*, 2015.

Conference papers:

- **S. Ben Chabane**, C. Stoica Maniu, T. Alamo, E. F. Camacho and D. Dumur. Sensor fault detection and diagnosis using zonotopic set-membership estimation. *Proceedings of the 22nd Mediterranean Conference on Control and Automation*, Palermo, Italy, pp. 261-266, June 16-19, 2014.

- **S. Ben Chabane**, C. Stoica Maniu, T. Alamo, E. F. Camacho and D. Dumur. Improved set-membership estimation approach based on zonotopes and ellipsoids. *European Control Conference*, Strasbourg, France, pp. 993-998, June 24-27, 2014.

- **S. Ben Chabane**, C. Stoica Maniu, T. Alamo, E. F. Camacho and D. Dumur. A new approach for guaranteed ellipsoidal state estimation. *Proceedings of the 19th IFAC World Congress*, Cape Town, South Africa, pp. 6533-6538, August 24-29, 2014.

- **S. Ben Chabane**, C. Stoica Maniu, T. Alamo, E. F. Camacho and D. Dumur. Ellipsoidal state estimation for systems with interval uncertainties. *Proceedings of the 53rd IEEE Conference on Decision and Control*, Los Angeles, California, USA, pp. 2603-2608, December 15-17, 2014.

- **S. Ben Chabane**, C. Stoica Maniu, E. F. Camacho, T. Alamo and D. Dumur. A Multiple Models Approach for Fault Detection based on Set-Membership State Estimation. *Submitted to European Control Conference*, Aalborg, Denmark, 2016.

Others (*oral presentation*):

- **S. Ben Chabane**, C. Stoica Maniu, D. Dumur, T. Alamo, E.F. Camacho. Set-membership state estimation for uncertain systems based on zonotopes and ellipsoids, *Journée commune du Groupe de Travail de Commande Prédictive Non Linéaire et du Groupe de Travail de Méthodes Ensemblistes pour l'Automatique*, Paris, April 3, 2014.

Chapter 3

Useful tools for uncertain linear systems

Modeling is the first step when designing a control system. In this context, it is important to obtain a mathematical representation as properly as possible reproducing the behavior of the system to be controlled.

The systems addressed in this thesis belong to the class of linear, finite dimensions, deterministic, and multivariable systems. This class of systems, which a priori seems very restricted, allows to study a large number of systems encountered in a large number of real systems. This type of systems allows to manage in an efficient way the compromise between the complexity of system modeling and the simplicity of the control design. In particular, many linearization techniques and identification procedures provide simplified linear models to achieve quite satisfactory practical results [59], [89]. But any mathematical model can not exactly represent the real system. In this context, uncertain models are used in order to ensure a behavior similar to the real system.

The importance of uncertainties is addressed in [72], [7], [8]. In literature, there exist two ways to model uncertainties: the stochastic approach [10], [102], [72] and the deterministic approach [95], [106], [16]. In the first approach, uncertainties are represented by a random process with known statistical properties (average, covariance, etc.). But in practice, the probability distribution of the uncertain parameters and perturbations is not known. Generally, only bounds of these uncertainties can be fixed. Thus, the probabilistic assumptions can not be used. In the second approach, uncertainties are supposed unknown but bounded. In general, these uncertainties can be represented by convex sets (intervals, ellipsoids, polytopes, zonotopes, etc.).

Several tools used to model uncertain linear systems in the deterministic framework will be detailed in this chapter. Section 3.1 addresses several basic

definitions and properties that will be used in this thesis. Widely used sets in the set-membership state estimation domain are presented in Section 3.2. Section 3.3 draws the conclusion of this chapter.

3.1 Basic matrix definitions and properties

In this section, basic definitions and properties are introduced. Some of these definitions concern some matrix operations which will be used in Chapter 5.

***Definition* 3.1.** A matrix $M = M^\top \in \mathbb{R}^{n\times n}$ is called a *semi positive-definite matrix* (respectively *semi negative-definite matrix*), denoted $M \succeq 0$ (resp. $M \preceq 0$), if $z^\top Mz \geq 0$ (resp. $z^\top Mz \leq 0$) for all non-zero vectors z with real entries ($z \in \mathbb{R}^n \backslash \{0_n\}$).

***Definition* 3.2.** A matrix $M = M^\top \in \mathbb{R}^{n\times n}$ is called a *strictly positive-definite matrix* (respectively *strictly negative-definite matrix*), denoted $M \succ 0$ (resp. $M \prec 0$), if $z^\top Mz > 0$ (resp. $z^\top Mz < 0$) for all non-zero vectors z with real entries ($z \in \mathbb{R}^n \backslash \{0_n\}$).

***Definition* 3.3.** The *image of a matrix* $M \in \mathbb{R}^{n\times m}$ is defined by a set of the outputs $y \in \mathbb{R}^n$ by the linear mapping $T : x \mapsto Mx$:

$$\mathrm{Im}(M) = \{y \in \mathbb{R}^n : y = Mx \text{ such that } x \in \mathbb{R}^m\}. \tag{3.1}$$

***Definition* 3.4.** An *Euclidean norm* is defined by the quantity $x^\top Px = \|x\|_P^2$, with $x \in \mathbb{R}^n$, $P \in \mathbb{R}^{n\times n}$ and $P = P^\top \succ 0$.

***Definition* 3.5.** A *Frobenius norm* of a matrix $M \in \mathbb{R}^{n\times m}$ is given by

$$\|M\|_F = \sqrt{\sum_{i=1}^{n}\sum_{j=1}^{m} |m_{ij}|} = \sqrt{Tr(MM^\top)}, \tag{3.2}$$

where m_{ij} are the elements of M.

***Definition* 3.6.** A *Linear Matrix Inequality* (LMI) has the form

$$F(x) \triangleq F_0 + \sum_{i=1}^{m} x_i F_i \succ 0 \tag{3.3}$$

where $x = \begin{bmatrix} x_1 & x_2 & \dots & x_m \end{bmatrix}^\top \in \mathbb{R}^m$ is the vector of decision variables and the matrices $F_i = F_i^\top \in \mathbb{R}^{n\times n}$, with $i = 0, \dots, m$, are given. The variables x_i, with $i = 1, \dots, m$ are called the scalar decision variables.

The LMI (3.3) is a convex constraint on x, i.e., the set $\{x \in \mathbb{R}^m : F(x) \succ 0\}$ is convex (see *Definition* 3.10 of convexity). When the matrices F_i, $i = 0, \ldots, m$, are diagonal, the LMI $F(x) \succ 0$ is reduced to a set of scalar linear inequalities.

The Linear Matrix Inequality (3.3) is given in a *strict* formulation. There is also a *non-strict* LMI which has the form

$$F(x) \succeq 0.$$

In general, the LMI problems are formulated using matrix decision variables, e.g., the Lyapunov inequality

$$A^\top P + PA \prec 0, \tag{3.4}$$

with the given matrix $A \in \mathbb{R}^{n\times n}$ and the decision variable $P = P^\top \in \mathbb{R}^{n\times n}$. In literature, the phrase "the LMI $A^\top P + PA \prec 0$ in P" is used [19], [93].

***Remark* 3.1.** In Linear Matrix Inequalities, the decision variables appear in an affine way.

Some LMI problems present constraints (called constrained LMI problems), e.g.,

$$P \succ 0, \;\; A^\top P + PA \prec 0, \;\; Tr(P) = 1, \tag{3.5}$$

where $P \in \mathbb{R}^{n\times n}$ is the decision variable.

The two following problems related to LMIs are considered in this thesis:

1. *Feasibility problem*: Does it exist a solution $x \in \mathbb{R}^n$ such that the LMI $F(x) \succ 0$ is feasible?

2. *Eigenvalue problem*: The eigenvalue problem consists in minimizing the maximum eigenvalue of a matrix that depends affinely on a variable, subject to a LMI constraint, i.e.,

$$\begin{array}{l} \min\limits_{x,\lambda} \lambda \\ \text{subject to } \; \lambda I_n - A(x) \succ 0, \;\; B(x) \succ 0, \end{array} \tag{3.6}$$

   where $A \in \mathbb{R}^{n\times n}$ and $B \in \mathbb{R}^{n\times n}$ are symmetric matrices that depend affinely on the optimization variable x. This problem has another equivalent form:

$$\begin{array}{l} \min\limits_{x,\lambda} \lambda \\ \text{subject to } \; C(x,\lambda) \succ 0, \end{array} \tag{3.7}$$

   where C is affine both in x and λ. The problem (3.7) is an LMI optimization problem.

***Remark* 3.2.** Once a LMI problem is specified, it can be solved numerically by calling the appropriate LMI solver. Two solvers (*feasp* for feasibility problems and *mincx* for general optimization problems) constitute the computational engine of the LMI part of *Matlab*/Robust Control Toolbox^{TM} software.

***Definition* 3.7.** A *Bilinear Matrix Inequality* (BMI) is defined by the following expression:

$$F(x) = F_0 + \sum_{i=1}^{n} x_i F_i + \sum_{i=1}^{n}\sum_{j=1}^{m} x_i x_j F_{ij} \succ 0, \tag{3.8}$$

where

$$x = \begin{cases} \begin{bmatrix} x_1 & x_2 & \dots & x_n \end{bmatrix}^\top \in \mathbb{R}^n \text{ if } n \geq m \\ \begin{bmatrix} x_1 & x_2 & \dots & x_m \end{bmatrix}^\top \in \mathbb{R}^m \text{ otherwise} \end{cases} \tag{3.9}$$

is the vector of decision variables and F_0, F_i, F_{ij}, with $i = 1, \dots, n$ and $j = 1, \dots, m$, are given symmetric matrices.

***Remark* 3.3.** The solver *penbmi* of *Matlab* can be used to solve a BMI (3.8).

The Bilinear Matrix Inequality (3.8) is given in a *strict* formulation. There is also a *non-strict* BMI which has the form

$$F(x) = F_0 + \sum_{i=1}^{n} x_i F_i + \sum_{i=1}^{n}\sum_{j=1}^{m} x_i x_j F_{ij} \succeq 0. \tag{3.10}$$

In general, the BMI problems are formulated using matrix decision variables, e.g., the Lyapunov inequality

$$A^\top P + PA \prec 0, \tag{3.11}$$

with the decision variables are the matrices $A \in \mathbb{R}^{n\times n}$ and $P = P^\top \in \mathbb{R}^{n\times n}$.

***Remark* 3.4.** It is easy to solve a BMI when the bilinearity concerns the product between a scalar decision variable and matrix decision variable or between two scalar decision variables.

***Definition* 3.8.** *Schur complement.* [19], [93] Consider the following LMI:

$$\begin{bmatrix} Q(x) & S(x) \\ S^\top(x) & R(x) \end{bmatrix} \succ 0, \tag{3.12}$$

where $Q(x)$, $R(x)$ are symmetric matrices and $Q(x)$, $R(x)$ and $S(x)$ are affine in x. Then this LMI is equivalent to:

$$\begin{cases} Q(x) \succ 0, \\ Q(x) - S(x)R^{-1}(x)S^{\top}(x) \succ 0, \end{cases} \tag{3.13}$$

or

$$\begin{cases} R(x) \succ 0, \\ R(x) - S^{\top}(x)Q^{-1}(x)S(x) \succ 0. \end{cases} \tag{3.14}$$

With this definition, nonlinear matrix inequalities (3.13) or (3.14) can be converted to an LMI problem (3.12). Then, it is possible to convert a BMI to an LMI and vice versa.

***Definition* 3.9.** *S-procedure.* [19] Let $F_0, \ldots, F_p$ be quadratic functions of variable $\zeta \in \mathbb{R}^n$:

$$F_i(\zeta) \triangleq \zeta^{\top} T_i \zeta + 2\mu_i^{\top} \zeta + v_i,$$

with $i = 0, \ldots, p$ and $T_i = T_i^{\top}$. Consider:

$$F_0(\zeta) \geq 0 \text{ for all } \zeta \text{ such that } F_i(\zeta) \geq 0,\ i = 1, \ldots, p. \tag{3.15}$$

If

$$\exists \tau_i \geq 0,\ i = 1, \ldots, p, \text{ such that } F_0(\zeta) - \sum_{i=0}^{p} \tau_i F_i(\zeta) \geq 0 \tag{3.16}$$

then expression (3.15) holds.
It is a non trivial fact that when $p = 1$, the converse holds meaning that there is some ζ_0 such that $F_0(\zeta_0) \geq 0$.

If the functions F_i are affine in ζ, then (3.15) and (3.16) are equivalent (see the affine form of the Farkas lemma [45]).

***Remark* 3.5.** Generally, the S-procedure is used to express some quadratic constraints as LMIs; in some cases, these LMIs can be more conservative than the initial constraints but more often useful approximations of these constraints can be formed.

3.2 Sets preliminaries

Set-membership state estimation represents a large part of this thesis. In this context, it is necessary to analyze the most used sets in the literature with their main properties. Several sets are used in the set-membership estimation domain: intervals [76], [55], polytopes [105], [63], [111], parallelotopes [26], zonotopes [27], [2], [67] and ellipsoids [61], [36], [80].

Before presenting these sets, some basic set definitions and operations are introduced.

***Definition* 3.10.** A set $\mathcal{S} \subset \mathbb{R}^n$ is called *convex set* if for any $x_1, x_2, \ldots, x_k \in \mathcal{S}$, with $k \geq 2$, and any $\alpha_1, \alpha_2, \ldots, \alpha_k \in \mathbb{R}^+$ such that $\sum_{i=1}^{k} \alpha_i = 1$, the element $\sum_{i=1}^{k} \alpha_i x_i$ is in $\mathcal{S}$.

***Definition* 3.11.** A *convex hull* of a given set $\mathcal{S}$, denoted $conv(\mathcal{S})$ is the smallest convex set containing $\mathcal{S}$.

***Definition* 3.12.** *Inclusion* operator. A set $\mathcal{X}$ is included in a set $\mathcal{Y}$, i.e. $\mathcal{X} \subseteq \mathcal{Y}$, if and only if $x \in \mathcal{Y}$, $\forall x \in \mathcal{X}$.

***Definition* 3.13.** *Intersection* operator. The intersection of two sets $\mathcal{X}$ and $\mathcal{Y}$ is defined as $\mathcal{X} \cap \mathcal{Y} = \{z : z \in \mathcal{X} \text{ and } z \in \mathcal{Y}\}$.

***Definition* 3.14.** The *image of a set $\mathcal{S}$ under a map (projection) M* is the set $M(\mathcal{S}) = \{y : y = M(x), x \in \mathcal{S}\}$.

***Definition* 3.15.** The *Minkowski sum* of two sets $\mathcal{X}$ and $\mathcal{Y}$ is defined by $\mathcal{X} \oplus \mathcal{Y} = \{x + y : x \in \mathcal{X}, y \in \mathcal{Y}\}$.

***Definition* 3.16.** The distance of two non empty sets $\mathcal{X}$ and $\mathcal{Y}$ is defined as $d(\mathcal{X}, \mathcal{Y}) = min\{d(x, y) : x \in \mathcal{X}, y \in \mathcal{Y}\}$, where $d(x, y)$ is the distance between a point $x \in \mathcal{X}$ and a point $y \in \mathcal{Y}$.

***Definition* 3.17.** The quantity $\mathcal{F}(\mathcal{X}|l) = \sup_{x \in \mathcal{X}} \langle x, l \rangle$ is the value of the *support function* for the compact convex set $\mathcal{X}$ in the l direction, where $\langle x, l \rangle$ denotes the dot product of x and l.

***Example* 3.1.** Figure 3.1 illustrates the *support function* of the compact convex set $\mathcal{X} \in \mathbb{R}^2$. Here, $\mathcal{F}(\mathcal{X}|l_1)$ represents the *support function* of $\mathcal{X}$ in the direction $l_1 = \begin{bmatrix} 1 & 0 \end{bmatrix}^\top$ and $\mathcal{F}(\mathcal{X}|l_2)$ represents the *support function* of $\mathcal{X}$ in the direction $l_2 = \begin{bmatrix} 0 & 1 \end{bmatrix}^\top$.

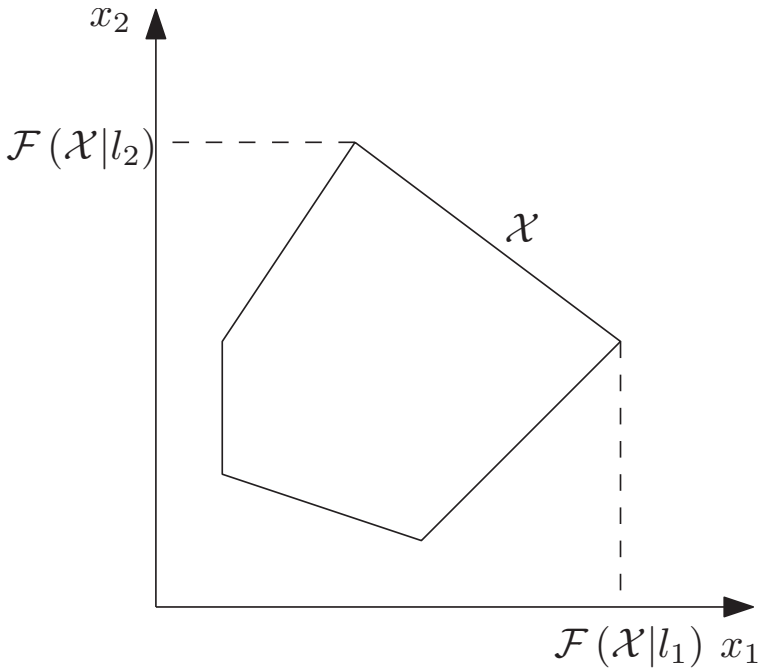

Figure 3.1: Illustration of the notion of support function of a convex set $\mathcal{X}$

3.2.1 Interval set

A simple way to define uncertainties is using *interval* sets. It consists in enclosing numerical errors into an interval, by affecting upper and lower bounds to this error. The idea of bounding errors using intervals was introduced in the 1950's. However, interval analysis is said to have begun with a book of Moore [76] in 1966. Since then, thousands of articles have appeared and numerous books have been published on this subject. The interval analysis permits to simplify most of the standard operations [49].

***Definition* 3.18.** An *interval* $[a, b]$ is defined as the set $\{x \in \mathbb{R} : a \leq x \leq b\}$.

***Definition* 3.19.** A *unitary interval* is denoted by $\mathbf{B} = [-1, 1]$.

***Definition* 3.20.** A *set of real compact intervals* $[a, b]$, where $a, b \in \mathbb{R}$ and $a \leq b$, is denoted by $\mathbb{I}$.

***Definition* 3.21.** A *box* $([a_1, b_1], \ldots, [a_n, b_n])^\top$, with $a_i \leq b_i$ for $i = 1, \ldots, n$, is an interval vector.

***Definition* 3.22.** A *unitary box* $\mathbf{B}^n$ is composed by n unitary intervals given by $\{x \in ([a_1, b_1], \ldots, [a_n, b_n])^\top : a_i = -1, b_i = 1, i = 1, \ldots, n\} \subset \mathbb{R}^n$.

Consider two given intervals $[x] = [\underline{x}, \bar{x}]$ and $[y] = [\underline{y}, \bar{y}]$. If $\circ$ denotes an operation between the two intervals $[x]$ and $[y]$, then this can be formalized as:

$$[x] \circ [y] = \{x \circ y : x \in [x], y \in [y]\} \tag{3.17}$$

The four basic operations of interval analysis applied for linear uncertain systems, are defined as follows:

1. $[x] + [y] = [\underline{x} + \underline{y}, \bar{x} + \bar{y}]$,
2. $[x] - [y] = [\underline{x} - \bar{y}, \bar{x} - \underline{y}]$,
3. $[x] * [y] = [min(\underline{x} \cdot \underline{y}, \underline{x} \cdot \bar{y}, \bar{x} \cdot \underline{y}, \bar{x} \cdot \bar{y}), max(\underline{x} \cdot \underline{y}, \underline{x} \cdot \bar{y}, \bar{x} \cdot \underline{y}, \bar{x} \cdot \bar{y})]$,
4. $[x]/[y] = [x] * [1/\bar{y}, 1/\underline{y}]$, if $0 \notin [y]$.

***Definition* 3.23.** A *strip* is defined by the following set $\mathcal{S}(y, d, \sigma) = \{x \in \mathbb{R}^n : |y - d^\top x| \leq \sigma\}$, where $y \in \mathbb{R}$, $d \in \mathbb{R}^n$ and $\sigma \in \mathbb{R}_+^*$.

Figure 3.2 represents the strip $\mathcal{S}(y, d, \sigma)$ in dimension 2, with $y = 1$, $d = \begin{bmatrix} 1 \\ -1 \end{bmatrix}$ and $\sigma = 1$.

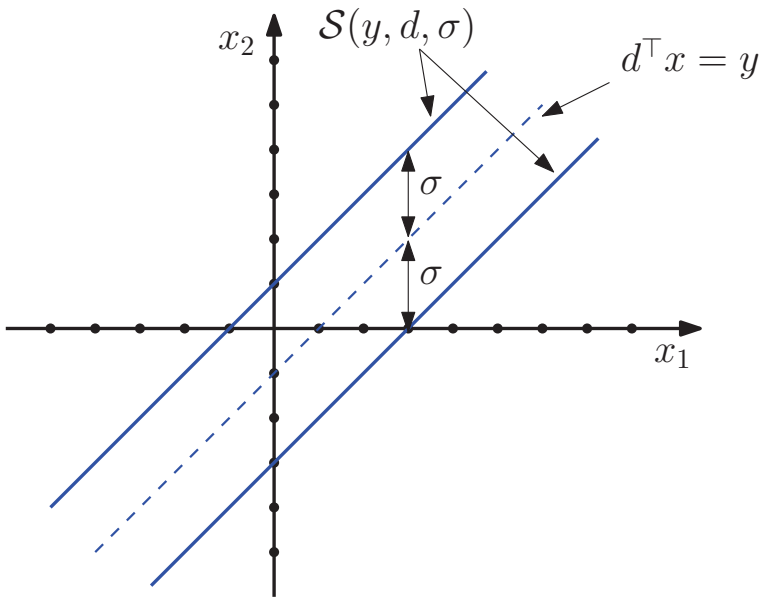

Figure 3.2: Representation of a strip in dimension 2

***Definition* 3.24.** An *interval matrix* is defined by $[M] \subset \mathbb{I}^{n\times m}$, with $a_{ij} \leq m_{ij} \leq b_{ij}$, $i = 1, ..., n$, and $j = 1, ..., m$, with $mid[M]_{ij} = \frac{a_{ij}+b_{ij}}{2}$ and $rad[M]_{ij} = \frac{a_{ij}-b_{ij}}{2}$ defining the center and the radius of the interval matrix $[M]$, respectively, $i = 1, \ldots, n$, $j = 1, \ldots, m$.

***Definition* 3.25.** A set $\mathcal{V}_{[M]}$ defines the set of all vertices of the interval matrix $[M]$.

The fact that $[M]$ is an interval matrix permits to write

$$M = mid[M] + \Delta M, \tag{3.18}$$

with ΔM the uncertain part of the matrix M. If n_δ is the number of the uncertain scalar terms δ_i of ΔM, with $\delta_i \in \mathbf{B}$, then ΔM can be decomposed as:

$$\Delta M = \sum_{i=1}^{n_\delta} M_{\delta_i}\delta_i \tag{3.19}$$

where the matrices M_{δ_i}, $i = 1, ..., n_\delta$, have only one non-zero element corresponding to the coefficient of δ_i. This decomposition is illustrated in the Example (3.2).

***Example* 3.2.** Consider the matrix $M = \begin{bmatrix} 2 & -2+0.1\delta_1 \\ 1+0.2\delta_2 & -1 \end{bmatrix}$. Then, $mid[M] = \begin{bmatrix} 2 & -2 \\ 1 & -1 \end{bmatrix}$, $\Delta M = \begin{bmatrix} 0 & 0.1\delta_1 \\ 0.2\delta_2 & 0 \end{bmatrix}$, $M_{\delta_1} = \begin{bmatrix} 0 & 0.1 \\ 0 & 0 \end{bmatrix}$, $M_{\delta_2} = \begin{bmatrix} 0 & 0 \\ 0.2 & 0 \end{bmatrix}$.

Despite its overall success, interval arithmetic suffers from two drawbacks: the *dependency problem*[1] and the so-called *wrapping effect*[2], which both can overestimate the true error of some computation [76], [60], [55].

3.2.2 Polyhedral set

Polyhedral sets provide a useful geometrical representation for the linear constraints that appear in diverse fields such as control and optimization. It can be bounded or not, and a bounded polyhedral set is called a *polytope*. A polytope has two representations: half-space representation (definition 3.26) and vertex representation (definition 3.28). This permits to choose a suitable

[1] If a variable occurs more than once in a map, it is treated independently at each occurrence. This causes widening of computed intervals and makes it difficult to obtain tighter bounds.

[2] The wrapping effect is due to the fact that the image of an interval vector under a map is not an interval vector, and it leads to overestimate this image.

representation for a given problem. Due to its flexibility, polytopes offer a good approximation of any convex set [63], [20], [96]. Another advantage of polytopes is that they are closed under the mentioned operations (inclusion, intersection, Minkovsky sum). The disadvantage of polytopes is related to its dependency on the number of vertices, which is not fixed by the space dimension. Therefore, even if a polytope can well approximate any convex set, the complexity can quickly increase with the number of vertices even in a low space dimension. Despite this disadvantage, polytopes are one of the most popular convex sets used in automatic control. This section recalls some theoretical concepts related to polyhedral sets.

***Definition* 3.26.** *Half-space representation.* A *polyhedral set* $\mathcal{P} \in \mathbb{R}^n$ in a finite-dimensional euclidean space is the intersection of a finite number of closed half-spaces as follows:

$$\mathcal{P} = \{x \in \mathbb{R}^n : Ax \leq b\}, \tag{3.20}$$

with $A \in \mathbb{R}^{m \times n}$ and $b \in \mathbb{R}^n$.

***Definition* 3.27.** A *polytope* is a bounded polyhedral set.

***Example* 3.3.** Figure 3.3 shows the half-space representation of a polytope with $A = \begin{bmatrix} -1 & 0 & 1 & -1 \\ 0 & -1 & 1 & -1 \end{bmatrix}^\top$ and $b = \begin{bmatrix} 1 & 1 & 1 & 1 \end{bmatrix}^\top$.

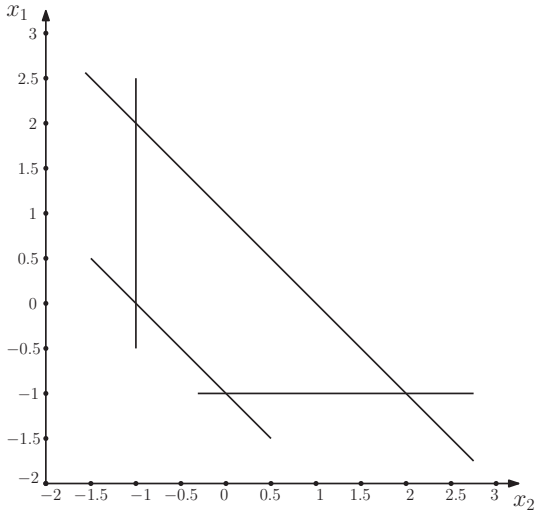

Figure 3.3: Half-space representation of a polytope

***Definition* 3.28.** (*Vertex representation* or *V-polytope*) For a finite set of points $\mathcal{V} = \{v_1, v_2, \ldots, v_m\} \in \mathbb{R}^n$, a polytope $\mathcal{P}$ can be defined as the convex hull of the set $\mathcal{V}$:

$$\mathcal{P} = conv(\mathcal{V}) = \{\alpha_1 v_1 + \alpha_2 v_2 + \ldots + \alpha_m v_m : \alpha_i \in \mathbb{R}^+, \sum_{i=1}^{m} \alpha_i = 1\} \quad (3.21)$$

***Example* 3.4.** Figure 3.4 shows the vertex representation of a polytope with $\mathcal{V} = \left\{ \begin{bmatrix} 0 \\ 2 \end{bmatrix}, \begin{bmatrix} 1.5 \\ 1.5 \end{bmatrix}, \begin{bmatrix} 2 \\ 0.5 \end{bmatrix}, \begin{bmatrix} 0 \\ -1 \end{bmatrix} \right\}$.

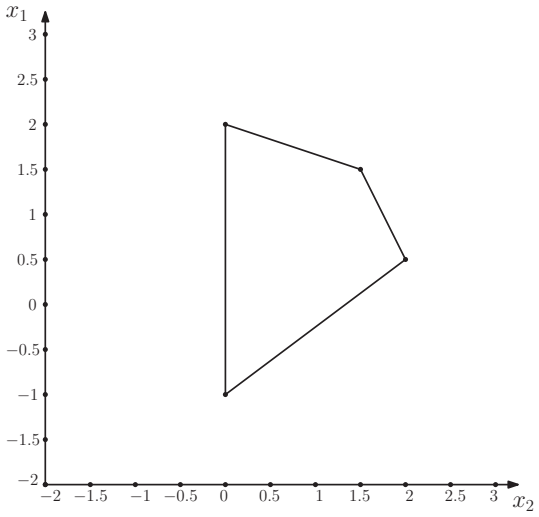

Figure 3.4: Vertex representation of a polytope

***Theorem* 3.1.** *Equivalence of the two polytopic representations.* [111] A subset $\mathcal{P} \in \mathbb{R}^n$ is the convex hull of a finite point set (a V-polytope) if and only if it is a bounded intersection of half-spaces (a H-polytope).

This theorem shows that the H-representation can be transformed to the V-representation of a polytope and vice versa. In the literature this problem is well known as the *vertex enumeration problem* for the transformation of a V-polytope to a H-polytope and the *facet enumeration problem* for the transformation of a H-polytope to a V-polytope. There exist algorithms to solve these transformation problems, but they are time consuming (e.g. [31], [40]). More details on polytopes can be found in [111], [17].

3.2.3 Zonotopic set

Zonotopes represent a particular class of polytopes which exhibit symmetry with respect to their center (a zonotope has a center). Similar to polytopes, zonotopes can be represented by the half-space representation and the vertex representation. Two additional specific definitions of zonotopes will be given here: the generator representation and the hypercube linear transformation. The last representation is used to summarize the set-membership estimation technique using zonotopes in the next chapter.

***Definition* 3.29.** *Generator representation.* Given a vector $p \in \mathbb{R}^n$ and a set of vectors $\mathcal{G} = \{g_1, g_2, ..., g_m\} \subset \mathbb{R}^n$, with $m \geq n$. A *zonotope* $\mathcal{Z}$ of order m (also called *m-zonotope*) is defined as follows:

$$\mathcal{Z} = (p; g_1, g_2, ..., g_m) = \{x \in \mathbb{R}^n : x = p + \sum_{i=1}^{m} \alpha_i g_i; |\alpha_i| \leq 1\}. \tag{3.22}$$

The vector p is called the *center* of the zonotope $\mathcal{Z}$. The vectors $g_1, \ldots, g_m$ are called *generators* of $\mathcal{Z}$. The *order* of a zonotope is defined by the number of its generators (m in this case). The case of $m < n$ is called degenerated zonotope. The line segment of a zonotope is a straight line between two vertices of this zonotope.

This definition is equivalent to the definition of zonotopes by the Minskowski sum of a finite number of line segments defined by

$$Z = (p; g_1, g_2, ..., g_m) = p \oplus g_1\mathbf{B}^1 \oplus \ldots \oplus g_m\mathbf{B}^1. \tag{3.23}$$

***Remark* 3.6.** The complexity of zonotopes grows up with respect to the number of its generators m and the dimension of the space n.

***Definition* 3.30.** *Hypercube linear projection.* A zonotope of order m in $\mathbb{R}^n$ ($m \geq n$) is the translation by the center $p \in \mathbb{R}^n$ of the image of an unitary hypercube of dimension m in $\mathbb{R}^n$ under a linear transformation. Given a matrix $H \in \mathbb{R}^{n \times m}$ representing the linear transformation, the zonotope $\mathcal{Z}$ is defined by:

$$\mathcal{Z} = (p; H) = p \oplus H\mathbf{B}^m. \tag{3.24}$$

The proposed definitions of zonotopes are equivalent if we consider the matrix $H = \begin{bmatrix} g_1 & g_2 & \ldots & g_m \end{bmatrix}$. From now on, to simplify the manuscript, the zonotope $\mathcal{Z}$ will be described by $\mathcal{Z}(p; H)$.

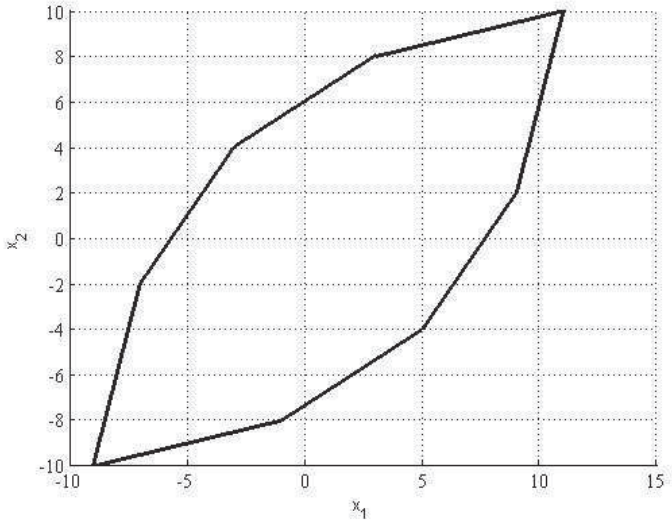

Figure 3.5: 4-zonotope in a two dimension space

***Example* 3.5.** Figure 3.5 shows a fourth order zonotope in two dimensions $\mathcal{Z} = p \oplus H\mathbf{B}^4$, with $p = \begin{bmatrix} 1 & 0 \end{bmatrix}^\top$ and $H = \begin{bmatrix} 1 & 2 & 3 & 4 \\ 4 & 3 & 2 & 1 \end{bmatrix}$.

Note that each vertex $v_{\mathcal{Z}_i} \in \mathcal{V}_{\mathcal{Z}}$, with $i = 1, \ldots, 2^4$, of this zonotope is computed as $v_{\mathcal{Z}_i} = p + Hv_i$ such that $v_i \in \mathcal{V}_{\mathbf{B}^4}$ (i.e. $v_i \in \{\begin{bmatrix} \pm 1 & \pm 1 & \pm 1 & \pm 1 \end{bmatrix}^\top\}$).

The generator representation of a zonotope can be converted to the V-representation and also to the H-representation. These conversions are related to the Minkowski sum of two polytopes because the generator representation is equivalent to the Minkowski sum of a finite number of line segments, which is a polytope. The conversion between the zonotopic representations is studied by several authors such as [44], [99], [41], [94], [6].

The generator representation illustrates a significant advantage of zonotopes: a complex geometrical form can be represented using one vector and one matrix. In addition, a centered zonotope (i.e. the $p = \mathbb{0}_{n \times 1}$) is represented only using a matrix.

***Definition* 3.31.** The *P-radius* of a zonotope $\mathcal{Z} = p \oplus H\mathbf{B}^m$ is defined by the following expression:

$$r = \max_{z \in \mathcal{Z}} (\|z - p\|_P^2) \tag{3.25}$$

where P is a symmetric and positive definite matrix ($P = P^T \succeq 0$).

This notation provides a criterion to evaluate the size of a zonotope. A small value of P-radius signifies a small size of a zonotope.

***Example* 3.6.** The P-radius definition is illustrated in Figure 3.6. In red the ellipsoid (see definition 3.33) related to the P-radius of the blue zonotope $\mathcal{Z} = p \oplus H\mathbf{B}^m$ with $p = \begin{bmatrix}1 & 0\end{bmatrix}^\top$, $H = \begin{bmatrix}1 & 2 & 3 & 4\\ 4 & 3 & 2 & 1\end{bmatrix}$ and $P = I_3$. The P-radius is $r_1 = 200$. In green, the ellipsoid related to the P-radius of the blue zonotope $\mathcal{Z} = p \oplus H\mathbf{B}^m$ with $p = \begin{bmatrix}1 & 0\end{bmatrix}^\top$, $H = \begin{bmatrix}1 & 2 & 3 & 4\\ 4 & 3 & 2 & 1\end{bmatrix}$ and $P = 0.5 \cdot I_3$. The P-radius is $r_2 = 100$.

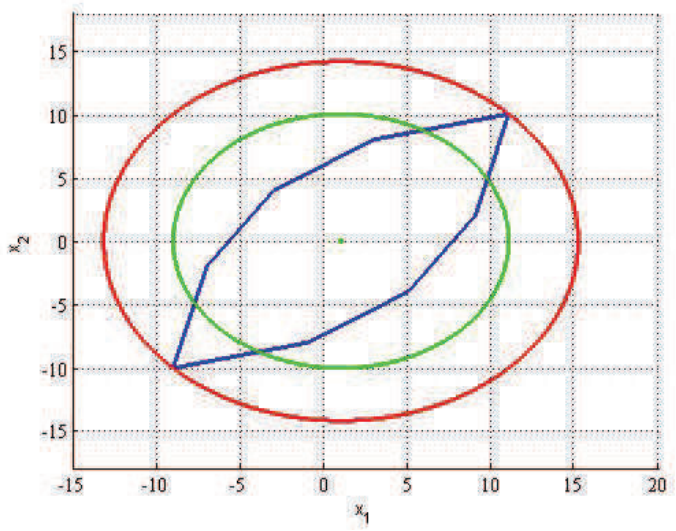

Figure 3.6: Ellipsoid related to the P-radius of a zonotope

Zonotopes present some important properties. A synthesis of these properties is given in [64]. Several properties that will be further used are summarized below.

***Property* 3.1.** *Sum of two zonotopes.* Given two zonotopes $\mathcal{Z}_1 = p_1 \oplus H_1\mathbf{B}^{m_1} \in \mathbb{R}^n$ and $\mathcal{Z}_2 = p_2 \oplus H_2\mathbf{B}^{m_2} \in \mathbb{R}^n$, the Minkowski sum of two zonotopes is also a zonotope defined by $\mathcal{Z} = \mathcal{Z}_1 \oplus \mathcal{Z}_2 = (p_1 + p_2) \oplus \begin{bmatrix}H_1 & H_2\end{bmatrix} \mathbf{B}^{m_1+m_2}$.

***Property* 3.2.** *Affine transformation of a zonotope.* Given a zonotope $\mathcal{Z} = p \oplus H\mathbf{B}^m$ and a matrix $A \in \mathbb{R}^{n\times n}$, the linear transformation of $\mathcal{Z}$ by the matrix A is $A \cdot \mathcal{Z} = (A \cdot p) \oplus (A \cdot H)\mathbf{B}^m$.

***Property* 3.3.** *Interval hull method.* Considering a zonotope $\mathcal{Z} = p \oplus H\mathbf{B}^m \in \mathbb{R}^n$, the smallest box containing this zonotope is computed by:

$$box(\mathcal{Z}) = p \oplus rs(H)\mathbf{B}^n, \tag{3.26}$$

with $rs(H)$ a diagonal matrix such that $rs(H)_{ii} = \sum_{j=1}^{m} |H_{ij}|$, $i = 1, ..., n$.

***Property* 3.4.** *Criterion-based reduction.* [2] Given a zonotope $\mathcal{Z} = p \oplus H\mathbf{B}^m$, an integer s, with $n < s < m$, and denote by $\hat{H} = \begin{bmatrix} \hat{h}_1 & \hat{h}_2 & \dots & \hat{h}_m \end{bmatrix}$ the matrix resulting from the reordering of the columns of H in decreasing order of the euclidean norm. The following expression holds:

$$\mathcal{Z} \subseteq p \oplus \begin{bmatrix} \hat{H}_T & Q \end{bmatrix} \mathbf{B}^s, \tag{3.27}$$

where $\hat{H}_T$ is composed by the first $s - n$ columns of the matrix $\hat{H}$ and $Q \in \mathbb{R}^{n \times n}$ is a diagonal matrix satisfying $Q_{ii} = \sum_{j=s-n+1}^{m} |\hat{H}_{ij}|$, with $i = 1, \dots, n$.

This property allows reducing the complexity of a zonotope. It permits to limit the number of generators of a zonotope, which is an important problem in the computation of zonotopes. There are also other reduction properties for zonotopes as *interval hull property*, *parallelotope hull property* and *cascade reduction property* (for details, see [64], [66]).

***Property* 3.5.** *Intersection between a zonotope and a strip.* [2] Given a zonotope $\mathcal{Z} = p \oplus H\mathbf{B}^m$, a strip $\mathcal{S}(d, c, \sigma) = \{x \in \mathbb{R}^n, \sigma \in \mathbb{R}_+^* : |c^\top x - d| \leq \sigma\}$ and a vector $\lambda \in \mathbb{R}^n$, the family of zonotopes $\hat{\mathcal{Z}}$ that contains the intersection of the zonotope $\mathcal{Z}$ and the strip $\mathcal{S}(d, c, \sigma)$ is obtained by

$$\mathcal{Z} \cap \mathcal{S}(d, c, \sigma) \subseteq \hat{\mathcal{Z}}(\lambda) = \hat{p}(\lambda) \oplus \hat{H}(\lambda)\mathbf{B}^{m+1}, \tag{3.28}$$

where $\hat{p}(\lambda) = p + \lambda(d^\top - c^\top p)$ and $\hat{H}(\lambda) = \begin{bmatrix} (I - \lambda c^\top)H & \sigma\lambda \end{bmatrix}$.

This property is very useful for zonotopic set-membership estimation in the case of linear systems.

***Definition* 3.32.** *Zonotope support strip.* Given a zonotope $\mathcal{Z} = p \oplus H\mathbf{B}^m$ and a vector $c \in \mathbb{R}^n$, the *zonotope support strip* is defined by

$$\mathcal{F}(\mathcal{Z}|c) = \{x \in \mathbb{R}^n : q_l \leq c^\top x \leq q_u\},$$

where the upper bound q_u and the lower bound q_l satisfy:

$$\begin{cases} q_u = \max\limits_{x \in \mathcal{Z}} c^\top x \\ q_l = \min\limits_{x \in \mathcal{Z}} c^\top x \end{cases} \tag{3.29}$$

and can be calculated as follows:

$$q_u = c^\top p + \|H^\top c\|_1 \tag{3.30}$$

$$q_l = c^\top p - \|H^\top c\|_1 \tag{3.31}$$

where $\|.\|_1$ is the 1-norm of a vector.

***Property* 3.6.** [104] *Checking consistency between a zonotope and a strip.* The intersection between the zonotope $\mathcal{Z} = p \oplus H\mathbf{B}^m$ and the strip $\mathcal{S}(y, c, \sigma)$ is empty if and only if:

$$q_u < y - \sigma \quad \text{or} \quad q_l > y + \sigma. \tag{3.32}$$

Figure 3.7 shows the upper bound q_u and the lower bound q_l of the zonotope support function for the red zonotope. Consider the blue strip $\mathcal{S}(y, c, \sigma)$. The unidimensional frame R is orthogonal to the vector $c^\top$ (which is the direction of the strip). Note that the projection of strip center on the R frame is y.

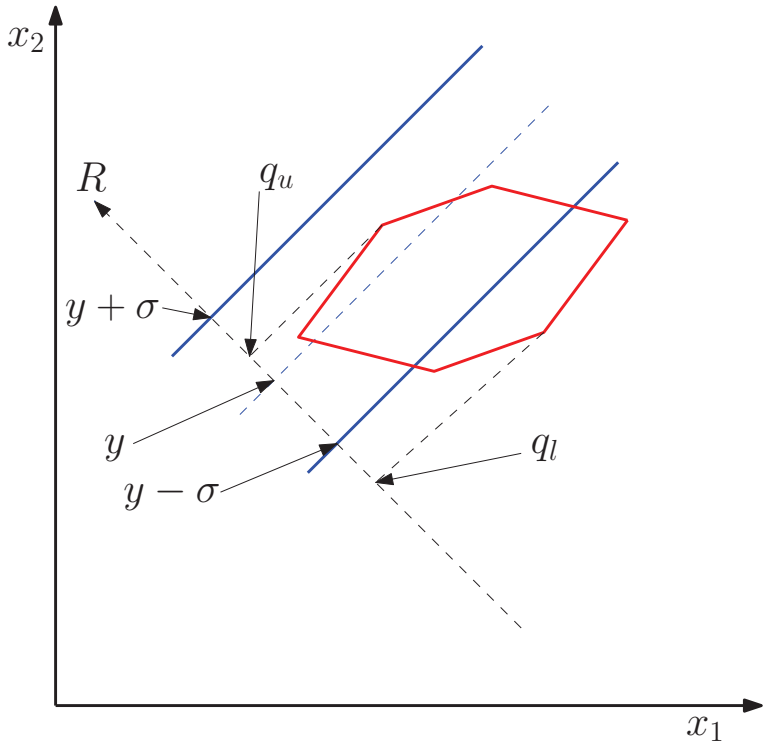

Figure 3.7: Representation of the zonotope support strip

Definition 3.32 and Property 3.6 will be used in Chapter 6 for fault detection purpose.

3.2.4 Ellipsoidal set

Ellipsoids are widely used in a large class of control system applications due to the simplicity of their formulations [95] and the resulting estimation stability properties [52]. In the domain of set-membership estimation, the ellipsoidal set occupies a large place. Effectively, it is used by several authors [36], [24], [80], [62] in many fields of control systems as identification, estimation, diagnosis, etc. Several definitions and properties of the ellipsoidal sets are further presented.

***Definition* 3.33.** *Ellipsoidal set.* Given a symmetric definite matrix $P = P^\top \succ 0$, a real vector $\bar{x} \in \mathbb{R}^n$ and a strictly positive real scalar $\rho \in \mathbb{R}_+^*$, the bounded *ellipsoid* $\mathcal{E}(P, \bar{x}, \rho)$ is defined by the set

$$\mathcal{E}(P, \bar{x}, \rho) = \{x \in \mathbb{R}^n : (x - \bar{x})^\top P(x - \bar{x}) \leq \rho\}, \tag{3.33}$$

where $P = P^\top \succ 0$ is the *shape matrix* of the ellipsoid, $\bar{x}$ its *center* and ρ its *radius*.

***Example* 3.7.** Figure 3.8 proposes an example of an ellipsoidal set in a two-dimension space with $\bar{x} = \begin{bmatrix} 0 & 0 \end{bmatrix}^\top$, $P = \begin{bmatrix} 1 & 1 \\ 1 & 4 \end{bmatrix}$ and $\rho = 1$.

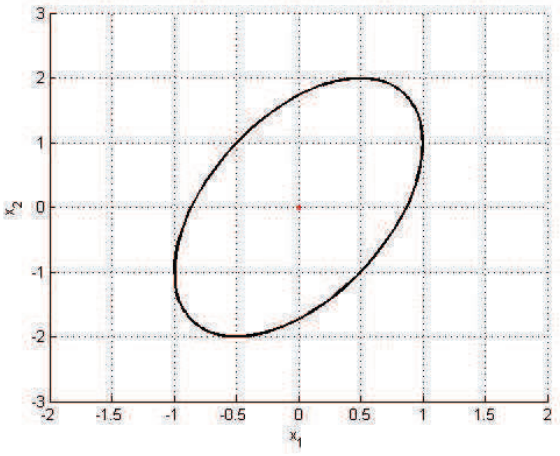

Figure 3.8: Ellipsoidal set

***Remark* 3.7.** The normalized ellipsoidal set is defined by

$$\mathcal{E}(P, \bar{x}, 1) = \mathcal{E}(P, \bar{x}) = \{x \in \mathbb{R}^n : (x - \bar{x})^\top P(x - \bar{x}) \leq 1\}, \tag{3.34}$$

where the matrix $P = P^\top \succ 0$ characterizes its shape and size and $\bar{x}$ its center.

Note that for the normalized ellipsoid, the radius $\rho = 1$ can be omitted leading to the simplified notation $\mathcal{E}(P, \bar{x})$. In this context, the normalized ellipsoid $\mathcal{E}(P^{-1}, \bar{x})$, which is used largely in literature, has the following form:

$$\mathcal{E}(P^{-1}, \bar{x}) = \{x \in \mathbb{R}^n : (x - \bar{x})^\top P^{-1}(x - \bar{x}) \leq 1\}. \tag{3.35}$$

In order to keep a simple formulation, all the properties that will be given below concern the normalized form (3.35) but they can be extended to the generalized representation of an ellipsoid.

***Definition* 3.34.** The *support function of the ellipsoid* $\mathcal{E}(P^{-1}, c)$ in a direction l is $\mathcal{F}(\mathcal{E}(P^{-1}, c)|l)$ given by

$$\begin{cases} \mathcal{F}(\mathcal{E}(P^{-1}, c)|l)_u = \langle l, c\rangle + \langle l, P^{-1}l\rangle^{\frac{1}{2}}, \\ \mathcal{F}(\mathcal{E}(P^{-1}, c)|l)_l = \langle l, c\rangle - \langle l, P^{-1}l\rangle^{\frac{1}{2}}, \end{cases} \tag{3.36}$$

where $\mathcal{F}(\mathcal{E}(P^{-1}, c)|l)_u$ and $\mathcal{F}(\mathcal{E}(P^{-1}, c)|l)_l$ are the upper and the lower bounds respectively.

***Property* 3.7.** *Affine transformation of an ellipsoid.* Given a normalized ellipsoidal set $\mathcal{E}(P^{-1}, c) \subseteq \mathbb{R}^n$, a matrix $A \in \mathbb{R}^{n\times n}$ and a vector $b \in \mathbb{R}^n$, the affine transformation of this ellipsoid by the matrix A and the vector b is defined by

$$A\mathcal{E}(P^{-1}, c) + b = \mathcal{E}((APA^\top)^{-1}, Ac + b). \tag{3.37}$$

***Property* 3.8.** *Outer ellipsoidal approximation of the union of two ellipsoids.* [36] Given two normalized ellipsoids $\mathcal{E}_1(P_1^{-1}, c_1)$, $\mathcal{E}_2(P_2^{-1}, c_2)$ and a vector $\phi \in \mathbb{R}^2$, with $\phi = \begin{bmatrix}\phi_1 & \phi_2\end{bmatrix}^\top$ and $\phi_1 + \phi_2 = 1$, then

$$\mathcal{E}_1(P_1^{-1}, c_1) \cup \mathcal{E}_2(P_2^{-1}, c_2) \subseteq \mathcal{E}(P^{-1}, c), \tag{3.38}$$

with $c = c_1 + c_2$ and $P = \phi_1^{-1}P_1 + \phi_2^{-1}P_2$.

***Property* 3.9.** *Intersection between an ellipsoid and a strip.* [39] Given a normalized ellipsoid $\mathcal{E}(P^{-1}, c)$ and a normalized strip $\mathcal{S}(y, d, 1) = \mathcal{S}(y, d)$, then the intersection between $\mathcal{E}(P^{-1}, c)$ and $\mathcal{S}(y, d, 1)$ is outer bounded by

$$\mathcal{E}(P^{-1}, c) \cap \mathcal{S}(y, d) \subseteq \mathcal{E}'(P'^{-1}, c'), \tag{3.39}$$

with

$$\begin{cases} \mathcal{E}'(P'^{-1}, c') = \{x \in \mathbb{R}^n : (x - c')^\top P'^{-1}(x - c') \leq 1\}, \\ c' = c + \dfrac{\psi\delta}{1 + \psi g} Pd, \\ P' = (1 + \psi - \dfrac{\psi\delta^2}{1 + \psi g})(P - \dfrac{\psi}{1 + \psi g} Pdd^\top P), \\ \psi \geq 0, \\ g = d^\top Pd, \\ \delta = y - d^\top c. \end{cases} \tag{3.40}$$

Two criteria are used in the literature to minimize the size of an ellipsoid $\mathcal{E}(P^{-1}, c)$: the minimization of its volume and the minimization of the sum of its semi-axes. The minimization of the volume is proportional to the minimization of the determinant of the shape and size matrix P and the minimization of the sum of the semi-axes is proportional to the trace of the matrix P [36].

3.3 Conclusion

This chapter presented a general representation of uncertainties that will be used in the context of linear uncertain systems. The interval set is a strong tool to deal with uncertainties but its application is limited due to the wrapping and dependency effects. Polytopes are largely used due to their higher accuracy, but they can not be used for systems with a fast dynamics due to their complexity. Zonotopes and ellipsoids are the most popular sets used in the domain of set-membership estimation due to their simplicity and interesting properties mentioned above. The next chapter focuses on the state of the art of set-membership state estimation using zonotopes and ellipsoids for uncertain linear systems.

Chapter 4

Zonotopic and ellipsoidal set-membership state estimation

4.1 Introduction

Knowing the full state of an industrial plant may be important for both safety and efficient control. However, sometimes only a limited amount of measurement data can be available. This could be due to the expensive costs or to the difficulty of incorporating sensors into this plant and sometimes to the presence of perturbations or measurement noises which affect the system. For these reasons, in many problems (control systems, fault detection, etc.) there is a need for state estimation. State estimators provide an economical alternative to adding new sensors or upgrading existing ones.

Most often, the state estimation problems are solved by implementing a stochastic approach based on a probabilistic description of the perturbations and measurement noises. This requires to assume that the individual perturbations are realizations of random variables characterized statistically by their average, covariance, probability density, etc. A lot of works are developed in this topic [72], [21], [68], [56], using generally the Kalman filter [57] and/or the Luenberger observer [68].

However, sometimes the probabilistic assumptions are difficult to verify. Thus, it can be more realistic to assume that the perturbations and measurement noises belong to compact bounded sets. This corresponds to the deterministic approach or the set-membership estimation [95], [38], [16], [106]. Set-membership estimation techniques provide a compact set containing the set of states that are consistent with the model and measurements. In this context, the evolution of the systems states at each time instant is not described by a point in the state-space but by a set. While their use was

severely restricted in the 80s due to the low capacity of available computers, set-membership-based approaches have been widely used over the last two decades by many researchers [39], [25], [105], [26], [61]. To implement set-membership estimation techniques, several sets are used: ellipsoids [61], [36], [22], [80], [33], [32], [24], polytopes and parallelotopes [105], [26], [11], [42], [86], [88] and zonotopes [83], [27], [2], [43], [67]. Polytopes offer a very good accuracy of the estimation while requiring a large computation time. Zonotopes, which are a special case of polytopes (symmetric polytopes) offer a good quality of the estimation with reduced computation time compared to polytopes. As a consequence, zonotopes are widely used in the context of linear systems. Ellipsoids are also largely used in set-membership estimation domain. They offer a less complex (lower computation time) but less accurate estimation compared to zonotopes [36]. Recently, a link between the zonotopic set-membership estimation and the stochastic paradigm of the Kalman filter is given in [30]. In this chapter, an improved method which combines the advantages of the zonotopic set-membership state estimation (i.e. accuracy) and of the ellipsoidal set-membership estimation (i.e. reduced complexity) is proposed. This is one of the contributions of this thesis.

This chapter is organized as follows. Section 4.2 presents the class of linear systems used in this thesis and formulates the state estimation problem. Several zonotopic and ellipsoidal set-membership state estimation techniques used in literature are presented is Section 4.3 and 4.4. Section 4.5 presents a new set-membership method based on both zonotopic and ellipsoidal estimation methods [12]. Section 4.6 concludes this chapter.

4.2 Problem statement of state estimation

The first step in the design of a control system is modeling. It is very important to obtain a simple mathematical representation as properly as possible reproducing the behavior of the system to be controlled. The class of systems addressed in this thesis is that of linear systems which are deterministic, discrete-time with finite dimension. This class of systems (that seems very restricted a priori) allows studying a large number of systems encountered in practice. It represents a trade-off between the complexity of system modeling and the simplicity of designed estimators, controllers, etc. In particular, many linearization techniques provide simplified linear models that achieve practical results quite satisfactory.

The following linear discrete-time autonomous system is further consid-

ered:

$$\begin{cases} x_{k+1} = Ax_k + \omega_k \\ y_k = Cx_k + v_k \end{cases} \tag{4.1}$$

where $x_k \in \mathbb{R}^{n_x}$ is the state of the system, $y_k \in \mathbb{R}^{n_y}$ is the measured output at sample time k, the matrices A and C have appropriate dimensions ($A \in \mathbb{R}^{n_x \times n_x}$, $C \in \mathbb{R}^{n_y \times n_x}$) and the couple ($A$,$C$) is detectable. The vector $\omega_k \in \mathbb{R}^{n_x}$ represents the state perturbation vector and $v_k \in \mathbb{R}^{n_y}$ is the measurement perturbation (noise, offset, etc.). It is assumed that the initial state belongs to a compact set $x_0 \in \mathcal{X}_0$ which can be chosen large enough due to the lack of knowledge on the system. Another assumption is that the perturbations are bounded by compact sets: $\omega_k \in \mathcal{W}, v_k \in \mathcal{V}$.

Given an initial state set $\mathcal{X}_0$ (with $x_0 \in \mathcal{X}_0$) and considering that at time k the state estimation set is $\hat{\mathcal{X}}_k$ (with $x_k \in \hat{\mathcal{X}}_k$), the objective is to find the state estimation set $\hat{\mathcal{X}}_{k+1}$ that guarantees to contain the state x_{k+1} of the system (4.1) at time $k+1$.

In the literature, this problem is solved in general by following three steps:

- *Prediction step*: the predicted state set $\bar{\mathcal{X}}_{k+1}$ is given by

$$\bar{\mathcal{X}}_{k+1} \subseteq A\hat{\mathcal{X}}_k \cup \mathcal{W}. \tag{4.2}$$

  This set offers a bound for the uncertain trajectory of the system (4.1).

- *Measurement step*: Compute the consistent state set with the measurements $\mathcal{X}_{y_{k+1}}$ given by

$$\mathcal{X}_{y_{k+1}} = \{x_{k+1} \in \mathbb{R}^{n_x} : (y_{k+1} - Cx_{k+1}) \in \mathcal{V}\}. \tag{4.3}$$

- *Correction step*: Compute the guaranteed state estimation set $\hat{\mathcal{X}}_{k+1}$ at time k given by

$$\hat{\mathcal{X}}_{k+1} = \bar{\mathcal{X}}_{k+1} \cap \mathcal{X}_{y_{k+1}}. \tag{4.4}$$

Figure 4.1 illustrates the three steps necessary to compute the guaranteed state estimation set $\hat{\mathcal{X}}_{k+1}$ for the multivariable system (4.1). At time k, the blue set $\hat{\mathcal{X}}_k$ contains the state x_k. The red set represents the predicted state estimation set $\bar{X}_{k+1}$ computed using (4.2). The green set represents the consistent state set $\mathcal{X}_{y_{k+1}}$ with the output measurement y_{k+1}. This set is intersected with the predicted state estimation set according to (4.4) to construct the red set $\hat{\mathcal{X}}_{k+1}$.

Generally, the set that contains the state is assumed to have a particular geometrical form (zonotope, ellipsoid, etc.). Thus, the exact state estimation set $\hat{\mathcal{X}}_{k+1}$ that contains x_{k+1} at time $k+1$, which is the intersection between

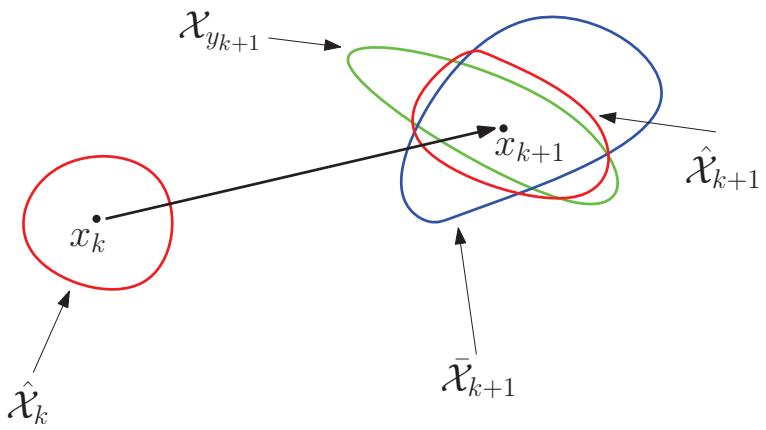

Figure 4.1: Illustration of set-membership estimation steps

$\bar{\mathcal{X}}_{k+1}$ and $\mathcal{X}_{y_{k+1}}$, has not this particular form and has to be approximated (outerbounded to guarantee the estimation) by a set having the same particular form with the previous state estimation set. The aim is to find the tightest set $\hat{\mathcal{X}}_{k+1}$ that outer-bound $\bar{\mathcal{X}}_{k+1} \cap \mathcal{X}_{y_{k+1}}$ in terms of the estimation accuracy and complexity.

In the literature, there are several authors interested in this estimation problem by using zonotopes (e.g. [26], [27]) and ellipsoids (e.g. [61], [24]). These methods are analyzed in the two next sections.

4.3 Zonotopic state estimation

Zonotopes are largely used to solve the estimation problem for systems with bounded perturbations and bounded measurement noises. The two first steps (prediction and measurement steps) are similar in all the methods. The difference is in the construction of the state estimation set in the correction step which outerbounds the intersection between the predicted state estimation set and the set consistent with the measurements. Four methods will be presented: Singular Value Decomposition-based method [27], segments minimization method [2], volume minimization method [2] and the P-radius minimization method [67]. A synthesis of these methods can be found in [64].

4.3.1 Singular Value Decomposition-based method

The zonotope bounding the perturbations ω_k is supposed to be a centered zonotope represented by $\mathcal{W} = F\mathbf{B}^{n_x}$ and the measurement noises are supposed to belong to a centered parallelotope $\mathcal{V}$ which can be described by $\mathcal{V} = \Sigma\mathbf{B}^{n_y}$, with $\Sigma \in \mathbb{R}^{n_y \times n_y}$ an invertible matrix. With these notations, at each sample time k there exists a vector $b_k \in \mathbf{B}^{n_y}$ such that the measurement noise at time instant k is computed by $v_k = \Sigma b_k$.

Assume that at time k the zonotopic guaranteed state estimation is $\hat{\mathcal{Z}}_k = \hat{p}_k \oplus \hat{H}_k\mathbf{B}^r$, with $r \in \mathbb{N}^*$ (i.e. $x_k \in \hat{\mathcal{Z}}_k$). Using the state equation of the mathematical model (4.1), the predicted zonotopic state estimation $\bar{\mathcal{Z}}_{k+1}$ that contains the state x_k at time $k+1$ is given by

$$\bar{\mathcal{Z}}_{k+1} = A \cdot \bar{\mathcal{Z}}_k \oplus F\mathbf{B}^r = A \cdot \left(\hat{p}_k \oplus \hat{H}_k\mathbf{B}^r\right) \oplus F\mathbf{B}^{n_x}. \tag{4.5}$$

Using *Property* 3.1 and *Property* 3.2, the predicted zonotopic state estimation $\bar{\mathcal{Z}}_{k+1}$ is

$$\bar{\mathcal{Z}}_{k+1} = \bar{p}_{k+1} \oplus \bar{H}_{k+1}\mathbf{B}^{r+n_x}, \tag{4.6}$$

with $\bar{p}_{k+1} = A\hat{p}_k$ and $\bar{H}_{k+1} = \begin{bmatrix} A\hat{H}_k & F \end{bmatrix}$.

There is a small difference with the set-membership steps presented in Section 4.2. Indeed, the consistent state set with the measurement $\mathcal{X}_{y_{k+1}}$ is not explicitly used. The extended space $\mathbb{R}^{r+n_x}$ of $\bar{\mathcal{X}}_{k+1}$, called *abstract space*, is decomposed into two complementary sub-spaces by using the singular value decomposition: the first is influenced by the measurement, while the second is not affected by the measurement.

Consider the prediction of the measurement at time $k+1$ given by:

$$\bar{y}_{k+1} = C\bar{p}_{k+1}, \tag{4.7}$$

where the state is chosen equal to the center of the predicted zonotopic estimation set $x_{k+1} = \bar{p}_{k+1}$.

The difference between the measurement y_{k+1} and the predicted measurement $\bar{y}_{k+1}$ has the following expression:

$$y_{k+1} - \bar{y}_{k+1} = C(x_{k+1} - \bar{p}_{k+1}) + \Sigma b_{k+1}. \tag{4.8}$$

As Σ is an invertible matrix, multiplying (4.8) with Σ^{-1} gives:

$$\Sigma^{-1}(y_{k+1} - \bar{y}_{k+1}) = \Sigma^{-1}C(x_{k+1} - \bar{p}_{k+1}) + b_{k+1}. \tag{4.9}$$

As $x_{k+1} \in \bar{\mathcal{Z}}_{k+1}$, there exists a value $s \in \mathbf{B}^{r+n_x}$ such that $x_{k+1} = \bar{p}_{k+1} + \bar{H}_{k+1}s$. Thus, the following expression is verified:

$$\eta - b_{k+1} = M\bar{H}_{k+1}s, \tag{4.10}$$

with $\eta = \Sigma^{-1}(y_{k+1} - \bar{y}_{k+1})$ and $M = \Sigma^{-1}C$. The correction step consists in outerbounding the intersection between the box $\mathbf{B}^{r+n_x}$ and the domain of the possible values of s resulting from the equation (4.10).

The procedure proposed in [27] for computing the zonotopic guaranteed state estimation is based on the Singular Value Decomposition (SVD) of the matrix resulted from the product $M\bar{H}_{k+1} \in \mathbb{R}^{n_y \times (r+n_x)}$:

$$M\bar{H}_{k+1} = USV^\top = \begin{bmatrix} U_1 & U_0 \end{bmatrix} \begin{bmatrix} S_1 & 0 \\ 0 & 0 \end{bmatrix} \begin{bmatrix} V_1^\top \\ V_0^\top \end{bmatrix}, \tag{4.11}$$

with $U^\top U = I$ and $V^\top V = I$ and S_1 a diagonal matrix with non-zero elements which are the singular values of $M\bar{H}_{k+1}$.

In (4.11) V_0 and V_1 are the new base and, thus, in the new base, the vector s can be decomposed as:

$$s = V_0\delta_0 + V_1\delta_1, \tag{4.12}$$

where, $\delta_0 = V_0^\top s$, $\delta_1 = V_1^\top s$, with δ_0, δ_1 the coordinates of s in the new base. With these new notations, the equation (4.10) is equivalent to:

$$\eta - b_{k+1} = M\bar{H}_{k+1}(V_0\delta_0 + V_1\delta_1). \tag{4.13}$$

Replacing $M\bar{H}_{k+1}$ by its Singular Value Decomposition leads to:

$$\eta - b_{k+1} = U_1 S_1 V_1^\top (V_0\delta_0 + V_1\delta_1). \tag{4.14}$$

From the expressions $U^\top U = I$ and $V^\top V = I$, it leads to $U_1^\top U_1 = I$, $V_0^\top V_0 = I$, $V_1^\top V_1 = I$, $V_1^\top V_0 = 0$, $V_0^\top V_1 = 0$. Thus, the equation (4.14) is equivalent to:

$$\delta_1 = S_1^{-1}U_1^\top \eta - S_1^{-1}U_1^\top b_{k+1}. \tag{4.15}$$

Because b_{k+1} is an interval vector, from the definition of a zonotope, a sufficient condition for the equation (4.15) or (4.10) is the following:

$$\delta_1 \in \mathcal{Z}_1 = \mathcal{Z}(S_1^{-1}U_1^\top \eta; S_1^{-1}U_1^\top). \tag{4.16}$$

From the equation (4.12), the images of s in the sub-space generated by V_1 and the sub-space generated by V_0 are shown by:

$$\delta_1 \in \mathcal{Z}(0; V_1^\top), \delta_0 \in \mathcal{Z}(0; V_0^\top). \tag{4.17}$$

Combining the results of (4.16) and (4.17), it leads to:

$$\delta_1 \in \mathcal{Z}_1 \cap \mathcal{Z}(0; V_1^\top), \quad \delta_0 \in \mathcal{Z}(0; V_0^\top). \tag{4.18}$$

Then, the next step consists in outerbounding the intersection between the zonotope $\mathcal{Z}_1$ and $\mathcal{Z}(0; V_1^\top)$. In [27], the intersection of the interval hull of two zonotopes is used (*Property* 3.3). This intersection is given by:

$$\mathcal{Z}(p_{temp}; H_{temp}) = \mathcal{Z}(S_1^{-1}U_1^\top \eta; rs(S_1^{-1}U_1^\top)) \cap \mathcal{Z}(0; rs(V_1^\top)). \tag{4.19}$$

Combining between (4.12), (4.18) and (4.19), s belongs to the following zonotopic set

$$s \in \mathcal{Z}(V_1 p_{temp}; \begin{bmatrix} V_1 H_{temp} & V_0 V_0^\top \end{bmatrix}). \tag{4.20}$$

Thus, the guaranteed state estimation set at time $k+1$ is:

$$\hat{\mathcal{Z}}_{k+1} = \mathcal{Z}(\bar{p}_{k+1} + \bar{H}_{k+1} V_1 p_{temp}; \begin{bmatrix} \bar{H}_{k+1} V_1 H_{temp} & \bar{H}_{k+1} V_0 V_0^\top \end{bmatrix}). \tag{4.21}$$

Detailed explanations about this zonotope-based estimation method can be found in [27], [29]. This method is used for fault detection purpose in [77]. An improved version of this algorithm which consists in replacing the intersection of two boxes (4.19) by a zonotopic outer approximation of the intersection between two zonotopes is presented in [28]. The Singular Value Decomposition method permits to rapidly obtain a guaranteed state estimation but it can not guarantee that the size of this guaranteed state estimation is optimized at each sampling time.

4.3.2 Segments minimization method

In this method [2], the case of Single-Output systems (i.e. $n_y = 1$ in (4.1)) is considered. Then the output is written as:

$$y_k = c^\top x_k + v_k, \tag{4.22}$$

with $v_k \in \mathcal{V}$ and $c \in \mathbb{R}^{n_x \times 1}$. The disturbances are bounded by a centered zonotope $\mathcal{W} = F\mathbf{B}^{n_x}$ and the measurement noise is bounded by a centered interval $\mathcal{V} = \sigma\mathbf{B}^1$ with $\sigma \in \mathbb{R}^+$.

Suppose that at time k the guaranteed zonotopic state estimation is $\hat{\mathcal{Z}}_k = \hat{p}_k \oplus \hat{H}_k \mathbf{B}^r$. Similar to (4.6) in the Singular Value Decomposition-based method, the predicted zonotopic state estimation $\bar{\mathcal{Z}}_{k+1}$ at time $k+1$ is given by:

$$\bar{\mathcal{Z}}_{k+1} = \bar{p}_{k+1} \oplus \bar{H}_{k+1} \mathbf{B}^{r+n_x}, \tag{4.23}$$

with $\bar{p}_{k+1} = A\hat{p}_k$ and $\bar{H}_{k+1} = \begin{bmatrix} A\hat{H}_k & F \end{bmatrix}$.

According to (4.22), the consistent state set with the measurement is a strip:

$$\mathcal{X}_{y_{k+1}} = \mathcal{S}(y_{k+1}, c, \sigma) = \{x_{k+1} \in \mathbb{R}^{n_x}, \sigma \in \mathbb{R}_+^* : |c^\top x_{k+1} - y_{k+1}| \leq \sigma\}. \tag{4.24}$$

The guaranteed zonotopic state estimation $\hat{\mathcal{Z}}_{k+1}$ containing the state x_{k+1} is the intersection between the predicted zonotopic state estimation $\bar{\mathcal{Z}}_{k+1}$ and the strip $\mathcal{X}_{y_{k+1}}$. Using the *Property* 3.5, this intersection is outerbounded by a family of zonotopes parametrized by the vector λ, i.e. $\hat{\mathcal{Z}}_{k+1}(\lambda) \supseteq \bar{\mathcal{Z}}_{k+1} \cap \mathcal{X}_{y_{k+1}}$, as follows:

$$\hat{\mathcal{Z}}_{k+1}(\lambda) = \hat{p}_{k+1}(\lambda) \oplus \hat{H}_{k+1}(\lambda)\mathbf{B}^{r+n_x+1}, \tag{4.25}$$

with $\hat{p}_{k+1}(\lambda) = A\hat{p}_k + \lambda(y_{k+1} - c^\top A\hat{p}_k)$ and
$\hat{H}_{k+1}(\lambda) = \begin{bmatrix}(I - \lambda c^\top)A\hat{H}_k & (I - \lambda c^\top)F & \sigma\lambda\end{bmatrix}$.

Then, the objective is to determine the vector λ in order to minimize the size of the zonotopic state estimation $\hat{\mathcal{Z}}_{k+1}(\lambda)$ given by (4.25).

In order to minimize the size of the zonotope $\hat{\mathcal{Z}}_{k+1}(\lambda)$, this subsection proposes to compute λ in such a way that the size of the segments that generate $\hat{\mathcal{Z}}_{k+1}(\lambda)$ is minimized [2]. Taking into account that the segments of the zonotope $\hat{\mathcal{Z}}_{k+1}(\lambda) = \hat{p}_{k+1}(\lambda) \oplus \hat{H}_{k+1}(\lambda)\mathbf{B}^{r+n_x+1}$ are represented by means of the columns of the matrix $\hat{H}_{k+1}(\lambda)$, a measure of the size of the zonotope $\hat{\mathcal{Z}}_{k+1}(\lambda)$ is the Frobenius norm of $\hat{H}_{k+1}(\lambda)$. In this case, an optimal value λ^* minimizing this Frobenius norm is obtained.

To do this, the matrix $\hat{H}_{k+1}(\lambda)$ is decomposed in the following form:

$$\hat{H}_{k+1}(\lambda) = M + \lambda a^\top, \tag{4.26}$$

with

$$M = \begin{bmatrix}A\hat{H}_k & F & \mathbb{0}_{n_x \times 1}\end{bmatrix} \text{ and } a^\top = \begin{bmatrix}-c^\top A\hat{H}_k & -c^\top F & \sigma\end{bmatrix}. \tag{4.27}$$

The Frobenius norm of $\hat{H}_{k+1}(\lambda)$ is computed by:

$$\begin{aligned}\|\hat{H}_{k+1}(\lambda)\|_F^2 &= \|M + \lambda a^\top\|_F^2, \\ &= Tr((M^\top + a\lambda^\top)(M + \lambda a^\top)), \\ &= Tr(M^\top M) + Tr(a\lambda^\top M) + Tr(M^\top \lambda a^\top) + Tr(a\lambda^\top \lambda a^\top), \\ &= 2\lambda^\top Ma + a^\top a\lambda^\top \lambda + Tr(M^\top M).\end{aligned} \tag{4.28}$$

The minimum of $\|\hat{H}_{k+1}(\lambda)\|_F^2$ is obtained when $\dfrac{d\|\hat{H}_{k+1}(\lambda)\|_F^2}{d\lambda} = 0$. This means that:

$$\frac{d(2\lambda^\top Ma + a^\top a\lambda^\top \lambda + Tr(M^\top M))}{d\lambda} = 0, \tag{4.29}$$

or:

$$2Ma + 2a^\top a\lambda^* = 0. \tag{4.30}$$

The optimal value of the vector λ is then computed by:

$$\lambda^* = \frac{-Ma}{a^\top a}. \tag{4.31}$$

Using the expressions of M and a in (4.27), λ^* is

$$\lambda^* = \frac{\hat{H}_k \hat{H}_k^\top c}{c^\top \hat{H}_k \hat{H}_k^\top c + \sigma^2}. \tag{4.32}$$

This method permits a fast computation of the vector λ which can be used in fast real-time systems. However the result of approximation is sometimes conservative as illustrated in [2].

4.3.3 Volume minimization method

This method [2] is proposed in order to improve the accuracy of the estimation obtained with the method presented in Subsection 4.3.2. Here, the case of Single-Output systems is also considered and the zonotope $\hat{\mathcal{Z}}_k$ is supposed to contain the state x_k at time k. Similar to the minimization of the segments of the zonotopes, the zonotopic state estimation $\hat{\mathcal{Z}}_{k+1}$ is given by the equation (4.25) and parametrized by the vector λ:

$$\hat{\mathcal{Z}}_{k+1}(\lambda) = \hat{p}_{k+1}(\lambda) \oplus \hat{H}_{k+1}(\lambda)\mathbf{B}^{r+n_x+1}, \tag{4.33}$$

with $\hat{p}_{k+1}(\lambda) = A\hat{p}_k + \lambda(y_{k+1} - c^\top A\hat{p}_k)$ and
$\hat{H}_{k+1}(\lambda) = \begin{bmatrix}(I - \lambda c^\top)A\hat{H}_k & (I - \lambda c^\top)F & \sigma\lambda\end{bmatrix}$.

The vector λ is determined such that the volume of the zonotope $\hat{\mathcal{Z}}_{k+1}(\lambda)$ is minimized. The volume of a zonotope $\mathcal{Z} = p \oplus H\mathbf{B}^m \in \mathbb{R}^n$, with $m \geq n$ is given by the following formula [100], [75]:

$$Vol(\mathcal{Z}) = 2^n \sum_{i=1}^{\binom{n}{m}} |det\begin{bmatrix}H_{s_1(i)} & H_{s_2(i)} & \dots & H_{s_n(i)}\end{bmatrix}|, \tag{4.34}$$

where $\binom{n}{m}$ is the number of all the different ways of choosing n elements between m elements, H_i is the ith column of H and $s_j(i)$ (with $j = 1, \dots, n$

and $i = 1, \ldots, \binom{n}{m}$) denotes each one of different ways of choosing n elements from a set of m elements. These integers satisfy $1 \leq s_1(i) < s_2(i) < \ldots < s_n(i) \leq m$.

Using this formula, the volume of the zonotope $\hat{\mathcal{Z}}_{k+1}(\lambda)$ is given by:

$$\begin{aligned} Vol(\hat{\mathcal{Z}}_{k+1}(\lambda)) = 2^{n_x} \sum_{i=1}^{\binom{n_x}{r+n_x}} det((I - \lambda c^\top) D_i) + \\ +2^{n_x} \sum_{i=1}^{\binom{n_x-1}{r+n_x}} det(\begin{bmatrix}(I - \lambda c^\top) E_i & \sigma\lambda\end{bmatrix}), \end{aligned} \tag{4.35}$$

where D_i is each of different matrices obtained by choosing n_x columns of matrix $\hat{H}_{k+1}$, E_i is each of different matrices obtained by choosing $n_x - 1$ columns of matrix $\hat{H}_{k+1}$. In [2], it is proven that the expression (4.35) can be rewritten in the form:

$$\begin{aligned} Vol(\hat{\mathcal{Z}}_{k+1}(\lambda)) = 2^{n_x} \sum_{i=1}^{\binom{n_x}{r+n_x}} |1 - c^\top \lambda| |det(D_i)| + \\ +2^{n_x} \sum_{i=1}^{\binom{n_x-1}{r+n_x}} \sigma |det\begin{bmatrix}E_i & q_i\end{bmatrix}| |q_i^\top \sigma|, \end{aligned} \tag{4.36}$$

where q_i is orthonormal to $\mathrm{Im}(E_i)$ (image of E_i) with $q_i^\top q_i = 1$ and $q_i^\top E_i = 0$. Note that expression (4.36) is a convex function of λ. Then the volume of the zonotope $\hat{\mathcal{Z}}_{k+1}$ is a convex function of λ. This means that obtaining the optimal value of the vector λ (denoted by λ^*) that minimizes the volume of the zonotopes $\hat{\mathcal{Z}}_{k+1}$ is a convex problem. Therefore, specialized algorithms can be used.

This volume based criterion gives an improved result of the approximation in comparison to the segment based criterion. But the complexity of the equation (4.36) leads to a considerable increase of the computation time. Moreover, minimizing the volume of the zonotope can lead to a very narrow zonotope [2] (i.e. the uncertainty in some directions can remain extremely large, even when the volume of the zonotope tends to zero).

4.3.4 P-radius minimization method

The zonotopic P-radius minimization method, [64] and [67], is proposed in order to overcome the complexity of the volume minimization method and the low accuracy of the segments minimization method. A comparison was made in [65] between the P-radius minimization method and the Singular Value Decomposition (SVD) method. The two methods have a similar computation time, while the accuracy of the P-radius minimization method is better than the accuracy obtained by the SVD method. The P-radius minimization method is firstly applied to systems with Single-Output ($n_y = 1$). As shown in the two last subsections, the guaranteed zonotopic state estimation set at time $k+1$, by knowing the guaranteed zonotopic state estimation set $\hat{\mathcal{Z}}_k$ at time k, is given by:

$$\hat{\mathcal{Z}}_{k+1}(\lambda) = \hat{p}_{k+1}(\lambda) \oplus \hat{H}_{k+1}(\lambda)\mathbf{B}^{r+n_x+1}, \tag{4.37}$$

with

$$\begin{cases} \hat{p}_{k+1}(\lambda) = A\hat{p}_k + \lambda\left(y_{k+1} - c^\top A\hat{p}_k\right), \\ \hat{H}_{k+1}(\lambda) = \left[\left(I - \lambda c^\top\right)A\hat{H}_k \quad \left(I - \lambda c^\top\right)F \quad \sigma\lambda\right]. \end{cases} \tag{4.38}$$

The vector $\lambda \in \mathbb{R}^{n_x}$ is determined in order to minimize the P-radius of the zonotope $\hat{\mathcal{Z}}_{k+1}(\lambda)$.

The idea is to compute a matrix $P = P^\top \succeq 0$ and a vector $\lambda \in \mathbb{R}^{n_x}$ such that, at each iteration the P-radius of the zonotopic state estimation set is not increased.

Consider the P-radius of the state estimation set at time instant k:

$$r_k = \max_{x_k \in \hat{\mathcal{Z}}_k(\lambda)} \|x_k - \hat{p}_k\|_P^2 = \max_{x_k \in \hat{\mathcal{Z}}_k(\lambda)} (x_k - \hat{p}_k)^\top P (x_k - \hat{p}_k) \tag{4.39}$$

Note that the ellipsoid related to the P-radius of the zonotopic state estimation $\hat{\mathcal{Z}}_k$ is represented by:

$$\mathcal{E}(\hat{p}_k, P, r_k) = \{x_k \in \mathbb{R}^{n_x} : \|x_k - \hat{p}_k\|_P^2 \leq r_k\}. \tag{4.40}$$

The contractiveness of the P-radius r_k is ensured by the expression $r_{k+1} \leq \beta r_k$, with $\beta \in (0, 1)$. Due to the presence of disturbances and measurement noises, this condition is difficult to verify. A relaxation of this condition can be $r_{k+1} \leq \beta r_k + \epsilon$ (see [67]), where ϵ is a positive constant which permits to bound the influence of disturbances and measurement noises. For $\epsilon = \max_{\omega \in \mathbf{B}^{n_x}} \|F\omega\|_2^2 + \sigma^2$, the non-increasing condition of the P-radius can be expressed as follows [67]:

$$r_{k+1} \leq \beta r_k + \max_{\omega \in \mathbf{B}^{n_x}} \|F\omega\|_2^2 + \sigma^2, \tag{4.41}$$

with $\beta \in (0,1)$.

Expression (4.41) is equivalent to:

$$\max_{z\in\mathbf{B}^{r+n_x+1}} \|\hat{H}_{k+1}\hat{z}\|_P^2 \leq \max_{z\in\mathbf{B}^{r}} \beta\|\hat{H}_{k}z\|_P^2 + \max_{\omega\in\mathbf{B}^{n_x}} \|F\omega\|_2^2 + \sigma^2 \tag{4.42}$$

with $\hat{z} = [z^\top \omega^\top \eta]^\top \in \mathbf{B}^{r+n_x+1}$, $z \in \mathbf{B}^r$, $\omega \in \mathbf{B}^{n_x}$, $\eta \in \mathbf{B}$ and $\beta \in (0,1)$. A sufficient condition for the inequality (4.42) is given in [67]. This consists in finding the smallest value of $\beta \in (0,1)$ (for instance via the bisection algorithm) such that the following LMI optimization is feasible:

$$\begin{array}{l} \max\limits_{\tau,P,\beta,Y} \tau \\ \text{subject to} \end{array}$$

$$\left\{ \begin{array}{l} \frac{(1-\beta)P}{\sigma^2+const} \succeq \tau I \\ \begin{bmatrix} \beta P & 0 & 0 & A^\top P - A^\top cY^\top \\ * & F^\top F & 0 & F^\top P - F^\top cY^\top \\ * & * & \sigma^2 & Y^\top \sigma \\ * & * & * & P \end{bmatrix} \succeq 0 \end{array} \right. \tag{4.43}$$

with $const = \max\limits_{\omega\in\mathbf{B}^{n_x}} \|F\omega\|_2^2$ and $*$ denote the terms required for the symmetry of a matrix. The decision variables are $\tau > 0$, $P \in \mathbb{R}^{n_x\times n_x}$, $\beta \in (0,1)$ and $Y = P\lambda \in \mathbb{R}^{n_x}$.

The LMI optimization problem (4.43) is computed off-line which leads to a small computation complexity compared to the zonotope volume minimization [67] for a similar accuracy.

***Remark* 4.1.** This method is also applied for the following linear uncertain discrete-time invariant systems with Single-Output [67]:

$$\left\{ \begin{array}{l} x_{k+1} = A_\delta x_k + \omega_k \\ y_k = c^\top x_k + v_k \end{array} \right. \tag{4.44}$$

where A_δ belongs to the Schur stable interval matrix $[A]$, the perturbations ω_k belongs to the centered zonotope $\mathcal{W} = F\mathbf{B}^{n_x}$ and the measurement noise $v_k \in \mathcal{V} = \sigma\mathbf{B}$.

Consider that at time k, the guaranteed zonotope that contains x_k is $\hat{\mathcal{Z}}_k = \hat{p}_k \oplus \hat{H}_k\mathbf{B}^r$. Then, it is proved in [64] that the guaranteed zonotopic state estimation set that contains the state x_{k+1} at time $k+1$ is given by:

$$\hat{\mathcal{Z}}_{k+1}(\lambda) = \hat{p}_{k+1}(\lambda) \oplus \hat{H}_{k+1}(\lambda)\mathbf{B}^{r+n_x+1}, \tag{4.45}$$

with

$$\left\{ \begin{array}{l} \hat{p}_{k+1}(\lambda) = mid[A]\hat{p}_k + \lambda\left(y_{k+1} - c^\top mid[A]\hat{p}_k\right), \\ \hat{H}_{k+1}(\lambda) = \begin{bmatrix} \left(I - \lambda c^\top\right)\bar{H}_{k+1} & \sigma\lambda \end{bmatrix}, \end{array} \right. \tag{4.46}$$

where $\bar{H}_{k+1} = \begin{bmatrix} mid[A]\hat{H}_k & rs(rad[A]|\hat{H}_k|) & rs(rad[A]|\hat{p}_k|) & F \end{bmatrix}$.

The objective is also to compute the optimal λ that minimizes the P-radius of the zonotopes $\hat{\mathcal{Z}}_{k+1}(\lambda)$. The solution is given by solving the following LMI optimization problem:

$$\max_{\tau,\beta,P,Y} \tau$$

subject to

$$\begin{cases} \frac{(1-\beta)P}{\epsilon} \succeq \tau I \\ \begin{bmatrix} \beta P & 0 & 0 & \tilde{A}_i^T P - \tilde{A}_i^T c Y^T \\ * & F^T F & 0 & F^T P - F^T c Y^T \\ * & * & \sigma^2 & Y^T \sigma \\ * & * & * & P \end{bmatrix} \succeq 0 \\ \tau > 0 \end{cases} \tag{4.47}$$

for $i = 1, ..., 2^q$, where $\tilde{A}_i$ are the vertices of the interval matrix $[A]$, q is the number of interval elements of $[A]$ and $Y = P\lambda$.

***Remark* 4.2.** Another extension of the P-radius minimization method is proposed [64] for the case of linear Multi-Output systems ($n_y > 1$ and $\omega_k \in \mathcal{V} = \Sigma\mathbf{B}^{n_y}$).

Firstly, Natural Single Output extensions are applied by considering each measurement as a strip in the state-space, then the guaranteed state estimation is obtained by repeating the intersection with each measurement strip. In these methods, n_y correction factors λ_i, with $i = 1, \ldots, n_y$, are computed. Three Natural Single extensions approaches are considered in the literature [64]. The first approach, called Equivalent Single-Output (ESO), considers the Multi-Output system as several separated Single-Output systems. This solution leads to a conservative result due to neglecting the coupling effect of the initial Multi-Output system. The second approach is the Extended Single-Output with Coupling Effect (ESOCE). Here, the performance of the estimation is improved by computing successively, in the same way to the first approach (ESO), the correction factors λ_i by considering available the previous correction factors $\lambda_1, \ldots, \lambda_{i-1}$. The Polynomial Matrix Inequality (PMI) technique is the third approach of the Natural Single Output extensions. Here, the factors λ_i, with $i = 1, \ldots, n_y$, are computed in the same time contrary to the ESO and ESOCE approaches. The PMI optimization problem is solved using a LMI relaxation approach proposed by [50], [51] to find a sub-optimal solution to this PMI problem. This leads to a good accuracy of the estimation compared to the ESO and ESOCE approaches.

Secondly, a Direct Multi-Output solution permitting to consider the information of all measurements at the same time is proposed to overcome the

complex problems of the Natural Single Output extensions. Here, the consistent state set with measurements, which is a polytope, is intersected with a predicted zonotopic state estimation directly (Figure 4.2). This solution is called Polytope and Zonotope Intersection (PAZI) [64]. This intersection is outerbounded by a family of zonotopes parametrized by a matrix Λ as follows [64]:

$$\hat{\mathcal{Z}}_{k+1}(\Lambda) = \hat{p}_{k+1}(\Lambda) \oplus \hat{H}_{k+1}(\Lambda)\mathbf{B}^{r+n_x+n_y} \tag{4.48}$$

with $\hat{p}_{k+1}(\Lambda) = A\hat{p}_k + \Lambda(y_{k+1} - CA\hat{p}_k)$ and
$\hat{H}_{k+1}(\Lambda) = \begin{bmatrix}(I - \Lambda C^\top)A\hat{H}_k & (I - \Lambda C^\top)F & \Lambda\Sigma\end{bmatrix}$.

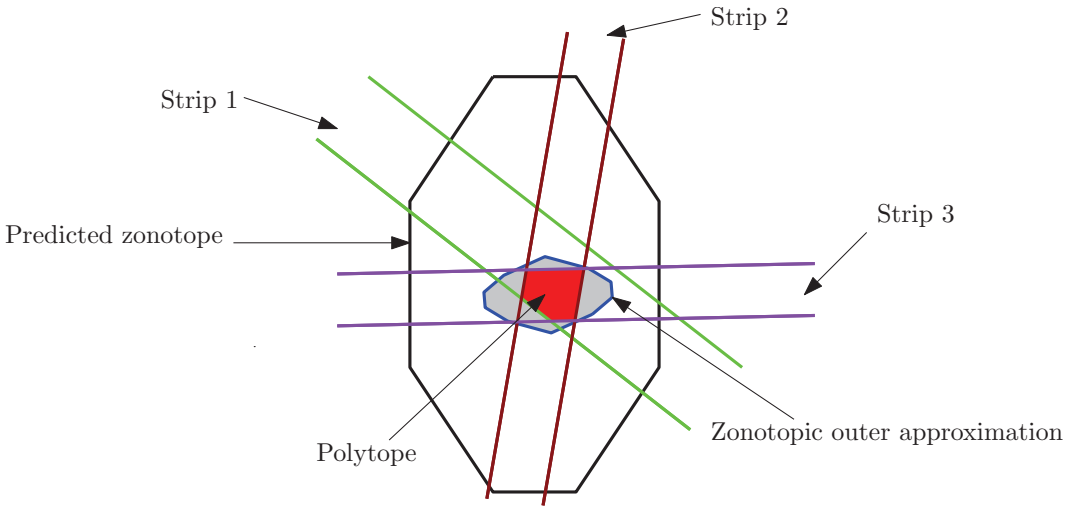

Figure 4.2: Outer approximation of the intersection between a zonotope and a polytope

The computation of the optimal matrix Λ, such that the P-radius of a guaranteed zonotopic estimation set $\hat{\mathcal{Z}}_{k+1}$ is non-increased, leads to solve the following optimization problem:

$$\max_{\tau,\beta,P,Y} \tau$$

subject to

$$\begin{cases} \dfrac{(1-\beta)P}{\sigma_1^2 + \ldots + \sigma_{n_y}^2 + \max\limits_{s\in\mathbf{B}^{n_x}} \|Fs\|_2^2} \succeq \tau I \\ \begin{bmatrix} \beta P & 0 & 0 & A^\top P - A^\top C^\top Y^\top \\ * & F^\top F & 0 & F^\top P - F^\top C^\top Y^\top \\ * & * & \Sigma^\top\Sigma & \Sigma^\top Y^\top \\ * & * & * & P \end{bmatrix} \succeq 0 \\ \tau > 0 \end{cases} \tag{4.49}$$

with a change of variables $Y = P\Lambda$ and $*$ denoting the terms required for the symmetry of a matrix. The Direct Multi-Output solution using a Polytope and Zonotope Intersection (PAZI) improves the estimation performance compared to the Single Output extensions applied for Multi-Output systems.

The P-radius minimization leads to a good trade-off between the rapidity of the segments minimization and the accuracy of the volume minimization of a zonotope making suitable this method for set-membership state estimation.

It is also important to note that each zonotopic state estimation set implies an ellipsoid related to the P-radius of this zonotope. Set-membership state estimation approaches using ellipsoids will be presented in the next section.

4.4 Ellipsoidal state estimation

Ellipsoids have been used by different authors [36], [80], [81] due to the simplicity of formulation. This method is applied for systems with Single-Output, but can be easily extended to the case of Multi-Output systems by considering each measurement given as a strip in the state-space, and the guaranteed state estimation is obtained by repeating the intersection with each strip measurement[1]. Then, the system is as follows:

$$\begin{cases} x_{k+1} = Ax_k + F\omega_k, \\ y_k = c^\top x_k + \sigma v_k, \end{cases} \tag{4.50}$$

where $x_k \in \mathbb{R}^{n_x}$ is the state vector, $y_k \in \mathbb{R}$ is the measurement output, $\omega_k \in \mathbb{R}^{n_x}$ and $v_k \in \mathbb{R}$ represent the state disturbances and the measurement noises, respectively. Here, A, c, F and σ have the appropriate dimensions, with the additional hypothesis that the pair $(c^\top, A)$ is detectable. It is assumed that the initial state x_0 belongs to the bounded ellipsoidal set $\mathcal{E}(P_0^{-1}, c_0)$, the perturbations are bounded by the ellipsoidal sets $\omega_k \in \mathcal{E}(I_{n_x}, \mathbb{0}_{n_x \times 1})$ and the measurement noise is bounded by the unitary interval $v_k \in \mathbf{B}$. Suppose that at time k the ellipsoidal set $\hat{\mathcal{E}}_k(\hat{P}_k^{-1}, \hat{c}_k)$ contains the state x_k. The objective is to compute the ellipsoidal set $\hat{\mathcal{E}}_{k+1}(\hat{P}_{k+1}^{-1}, \hat{c}_{k+1})$ that guarantees to contain the state x_{k+1} at time $k+1$.

The predicted ellipsoidal set $\bar{\mathcal{E}}_{k+1}(\bar{P}_{k+1}^{-1}, \bar{c}_{k+1})$ at time $k+1$ is given by:

$$\bar{\mathcal{E}}_{k+1}(\bar{P}_{k+1}^{-1}, \bar{c}_{k+1}) = A\hat{\mathcal{E}}_k(\hat{P}_k^{-1}, \hat{c}_k) \cup F\mathcal{E}(I_{n_x}, \mathbb{0}_{n_x \times 1}). \tag{4.51}$$

[1]It is better to perform the intersection between the predicted ellipsoidal estimation set directly with the consistent state set with measurements, which is a polytope instead of computing succesive intersections with the measurement strips. This is similar to the PAZI approach (Direct Multi-Output solution) compared to the Natural Single Output extensions as detailed in [64].

Using *Property* 3.7, with $b = \mathbb{0}_{n_x \times 1}$, (4.51) can be rewritten as:

$$\bar{\mathcal{E}}_{k+1}(\bar{P}_{k+1}, \bar{c}_{k+1}) = \hat{\mathcal{E}}_k((A\hat{P}_k A^\top)^{-1}, A\hat{c}_k) \cup \mathcal{E}(FF^\top, \mathbb{0}_{n_x \times 1}). \tag{4.52}$$

Applying *Property* 3.8 means that there exists $\phi = [\phi_1, \phi_2]^\top \in \mathbb{R}^2$ such that:

$$\begin{cases} \bar{c}_{k+1} = A\hat{c}_k \\ \bar{P}_{k+1} = \phi_1^{-1} P_{1_k} + \phi_2^{-1} P_{2_k} \end{cases} \tag{4.53}$$

with $P_{1_k} = A\hat{P}_k A^\top$, $P_{2_k} = FF^\top$ and $\phi_1 + \phi_2 = 1$. The objective is to find ϕ which minimizes the size of the ellipsoid $\bar{\mathcal{E}}_{k+1}(\bar{P}_{k+1}^{-1}, \bar{c}_{k+1})$. This problem can be solved using the trace or the determinant criteria. This will be developed in the next two subsections.

The consistent state set measurement is represented by the following strip (see (4.24) for more details):

$$\mathcal{X}_{y_{k+1}} = \mathcal{S}\left(y_{k+1}, c, \sigma\right) = \{x_{k+1} \in \mathbb{R}^{n_x}, \sigma \in \mathbb{R}_+^* : |c^\top x_{k+1} - y_{k+1}| \leq \sigma\}. \tag{4.54}$$

The correction step consists in computing the intersection between the ellipsoid resulting after the prediction step and the strip representing the measured output. For this, the Outer Bounding Ellipsoid (OBE) algorithm [39] is used. In this step, the set $\hat{\mathcal{E}}_{k+1}(\hat{P}_{k+1}^{-1}, \hat{c}_{k+1})$ is found. This set is computed as follows:

$$\bar{\mathcal{E}}_{k+1}(\bar{P}_{k+1}^{-1}, \bar{c}_{k+1}) \cap \mathcal{X}_{y_{k+1}} \subseteq \hat{\mathcal{E}}_{k+1}(\hat{P}_{k+1}^{-1}, \hat{c}_{k+1}) \tag{4.55}$$

with the measurement consistent state set
$\mathcal{X}_{y_{k+1}} = \{x_{k+1} \in \mathbb{R}^{n_x} : |y'_{k+1} - c'^\top x_{k+1}| \leq 1\}$, with $y'_{k+1} = y_{k+1}\sigma$ and $c' = c\sigma$.

This allows us to apply *Property* 3.9 in (4.55), leading to:

$$\begin{cases} \hat{c}_{k+1} = \bar{c}_{k+1} + \dfrac{\psi\delta}{1+\psi g}\bar{P}_{k+1}c' \\ \hat{P}_{k+1} = \left(1 + \psi - \dfrac{\psi\delta^2}{1+\psi g}\right)\left(\bar{P}_{k+1} - \dfrac{\psi}{1+\psi g}\bar{P}_{k+1}c'c'^\top\bar{P}_{k+1}\right) \end{cases} \tag{4.56}$$

with $g = c'^\top \bar{P}_{k+1} c'$, $\delta = y'_{k+1} - c'^\top \bar{c}_{k+1}$ and $\psi \geq 0$.

The resulting solution may be suboptimal if an hyperplane does not intersect the predicted ellipsoid $\bar{\mathcal{E}}_{k+1}(P_{k+1}^{-1}, c_{k+1})$. In this case, a contraction of the strip by translating the hyperplane parallel to itself is done until it becomes tangent to the predicted ellipsoid (see Fig.4.3) [39].

The new ellipsoid contains the free parameter $\psi \geq 0$ which actually defines its position, size and orientation. Several criteria were developed to calculate this parameter. In the next two subsections, the trace criterion [39] and the determinant criterion [39] will be presented.

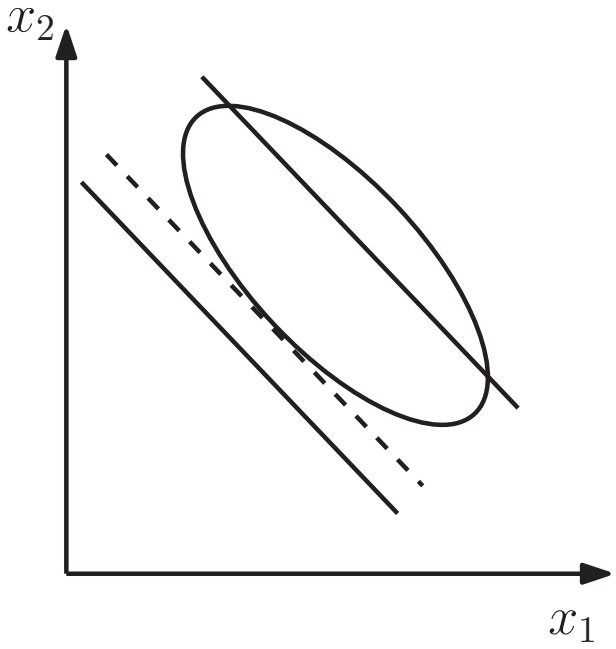

Figure 4.3: Relative position between the strip and the predicted ellipsoid

4.4.1 Trace criterion

The size of an ellipsoid can be measured by its sum of square of the length of its semi-axes. It corresponds to the trace of its shape and size matrix. Minimizing the trace of the size and shape matrix of an ellipsoid is largely used in the literature [36], [39].

For the prediction step, the objective is to find ϕ that minimizes the size of the ellipsoid $\bar{\mathcal{E}}_{k+1}(\bar{P}_{k+1}^{-1}, \bar{c}_{k+1})$. The criterion is the following:

$$\phi^* = \arg\min_{\phi} Tr(\bar{P}_{k+1}), \tag{4.57}$$

with $\bar{P}_{k+1}$ is given by (4.53).

The advantage of this method is that an explicit solution for ϕ^* can be given (see [36] for the proof of concept):

$$\phi_i^* = \left(\sqrt{Tr(P_{1_k})} + \sqrt{Tr(P_{2_k})}\right)^{-1} \sqrt{Tr(P_{i_k})}, \tag{4.58}$$

leading to the following optimal value of $\bar{P}_{k+1}$:

$$\bar{P}_{k+1} = \left(\sqrt{Tr(P_{1_k})} + \sqrt{Tr(P_{2_k})}\right) \left(\frac{P_{1_k}}{\sqrt{Tr(P_{1_k})}} + \frac{P_{2_k}}{\sqrt{Tr(P_{2_k})}}\right). \tag{4.59}$$

For the correction step, the objective is to find $\psi > 0$ that minimizes the size of the ellipsoid $\hat{\mathcal{E}}_{k+1}(\hat{P}_{k+1}^{-1}, \hat{c}_{k+1})$ given by (4.56). The minimal trace ellipsoid is obtained by solving the following optimization problem:

$$\psi^* = \arg\min_{\psi \geq 0} Tr(\hat{P}_{k+1}). \tag{4.60}$$

Applying the fact that $Tr(M + uv^\top) = Tr(M) + v^\top u$ with $M = \bar{P}_{k+1}$, $u = \bar{P}_{k+1}c'$ and $v = -\dfrac{\psi}{1+\psi g}\bar{P}_{k+1}c'$ to the trace of $\hat{P}_{k+1}$ in (4.56) leads to:

$$Tr(\hat{P}_{k+1}) = \left(1 + \psi - \frac{\psi\delta^2}{1+\psi g}\right)\left(\mu - \frac{\psi\gamma}{1+\psi g}\right) \tag{4.61}$$

with $\mu = Tr(\bar{P}_{k+1})$ and $\gamma = c'^\top \bar{P}_{k+1}^2 c'$.

The optimal value of ψ is the solution of:

$$\frac{d\hat{P}_{k+1}(\psi)}{d\psi} = 0. \tag{4.62}$$

As ψ has to verify a condition of positivity ($\psi \geq 0$) while satisfying (4.62), it means that ψ is the unique positive real root (*Descartes's Rule of Signs* [5]) of the following third degree polynomial:

$$\frac{d\hat{P}_{k+1}(\psi)}{d\psi} = 0 \Longleftrightarrow \psi^3 + \beta_1\psi^2 + \beta_2\psi + \beta_3 = 0 \tag{4.63}$$

with

$$\begin{cases} \beta_1 = \dfrac{3}{g} > 0 \\ \beta_2 = \dfrac{g\left[\mu\left(1-\delta^2\right) - \gamma\right] + 2\left[g\mu - \gamma\left(1-\delta^2\right)\right]}{g^2\left(g\mu - \gamma\right)} \\ \beta_3 = \dfrac{\mu\left(1-\delta^2\right) - \gamma}{g^2\left(g\mu - \gamma\right)} \end{cases} \tag{4.64}$$

where β_3 and β_2 have the same sign.

4.4.2 Determinant criterion

Minimizing the volume of an ellipsoid in also used in literature. It is proportional to the square of the product of the length of its axes, which corresponds to the determinant of the shape and size matrix. The logarithm[2] of this matrix is generally minimized.

[2]For example if the matrix P is diagonal, $det(P)$ is the product of its diagonal elements. Then $\log det(P)$ will be the sum of these diagonal elements. This permits to linearize the criterion.

For the prediction step, it leads to minimize the following criterion:

$$\phi^* = \arg\min_{\phi} \log det(\bar{P}_{k+1}), \tag{4.65}$$

with $\bar{P}_{k+1}$ given by (4.53).

There is no explicit solution for this minimization (4.53) problem. The recursive algorithm gives:

$$\bar{P}_{k+1} = \alpha_{k+1}^{-1} P_{1_k} + (1-\alpha_{k+1})^{-1} P_{2_k}, \text{ such that } \alpha_{k+1} \in (0,1). \tag{4.66}$$

The optimal value α_{k+1}^* is obtained by solving a convex optimization problem of one dimension:

$$\alpha_{k+1}^* = \arg \min_{0<\alpha_{k+1}<1} \log det(\alpha_{k+1}^{-1} P_{1_k} + (1-\alpha_{k+1})^{-1} P_{2_k}) \tag{4.67}$$

Then, standard iterative methods for solving convex constrained optimization problems can be applied. Finally, ϕ^* can be rewritten as $\phi^* = \begin{bmatrix} \alpha_{k+1}^* & 1-\alpha_{k+1}^* \end{bmatrix}^\top$.

For the correction step, the objective is to minimize the size of the ellipsoid $\hat{\mathcal{E}}_{k+1}(\hat{P}_{k+1}^{-1}, \hat{c}_{k+1})$ by solving:

$$\psi^* = \arg\min_{\psi \geq 0} \log det(\hat{P}_{k+1}), \tag{4.68}$$

with $\hat{P}_{k+1}$ given by (4.56).

Applying the fact that $\det(\theta K) = \theta^{n_x} det(K)$, with $\theta = 1+\psi-\dfrac{\psi\delta^2}{1+\psi g} \in \mathbb{R}$ and $K \in \mathbb{R}^{n_x \times n_x}$ and the fact that $det(I + uv^\top) = 1 + v^\top u$, with $u = \bar{P}_{k+1} c'$ and $v = -\dfrac{\psi}{1+\psi g} c'$, then the determinant of $\hat{P}_{k+1}$ in (4.56) can be computed as follows:

$$\det(\hat{P}_{k+1}) = \left(1 + \psi - \frac{\psi\delta^2}{1+\psi g}\right)^{n_x} \frac{det(\bar{P}_{k+1})}{1+\psi g} \tag{4.69}$$

The minimal volume ellipsoid is obtained by solving the following optimization problem:

$$\psi^* = \arg\min_{\psi \geq 0} h(\psi) \tag{4.70}$$

with $h(\psi) = \dfrac{\left(1 + \psi - \dfrac{\psi\delta^2}{1+\psi g}\right)^{n_x}}{1+\psi g}$.

A sufficient condition for ψ is that:

$$\frac{dh(\psi)}{d\psi} = 0, \text{ with } \psi \geq 0, \tag{4.71}$$

which leads to the following solution (see [39] for more details):

$$\psi^* = \begin{cases} \dfrac{-\left(2n_x - g - 1 + \delta^2\right) + \sqrt{\Delta}}{2\left(n_x - 1\right) g}, & \text{if } \Delta \geq 0 \\ 0, \quad \text{otherwise} \end{cases} \tag{4.72}$$

with $\Delta = \left(g - 1 - \delta^2\right)^2 + 4\delta^2\left(\delta^2 - 1\right)$ and n_x equal to the dimension of x_k. It can be noticed that $\psi^* = 0$ means that the ellipsoid $\bar{\mathcal{E}}_{k+1}(\bar{P}_{k+1}^{-1}, \bar{c}_{k+1})$ does not change compared to $\hat{\mathcal{E}}_{k+1}(\hat{P}_{k+1}^{-1}, \hat{c}_{k+1})$ (i.e. $\hat{\mathcal{E}}_{k+1} = \bar{\mathcal{E}}_{k+1}$).

Ellipsoids are also largely used in set-membership estimation domain. It offers an estimation with lower accuracy but with a gain in complexity comparing to zonotopes (lower computation time) [36].

4.5 Combined estimation based on zonotopes and ellipsoids

This section proposes an improved method which takes advantage of the good estimation accuracy obtained via the zonotopic minimization and the low complexity proven by the ellipsoidal minimization [12], which is the first contribution in this thesis. The P-radius zonotopic estimation method is chosen for the reason that an ellipsoid is associated to the zonotopic estimation set related to the P-radius. For the ellipsoidal estimation method, the trace criterion is chosen due the simplicity of the method (explicit solution for the prediction step) with good estimation accuracy. In fact, when the P-radius is decreasing slowly during the last iterations of the zonotopic estimation, (i.e. the solution is close enough to an optimum), we propose to outer approximate the zonotopic estimation set by an ellipsoid and to continue the procedure via the ellipsoidal set-membership estimation. This leads to gain in rapidity of the estimation, while keeping an acceptable level of accuracy.

Computing the zonotopic state estimation set via the minimization of the P-radius (i.e. solving the optimization problem (4.43)) allows computing the P-radius of the zonotope and its associated ellipsoid. At infinity, the non-increasing condition of the P-radius (4.41) leads to:

$$r_\infty = \frac{\sigma^2 + const}{1 - \beta}, \tag{4.73}$$

with $const = \max\limits_{\omega \in \mathbf{B}^{n_x}} \|F\omega\|_2^2$. This can be visualized in Figure 4.4, where the blue zonotope is the guaranteed state estimation at each iteration and the red ellipsoid is related to the P-radius of the zonotopic state estimation set.

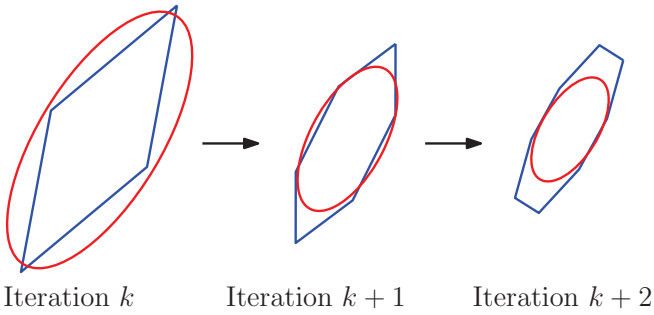

Figure 4.4: Evolution of the guaranteed state estimation

The ellipsoid related to the P-radius is usually an approximation of the zonotope, with the same center and direction as the zonotope (e.g. the blue ellipsoid in Fig. (4.5)). In order to obtain an outer ellipsoid that will outer approximate the zonotope, the ellipsoid related to the P-radius will be scaled by a positive scalar α (as illustrated by the red ellipsoid in Fig. (4.5)). *Algorithm* 1 formulates the proposed method.

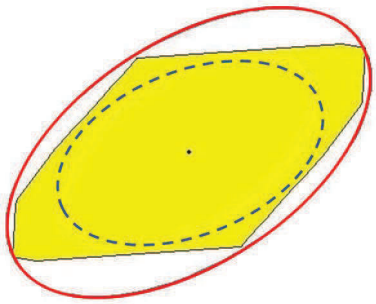

Figure 4.5: Scaled ellipsoidal outer-bounding approximation of a zonotope based on the P-radius technique

Algorithm 1:

Inputs:

N: length of the simulation horizon;
ϵ: desired level of accuracy of the P-radius;
x_0: initial state vector;
$\hat{\mathcal{Z}}_0$: initial state set;
l: length of the horizon of slow variation of the P-radius;

Outputs:
$test = 1$;
for $k = 1 : N$
  if $(|r_k - r_{k-l}| \geq \epsilon$ and $test = 1)$ or $(k \leq l)$ then
    Compute the zonotope estimation $\hat{\mathcal{Z}}_k$ and its P-radius according to (4.37), (4.38) and (4.43);
    $test = 1$;
  else if $|r_k - r_{k-l}| \leq \epsilon$ and $test = 1$ then
    Compute the scaled ellipsoid $\hat{\mathcal{E}}_k$ by finding the optimal α according to *Proposition* 4.1;
    $test = 0$;
  else
    Compute the ellipsoid estimation $\hat{\mathcal{E}}_k$ via the trace minimization estimation according to (4.53), (4.56), (4.59) and (4.60);
    $test = 0$;
  end
  Collect the measurement y_k;
end

Figure 4.6 shows a diagram that summarizes the proposed approach.

It means that if the P-radius does not change with respect to a relative accuracy during the last l iterations, a transition to the ellipsoidal estimation is made and the algorithm continues with the ellipsoidal estimation until the end of the simulation. In addition, the scalar ϵ is fixing the speed of transition to the ellipsoidal estimation method (i.e. it is inversely proportional to the speed of this transition). At the moment of transition, an ellipsoidal outer approximation is chosen as an outer bound of the zonotopic estimation with the same center and direction (given by the P matrix) as the ellipsoid related to the P-radius of the zonotopic estimation. This can be conservative but guarantees the estimation. Therefore, the parameter $\alpha \in (0, 1)$ has to be found in order to minimize the size of the ellipsoid $\hat{\mathcal{E}}_k = \{x_k \in \mathbb{R}^{n_x} : (x_k - \hat{p}_k)^\top \alpha (r_k P^{-1})^{-1} (x_k - \hat{p}_k) \leq 1\}$, where $\hat{p}_k$ is the center of the zonotope to be outer bounded and r_k its P-radius.

This can be formulated as an optimization problem that has to be verified for all the vertices of the zonotope $\hat{\mathcal{Z}}_k$:

$$\max_{\alpha \in \mathbb{R}} \alpha$$

subject to

$$\begin{cases} 0 < \alpha \leq 1 \\ (x_k - \hat{p}_k)^\top \alpha P r_k^{-1} (x_k - \hat{p}_k) \leq 1, \ \ \forall x_k \in \mathcal{V}_{\hat{\mathcal{Z}}_k}. \end{cases} \tag{4.74}$$

The reader will note that this optimization problem has to be verified for all

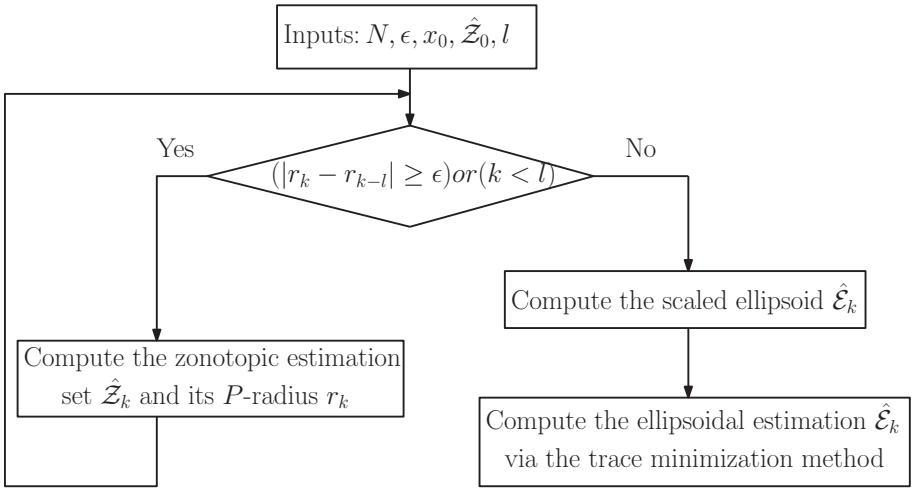

Figure 4.6: Diagram of the combined method

the vertices $\mathcal{V}_{\hat{\mathcal{Z}}_k}$ of the zonotope $\hat{\mathcal{Z}}_k$. This requires a large computation time to solve the optimization problem (4.74). For this, it is suitable to find a method reducing the number of vertices to be checked to compute α.

Let us denote by $\bar{x}_{\hat{\mathcal{Z}}_k}$ the furthest vertex from the center of the zonotope. Then, the following proposition avoids the vertex enumeration when solving the optimization problem (4.74). In fact, this allow us to reformulate (4.74) by computing the maximum of a given functional in the set of vertices.

***Proposition* 4.1.** Consider a symmetric positive definite matrix $P = P^\top \succ 0 \in \mathbb{R}^{n_x \times n_x}$, the state vector $x_k \in \mathbb{R}^{n_x}$, the furthest vertex $\bar{x}_{\mathcal{Z}_k} \in \mathbb{R}^{n_x}$, the P-radius $r_k > 0$ of the zonotope $\hat{\mathcal{Z}}_k$ and $\hat{p}_k \in \mathbb{R}^{n_x}$ its center and the scalar $\alpha \in (0,1)$. If $(\bar{x}_{\hat{\mathcal{Z}}_k} - \hat{p}_k)^\top \alpha P r_k^{-1} (\bar{x}_{\hat{\mathcal{Z}}_k} - \hat{p}_k) \leq 1$, then $(x_k - \hat{p}_k)^\top \alpha P r_k^{-1} (x_k - \hat{p}_k) \leq 1, \ \ \forall x_k \in \mathcal{V}_{\hat{\mathcal{Z}}_k}$.

Proof

Expression (4.39) can be formulated as follows

$$(\bar{x}_{\hat{\mathcal{Z}}_k} - \hat{p}_k)^\top P (\bar{x}_{\hat{\mathcal{Z}}_k} - \hat{p}_k) = r_k, \tag{4.75}$$

with $\bar{x}_{\hat{\mathcal{Z}}_k}$ the furthest vertex from the center of the zonotope $\hat{\mathcal{Z}}_k$.

This means that

$$(x_k - \hat{p}_k)^\top P (x_k - \hat{p}_k) \leq (\bar{x}_{\hat{\mathcal{Z}}_k} - \hat{p}_k)^\top P (\bar{x}_{\hat{\mathcal{Z}}_k} - \hat{p}_k), \ \ \forall x_k \in \mathcal{V}_{\hat{\mathcal{Z}}_k}. \tag{4.76}$$

Assume that $\exists \alpha \in (0,1)$ such that

$$(\bar{x}_{\hat{\mathcal{Z}}_k} - \hat{p}_k)^\top \alpha P r_k^{-1} (\bar{x}_{\hat{\mathcal{Z}}_k} - \hat{p}_k) \leq 1. \tag{4.77}$$

This inequality can be rewritten as

$$(\bar{x}_{\hat{\mathcal{Z}}_k} - \hat{p}_k)^\top P(\bar{x}_{\hat{\mathcal{Z}}_k} - \hat{p}_k) \leq \frac{r_k}{\alpha}. \tag{4.78}$$

From (4.76) and (4.78) it is inferred that

$$(x_k - \hat{p}_k)^\top P(x_k - \hat{p}_k) \leq \frac{r_k}{\alpha}, \ \ \forall x_k \in \mathcal{V}_{\hat{\mathcal{Z}}_k} \tag{4.79}$$

which is equivalent to

$$(x_k - \hat{p}_k)^\top \alpha P r_k^{-1}(x_k - \hat{p}_k) \leq 1, \ \ \forall x \in \mathcal{V}_{\hat{\mathcal{Z}}_k}. \tag{4.80}$$

□

This proposition avoids solving the optimization problem (4.74) for all the vertices of the zonotope (only the furthest vertex will be now considered in (4.74)) and gives a reduced computation time. The next example shows the performances of this combination method.

***Example* 4.1.** Consider the following linear discrete-time invariant system:

$$\begin{cases} x_{k+1} = \begin{bmatrix} 1 & 1 \\ 0 & 0.8 \end{bmatrix} x_k + \begin{bmatrix} -0.24 \\ 0.04 \end{bmatrix} \omega_k \\ \\ y_k = \begin{bmatrix} -2 & 1 \end{bmatrix} x_k + 0.4 v_k \end{cases} \tag{4.81}$$

with $\|v_k\|_\infty \leq 1$, $\|\omega_k\|_\infty \leq 1$. The initial state belongs to the box $3\mathbf{B}^2$. The order of the zonotope is limited to $m \leq 20$ in order to have a fast simulation.

Figure 4.7 and its zoom (Fig. 4.8) show the evolution domains containing the state set for the 20 first iterations.

In red, the P-radius-based zonotopic guaranteed state estimation sets at each iteration and in green the ellipsoid related to its P-radius. The blue ellipsoid is the guaranteed state estimation domain obtained by the ellipsoidal estimation using the trace criterion. Note that the non-increasing condition of the P-radius is verified. After 15 iterations, the green ellipsoid related to the P-radius is completely contained into the zonotopic estimated set (Fig. (4.8)).

Figures 4.9 and 4.11 and their zoom (Fig. 4.10 and 4.12, respectively) illustrate the bounds of x_1 and x_2 after 120 iterations obtained with the three estimation method: the P-radius based zonotopic estimation, the trace-based ellipsoidal estimation and the proposed method.

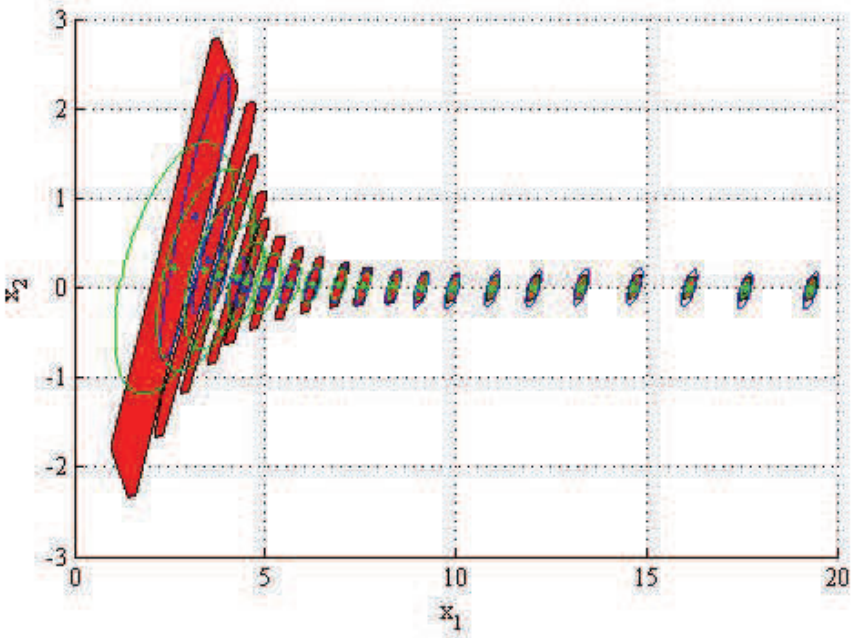

Figure 4.7: State-space sets

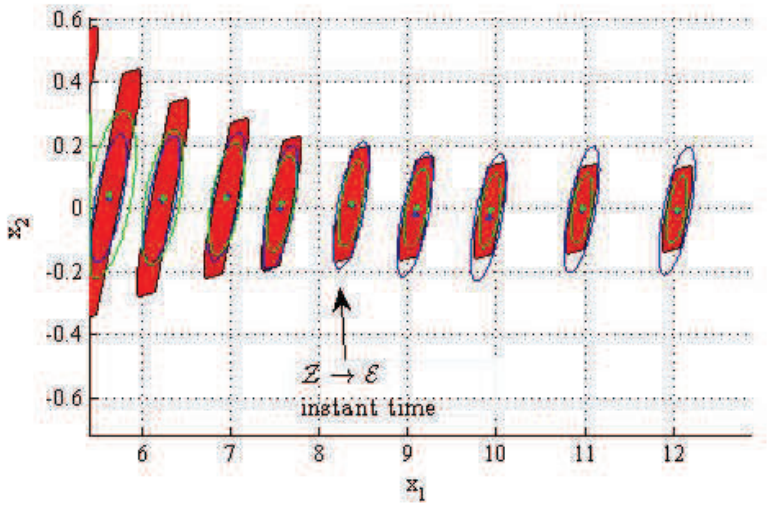

Figure 4.8: Zoom of state-space sets

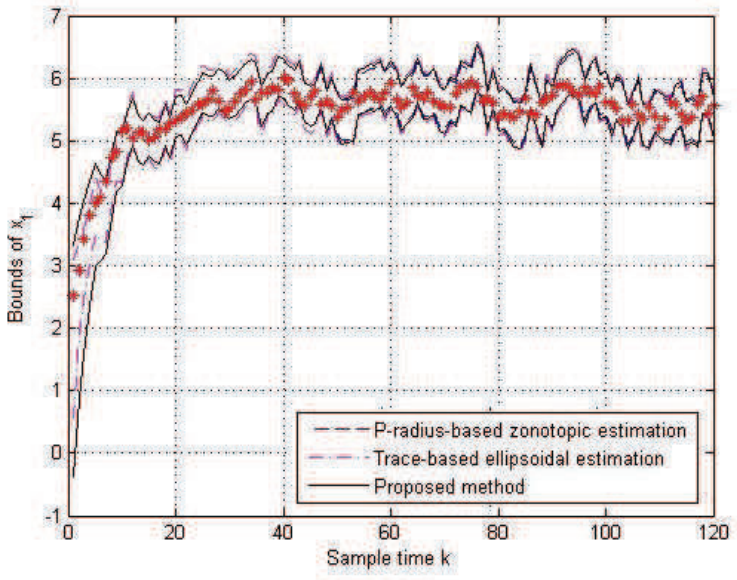

Figure 4.9: Bounds of x_1

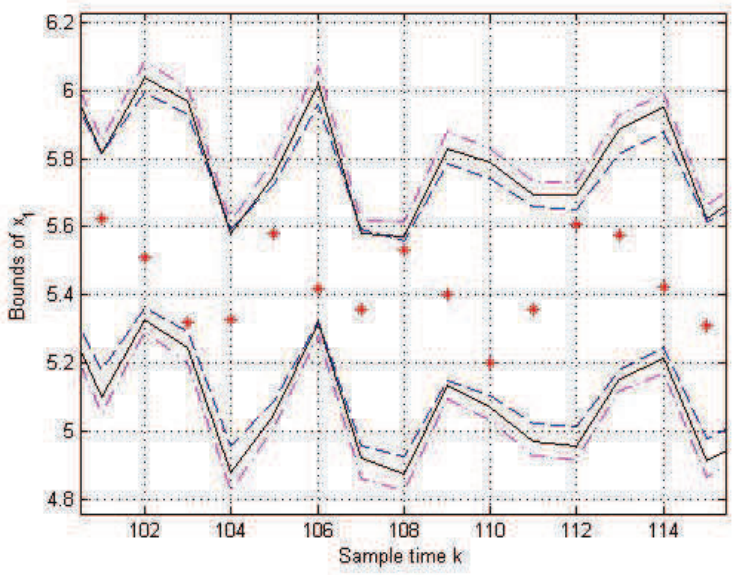

Figure 4.10: Zoom of x_1

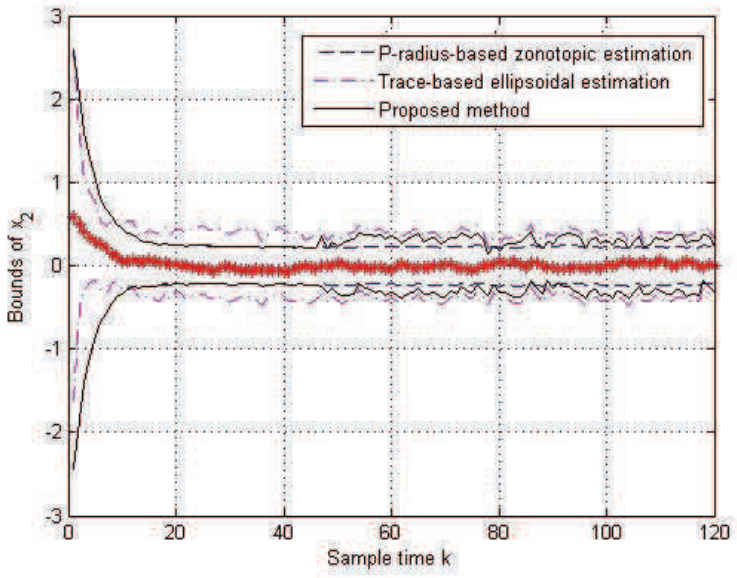

Figure 4.11: Bounds of x_2

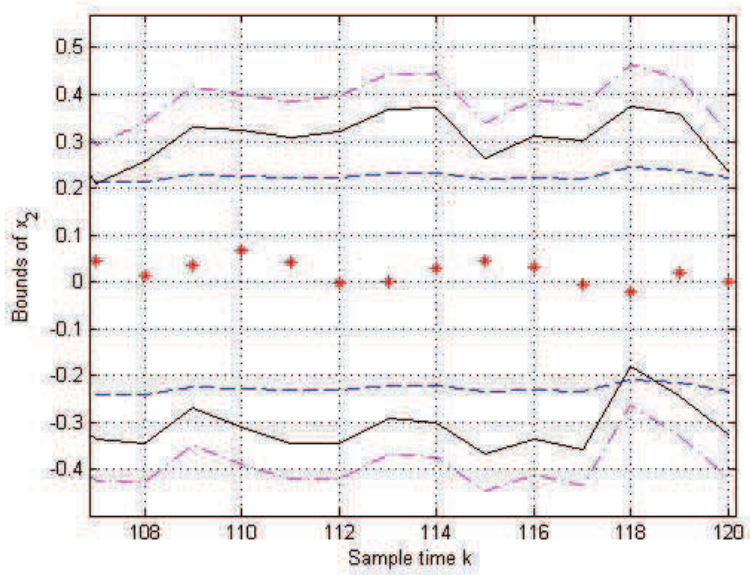

Figure 4.12: Zoom of x_2

The magenta dashed lines are obtained by the ellipsoidal estimation using

the trace minimization criterion. The blue lines are obtained by the zonotopic estimation based on the P-radius minimization and red dashdot lines are obtained using the proposed method. The red stars represent the real state of the system, which is inside the estimated sets.

The computation time after 120 iterations is $0.27s$ for P-radius-based zonotopic estimation, $0.08s$ for the trace-based ellipsoidal estimation and $0.15s$ for the proposed method, which is a good trade-off (see Table 4.1). These results are obtained using an Intel Core Duo E8500 3.16GHz. The tuning parameters used in *Algorithm 1* are: $\epsilon = 10^{-5}$ and $l = 5$.

Table 4.1: Total computation time after 120 time instants

Algorithm	Time (second)
Proposed method	0.15
Trace-based ellipsoidal estimation	0.08
P-radius-based zonotopic estimation	0.27

Figure 4.13 shows the P-radius evolution using the zonotopic estimation. Note that the P-radius is decreasing at each iteration. At the moment of transition to the ellipsoidal estimation, the value of the P-radius is equal to 0.1463.

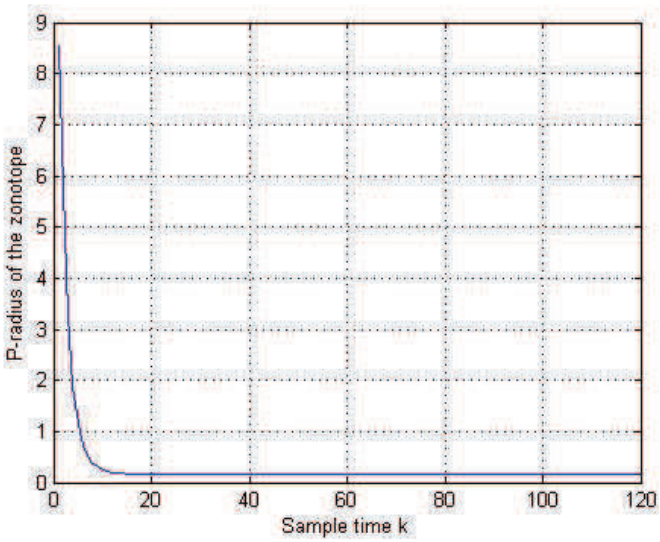

Figure 4.13: P-radius evolution of the zonotopic estimation

Figure 4.14 compares the volume of the state estimation sets obtained

by the considered approaches. The minimal volume is obtained by the P-radius-based method, while with the proposed method the volume is the same until just before the transition and it does not degrade too much after the transition. The proposed method permits to gain 59% in computation time compared to the P-radius-based zonotopic estimation with a degradation of volume of 36% compared to the P-radius-based zonotopic estimation, which remains reasonable.

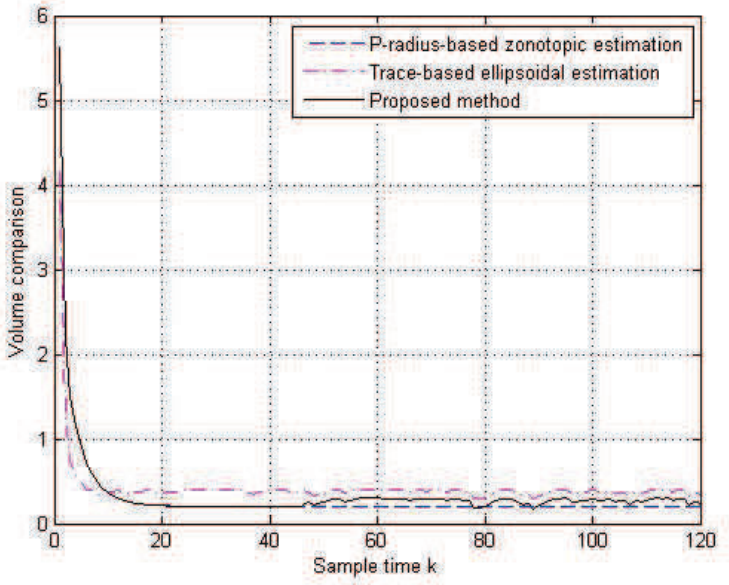

Figure 4.14: Comparison of the volume of state estimation sets

This confirms the objective of the proposed algorithm offering good accuracy compared to the ellipsoidal estimation, while reducing the complexity compared to the zonotopic estimation.

4.6 Conclusion

The aim of this chapter was twofold: comparing zonotopic and ellipsoidal set-membership estimation techniques, and proposing a new approach allowing a trade-off between zonotopic and ellipsoidal state estimation approaches.

This chapter begins with the state-of-the-art on the state estimation techniques using zonotopes and ellipsoids for linear systems.

The main part of this chapter consists in proposing an improved method which combines the advantages of the zonotopic set-membership state esti-

mation (i.e. accuracy) and of the ellipsoidal set-membership estimation (i.e. reduced complexity). This is formulated as an optimization problem which starts with the zonotopic estimation and continues with the ellipsoidal estimation. A new criterion based on the P-radius of the zonotopic estimation is used to make the transition. In fact, when the P-radius of the zonotope is decreasing very slowly in the last iterations, an outer ellipsoidal approximation of the zonotope is considered to continue the state estimation with the ellipsoidal set-membership technique. This outer ellipsoid is obtained by scaling the ellipsoid related to the P-radius of the zonotope after solving an optimization problem. This combined method (which is the first novelty of this thesis) leads to a less complex estimation than the zonotopic estimation based on the minimization of the P-radius and more accurate than the ellipsoidal estimation.

In the next chapter, a new ellipsoidal state estimation approach based on the minimization of the ellipsoidal radius will be presented.

Chapter 5

Ellipsoidal state estimation based on the radius minimization

5.1 Introduction

The set-membership estimation approaches compute at each sample time instant the estimated set containing all the possible states consistent with the measurements, the possible perturbations and uncertainties. As shown in the previous chapter, several sets are used to implement these techniques: polytopes, parallelotopes, zonotopes, ellipsoids, etc.

Chapter 4 focused on set membership state estimation using ellipsoids and zonotopes. In fact, ellipsoidal estimation has increased the attention among researchers in the last years. Indeed, ellipsoids are widely used due to the simplicity of their formulation. This topic is considerably covered in [61], which in particular provides an exhaustive solution of the problem for the sum and the geometrical difference of two ellipsoids. Less efforts have been devoted to the study of other important operations, such as the union and the intersection of ellipsoids, although the construction of external approximations for the intersection of ellipsoids plays a key role for control design in dynamical systems with ellipsoidal constraints [24]. To minimize the size of the estimation ellipsoidal set, two methods are mainly considered. Firstly, the determinant-based criterion is minimized [36], which is equivalent to minimize the volume of the ellipsoidal set. Secondly, the minimization of the trace criterion, which is equivalent to minimize the sum of squares of the half length of the axes of the ellipsoid, is considered in the literature [36]. These two methods offer low complexity suitable for online implementation, but with a loss of accuracy compared to the polytopic estimation [36].

In addition, as seen in the previous chapter, zonotopes are proposed to

obtain a trade-off between the estimation accuracy of polytopes and the reduced complexity of ellipsoids. To minimize the size of the zonotopic estimation, several methods are proposed in the literature: the Singular Value Decomposition-based method [27], the minimization of the zonotope segments [2], the minimization of the zonotope volume [2]. In [67], the minimization of the P-radius of the zonotope leads to a trade-off between the rapidity of the segments minimization and the estimation accuracy of the volume minimization of a zonotope. Quite similar results are obtained comparing the Singular Value Decomposition-based method and the P-radius minimization zonotopic method [65]. The P-radius minimization zonotopic method [67] is also used for linear time-invariant systems with interval uncertainties. However, the P-radius based method imposes a fixed gain to construct the zonotopic estimation set which is parametrized by a vector/matrix computed off-line.

In order to overcome these disadvantages, this chapter proposes a new approach for guaranteed state estimation Multi-Input Multi-Output linear systems by minimizing the radius of the ellipsoidal estimation set. In this context, four methods are developed (as illustrated in Figure 5.1):

- *Method 1* considers a constant observer gain matrix;
- *Method 2* considers an updated observer gain matrix;
- *Method 3* considers an updated observer gain with vector scaling technique;
- *Method 4* considers a flexible shape matrix for the ellipsoidal estimation set.

Methods *1*, *2* and *3* are applied for multivariable Linear Time Invariant (LTI) systems with bounded perturbations and bounded measurement noises. In *Method 1*, a constant observer gain matrix related to the center of the ellipsoid is obtained by solving a Linear Matrix Inequality (LMI) problem. This result is based on the use of the S-procedure for quadratic functions [19]. To improve the state estimation, the observer gain is updated online by solving an LMI optimization problem at each iteration in *Method 2*. This leads to a more accurate estimation than *Method 1*, but with a significant increase of the computation burden. In order to reduce the computation load, while keeping a suitable level of the estimation accuracy, *Method 3* proposes a new vector scaling technique. *Method 3* is extended to the case of uncertain LTI systems (the evolution and observations matrices have interval uncertainties). It consists in minimizing the radius of the ellipsoidal estimation set by solving

an online Linear Matrix Inequality (LMI) problem. It offers less conservative results than the estimation obtained by the P-radius-based zonotopic estimation method [67] due to the minimization of the ellipsoid radius at each time instant. For these methods applied for LTI systems and uncertain LTI systems (Methods *1*, *2* and *3*), the shape of the ellipsoidal estimation set is initially fixed and does not change along the estimation horizon. Finally, *Method 4* proposes an extension for the case of uncertain Linear Time Variant (LTV) systems using a flexible shape matrix [14]. The novelty of this method consists in minimizing the size of the ellipsoidal estimation set by solving an online Linear Matrix Inequality (LMI) problem, while allowing to adjust the shape of the ellipsoid, which reduces the conservativeness of the estimation. This method based on the use of the S-procedure for quadratic functions [19] is applied to linear time-varying systems with interval uncertainties, bounded perturbations and measurement noises. To improve the accuracy of the proposed ellipsoidal estimation, quadratic constraints on the output measurement are added, allowing to reduce the predicted estimation set due to more accurate measurement data.

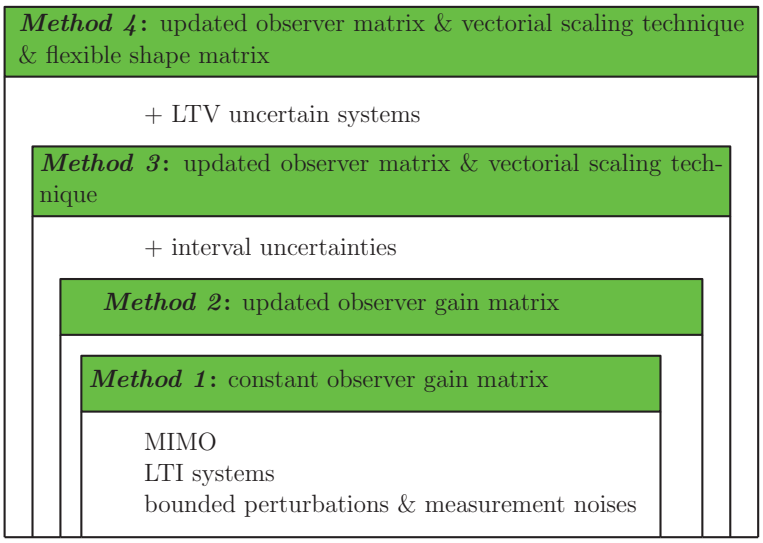

Figure 5.1: Different methods of a new guaranteed ellipsoidal state estimation approach

In the following, the general problem of the ellipsoidal estimation is presented.

Consider the following discrete-time Linear Time Invariant (LTI) system:

$$\begin{cases} x_{k+1} = Ax_k + Bu_k + E\omega_k, \\ y_k = Cx_k + Du_k + F\omega_k, \end{cases} \tag{5.1}$$

where $x_k \in \mathbb{R}^{n_x}$ is the state vector of the system, $u_k \in \mathbb{R}^{n_u}$ is the input vector, and $y_k \in \mathbb{R}^{n_y}$ is the measured output vector at sample time k. The vector $\omega_k \in \mathbb{R}^{n_x+n_y}$ contains the state perturbations and the measurement perturbations[1] (noise, offset, etc.), which are non-correlated. Matrices A, B, C, D, E, and F have the appropriate dimensions, with the pair (C, A) detectable and the pair (A, B) stabilizable[2]. It is assumed that the perturbations ω_k are bounded by the unitary interval $\mathbf{B}^{n_x+n_y}$ and the initial state x_0 is bounded by the ellipsoid $\mathcal{E}(P_0, \bar{x}_0, \rho_0) = \{x \in \mathbb{R}^{n_x} : (x - \bar{x}_0)^\top P_0 (x - \bar{x}_0) \leq \rho_0\}$, with $\bar{x}_0$ the initial nominal state. In fact, the matrices E and F represent weights for the normalized perturbations $\omega_k \in \mathbf{B}^{n_x+n_y}$.

Given an ellipsoidal estimation set for x_k of the form $\mathcal{E}(P, \bar{x}_k, \rho_k)$, with $\bar{x}_k$ the nominal estimated state, the aim of this chapter is to provide an ellipsoidal state estimation set for x_{k+1} of the form $\mathcal{E}(P, \bar{x}_{k+1}, \rho_{k+1})$.

5.2 Linear Time Invariant systems

In this section, the matrices A, B, C, D, E, and F are supposed constant for the system (5.1). Three solutions to the proposed ellipsoidal state estimation problem are given for LTI case: *Method 1* with constant observer matrix gain (*Method 1*), *Method 2* with updated observer matrix gain and *Method 3* with new vector scaling technique. In *Method 2* and *Method 3*, the radius of the ellipsoidal state estimation set is minimized at each sample time for.

5.2.1 *Method 1*: ellipsoidal state estimation method with a constant observer matrix gain

In the following, a constant observer gain matrix, related to the center of the ellipsoidal state estimation set, is computed by solving an off-line LMI optimization problem.

In this method, the ellipsoidal state estimation set $\mathcal{E}(P, \bar{x}_{k+1}, \rho_{k+1})$ that contains x_{k+1} is computed in such a way that:

$$\rho_{k+1} \leq \beta\rho_k + \sigma, \tag{5.2}$$

[1] In general, the vector ω_k could have any desired dimension $\omega_k \in \mathbb{R}^{\omega}$ with appropriate matrices E and F.

[2] Note that the control u_k will be omitted in Sections 5.3 and 5.4 in order to simplify the writing for estimation purposes.

where $\beta \in (0,1)$ and σ is a bounded positive scalar ($\sigma > 0$). Imposing this condition allows us to guarantee the non-increasing property of the ellipsoidal radius. A similar condition is considered for the P-radius-zonotopic guaranteed state estimation in [67].
Finding a guaranteed ellipsoid which contains the state vector x_k at each sampling time k is formulated by the following theorem.

***Theorem* 5.1.** Consider an initial state vector x_0 and assume that $x_k \in \mathcal{E}(P, \bar{x}_k, \rho_k)$ at time k. Given a scalar $\beta \in (0,1)$, if there exist a symmetric positive definite matrix $P = P^\top \succ 0$ in $\mathbb{R}^{n_x \times n_x}$, a matrix $Y \in \mathbb{R}^{n_x \times n_y}$ and a scalar $\sigma > 0$ for which the following LMI holds for every $\omega_k \in \mathcal{V}_{\mathbf{B}^{n_x+n_y}}$:

$$\begin{bmatrix} \beta P & 0 & A^\top P - C^\top Y^\top \\ 0 & \sigma & \omega_k^\top (E^\top P - F^\top Y^\top) \\ PA - YC & (PE - YF)\omega_k & P \end{bmatrix} \succ 0, \tag{5.3}$$

then the system state x_{k+1} at time $k+1$ is guaranteed to belong to the ellipsoid $\mathcal{E}(P, \bar{x}_{k+1}, \rho_{k+1})$, for all $\omega_k \in \mathbf{B}^{n_x+n_y}$, with the following notations:

$$Y = PL, \tag{5.4}$$
$$\bar{x}_{k+1} = A\bar{x}_k + Bu_k + L(y_k - C\bar{x}_k - Du_k), \tag{5.5}$$
$$\rho_{k+1} \leq \beta\rho_k + \sigma. \tag{5.6}$$

Proof

Since $y_k = Cx_k + Du_k + F\omega_k$, for every matrix L of appropriate dimensions, the following equation holds $x_{k+1} = Ax_k + Bu_k + E\omega_k + L(y_k - Cx_k - Du_k - F\omega_k)$. Denote by $z_k = x_k - \bar{x}_k$ the error between the real state and the nominal estimated state at time k. Computing the error z_{k+1} at the next time instant leads to

$$z_{k+1} = (A - LC)z_k + (E - LF)\omega_k = A_L z_k + \eta_k, \tag{5.7}$$

with $A_L = A - LC$ and $\eta_k = (E - LF)\omega_k$.

To prove the result of *Theorem* 5.1, we will show that

$$z_k^\top P z_k \leq \rho_k \Rightarrow z_{k+1}^\top P z_{k+1} \leq \rho_{k+1} \leq \beta\rho_k + \sigma. \tag{5.8}$$

Denote $F_0(z_k) = \beta\rho_k + \sigma - (A_L z_k + \eta_k)^\top P (A_L z_k + \eta_k) = \rho_{k+1} - z_{k+1}^\top P z_{k+1}$ and $F_1(z_k) = \rho_k - z_k^\top P z_k$. Using the S-Procedure (see *Definition* 3.9), with $p = 1$, expression (5.8) is verified if there exists $\mu > 0$ such that $F_0(z_k) - \mu F_1(z_k) \geq 0, \ \forall \omega_k \in \mathbf{B}^{n_x+n_y}$, which is equivalent to

$$z_{k+1}^\top P z_{k+1} + \mu(\rho_k - z_k^\top P z_k) \leq \beta\rho_k + \sigma, \ \ \forall \omega_k \in \mathbf{B}^{n_x+n_y}. \tag{5.9}$$

Fixing the value of μ equal to β, we obtain

$$z_{k+1}^\top P z_{k+1} + \beta(\rho_k - z_k^\top P z_k) \leq \beta\rho_k + \sigma, \;\; \forall \omega_k \in \mathbf{B}^{n_x+n_y}. \tag{5.10}$$

Replacing the term z_{k+1} with the equation (5.7) and after simplifying the terms in $\beta\rho_k$, the following inequality is obtained

$$(A_L z_k + \eta_k)^\top P (A_L z_k + \eta_k) - \beta z_k^\top P z_k \leq \sigma, \;\; \forall \omega_k \in \mathbf{B}^{n_x+n_y}. \tag{5.11}$$

This is equivalent to

$$z_k^\top A_L^\top P A_L z_k + \eta_k^\top P \eta_k + 2\eta_k^\top P A_L z_k - \beta z_k^\top P z_k - \sigma \leq 0, \;\; \forall \omega_k \in \mathbf{B}^{n_x+n_y}, \tag{5.12}$$

which can be rewritten as

$$\begin{bmatrix} z_k \\ 1 \end{bmatrix}^\top \begin{bmatrix} A_L^\top P A_L - \beta P & A_L^\top P \eta_k \\ \eta_k^\top P A_L & -\sigma + \eta_k^\top P \eta_k \end{bmatrix} \begin{bmatrix} z_k \\ 1 \end{bmatrix} \leq 0, \; \forall \omega_k \in \mathbf{B}^{n_x+n_y}, \; \forall z_k \in \mathbb{R}^{n_x} \tag{5.13}$$

The expression (5.13) is satisfied if

$$\begin{bmatrix} -A_L^\top P A_L + \beta P & -A_L^\top P \eta_k \\ -\eta_k^\top P A_L & \sigma - \eta_k^\top P \eta_k \end{bmatrix} \succ 0, \;\; \forall \omega_k \in \mathbf{B}^{n_x+n_y}, \tag{5.14}$$

which is equivalent to

$$\begin{bmatrix} \beta P & 0 \\ 0 & \sigma \end{bmatrix} - \begin{bmatrix} A_L^\top P \\ \eta_k^\top P \end{bmatrix} P^{-1} \begin{bmatrix} P A_L & P\eta_k \end{bmatrix} \succ 0, \;\; \forall \omega_k \in \mathbf{B}^{n_x+n_y}. \tag{5.15}$$

Applying Schur complement (see *Definition* 3.8) leads to

$$\begin{bmatrix} \beta P & 0 & A_L^\top P \\ 0 & \sigma & \eta_k^\top P \\ P A_L & P\eta_k & P \end{bmatrix} \succ 0, \;\; \forall \omega_k \in \mathbf{B}^{n_x+n_y}. \tag{5.16}$$

From the equalities $A_L = A - LC$, $\eta_k = (E - LF)\omega_k$ and $Y = PL$, the equivalent expression follows

$$\begin{bmatrix} \beta P & 0 & A^\top P - C^\top Y^\top \\ 0 & \sigma & \omega_k^\top (E^\top P - F^\top Y^\top) \\ PA - YC & (PE - YF)\omega_k & P \end{bmatrix} \succ 0, \;\; \forall \omega_k \in \mathbf{B}^{n_x+n_y}. \tag{5.17}$$

Since ω_k appears in an affine way in the previous LMI, the inequality is satisfied if and only if it is verified for all the vertices of $\mathbf{B}^{n_x+n_y}$. This completes the proof. □

***Remark* 5.1.** The center of the ellipsoid $\bar{x}_{k+1}$ (which is the nominal state estimation at time $k+1$) is computed like a Luenberger observer which is motivated by the fact that the system is linear. The gain $L = P^{-1}Y$ is obtained after solving the LMI (5.3). Note that when β is a free variable in the interval $(0,1)$, expression (5.3) becomes a very simple case of Bilinear Matrix Inequality (BMI). As $\beta \in (0,1)$ is a bounded scalar, this expression can be rewritten as a LMI problem by successively fixing the value of β via the bisection algorithm or using any available BMI solver from the literature (e.g. *penbmi* solver [58]).

***Remark* 5.2.** A sufficient condition is to choose $\rho_{k+1} = \beta\rho_k + \sigma$ in the equation (5.6), which means to consider the worst case.

***Remark* 5.3.** At infinity, the sequence ρ_k converges to $\rho_\infty = \dfrac{\sigma}{1-\beta}$. Reducing the size of the associated ellipsoid can be done by minimizing σ subject to the LMI (5.3) and the additional constraint $Tr(P) \leq 1$. Another possibility is to impose $P \preceq I$ as additional constraint.

The proposed optimization problem is solved off-line. Online, it is possible to take advantage of the knowledge of matrix P in order to obtain a different gain L_k at each time instant k. This method improves the rapidity of the convergence of the estimation. Given $\bar{x}_k$ and ρ_k, it consists in minimizing the radius ρ_{k+1} at each time instant. This method will be developed in the next subsection.

5.2.2 *Method 2*: ellipsoidal state estimation method with an updated observer matrix gain

This subsection proposes a method which improves the convergence of the radius of the state estimation with respect to the approach presented in the previous subsection. In fact, once the matrix P is computed off-line, it is possible to improve the convergence by computing an optimal value for L_k at each iteration. The existence of P, L, and β (initially computed via *Method 1*) guarantees the existence of L_k satisfying the considered constraints. This method allows minimizing the ellipsoidal radius ρ_{k+1} at each iteration. The following theorem formulates the proposed approach.

***Theorem* 5.2.** Consider that at time instant k the system state x_k belongs to the ellipsoid $\mathcal{E}(P, \bar{x}_k, \rho_k)$, with the matrix P, the radius ρ_k and the scalar σ computed off-line (using the result of *Theorem* 5.1). If there exist a matrix $Y_k \in \mathbb{R}^{n_x \times n_y}$, a scalar $\beta \in (0,1)$ and a radius ρ_{k+1} satisfying the following LMI optimization problem for all $\omega_k \in \mathcal{V}_{\mathbf{B}^{n_x+n_y}}$:

$$\min_{\beta, Y_k, \rho_{k+1}} \rho_{k+1}$$
subject to

$$\begin{cases} \begin{bmatrix} \beta P & 0 & A^\top P - C^\top Y_k^\top \\ 0 & \rho_{k+1} - \beta\rho_k & \omega_k^\top (E^\top P - F^\top Y_k^\top) \\ PA - Y_k C & (PE - Y_k F)\omega_k & P \end{bmatrix} \succ 0 \\ \rho_{k+1} \leq \beta\rho_k + \sigma \end{cases} \tag{5.18}$$

then the system state x_{k+1} at time $k+1$ is guaranteed to belong to the ellipsoid $\mathcal{E}(P, \bar{x}_{k+1}, \rho_{k+1})$, for all $\omega_k \in \mathbf{B}^{n_x+n_y}$, with:

$$PL_k = Y_k, \tag{5.19}$$

$$\bar{x}_{k+1} = A\bar{x}_k + Bu_k + L_k(y_k - C\bar{x}_k - Du_k). \tag{5.20}$$

Proof

The proof is similar to the proof of *Theorem 1*, replacing σ by $\rho_{k+1} - \beta\rho_k$ and L by L_k. □

The second constraint $\rho_{k+1} \leq \beta\rho_k + \sigma$ of LMIs (5.18) ensures the non-increasing condition of the ellipsoidal radius. In fact, this implies a reduction of the ellipsoidal radius only if the radius ρ_k is larger than $\rho_\infty = \dfrac{\sigma}{1-\beta}$.

Online verifying the LMI problem (5.18) for all the vertices of $\mathbf{B}^{n_x+n_y}$ requires a large computation time and thus it is suitable to find a technique for reducing the number of vertices to be checked.

5.2.3 *Method 3*: ellipsoidal state estimation method with vector scaling technique

To avoid the vertex enumeration and reduce the computation time when solving the online problem (5.18), a new *scaling technique* is proposed in this section. This technique is based on the results developed in [4] and will be applied to the LMI optimization problem (5.18).

Knowing that the perturbation ω_k is contained into a box $\mathbf{B}^{n_x+n_y}$, it is possible to take into account the structure of ω_k to avoid the vertex enumeration problem. Therefore, the perturbation vector ω_k can be written as: $\omega_k = [\omega_{k_1}\ \omega_{k_2}\ \ldots\ \omega_{k_{n_x+n_y}}]^\top \in \mathbf{B}^{n_x+n_y}$. In the element-wise formulation, the following expressions are true: $|\omega_k| \leq 1$ and $\omega_k^\top \omega_k \leq 1$.

Denote by e_i, with $i = 1, \ldots, n_{n_x+n_y}$, the columns of the following identity matrix $I_{n_x+n_y} = \begin{bmatrix} e_1 & e_2 & \ldots & e_{n_x+n_y} \end{bmatrix}$. This permits to write: $\omega_k^\top e_i e_i^\top \omega_k \leq 1$, for $i = 1, \ldots, n_x + n_y$. Then, denoting by $T_i = e_i e_i^\top$ the matrix having only the element (i,i) equal to 1, it leads to the following scalar inequalities:

$$\omega_k^\top T_i \omega_k \leq 1, \quad i = 1, \ldots, n_x + n_y. \tag{5.21}$$

This result is further used by the following property.

***Property* 5.1.** Consider a positive definite matrix $S \in \mathbb{R}^{(n_x+n_y)\times(n_x+n_y)}$ and the positive real scalars $\rho > 0$ and $\tau_i \geq 0$, with $i = 1, \ldots, n_x + n_y$. If the following conditions are verified:

$$\begin{cases} \omega_k^\top T_i \omega_k \leq 1, \quad i = 1, \ldots, n_x + n_y, & (a) \\ \sum\limits_{i=0}^{n_x+n_y} \tau_i < \rho, \quad i = 1, \ldots, n_x + n_y, & (b) \\ \sum\limits_{i=0}^{n_x+n_y} \tau_i T_i \succ S, & (c) \end{cases} \tag{5.22}$$

then the following inequality holds $\dfrac{1}{\rho}\omega_k\omega_k^\top \prec S^{-1}$.

Proof

From (5.22.b), we have that $\rho > \sum\limits_{i=0}^{n_x+n_y} \tau_i \geq 0$. Multiplying left and right expression (5.22.c) by $\omega_k^\top$ and ω_k, respectively, and then successively using (5.22.a) and (5.22.b), leads to the following scalar formulation $\omega_k^\top S \omega_k < \omega_k^\top (\sum\limits_{i=0}^{n_x+n_y} \tau_i T_i)\omega_k = \sum\limits_{i=0}^{n_x+n_y} \tau_i (\omega_k^\top T_i \omega_k) \leq \sum\limits_{i=0}^{n_x+n_y} \tau_i < \rho$. This can be rewritten as $\rho - \omega_k^\top S \omega_k > 0$, with $S \succ 0$ and further reformulated using the Schur complement

$$\begin{bmatrix} \rho & \omega_k^\top \\ \omega_k & S^{-1} \end{bmatrix} \succ 0, \quad S \succ 0,$$

or equivalently:

$$\begin{bmatrix} S^{-1} & \omega_k \\ \omega_k^\top & \rho \end{bmatrix} \succ 0, \quad \rho > 0. \tag{5.23}$$

Applying again the Schur complement, gives

$$S^{-1} - \omega_k \rho^{-1} \omega_k^\top \succ 0, \quad \rho > 0. \tag{5.24}$$

which leads to $\dfrac{\omega_k\omega_k^\top}{\rho} \prec S^{-1}$. This completes the proof. □

Applying *Property* 5.1 to problem (5.18), the following proposition is obtained.

***Proposition* 5.1.** If the first LMI constraint of the optimization problem (5.18) is verified:

$$\begin{bmatrix} \beta P & 0 & A^\top P - C^\top Y_k^\top \\ 0 & \rho_{k+1} - \beta\rho_k & \omega_k^\top (E^\top P - F^\top Y_k^\top) \\ PA - Y_k C & (PE - Y_k F)\omega_k & P \end{bmatrix} \succ 0, \quad \forall \omega_k \in \mathcal{V}_{\mathbf{B}^{n_x+n_y}}, \tag{5.25}$$

then there exist a scalar $\beta > 0$ and a matrix $S = S^\top \succ 0 \in \mathbb{R}^{(n_x+n_y)\times(n_x+n_y)}$ verifying the constraints (5.22.a), (5.22.b) and (5.22.c) of *Property* 5.1 such that:

$$\begin{cases} \begin{bmatrix} \beta P & A^\top P - C^\top Y_k^\top & 0 \\ PA - Y_k C & P & PE - Y_k F \\ 0 & E^\top P - F^\top Y_k^\top & S \end{bmatrix} \succ 0, \\ \rho_{k+1} - \beta\rho_k > 0. \end{cases} \tag{5.26}$$

Proof

Pre-multiplying and post-multiplying inequality (5.25) by $\begin{bmatrix} I & 0 & 0 \\ 0 & 0 & I \\ 0 & I & 0 \end{bmatrix}$ leads to

$$\begin{bmatrix} \beta P & A^\top P - C^\top Y_k^\top & 0 \\ PA - Y_k C & P & (PE - Y_k F)\omega_k \\ 0 & \omega_k^\top (E^\top P - F^\top Y_k^\top) & \rho_{k+1} - \beta\rho_k \end{bmatrix} \succ 0, \tag{5.27}$$

with $\rho_{k+1} - \beta\rho_k > 0$. Applying the Schur complement and using the notation $PE - Y_k F = H_k$, gives

$$\begin{bmatrix} \beta P & A^\top P - C^\top Y_k^\top \\ PA - Y_k C & P - H_k \omega_k \frac{1}{\rho_{k+1} - \beta\rho_k} \omega_k^\top H_k^\top \end{bmatrix} \succ 0, \tag{5.28}$$

with $\rho_{k+1} - \beta\rho_k > 0$. Applying *Property* 5.1 to the term $\omega_k \dfrac{1}{\rho_{k+1} - \beta\rho_k} \omega_k^\top$, with $\rho = \rho_{k+1} - \beta\rho_k$, means that $\exists S = S^\top \succ 0$ such that

$$\omega_k \frac{1}{\rho_{k+1} - \beta\rho_k} \omega_k^\top \prec S^{-1} \tag{5.29}$$

or equivalently:

$$-\omega_k \frac{1}{\rho_{k+1} - \beta\rho_k} \omega_k^\top \succ -S^{-1}, \;\; \rho_{k+1} - \beta\rho_k > 0. \tag{5.30}$$

Therefore, if the following expression is verified

$$\begin{bmatrix} \beta P & A^\top P - C^\top Y_k^\top \\ PA - Y_k C & P - (PE - Y_k F) S^{-1} (E^\top P - F^\top Y_k^\top) \end{bmatrix} \succ 0, \tag{5.31}$$

with $S \succ 0$, then expression (5.26) is verified. The constraint (5.31) can be decomposed as the following

$$\begin{aligned} &\begin{bmatrix} \beta P & A^\top P - C^\top Y_k^\top \\ PA - Y_k C & P \end{bmatrix} - \\ &- \begin{bmatrix} 0 \\ PE - Y_k F \end{bmatrix} S^{-1} \begin{bmatrix} 0 & E^\top P - F^\top Y_k^\top \end{bmatrix} \succ 0, \;\; S \succ 0. \end{aligned} \tag{5.32}$$

Applying the Schur complement leads to the expression (5.26), which completes the proof. □

***Remark* 5.4.** *Proposition* 5.1 permits avoiding the vertex enumeration used in *Theorem* 5.2.

These methods (*Method 1* (5.3), *Method 2* (5.18) and *Method 3* (5.26)) are applied to an example to illustrate the performances.

***Example* 5.1.** Consider the following linear discrete-time invariant system:

$$\begin{cases} x_{k+1} &= \begin{bmatrix} 1 & 0 & 0.2 \\ 0 & 0.8 & 1 \\ 0 & 0 & 1 \end{bmatrix} x_k + \begin{bmatrix} 0.1 & 0 & 0 & 0 & 0 \\ 0 & 0.05 & 0 & 0 & 0 \\ 0 & 0 & 0.05 & 0 & 0 \end{bmatrix} \omega_k \\ y_k &= \begin{bmatrix} 1 & 0 & 2 \\ 0 & -1 & 1 \end{bmatrix} x_k + \begin{bmatrix} 0 & 0 & 0 & 0.15 & 0 \\ 0 & 0 & 0 & 0 & 0.15 \end{bmatrix} \omega_k \end{cases} \tag{5.33}$$

where the perturbations and measurement noises are bounded by $\|\omega_k\|_\infty \leq 1$. The value of ω_k is generated by a random function. The initial state belongs to the ellipsoid $\mathcal{E}(diag(5,5,17), \begin{bmatrix} 0 & 0 & 0 \end{bmatrix}^\top, 10^4)$ as an arbitrary initialization. In this example, the results obtained by *Method 1*, *Method 2* and *Method 3* are analyzed.

These simulation results have been obtained with an Intel Core $i7-3770$ 3.40 GHz, using the LMI solver *mincx* of MATLAB$^{\text{TM}}$Robust Control Toolbox.

Figures 5.2, 5.4, 5.6 and the corresponding zoom figures (Fig. 5.3, 5.5, 5.7) compare the bounds of x_k obtained via the proposed methods: *Method 1* (blue dashed lines), *Method 2* (magenta dashdot lines), and *Method 3* (black solid lines). The red stars represent the real state of the system. These points are found between the upper and lower bounds of x_k, which confirms that the bounds are well estimated. *Method 2* offers a faster convergence rate of the estimation than *Method 1* (see Fig. 5.2, 5.4, 5.6).

Figures 5.8, 5.9 and 5.10 illustrate the comparison of the width of the bounds of x_k computed by the proposed methods, considering the estimation *Method 1* as reference. The best accuracy of the estimation is obtained using *Method 2*.

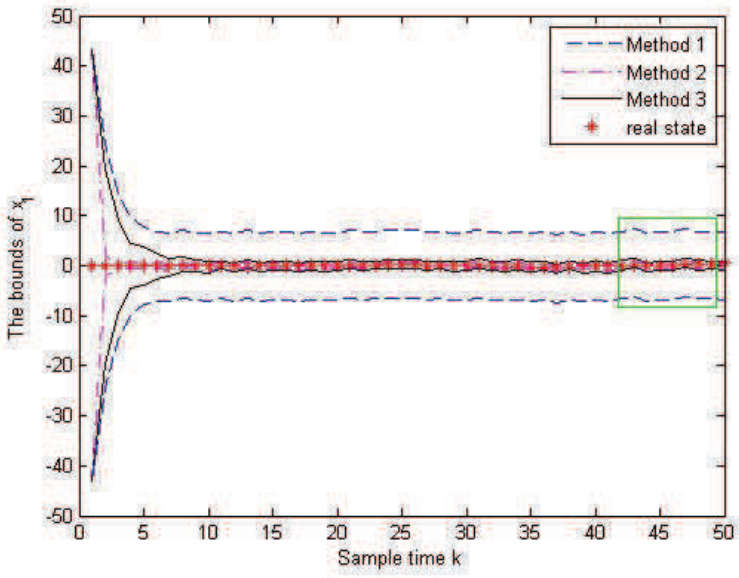

Figure 5.2: Bounds of x_1

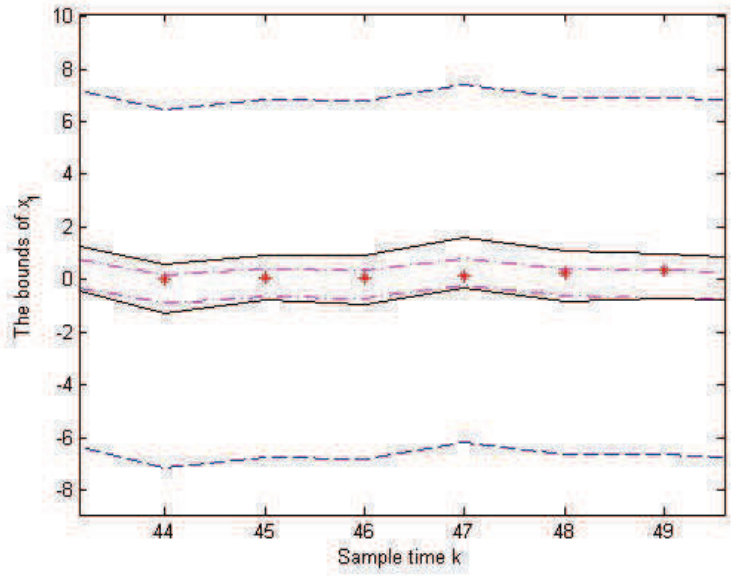

Figure 5.3: Bounds of x_1 (zoom of Fig. 5.2)

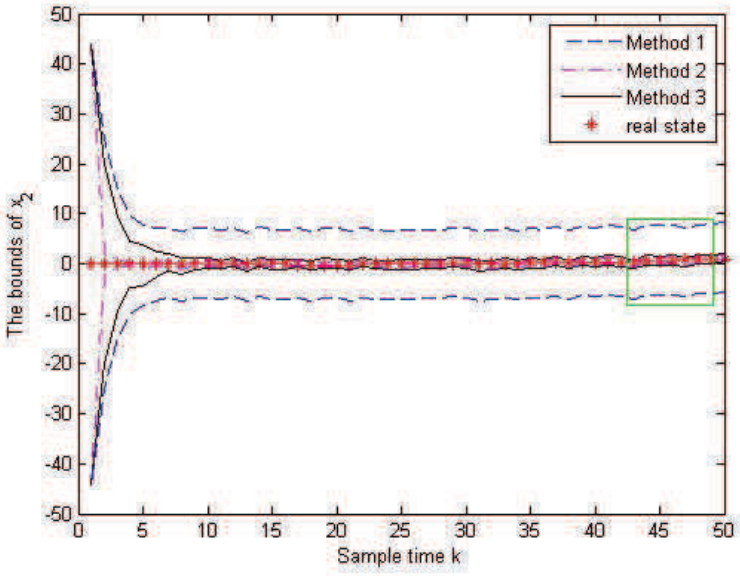

Figure 5.4: Bounds of x_2

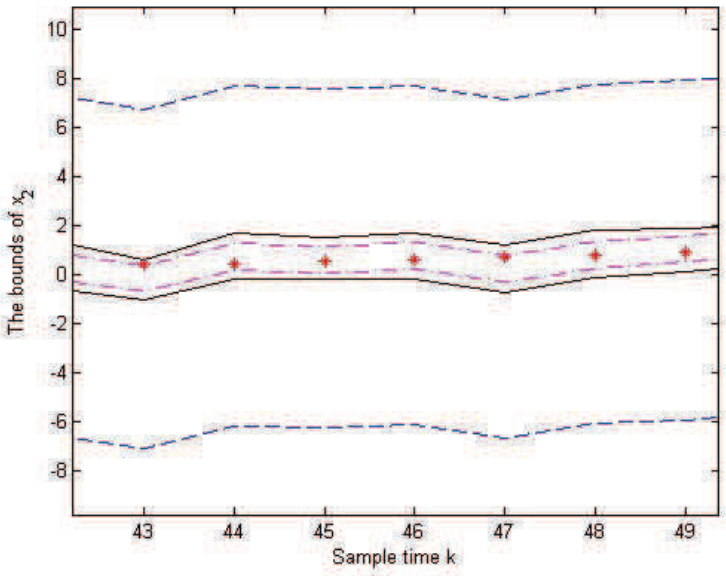

Figure 5.5: Bounds of x_2 (zoom of Fig. 5.4)

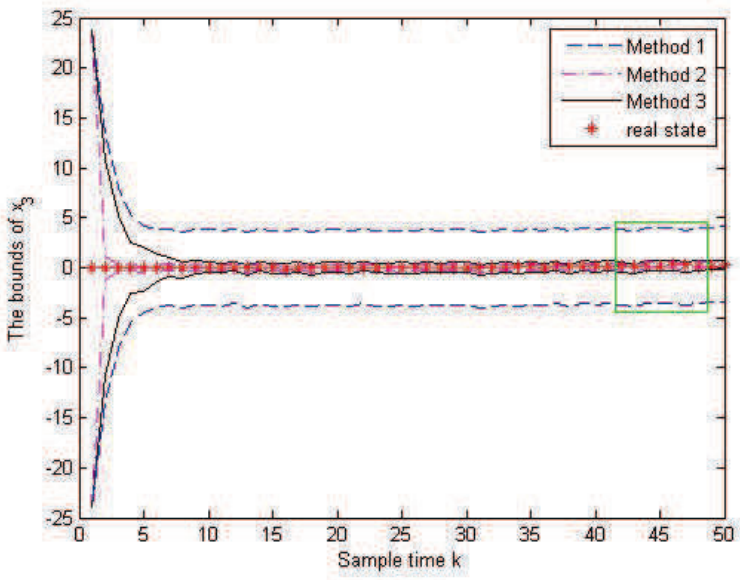

Figure 5.6: Bounds of x_3

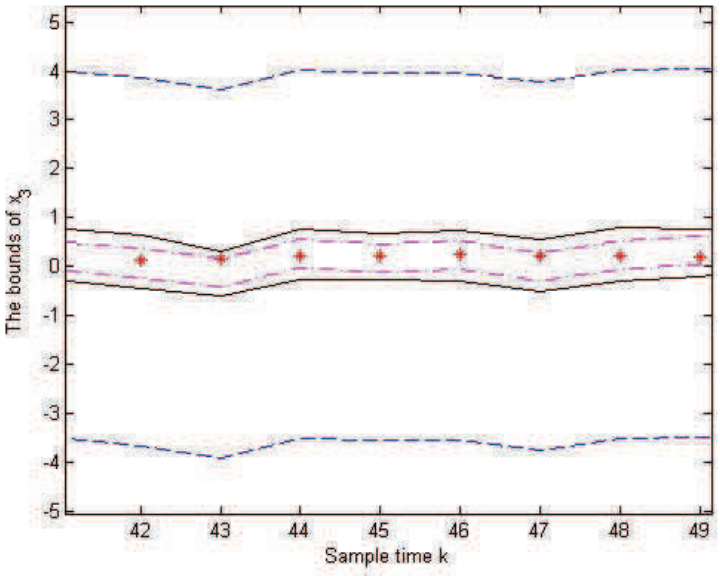

Figure 5.7: Bounds of x_3 (zoom of Fig. 5.6)

Using the vector scaling technique (*Method 3*) will significantly reduce the

computation time with 77% (see Table 5.1) compared to *Method 2*, but with a small loss on the accuracy compared to the results obtained via *Method 2* (Fig. 5.3, 5.5, 5.7). In conclusion, the estimation method with the scaling technique (*Method 3*) offers a good trade-off between the accuracy of the ellipsoidal state estimation and the computation time.

Table 5.1: Total computation time after 50 time instants

Algorithm	Time (second)
Method 1	1.12
Method 2	7.86
Method 3	1.76

Figure 5.11 and its zoom (Fig. 5.12) compare the volume of the state estimation sets obtained by the different methods. This confirms that the ellipsoidal estimation method with the scaling technique (*Method 3*) offers good accuracy compared to *Method 1*, with a gain on the computation time compared to *Method 2* (see Table 5.1).

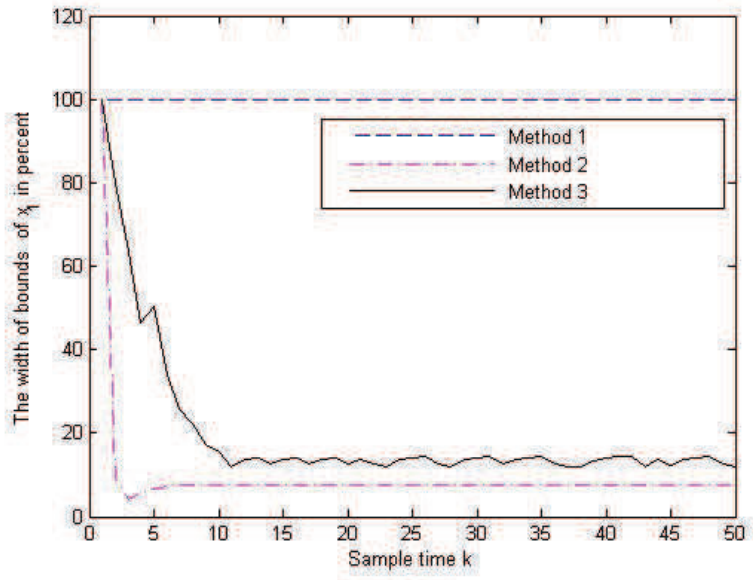

Figure 5.8: Comparison of the bound's width of x_1

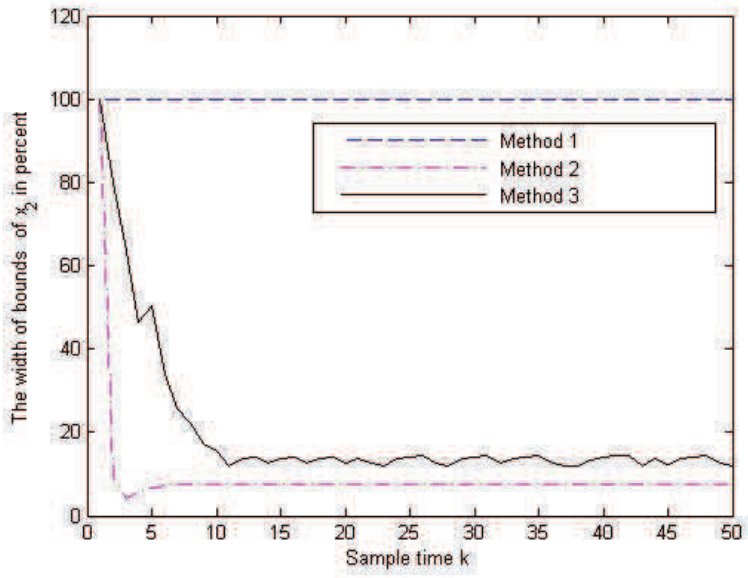

Figure 5.9: Comparison of the bound's width of x_2

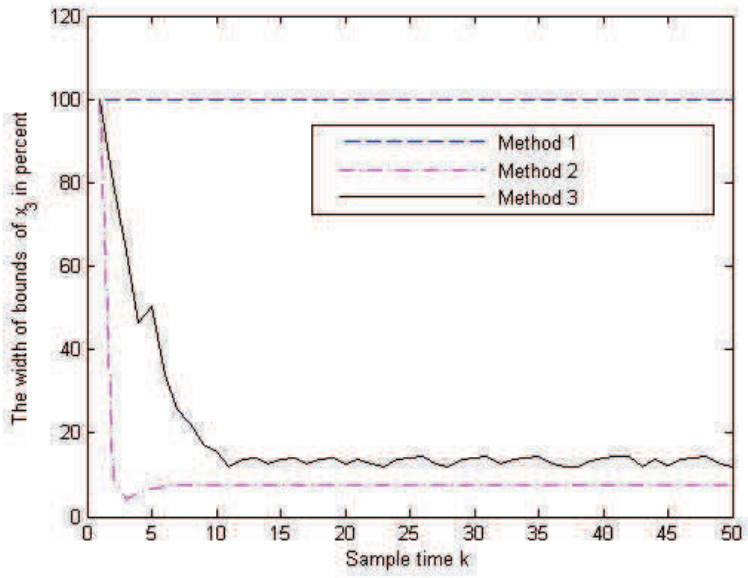

Figure 5.10: Comparison of the bound's width of x_3

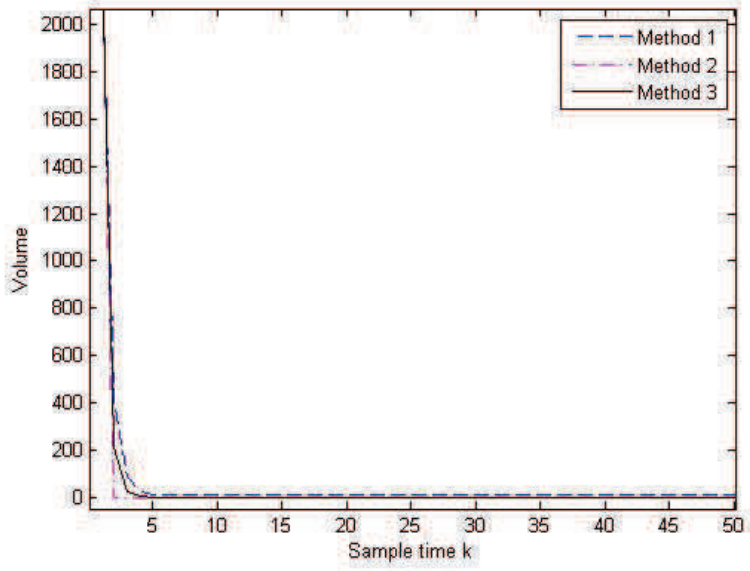

Figure 5.11: Comparison of the volume of the state estimation sets

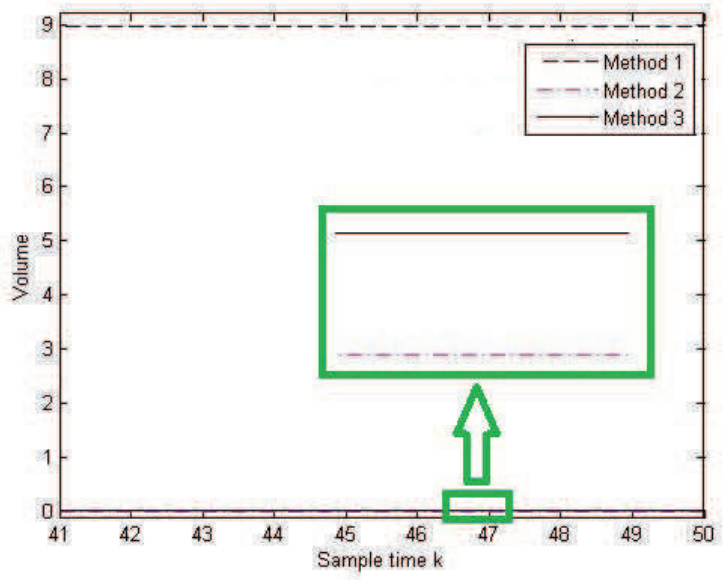

Figure 5.12: Zoom of comparison of the volume of the state estimation sets

5.3 Uncertain Linear Time Invariant systems

In this section, interval uncertainties are introduced for both evolution and observation matrices (A and C). This can be applied for linear systems with parametric uncertainties. For this system, *Method 3* will be applied due to the trade-off between the accuracy and the computation time (although *Method 1* and *Method 2* can also be considered). The following linear discrete-time invariant system is considered:

$$\begin{cases} x_{k+1} = A_\delta x_k + E\omega_k \\ y_k = C_\delta x_k + F\omega_k \end{cases} \tag{5.34}$$

where $x_k \in \mathbb{R}^{n_x}$ is the state vector of the system and $y_k \in \mathbb{R}^{n_y}$ is the measured output vector at sample time k. The vector $\omega_k \in \mathbb{R}^{n_x+n_y}$ contains both the state perturbations and the measurement perturbations (noise, offset, etc.). It is assumed that the perturbations ω_k are bounded by the unitary box $\mathbf{B}^{n_x+n_y}$ and the initial state x_0 is bounded by the ellipsoid: $\mathcal{E}(P_0, \bar{x}_0, \rho_0) = \{x \in \mathbb{R}^{n_x} : (x - \bar{x}_0)^\top P_0 (x - \bar{x}_0) \leq \rho_0\}$. Matrices A_δ, C_δ, E and F have the appropriate dimensions, with the pair (C_δ, A_δ) detectable (see [108] for the detectability of linear time invariant systems with interval uncertainties). An additional hypothesis is to consider a quadratically stable interval matrix $[A]$ for a common quadratic Lyapunov function[3]. A_δ and C_δ are constant unknown matrices belonging to interval matrices $[A]$ and $[C]$, which permits to structure the uncertainties ΔA_δ and ΔC_δ as follows:

$$\begin{cases} A_\delta = mid[A] + \Delta A_\delta, \\ C_\delta = mid[C] + \Delta C_\delta. \end{cases} \tag{5.35}$$

If n_{A_δ} is the number of the uncertain terms $\delta_i \in \mathbf{B}$ of ΔA_δ, with $i = 1, \ldots, n_{A_\delta}$, then the uncertain part ΔA_δ can be decomposed into elementary parts:

$$\Delta A_\delta = \sum_{i=1}^{n_{A_\delta}} A_{\delta_i} \delta_i, \tag{5.36}$$

where the matrices A_{δ_i} have only one non-zero element corresponding to the coefficient of δ_i. In a similar way, ΔC_δ can be decomposed into the following elementary parts:

$$\Delta C_\delta = \sum_{i=1}^{n_{C_\delta}} C_{\delta_i} \delta_i, \tag{5.37}$$

[3]This assumption is necessary for the stability of the estimation.

where n_{C_δ} is the number of the uncertain terms $\delta_i \in \mathbf{B}$ of ΔC_δ, with $i = 1, \ldots, n_{C_\delta}$ and the matrices C_{δ_i} have only one non-zero element corresponding to the coefficient of δ_i. The reader can notice that $n_\delta = n_{A_\delta} + n_{C_\delta}$.

At time $k > 0$, consider an ellipsoid $\mathcal{E}(P, \bar{x}_k, \rho_k)$ that contains the real system state x_k, with $\bar{x}_k$ the nominal estimated set. The idea is to provide at time $k+1$ an optimal ellipsoidal estimation $\mathcal{E}(P, \bar{x}_{k+1}, \rho_{k+1})$ that guarantees to contain the state x_{k+1}.

Finding a guaranteed ellipsoid which contains the state vector x_k at each sample time k is formulated by the following theorem.

***Theorem* 5.3.** Consider an initial state vector x_0 and at sample time k assume that $x_k \in \mathcal{E}(P, \bar{x}_k, \rho_k)$, with $P = P^\top \succ 0$ and $\rho_k > 0$. If there exist a matrix $Y_k \in \mathbb{R}^{n_x \times n_y}$, a matrix $S = S^\top \succ 0$ in $\mathbb{R}^{(n_x+n_y+n_\delta)\times(n_x+n_y+n_\delta)}$ and the scalars $\rho_{k+1} > 0$ and $\beta \in (0,1)$ for which the following LMI holds for all $A_\delta \in \mathcal{V}_{[A]}$ and $C_\delta \in \mathcal{V}_{[C]}$:

$\min\limits_{\beta, Y_k, S, \rho_{k+1}} \rho_{k+1}$

subject to

$$\begin{cases} \begin{bmatrix} \beta P & * & * \\ PA_\delta - Y_k C_\delta & P & * \\ & \begin{bmatrix} E^\top P - F^\top Y_k^\top \end{bmatrix} & \\ 0 & \begin{bmatrix} \mathcal{A}_k^\top \\ -\mathcal{C}_k^\top Y_k^\top \end{bmatrix} & S \end{bmatrix} \succ 0, \\ \rho_{k+1} - \beta\rho_k > 0, \\ \beta < 1, \end{cases} \tag{5.38}$$

with $\mathcal{A}_k = \begin{bmatrix} PA_{\delta_1}\bar{x}_k & \ldots & PA_{\delta_{n_{A_\delta}}}\bar{x}_k \end{bmatrix}$ and $\mathcal{C} = \begin{bmatrix} C_{\delta_1}\bar{x}_k & \ldots & C_{\delta_{n_{C_\delta}}}\bar{x}_k \end{bmatrix}$, then the system state x_{k+1} at time $k+1$ is guaranteed to belong to the ellipsoid $\mathcal{E}(P, \bar{x}_{k+1}, \rho_{k+1}), \forall \omega_k \in \mathbf{B}^{n_x+n_y+n_\delta}$, $\forall A_\delta \in [A]$ and $\forall C_\delta \in [C]$, with the following notations:

$$Y_k = PL_k, \tag{5.39}$$

$$\bar{x}_{k+1} = mid[A]\bar{x}_k + L_k(y_k - mid[C]\bar{x}_k) \tag{5.40}$$

Proof

Denote by $z_k = x_k - \bar{x}_k$ the error between the real state and the nominal estimated state at time k. At time instant $k+1$, the error z_{k+1} is computed as follows

$$z_{k+1} = x_{k+1} - \bar{x}_{k+1} = A_\delta x_k + E\omega_k - mid[A]\bar{x}_k - L_k(y_k - mid[C]\bar{x}_k).$$

Then, replacing y_k as in (5.34), we obtain

$$z_{k+1} = A_\delta x_k + E\omega_k - mid[A]\bar{x}_k - L_k(C_\delta x_k + F\omega_k - mid[C]\bar{x}_k),$$

which, after regrouping the terms in x_k, in ω_k and in $\bar{x}_k$, is equivalent to

$$z_{k+1} = (A_\delta - L_k C_\delta)x_k + (E - L_k F)\omega_k - (mid[A] - L_k mid[C])\bar{x}_k.$$

Replacing $mid[A]$ and $mid[C]$ as detailed in equations (5.35) gives

$$z_{k+1} = (A_\delta - L_k C_\delta)x_k + (E - L_k F)\omega_k - (A_\delta - \Delta A_\delta - L_k(C_\delta - \Delta C_\delta))\bar{x}_k.$$

Then, highlighting the error z_k, an equivalent form is obtained

$$z_{k+1} = A_{L_k} z_k + \eta_{L_k} + (\Delta A_\delta - L_k \Delta C_\delta)\bar{x}_k, \tag{5.41}$$

with $A_{L_k} = A_\delta - L_k C_\delta$ and $\eta_{L_k} = (E - L_k F)\omega_k$.
In order to verify the result, the next step is to prove the following expression

$$z_k^\top P z_k \leq \rho_k \Rightarrow z_{k+1}^\top P z_{k+1} \leq \rho_{k+1}. \tag{5.42}$$

Denote $F_0(z_k) = \rho_{k+1} - (A_{L_k} z_k + \eta_{L_k} + (\Delta A_\delta - L_k \Delta C_\delta)\bar{x}_k)^\top P(A_{L_k} z_k + \eta_{L_k} + (\Delta A_\delta - L_k \Delta C_\delta)\bar{x}_k) = \rho_{k+1} - z_{k+1}^\top P z_{k+1}$ and $F_1(z_k) = \rho_k - z_k^\top P z_k$. Using the S-Procedure defined in [19], the expression (5.42) is verified if there exists $\beta > 0$ such that
$F_0(z_k) - \beta F_1(z_k) \geq 0$, $\forall \omega_k \in \mathbf{B}^{n_x+n_y}$, $\forall A_\delta \in [A]$ and $\forall C_\delta \in [C]$,
which is equivalent to

$$z_{k+1}^\top P z_{k+1} + \beta(\rho_k - z_k^\top P z_k) \leq \rho_{k+1}, \quad \forall \omega_k \in \mathbf{B}^{n_x+n_y}, \forall A_\delta \in [A] \text{ and } \forall C_\delta \in [C].$$

Using the expression (5.41), this is further equivalent to $z_k^\top A_{L_k}^\top P A_{L_k} z_k + (\eta_{L_k} + (\Delta A_\delta - L_k \Delta C_\delta)\bar{x}_k)^\top P(\eta_{L_k} + (\Delta A_\delta - L_k \Delta C_\delta)\bar{x}_k) + 2(\eta_{L_k} + (\Delta A_\delta - L_k \Delta C_\delta)\bar{x}_k)^\top P A_{L_k} z_k - \beta z_k^\top P z_k - \rho_{k+1} + \beta \rho_k \leq 0$, $\forall \omega_k \in \mathbf{B}^{n_x+n_y}$, $\forall A_\delta \in [A]$ and $\forall C_\delta \in [C]$, which can be rewritten as

$$\begin{bmatrix} z_k \\ 1 \end{bmatrix}^\top \begin{bmatrix} A_{L_k}^\top P A_{L_k} - \beta P & * \\ (\eta_{L_k} + (\Delta A_\delta - L_k \Delta C_\delta)\bar{x}_k)^\top P A_{L_k} & \gamma \end{bmatrix} \begin{bmatrix} z_k \\ 1 \end{bmatrix} \prec 0, \tag{5.43}$$

with $\gamma = -\rho_{k+1} + \beta\rho_k + (\eta_{L_k} + (\Delta A_\delta - L_k \Delta C_\delta)\bar{x}_k)^\top P(\eta_{L_k} + (\Delta A_\delta - L_k \Delta C_\delta)\bar{x}_k)$, $\forall \omega_k \in \mathbf{B}^{n_x+n_y}$, $\forall A_\delta \in [A]$, $\forall C_\delta \in [C]$ and $\forall z_k \in \mathbb{R}^{n_x}$. The expression (5.43) is verified, $\forall z_k \in \mathbb{R}^{n_x}$, if:

$$\begin{bmatrix} -A_{L_k}^\top P A_{L_k} + \beta P & * \\ -(\eta_{L_k} + (\Delta A_\delta - L_k \Delta C_\delta)\bar{x}_k)^\top P A_{L_k} & -\gamma \end{bmatrix} \succ 0,$$

$\forall \omega_k \in \mathbf{B}^{n_x+n_y}$, $\forall A_\delta \in [A]$ and $\forall C_\delta \in [C]$, or equivalently to:

$$\begin{bmatrix} \beta P & 0 \\ 0 & \rho_{k+1} - \beta\rho_k \end{bmatrix} - \tilde{A}^\top P^{-1} \tilde{A} \succ 0,$$

$\forall \omega_k \in \mathbf{B}^{n_x+n_y}$, $\forall A_\delta \in [A]$ and $\forall C_\delta \in [C]$, with
$\tilde{A} = \begin{bmatrix} PA_{L_k} & P(\eta_{L_k} + (\Delta A_\delta - L_k \Delta C_\delta)\bar{x}_k) \end{bmatrix}$. Applying the Schur complement leads to

$$\begin{bmatrix} \beta P & * & * \\ 0 & \rho_{k+1} - \beta\rho_k & * \\ PA_{L_k} & P(\eta_{L_k} + (\Delta A_\delta - L_k \Delta C_\delta)\bar{x}_k) & P \end{bmatrix} \succ 0,$$

$\forall \omega_k \in \mathbf{B}^{n_x+n_y}$, $\forall A_\delta \in [A]$, $\forall C_\delta \in [C]$.
Using the explicit formulation of A_{L_k}, η_{L_k} and Y_k, the equivalent expression follows

$$\begin{bmatrix} \beta P & * & * \\ 0 & \rho_{k+1} - \beta\rho_k & * \\ PA_\delta - Y_k C_\delta & (PE - Y_k F)\omega_k + P(\Delta A_\delta - L_k \Delta C_\delta)\bar{x}_k & P \end{bmatrix} \succ 0, \quad (5.44)$$

$\forall \omega_k \in \mathbf{B}^{n_x+n_y}$, $\forall A_\delta \in [A]$, $\forall C_\delta \in [C]$.

Pre-multiplying and post-multiplying equation (5.36) by P and $\bar{x}_k$ and post-multiplying equation (5.37) by $\bar{x}_k$, respectively, gives

$$\begin{aligned} P\Delta A_\delta \bar{x}_k = P \sum_{i=1}^{n_{A_\delta}} A_{\delta_i} \delta_i \bar{x}_k = \sum_{i=1}^{n_{A_\delta}} PA_{\delta_i} \bar{x}_k \delta_i, \\ \Delta C_\delta \bar{x}_k = \sum_{i=1}^{n_{C_\delta}} C_{\delta_i} \delta_i \bar{x}_k = \sum_{i=1}^{n_{C_\delta}} C_{\delta_i} \bar{x}_k \delta_i. \end{aligned} \quad (5.45)$$

These expressions are equivalent to

$$\begin{aligned} P\Delta A_\delta \bar{x}_k = \mathcal{A}_k \delta_A, \\ \Delta C_\delta \bar{x}_k = \mathcal{C}_k \delta_C, \end{aligned} \quad (5.46)$$

where $\mathcal{A}_k = \begin{bmatrix} PA_{\delta_1}\bar{x}_k & \dots & PA_{\delta_{n_{A_\delta}}}\bar{x}_k \end{bmatrix} \in \mathbb{R}^{n_x \times n_{A_\delta}}$ and $\mathcal{C}_k = \begin{bmatrix} C_{\delta_1}\bar{x}_k & \dots & C_{\delta_{n_{C_\delta}}}\bar{x}_k \end{bmatrix} \in \mathbb{R}^{n_y \times n_{C_\delta}}$, with $\delta_A = \begin{bmatrix} \delta_1 & \dots & \delta_{n_{A_\delta}} \end{bmatrix}^\top \in \mathbb{R}^{n_{A_\delta}}$ and $\delta_C = \begin{bmatrix} \delta_1 & \dots & \delta_{n_{C_\delta}} \end{bmatrix}^\top \in \mathbb{R}^{n_{C_\delta}}$.
Replacing (5.46) in (5.44) gives:
$\begin{bmatrix} \beta P & * & * \\ 0 & \rho_{k+1} - \beta\rho_k & * \\ PA_\delta - Y_k C_\delta & (PE - Y_k F)\omega_k + \mathcal{A}_k \delta_A - Y_k \mathcal{C}_k \delta_C & P \end{bmatrix} \succ 0, \forall \omega_k \in \mathbf{B}^{n_x+n_y}$, $\delta_A \in \mathbf{B}^{n_{A_\delta}}$, $\delta_C \in \mathbf{B}^{n_{C_\delta}}$, $\forall A_\delta \in [A]$, $\forall C_\delta \in [C]$, or equivalently:

$$\begin{bmatrix} \beta P & * & * \\ 0 & \rho_{k+1} - \beta\rho_k & * \\ PA_\delta - Y_k C_\delta & \begin{bmatrix} PE - Y_k F & \mathcal{A}_k & -Y_k \mathcal{C}_k \end{bmatrix} r & P \end{bmatrix} \succ 0, \quad (5.47)$$

$\forall A_\delta \in [A]$, $\forall C_\delta \in [C]$, $\forall r \in \mathbf{B}^{n_x+n_y+n_\delta}$, with $r = \begin{bmatrix} \omega_k^\top & \delta_A^\top & \delta_C^\top \end{bmatrix}^\top$.

Pre-multiplying and post multiplying inequality (5.47) by $\begin{bmatrix} I & 0 & 0 \\ 0 & 0 & I \\ 0 & I & 0 \end{bmatrix}$ leads to

$$\begin{bmatrix} \beta P & * & * \\ PA_\delta - Y_k C_\delta & P & * \\ 0 & r^\top G_k^\top & \rho_{k+1} - \beta\rho_k \end{bmatrix} \succ 0 \tag{5.48}$$

$\forall r \in \mathbf{B}^{n_x+n_y+n_\delta}$ with $\rho_{k+1}-\beta\rho_k > 0$ and $G_k = \begin{bmatrix} PE - Y_k F & \mathcal{A}_k & -Y_k\mathcal{C}_k \end{bmatrix} \in \mathbb{R}^{n_x\times(n_x+n_\delta)}$. Applying the Schur complement gives

$$\begin{bmatrix} \beta P & * \\ PA_\delta - Y_k C_\delta & P - G_k r \dfrac{1}{\rho_{k+1} - \beta\rho_k} r^\top G_k^\top \end{bmatrix} \succ 0, \tag{5.49}$$

$\forall r \in \mathbf{B}^{n_x+n_y+n_\delta}$ with $\rho_{k+1} - \beta\rho_k > 0$. Applying *Property* 5.1 to the term $r\dfrac{1}{\rho_{k+1} - \beta\rho_k} r^\top$, with $\rho = \rho_{k+1} - \beta\rho_k$, means that $\exists S = S^\top \succ 0$ such that

$$r\frac{1}{\rho_{k+1} - \beta\rho_k} r^\top \prec S^{-1}$$

or equivalently:

$$-r\frac{1}{\rho_{k+1} - \beta\rho_k} r^\top \succ -S^{-1}, \text{ with } \rho_{k+1} - \beta\rho_k > 0.$$

Therefore, the following expression is verified

$$\begin{bmatrix} \beta P & * \\ PA_\delta - Y_k C_\delta & P - G_k S^{-1} G_k^\top \end{bmatrix} \succ 0, \tag{5.50}$$

$\forall r \in \mathbf{B}^{n_x+n_y+n_\delta}$, with $S \succ 0$. The constraint (5.50) can be further decomposed into

$$\begin{bmatrix} \beta P & * \\ PA_\delta - Y_k C_\delta & P \end{bmatrix} - \begin{bmatrix} 0 \\ G_k \end{bmatrix} S^{-1} \begin{bmatrix} 0 & G_k^\top \end{bmatrix} \succ 0, \tag{5.51}$$

with $S \succ 0$, $\forall r \in \mathbf{B}^{n_x+n_y+n_\delta}$. Applying the Schur Complement and replacing $G_k = \begin{bmatrix} PE - Y_k F & \mathcal{A}_k & -Y_k\mathcal{C}_k \end{bmatrix}$ leads to expression (5.38). Since A_δ and C_δ appear in an affine way in the LMI (5.51), the inequality is satisfied if and only if it is verified for all the vertices of $[A]$ and $[C]$. □

Given a scalar $\beta \in (0, 1)$ in the first step, an initialization is required to fix the positive definite matrix P.

***Remark* 5.5.** *(Initialisation)* Given the rate of the estimation convergence $\beta \in (0,1)$, the initial state x_0, the center $\bar{x}_0$ and the radius ρ_0 of the initial ellipsoid, the matrix P is computed off-line in the first step (i.e. $k=0$) by solving the following optimization problem:

$\min\limits_{P,S,Y_0,\rho_1} \rho_1$

subject to

$$\left\{ \begin{array}{l} \left[\begin{array}{ccc} \beta P & * & * \\ PA_\delta - Y_0 C & P & * \\ & \left[\begin{array}{c} E^\top P - F^\top Y_0^\top \\ \mathcal{A}_0^\top \\ -\mathcal{C}_0^\top Y_0^\top \end{array} \right] & \\ 0 & & S \end{array} \right] \succ 0, \\ \rho_1 - \beta\rho_0 > 0, \end{array} \right. \tag{5.52}$$

where $\mathcal{A}_0 = \left[\begin{array}{ccc} PA_{\delta_1}\bar{x}_0 & ... & PA_{\delta_{n_\delta}}\bar{x}_0 \end{array} \right]$, $\forall A_\delta \in [A]$, with the following notations:

$$Y_0 = PL_0, \tag{5.53}$$

$$\bar{x}_1 = mid[A]\bar{x}_0 + L_0(y_0 - mid[C]\bar{x}_0) \tag{5.54}$$

This initialization fixes the matrix P which the shape matrix of the ellipsoidal estimation set.

***Remark* 5.6.** The number of scalar decision variables in the problem (5.38) is equal to $2 + n_x n_y + (n_x + n_y + n_\delta)^2$ and equal to $1 + \frac{n_x \times (n_x - 1)}{2} + n_x n_y + (n_x + n_y + n_\delta)^2$ for the initialization problem (5.52).

***Remark* 5.7.** *(Vertex reduction)* The LMI problem (5.38) has to be verified in 2^{n_δ} vertices. In the general case when all the elements of the matrices A_δ and C_δ have interval uncertainties, the value of n_δ is equal to $n_x^2 + n_x n_y$. In order to reduce the number of vertices to be verified from 2^{n_δ} to 2^{4n_x}, the following optimization problem can be solved (applying the matrix scaling technique of *Theorem 1* of [4]):

$\min\limits_{\beta,Y_k,S,\rho_{k+1}} \rho_{k+1}$

subject to

$$\left\{ \begin{array}{l} \left[\begin{array}{ccc} \beta P & * & * \\ P\, mid[A] - Y_k mid[C] & P & * \\ 0 & \Xi_1^\top & S \end{array} \right] + \left[\begin{array}{ccc} 0 & * & * \\ \Xi_2 & 0 & * \\ 0 & 0 & 0 \end{array} \right] \succ 0, \\ \rho_{k+1} - \beta\rho_k > 0, \\ \beta < 1, \end{array} \right. \tag{5.55}$$

where

$$\begin{cases} \Xi_1 = \begin{bmatrix} PE - Y_k F & \mathcal{A}_k & -Y_k \mathcal{C}_k \end{bmatrix}, \\ \Xi_2 = \Delta_2 \; P \; rad[A] \Delta_1 + \Delta_4 \; Y_k \; rad[C] \Delta_3, \end{cases} \tag{5.56}$$

$\forall \Delta_1 \in \mathbf{\Delta}_{n_x}$, $\forall \Delta_2 \in \mathbf{\Delta}_{n_x}$, $\forall \Delta_3 \in \mathbf{\Delta}_{n_x}$ and $\forall \Delta_4 \in \mathbf{\Delta}_{n_x}$, with $\mathbf{\Delta}_{n_x}$ the set of $n_x \times n_x$ diagonal matrices with diagonal entries equal to 1 or -1.

Example 5.2 shows the performances of the proposed ellipsoidal state estimation approach (5.38).

***Example* 5.2.** Consider the following linear discrete-time invariant system:

$$\begin{cases} x_{k+1} = \begin{bmatrix} 0.7 + 0.3\delta_1 & 0.1 + 0.1\delta_2 \\ 0.6 + 0.1\delta_3 & 0.2 + 0.1\delta_4 \end{bmatrix} x_k + \begin{bmatrix} 0.05 & 0 & 0 & 0 \\ 0 & 0.02 & 0 & 0 \end{bmatrix} \omega_k \\ y_k = \begin{bmatrix} -2 + 0.1\delta_5 & 1 \\ 1 & 1 + 0.1\delta_6 \end{bmatrix} x_k + \begin{bmatrix} 0 & 0 & 0.05 & 0 \\ 0 & 0 & 0 & 0.05 \end{bmatrix} \omega_k \end{cases} \tag{5.57}$$

with the following bounds $\|\omega_k\|_\infty \leq 1$, $|\delta_i| < 1$, $i = 1, \ldots, 6$. The value of ω_k is randomly generated. The initial state belongs to the ellipsoid $\mathcal{E}(P_0, \bar{x}_0, \rho_0)$, with $P_0 = I_2$, $\bar{x}_0 = \begin{bmatrix} 0 & 0 \end{bmatrix}^\top$ and $\rho_0 = 1$ which is sufficiently large to contain the initial state. $\beta = 0.7$ in the first step as mentioned in Remark 5.5.

In this example, the results obtained by the proposed approach (5.38) are compared in terms of accuracy and complexity to the results obtained by the zonotopic estimation based on the minimization of the P-radius [66]. The order of the zonotope is limited to $m \leq 20$ (20 segments).

Note that the P-radius zonotopic estimation method is developed in the case of a constant known observation matrix C (only the evolution matrix A_δ is uncertain). To summarize, an interval matrix C_δ is used with the ellipsoidal estimation method (5.38), while a fixed matrix C is used with the zonotopic estimation [66]. So, the exact matrix C is used for the P-radius zonotopic estimation method while the unknown C_δ is considered for the proposed ellipsoidal estimation method.

Figures 5.13 and 5.14 illustrate the bounds of x_1 and x_2 after 50 iterations obtained by the ellipsoidal *Method 3* and the P-radius-based zonotopic estimation.

The blue dashed lines are obtained by the zonotopic estimation based on the zonotope P-radius minimization, the magenta dotted lines are obtained using the ellipsoidal estimation based on the minimization of the ellipsoid radius (5.38). The red stars, representing the real state of the system are situated inside the estimated bounds, which validates the guaranteed estimation.

In order to facilitate the comparison between theses methods, Figures 5.15 and 5.16 illustrate the bounds widths of x_1 and x_2, respectively. The zonotopic P-radius based method is considered as reference. The best accuracy of the estimation is obtained using *Method 3*.

Figure 5.17 compares the volume of the state estimation sets. The volume obtained by the ellipsoidal estimation is less than the volume of the estimation set obtained by the P-radius-based zonotopic estimation method (a gain of 47%) even in the case when more uncertainties have been considered for the ellipsoidal approach.

The proposed methods offer a good accuracy compared to the P-radius-based zonotopic estimation [66] but with increased complexity due to the online computation of the ellipsoidal radius (see Table 5.2). The mean computation time of one iteration is equal to: 0.1s for the ellipsoidal method (5.38) considering interval uncertainties both in A et C matrices and 0.02s using the P-radius-based zonotopic estimation considering interval uncertainties only in the A matrix.

Table 5.2: Total computation time after 50 time instants

Algorithm	Time (second)
P-radius-based zonotopic estimation	0.92
Ellipsoidal method (5.38)	5.31

The *Method 3* gives a better estimation than the estimation obtained by the P-radius zonotopic estimation due to the minimization of the radius at each sample time, but with higher computation time.

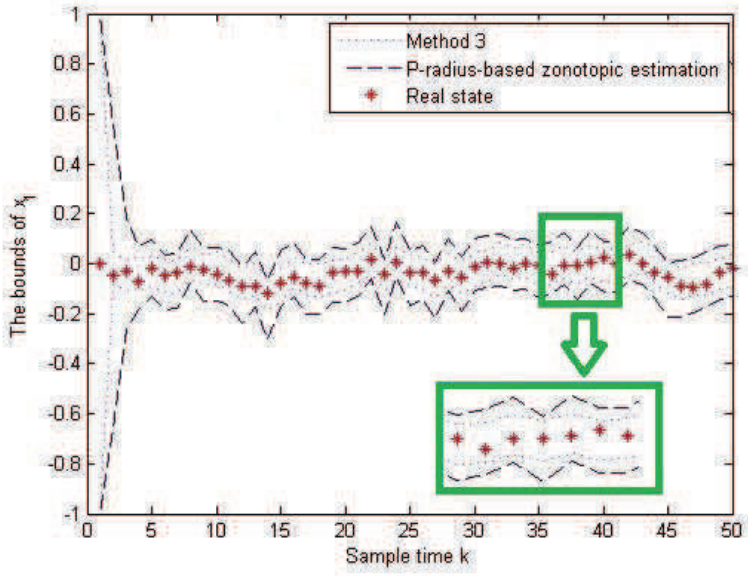

Figure 5.13: Bounds of x_1

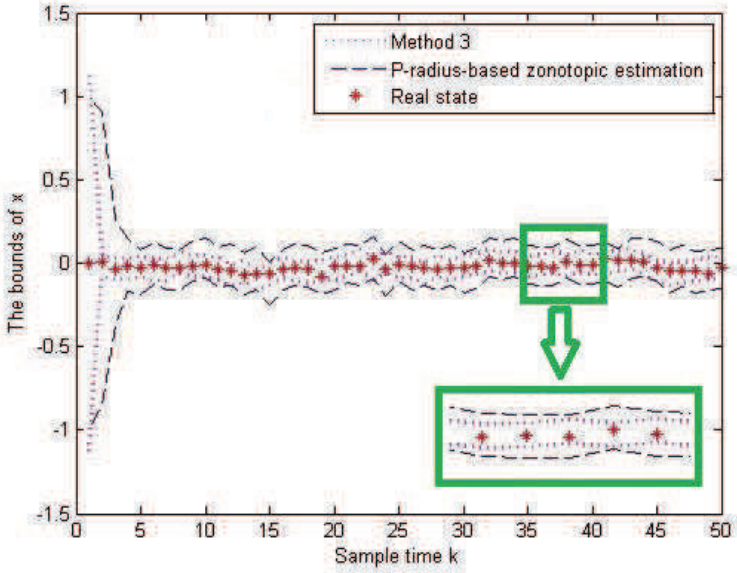

Figure 5.14: Bounds of x_2

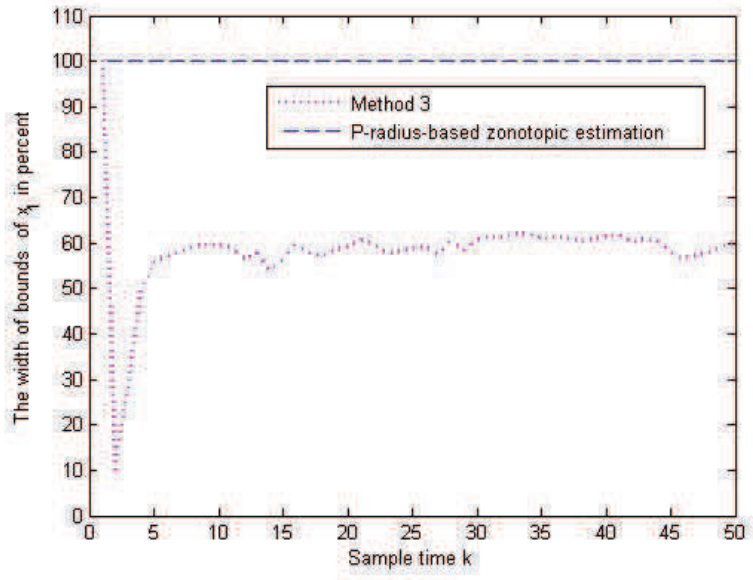

Figure 5.15: Comparison of the bounds width of x_1

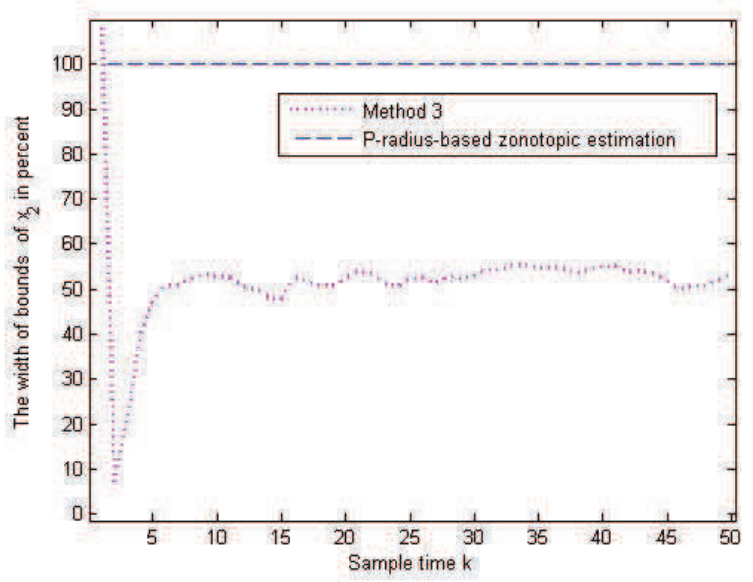

Figure 5.16: Comparison of the bounds width of x_2

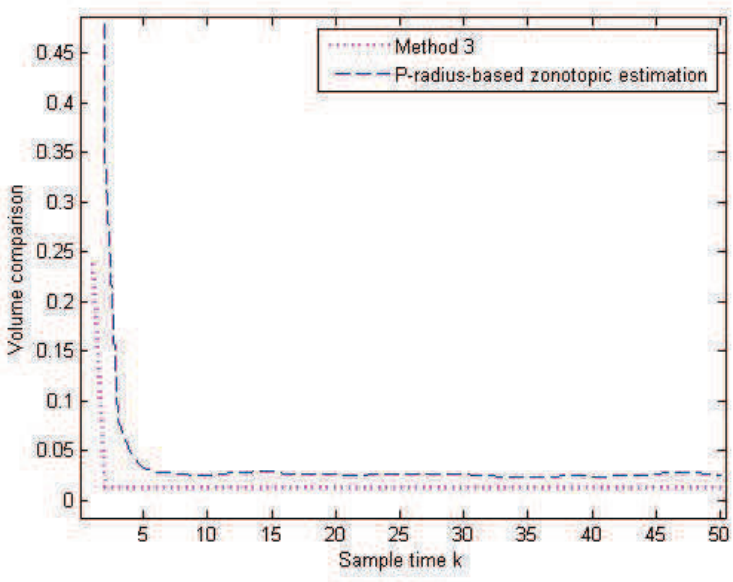

Figure 5.17: Comparison of the volume of the state estimation sets

5.4 Linear Time Variant systems

The aim of this section is to extend the previous state-estimation techniques to the case of linear time-variant systems with interval uncertainties, bounded perturbations and measurement noises. The novelty here (compared to Section 5.2 and Section 5.3) consists in considering a variable shape matrix for the ellipsoidal state estimation set in order to improve the accuracy of the estimation [14].

Consider the following linear discrete-time variant system:

$$\begin{cases} x_{k+1} = A_k x_k + E\omega_k \\ y_k = C_k x_k + F\omega_k \end{cases} \tag{5.58}$$

where $x_k \in \mathbb{R}^{n_x}$ is the state vector of the system and $y_k \in \mathbb{R}^{n_y}$ is the measured output vector at sample time k. The vector $\omega_k \in \mathbb{R}^{n_x+n_y}$ contains both the state perturbations and the measurement perturbations (noise, offset, etc.), which are non-correlated. It is assumed that the perturbations ω_k are bounded by the unitary box $\mathbf{B}^{n_x+n_y}$ and the initial state x_0 is bounded by the ellipsoid: $\mathcal{E}(P_0, \bar{x}_0, \rho_0) = \{x \in \mathbb{R}^{n_x} : (x - \bar{x}_0)^\top P_0 (x - \bar{x}_0) \leq \rho_0\}$. Matrices A_k, C_k, E and F have the appropriate dimensions. A_k and C_k are unknown time-varying matrices belonging to interval matrices $[A]$ and $[C]$.

At time $k > 0$, consider an ellipsoid $\mathcal{E}(P_k, \bar{x}_k, \rho_k)$ that contains the real system state x_k, with $\bar{x}_k$ the nominal estimated set. Note that the shape matrix P_k of the ellipsoid $\mathcal{E}(P_k, \bar{x}_k, \rho_k)$ depends on time instant k contrary to Section 5.2 and Section 5.3. The aim of this section is to provide at time $k+1$ an optimal ellipsoidal estimation $\mathcal{E}(P_{k+1}, \bar{x}_{k+1}, \rho_{k+1})$ that guarantees to contain the state x_{k+1}.

5.4.1 *Method 4*: ellipsoidal state estimation method with vector scaling technique and flexible shape matrix

This method consists in minimizing the size of the ellipsoidal estimation set by solving an online Linear Matrix Inequality (LMI) problem, while allowing to adjust the shape of the ellipsoid, which reduces the conservativeness of the estimation. This method based on the use of the S-procedure for quadratic functions [19] is applied on linear time-varying systems with interval uncertainties, bounded perturbations and measurement noises. The following theorem formulates the solution to this problem.

***Theorem* 5.4.** Considering the system (5.58), if the following assumptions hold:

(i) At time k, the system state x_k belongs to the ellipsoid $\mathcal{E}(P_k, \bar{x}_k, \rho_k)$;

(ii) At time k, the considered uncertainties are bounded by a convex set Ω_k, i.e. $(\omega_k, A_k, C_k) \in \Omega_k$, with $\mathcal{V}_{\Omega_k}$ denoting the vertices of Ω_k;

(iii) There exist the matrices $P_{k+1} = P_{k+1}^\top \succ 0$ with $P_{k+1} \in \mathbb{R}^{n_x \times n_x}$, $Y_{k+1} \in \mathbb{R}^{n_x \times n_y}$, $G_{k+1} \in \mathbb{R}^{n_x \times n_x}$, the vector $g_{k+1} \in \mathbb{R}^{n_x}$ and the positive scalars $\beta_{k+1}, \rho_{k+1} > 0$ such that the following LMI is satisfied for every $(\omega_k, A_k, C_k) \in \mathcal{V}_{\Omega_k}$:

$$\begin{bmatrix} \beta_{k+1}P_k & * & * \\ 0 & \rho_{k+1} - \beta_{k+1}\rho_k & * \\ P_{k+1}A_k - Y_{k+1}C_k & \tau_{k+1} & P_{k+1} \end{bmatrix} \succ 0, \tag{5.59}$$

with $\tau_{k+1} = (P_{k+1}A_k - Y_{k+1}C_k - G_{k+1})\bar{x}_k + (P_{k+1}E - Y_{k+1}F)\omega_k - g_{k+1}$;

then, at time $k+1$, the system state x_{k+1} belongs to the ellipsoid $\mathcal{E}(P_{k+1}, \bar{x}_{k+1}, \rho_{k+1})$, with $\bar{x}_{k+1} = P_{k+1}^{-1}(G_{k+1}\bar{x}_k + Y_{k+1}y_k + g_{k+1})$.

Proof

Denote by $z_k = x_k - \bar{x}_k$ the error between the real state and the nominal estimated state at time k. At time instant $k+1$, the error z_{k+1} is computed as follows

$$z_{k+1} = x_{k+1} - \bar{x}_{k+1} = A_k x_k + E\omega_k - P_{k+1}^{-1}(G_{k+1}\bar{x}_k + Y_{k+1}y_k + g_{k+1}).$$

Denoting $P_{k+1}^{-1}Y_{k+1} = L_{k+1}$ gives

$$z_{k+1} = A_k x_k + E\omega_k - L_{k+1}y_k - P_{k+1}^{-1}(G_{k+1}\bar{x}_k + g_{k+1}).$$

Then, replacing y_k as in (5.58) leads to

$$z_{k+1} = A_k x_k + E\omega_k - L_{k+1}C_k x_k - L_{k+1}F\omega_k - P_{k+1}^{-1}(G_{k+1}\bar{x}_k + g_{k+1}),$$

which, after regrouping the terms in z_k, ω_k and $\bar{x}_k$, is equivalent to

$$z_{k+1} = (A_k - L_{k+1}C_k)z_k + (A_k - L_{k+1}C_k)\bar{x}_k + (E - L_{k+1}F)\omega_k - P_{k+1}^{-1}(G_{k+1}\bar{x}_k + g_{k+1}).$$

Then, highlighting the error z_k, an equivalent form is obtained

$$z_{k+1} = \tilde{A}_{L_{k+1}} z_k + \tilde{\eta}_{k+1}, \tag{5.60}$$

with:

$$\begin{aligned} \tilde{A}_{L_{k+1}} &= A_k - L_{k+1}C_k \\ \tilde{\eta}_{k+1} &= (A_k - L_{k+1}C_k)\bar{x}_k + (E - L_{k+1}F)\omega_k - P_{k+1}^{-1}(G_{k+1}\bar{x}_k + g_{k+1}). \end{aligned}$$

In order to verify the result, the next step is to prove the following expression

$$z_k^\top P_k z_k \leq \rho_k \Rightarrow z_{k+1}^\top P_{k+1} z_{k+1} \leq \rho_{k+1}. \tag{5.61}$$

Denote $F_0(z_k) = \rho_{k+1} - z_{k+1}^\top P_{k+1} z_{k+1}$ and $F_1(z_k) = \rho_k - z_k^\top P_k z_k$. Using the S-Procedure, the expression (5.61) is verified if there exists $\beta_{k+1} > 0$ such that $F_0(z_k) - \beta_{k+1}F_1(z_k) \geq 0$, $\forall(\omega_k, A_k, C_k) \in \Omega_k$, which is equivalent to

$$z_{k+1}^\top P_{k+1} z_{k+1} + \beta_{k+1}(\rho_k - z_k^\top P_k z_k) \leq \rho_{k+1}, \quad \forall(\omega_k, A_k, C_k) \in \Omega_k.$$

Using expression (5.60), this is further equivalent to
$z_k^\top(\tilde{A}_{L_{k+1}}^\top P_{k+1}\tilde{A}_{L_{k+1}} - \beta_{k+1}P_k)z_k + 2\tilde{\eta}_{k+1}^\top P_{k+1}\tilde{A}_{L_{k+1}}z_k + \tilde{\eta}_{k+1}^\top P_{k+1}\tilde{\eta}_{k+1} + \beta_{k+1}\rho_k - \rho_{k+1} \leq 0$, $\forall(\omega_k, A_k, C_k) \in \Omega_k$, which can be rewritten as

$$\begin{bmatrix} z_k \\ 1 \end{bmatrix}^\top \begin{bmatrix} \tilde{A}_{L_{k+1}}^\top P_{k+1}\tilde{A}_{L_{k+1}} - \beta_{k+1}P_k & * \\ \tilde{\eta}_{k+1}^\top P_{k+1}\tilde{A}_{L_{k+1}} & \tilde{\eta}_{k+1}^\top P_{k+1}\tilde{\eta}_{k+1} + \beta_{k+1}\rho_k - \rho_{k+1} \end{bmatrix} \begin{bmatrix} z_k \\ 1 \end{bmatrix} \prec 0, \tag{5.62}$$

with $\forall(\omega_k, A_k, C_k) \in \Omega_k$ and $\forall z_k \in \mathbb{R}^{n_x}$. The expression (5.62) is verified, $\forall z_k \in \mathbb{R}^{n_x}$, if

$$\begin{bmatrix} -\tilde{A}_{L_{k+1}}^\top P_{k+1} \tilde{A}_{L_{k+1}} + \beta_{k+1} P_k & * \\ -\tilde{\eta}_{k+1}^\top P_{k+1} \tilde{A}_{L_{k+1}} & -\tilde{\eta}_{k+1}^\top P_{k+1} \tilde{\eta}_{k+1} - \beta_{k+1}\rho_k + \rho_{k+1} \end{bmatrix} \succ 0,$$

$\forall(\omega_k, A_k, C_k) \in \Omega_k$, or equivalently if

$$\begin{bmatrix} \beta_{k+1} P_k & 0 \\ 0 & \rho_{k+1} - \beta_{k+1}\rho_k \end{bmatrix} - \begin{bmatrix} \tilde{A}_{L_{k+1}}^\top P_{k+1} \\ \tilde{\eta}_{k+1}^\top P_{k+1} \end{bmatrix} P_{k+1}^{-1} \begin{bmatrix} P_{k+1}\tilde{A}_{L_{k+1}} & P_{k+1}\tilde{\eta}_{k+1} \end{bmatrix} \succ 0,$$

$\forall(\omega_k, A_k, C_k) \in \Omega_k$. Applying the Schur complement leads to

$$\begin{bmatrix} \beta_{k+1} P_k & * & * \\ 0 & \rho_{k+1} - \beta_{k+1}\rho_k & * \\ P_{k+1}\tilde{A}_{L_{k+1}} & P_{k+1}\tilde{\eta}_{k+1} & P_{k+1} \end{bmatrix} \succ 0, \quad \forall(\omega_k, A_k, C_k) \in \Omega_k.$$

Taking into account that $P_{k+1}\tilde{A}_{L_{k+1}} = P_{k+1}A_k - Y_{k+1}C_k$ and that

$$P_{k+1}\tilde{\eta}_{k+1} = (P_{k+1}A_k - Y_{k+1}C_k)\bar{x}_k + (P_{k+1}E - Y_{k+1}F)\omega_k - G_{k+1}\bar{x}_k - g_{k+1},$$

the following equivalent expression is found

$$\begin{bmatrix} \beta_{k+1} P_k & * & * \\ 0 & \rho_{k+1} - \beta_{k+1}\rho_k & * \\ P_{k+1}A_k - Y_{k+1}C_k & \tau_{k+1} & P_{k+1} \end{bmatrix} \succ 0, \quad \forall(\omega_k, A_k, C_k) \in \Omega_k, \tag{5.63}$$

where $\tau_{k+1} = (P_{k+1}A_k - Y_{k+1}C_k - G_{k+1})\bar{x}_k + (P_{k+1}E - Y_{k+1}F)\omega_k - g_{k+1}$. Since ω_k, A_k and C_k appear in an affine way in the LMI (5.63), the inequality is satisfied if and only if it is verified for all the vertices of Ω_k. □

***Remark* 5.8.** Some constraints on the matrix P_{k+1} and the radius ρ_{k+1} are added to the feasibility problem (5.59) in order to reduce the size of the ellipsoidal state estimation set. The LMI optimization problem to solve in this case is the following:

$$\min_{\beta_{k+1}, Y_{k+1}, P_{k+1}, \rho_{k+1}, G_{k+1}, g_{k+1}, \alpha, \gamma} \alpha$$

subject to

$$\begin{cases} \begin{bmatrix} \beta_{k+1} P_k & * & * \\ 0 & \rho_{k+1} - \beta_{k+1}\rho_k & * \\ P_{k+1}A_k - Y_{k+1}C_k & \tau_{k+1} & P_{k+1} \end{bmatrix} \succ 0, \\ P_{k+1} \geq P_k, \\ \rho_{k+1} \leq \alpha\rho_k + \gamma, \\ 0 < \alpha < 1, \\ \gamma > 0, \end{cases} \tag{5.64}$$

where $\tau_{k+1} = (P_{k+1}A_k - Y_{k+1}C_k - G_{k+1})\bar{x}_k + (P_{k+1}E - Y_{k+1}F)\omega_k - g_{k+1}$, $\forall(\omega_k, A_k, C_k) \in \Omega_k$ and $\bar{x}_{k+1} = P_{k+1}^{-1}(G_{k+1}\bar{x}_k + Y_{k+1}y_k + g_{k+1})$.

The constraint $\rho_{k+1} \leq \alpha\rho_k + \gamma$, with $\alpha \in (0, 1)$ and $\gamma > 0$, serves to bound the radius of the ellipsoidal estimation set $\mathcal{E}(P_{k+1}, x_{k+1}, \rho_{k+1})$ and then to reduce the size of this set. Here, the positive scalar γ serves to bound the effect of the additive terms. Using the matrix P_{k+1} as a decision variable offers the possibility to modify the shape of the ellipsoid $\mathcal{E}(P_{k+1}, x_{k+1}, \rho_{k+1})$ at time $k+1$ compared to the ellipsoid $\mathcal{E}(P_k, x_k, \rho_k)$ at time k. This allows an additional degree of freedom compared to the three previous ellipsoidal state estimation techniques (*Method 1*, *Method 2* and *Method 3*).

***Remark* 5.9.** The number of scalar decision variables in the problem (5.64) is equal to $4 + n_x(n_y + \frac{3}{2}n_x + \frac{3}{2})$.

***Remark* 5.10.** The LMI problem (5.64) has to be verified in $2^{n_{A_\delta}+n_{C_\delta}+n_x+n_y}$ vertices (where n_{A_δ} and n_{C_δ} are the number of scalar interval uncertainties in the interval matrices A_k and C_k, respectively). In the general case, when all the elements of the matrices A_k and C_k have interval uncertainties, the number of scalar interval uncertainties $n_{A_\delta} + n_{C_\delta}$ is equal to $n_x^2 + n_x n_y$. In order to reduce the number of vertices to be verified, the matrix scaling technique in *Theorem 1* of [4] can be applied.

5.4.2 *Improved Method 4*

The state estimation (5.64) computes the ellipsoidal set $\mathcal{E}(P_{k+1}, \bar{x}_{k+1}, \rho_{k+1})$ using the measurements y_k. It is convenient to the adjustment of the ellipsoidal estimation set the use the measurement y_{k+1} at time $k+1$. This will improve the accuracy of the estimation with respect to (5.64) taking into account the measurement y_{k+1}. To do this, additional quadratic constraints on the output measurement taking into account the structure of the perturbations and the measurement noise allow to improve the accuracy of the estimation. Starting from the ellipsoidal state estimation (5.64), the idea is to consider supplementary quadratic constraints on the measurement y_{k+1} and on the perturbations ω_{k+1} in order to compute the new ellipsoidal state estimation set. This is similar to a correction step based on the measurements at time $k+1$.

Consider the ellipsoidal estimation set $\mathcal{E}(P_{k+1}, \bar{x}_{k+1}, \rho_{k+1})$ obtained at sample time $k+1$ by the ellipsoidal estimation method (5.64) and the following measurements:

$$y_{k+1} - C_{k+1}x_{k+1} = F\omega_{k+1}, \tag{5.65}$$

and the perturbations $\omega_{k+1} \in \mathbf{B}^{n_x+n_y}$ verifying the following expression:

$$\omega_{k+1}^{\top} T_i \omega_{k+1} \leq 1, \quad i = 1, \ldots, n_x + n_y. \tag{5.66}$$

The objective is to find an updated ellipsoidal estimation set $\mathcal{E}'(P'_{k+1}, \bar{x}'_{k+1}, \rho'_{k+1})$ such that the equations (5.65) and (5.66) hold. The result of this problem is summarized by the following proposition.

***Proposition* 5.2.** Consider the ellipsoidal state estimation set $\mathcal{E}(P_{k+1}, \bar{x}_{k+1}, \rho_{k+1})$ obtained by solving the LMI problem (5.64) for system (5.58) at time $k+1$, based on the information available at time k. If there exist a matrix $P'_{k+1} = P'^{\top}_{k+1} \succ 0$ in $\mathbb{R}^{n_x \times n_x}$, a matrix $H = H^{\top} \succ 0$ in $\mathbb{R}^{n_y \times n_y}$, a vector $\bar{x}'_{k+1} \in \mathbb{R}^{n_x}$ and a real positive scalar $\rho'_{k+1} > 0$ such that the following LMI problem is verified for all $C_{k+1} \in \mathcal{V}_{[C]}$:

$$\begin{cases} \begin{bmatrix} \eta_1 & * & * \\ \eta_2 & \eta_3 - \sum_{i=1}^{n_x+n_y} \mu_i & * \\ P'_{k+1} & -b_{k+1} & P'_{k+1} \end{bmatrix} \succ 0, \\ F^{\top} H F < \sum_{i=1}^{n_x+n_y} \mu_i T_i, \\ \mu_i \geq 0, \quad i = 1, ..., n_x + n_y, \\ \theta \geq 0, \quad \theta < 1, \\ \rho'_{k+1} > \theta \rho_{k+1}, \end{cases} \tag{5.67}$$

with:

$$\begin{aligned} b_{k+1} &= P'_{k+1} \bar{x}'_{k+1} \\ \eta_1 &= \theta P_{k+1} + C_{k+1}^{\top} H C_{k+1} \\ \eta_2 &= -\theta \bar{x}_{k+1}^{\top} P_{k+1} - y_{k+1}^{\top} H C_{k+1} \\ \eta_3 &= \rho'_{k+1} - \theta \rho_{k+1} + \theta \|\bar{x}_{k+1}\|^2_{P_{k+1}} + \|y_{k+1}\|^2_H \end{aligned} \tag{5.68}$$

then the updated ellipsoidal state estimation set is $\mathcal{E}'(P'_{k+1}, \bar{x}'_{k+1}, \rho'_{k+1})$.

Proof

Denote $F_0(x_{k+1}) = \rho'_{k+1} - \|x_{k+1} - \bar{x}'_{k+1}\|^2_{P'_{k+1}} > 0$ and $F_1(x_{k+1}) = \rho_{k+1} - \|x_{k+1} - \bar{x}_{k+1}\|^2_{P_{k+1}} > 0$. Using the S-procedure, *Proposition* 5.2 is verified if there exists $\theta \geq 0$, such that $F_0(x_{k+1}) - \theta F_1(x_{k+1}) \geq 0$, for every[4] $\omega_{k+1} \in \mathbf{B}^{n_x+n_y}$ and $C_{k+1} \in [C]$, which is equivalent to

$$\rho'_{k+1} - \|x_{k+1} - \bar{x}'_{k+1}\|^2_{P'_{k+1}} - \theta(\rho_{k+1} - \|x_{k+1} - \bar{x}_{k+1}\|^2_{P_{k+1}}) \geq 0. \tag{5.69}$$

[4]In order to simplify the text, the rigorous notation $\forall \omega_{k+1} \in \mathbf{B}^{n_x+n_y}$ and $\forall C_{k+1} \in [C]$ will be further omitted.

From equation (5.65) it is inferred that, for every matrix $H \succ 0$, the following equality is satisfied

$$\|y_{k+1} - C_{k+1}x_{k+1}\|_H^2 - \|F\omega_{k+1}\|_H^2 = 0. \tag{5.70}$$

Summing (5.69) and (5.70), it gives

$$\begin{gathered}\rho'_{k+1} - \|x_{k+1} - \bar{x}'_{k+1}\|^2_{P'_{k+1}} - \theta(\rho_{k+1} - \|x_{k+1} - \bar{x}_{k+1}\|^2_{P_{k+1}}) - \|F\omega_{k+1}\|_H^2 + \\ + \|y_{k+1} - C_{k+1}x_{k+1}\|_H^2 \geq 0.\end{gathered}$$

Multiplying by -1 and developing $\|x_{k+1} - \bar{x}_{k+1}\|^2_{P_{k+1}}$ and $\|x_{k+1} - \bar{x}_{k+1}\|^2_{P'_{k+1}}$, the previous expression is equivalent to

$$\begin{gathered}\|x_{k+1}\|^2_{P'_{k+1}} - 2\bar{x}'^{\top}_{k+1}P'_{k+1}x_{k+1} + \|\bar{x}'_{k+1}\|^2_{P'_{k+1}} - \rho'_{k+1} + \theta\rho_{k+1} - \theta\|x_{k+1}\|^2_{P_{k+1}} + \\ + 2\theta\bar{x}^{\top}_{k+1}P_{k+1}x_{k+1} - \theta\|\bar{x}_{k+1}\|^2_{P_{k+1}} + \|F\omega_{k+1}\|_H^2 - \|C_{k+1}x_{k+1}\|_H^2 + \\ + 2y^{\top}_{k+1}HC_{k+1}x_{k+1} - \|y_{k+1}\|_H^2 \leq 0.\end{gathered} \tag{5.71}$$

Factorize the expression (5.71) to obtain

$$\begin{gathered}\|x_{k+1}\|^2_{P'_{k+1} - \theta P_{k+1} - C^{\top}_{k+1}HC_{k+1}} + \|\bar{x}'_{k+1}\|^2_{P'_{k+1}} - \rho'_{k+1} + \theta\rho_{k+1} - \theta\|\bar{x}_{k+1}\|^2_{P_{k+1}} + \\ + 2(-\bar{x}'^{\top}_{k+1}P'_{k+1} + \theta\bar{x}^{\top}_{k+1}P_{k+1} + y^{\top}_{k+1}HC_{k+1})x_{k+1} - \|y_{k+1}\|_H^2 + \|F\omega_{k+1}\|_H^2 \leq 0.\end{gathered}$$

With the considered notations of η_1, η_2 and η_3, the previous inequality is equivalent to

$$x^{\top}_{k+1}(P'_{k+1} - \eta_1)x_{k+1} + 2(-\bar{x}'^{\top}_{k+1}P'_{k+1} - \eta_2)x_{k+1} + \|\bar{x}'^{\top}_{k+1}\|^2_{P'_{k+1}} - \eta_3 + \|F\omega_{k+1}\|_H^2 \leq 0,$$

which can be rewritten using the following matrix formulation

$$\begin{bmatrix} x_{k+1} \\ 1 \end{bmatrix}^{\top} \begin{bmatrix} P'_{k+1} - \eta_1 & * \\ -\bar{x}'^{\top}_{k+1}P'_{k+1} - \eta_2 & \Gamma \end{bmatrix} \begin{bmatrix} x_{k+1} \\ 1 \end{bmatrix} \leq 0,$$

with $\Gamma = \|\bar{x}'_{k+1}\|^2_{P'_{k+1}} - \eta_3 + \|F\omega_{k+1}\|_H^2$. The previous inequality is verified if

$$\begin{bmatrix} -P'_{k+1} + \eta_1 & * \\ \bar{x}'^{\top}_{k+1}P'_{k+1} + \eta_2 & -\Gamma \end{bmatrix} \succeq 0.$$

Note that in order to guarantee the ellipsoidal bound, this inequality has to be satisfied for every $x_{k+1} \in \mathbb{R}^{n_x}$, $\omega_{k+1} \in \mathbf{B}^{n_x+n_y}$ and $C_{k+1} \in [C]$. Adding the quadratic constraint on the perturbation of the form $F^{\top}HF \prec \sum_{i=1}^{n_x+n_y} \mu_i T_i$,

and using condition (5.66) allow to remove ω_{k+1} from the previous inequality, i.e.

$$\omega_{k+1}^{\top} F^{\top} H F \omega_{k+1} \leq \omega_{k+1}^{\top} \sum_{i=1}^{n_x+n_y} \mu_i T_i \omega_{k+1} \leq \sum_{i=1}^{n_x+n_y} \mu_i (\omega_{k+1}^{\top} T_i \omega_{k+1}) \leq \leq \sum_{i=1}^{n_x+n_y} \mu_i. \tag{5.72}$$

Then, the following constraint holds

$$\begin{bmatrix} -P'_{k+1} + \eta_1 & * \\ \bar{x}'^{\top}_{k+1} P'_{k+1} + \eta_2 & -\bar{x}'^{\top}_{k+1} P'_{k+1} \bar{x}'_{k+1} + \eta_3 - \sum_{i=1}^{n_x+n_y} \mu_i \end{bmatrix} \succeq 0.$$

Applying the Schur complement to the previous inequality gives

$$\begin{bmatrix} \eta_1 & * & * \\ \eta_2 & \eta_3 - \sum_{i=1}^{n_x+n_y} \mu_i & * \\ P'_{k+1} & -P'_{k+1} \bar{x}'_{k+1} & P'_{k+1} \end{bmatrix} \succ 0.$$

Denoting $b_{k+1} = P'_{k+1} \bar{x}'_{k+1}$ (which becomes a decision variable) leads to

$$\begin{bmatrix} \eta_1 & * & * \\ \eta_2 & \eta_3 - \sum_{i=1}^{n_x+n_y} \mu_i & * \\ P'_{k+1} & -b_{k+1} & P'_{k+1} \end{bmatrix} \succ 0.$$

□

***Remark* 5.11.** In order to decrease the size of the ellipsoidal state estimation set $\mathcal{E}'(P'_{k+1}, \bar{x}'_{k+1}, \rho'_{k+1})$ obtained after solving the feasibility problem (5.67), some constraints (similar to Remark 5.8) on the matrix P_{k+1} and on the radius ρ_{k+1} are added, leading to the following LMI optimization problem:

$$\min_{\rho'_{k+1},P',b_{k+1},H,\theta,\mu_i,\alpha,\gamma} \alpha$$

subject to

$$\begin{cases} \begin{bmatrix} \eta_1 & \eta_2^\top & P'_{k+1} \\ \eta_2 & \eta_3 - \sum\limits_{i=1}^{n_x+n_y} \mu_i & -b_{k+1}^\top \\ P'_{k+1} & -b_{k+1} & P'_{k+1} \end{bmatrix} \succ 0, \\ F^\top H F < \sum\limits_{i=1}^{n_x+n_y} \mu_i T_i, \\ \mu_i \geq 0, \quad i = 1, ..., n_x + n_y, \\ \theta \geq 0, \quad \theta < 1, \\ \rho'_{k+1} > \theta \rho_{k+1}, \\ P'_{k+1} \geq P_{k+1}, \\ \rho_{k+1} \leq \alpha \rho_k + \gamma, \\ 0 < \alpha < 1, \\ \gamma > 0, \end{cases} \tag{5.73}$$

with the notations (5.68).

***Remark* 5.12.** The number of scalar decision variables in the optimization problem (5.73) is equal to $4 + n_x(\frac{1}{2}n_x + \frac{5}{2}) + n_y(\frac{1}{2}n_y + \frac{3}{2})$.

***Remark* 5.13.** It is important to note that the results obtained using the *Methods 1*, *2* and *3* can be improved in the same way as *Method 4*, i.e. by adding quadratic constraints on the measurements y_{k+1}.

Examples 5.3 and 5.4 show the performances of the proposed ellipsoidal state estimation approaches.

***Example* 5.3.** Consider the following linear discrete-time variant system:

$$\begin{cases} x_{k+1} = \begin{bmatrix} 0.7 + 0.3\delta_{1_k} & 0.1 + 0.1\delta_{2_k} \\ 0.6 & 0.2 + 0.1\delta_{3_k} \end{bmatrix} x_k + \begin{bmatrix} 0.05 & 0 & 0 & 0 \\ 0 & 0.02 & 0 & 0 \end{bmatrix} \omega_k \\ y_k = \begin{bmatrix} -2 + 0.1\delta_{4_k} & 1 \\ 1 & 1 + 0.1\delta_{5_k} \end{bmatrix} x_k + \begin{bmatrix} 0 & 0 & 0.05 & 0 \\ 0 & 0 & 0 & 0.05 \end{bmatrix} \omega_k \end{cases} \tag{5.74}$$

with $\|\omega_k\|_\infty \leq 1$, $|\delta_{i_k}| < 1$, $i = 1, \ldots, 5$. The value of ω_k and δ_{i_k} is randomly generated. The initial state belongs to the ellipsoid $\mathcal{E}(P_0, \bar{x}_0, \rho_0)$, with $P_0 = I_2$, $\bar{x}_0 = \begin{bmatrix} 0 & 0 \end{bmatrix}^\top$ and $\rho_0 = 1$, which is sufficiently large to contain the initial state. This example proposes a comparison (in terms of accuracy and complexity) between the state estimation results obtained by *Method 4* and *Improved Method 4*.

Figures 5.18 and 5.19 illustrate the bounds of x_1 and x_2 after 50 iterations obtained by the two considered ellipsoidal estimation methods: *Method 4* (5.64) in black solid line and *Improved Method 4* in magenta dashed line. The red stars, representing the real state of the system are situated inside the estimated bounds, which validates the guaranteed estimation bounds obtained with the proposed techniques. A better accuracy of the estimation is obtained using *Improved Method 4*.

The simulation results have been obtained with an Intel Core $i7-3770$ 3.40 GHz, using the LMI solver *mincx* of MATLAB^{TM}Robust Control Toolbox.

Figure 5.20 compares the volume of the state estimation sets. The smallest volume is obtained via *Improved Method 4*. Thus, *Improved Method 4* offers better accuracy than the *Method 4*, but with higher complexity (see Table 5.3).

Table 5.3: Total computation time after 50 time instants

Algorithm	Time (second)
Method 4	72.23
Improved Method 4	78.36

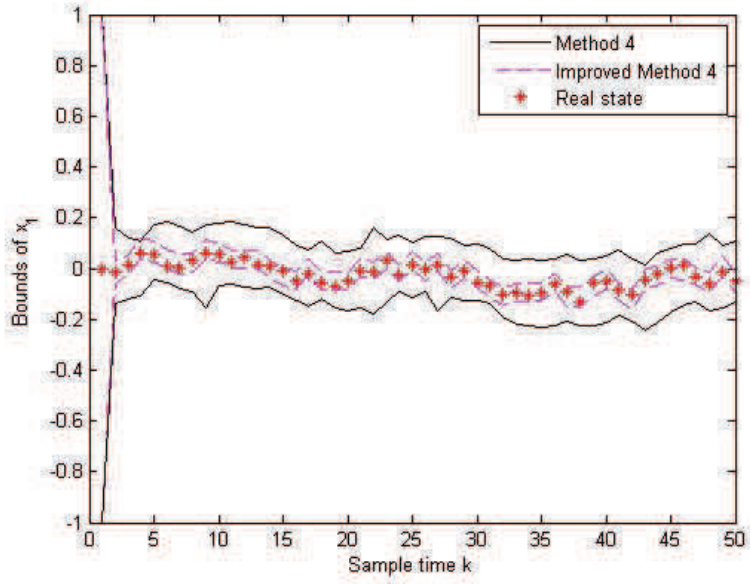

Figure 5.18: Bounds of x_1

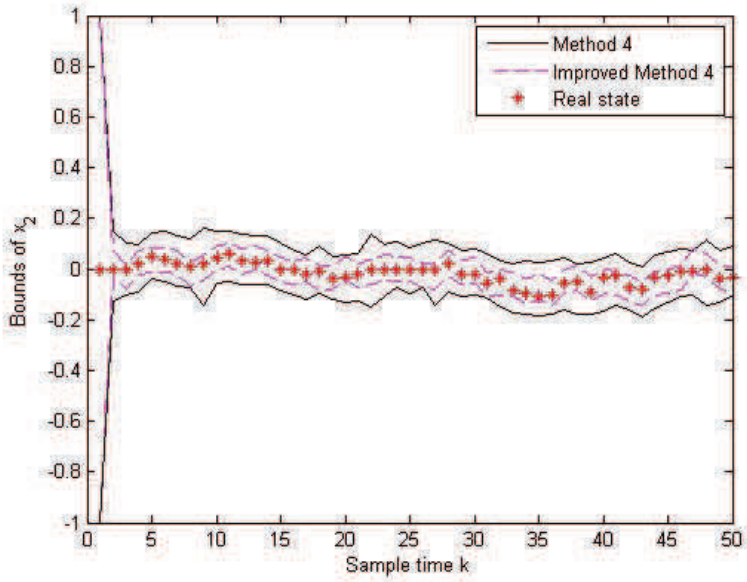

Figure 5.19: Bounds of x_2

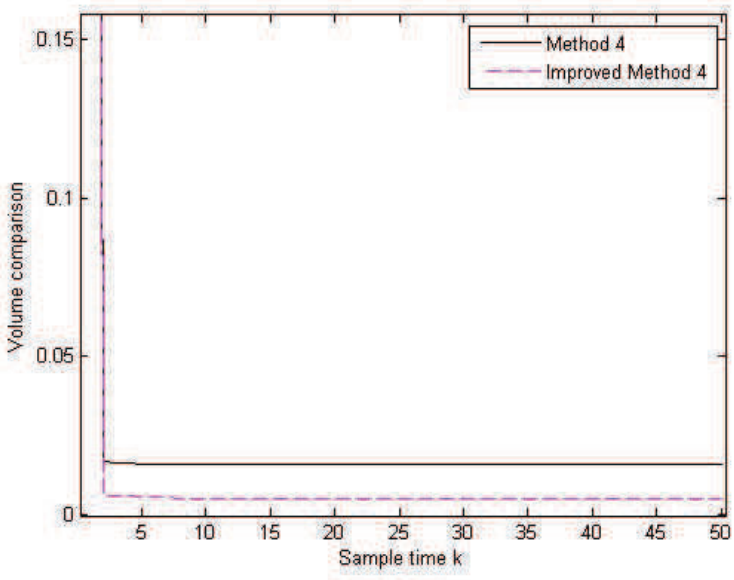

Figure 5.20: Comparison of the volume of the state estimation sets

***Example* 5.4.** This example proposes a comparison of the results obtained with *Method 4*, *Improved Method 4* and an existing zonotopic estimation approach based on the minimization of the P-radius [67]. The order of the zonotope is limited to $m \leq 20$. Due to the fact that the zonotopic estimation method [67] is developed only for interval systems with fixed observation matrices[5], a particular case of the linear discrete-time system (5.74) with a fixed observation matrix $\begin{bmatrix} -2 & 1 \\ 1 & 1 \end{bmatrix}$ will be further considered (i.e. $\delta_{4_k} = \delta_{5_k} = 0$ in (5.74)).

Figures 5.21 and 5.22 illustrate the bounds of x_1 and x_2 after 50 iterations, using the three methods: *Method 4* in black solid line, *Improved Method 4* in magenta dashed line and the zonotopic approach based on the zonotope P-radius minimization [67] in blue dashed line. The real state is represented by red stars and is found inside the estimated bounds.

To facilitate the comparison between these methods, Figures 5.23 and 5.24 illustrate the bounds width of x_1 and x_2, respectively. The P-radius-based zonotopic method is considered as reference. Due to the fact that the proposed ellipsoidal estimation methods allow to modify both the shape and the radius of the considered ellipsoid at each time instant, these methods offer a better estimation accuracy than the P-radius based zonotopic estimation [67]. The best accuracy of the estimation is obtained using *Improved Method 4*, but with the highest complexity (see Table 5.4).

Table 5.4: Total computation time after 50 time instants

Algorithm	Time (second)
P-radius based zonotopic estimation	0.92
Method 4	29.77
Improved Method 4	32.19

Figure 5.25 compares the volume of the state estimation sets. The volume of the estimation set obtained by the P-radius based zonotopic estimation method is larger than the volume obtained by the *Method 4*, which is also larger than the volume obtained by *Improved Method 4*.

The proposed ellipsoidal methods offer better accuracy compared to the P-radius based zonotopic estimation technique [67] but with increased complexity due to the online computation (see Table 5.4).

[5]Only interval uncertainties in the evolution matrix are considered in the approach proposed in [67].

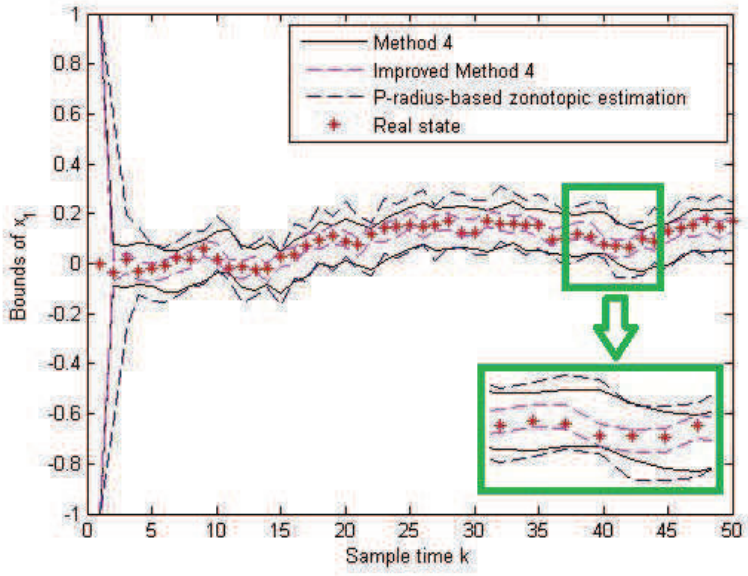

Figure 5.21: Bounds of x_1

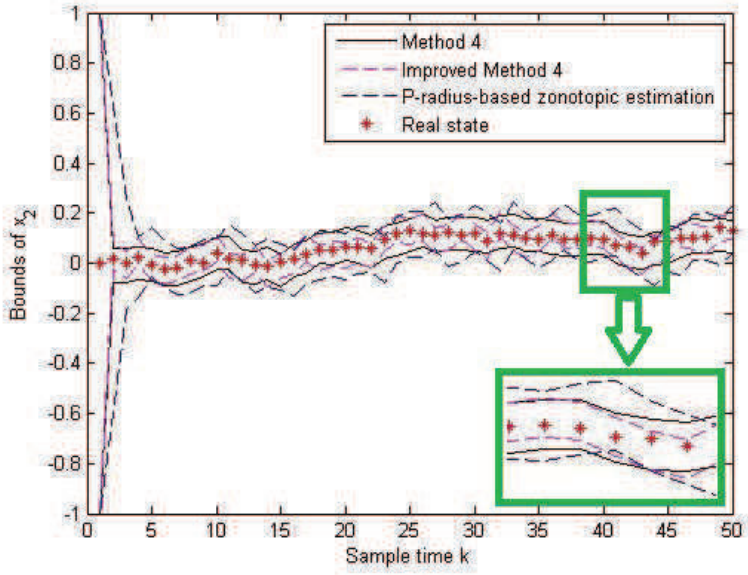

Figure 5.22: Bounds of x_2

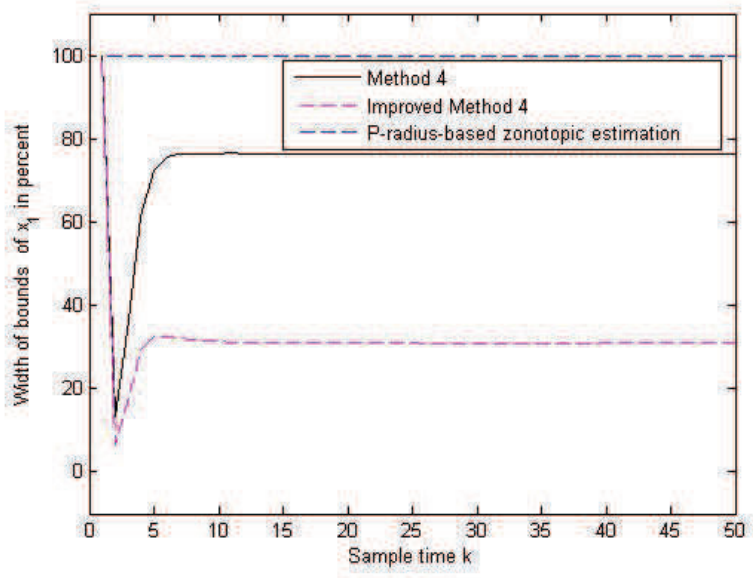

Figure 5.23: Comparison of the bounds width of x_1

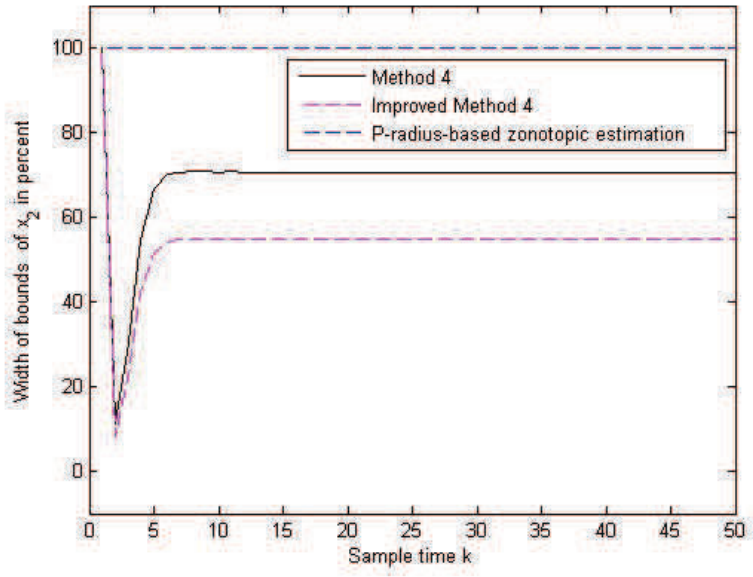

Figure 5.24: Comparison of the bounds width of x_2

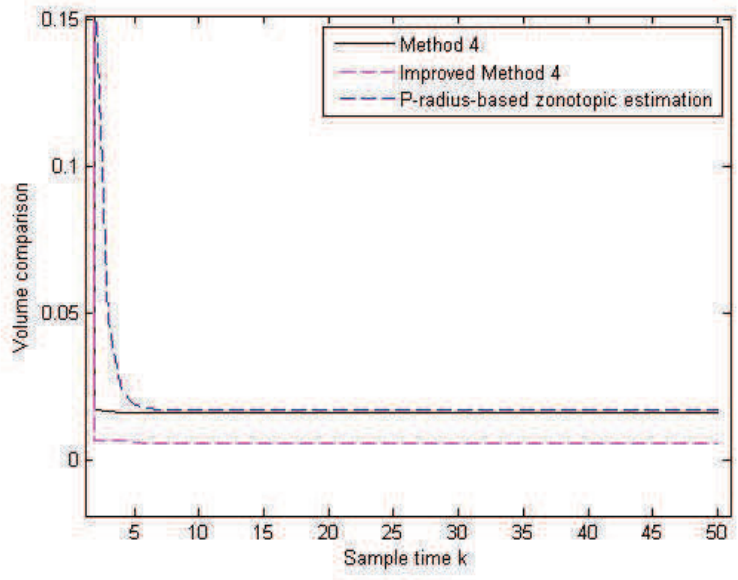

Figure 5.25: Comparison of the volume of the state estimation sets

Comparing Table 5.3 and Table 5.4 allows to quantify (in terms of the computation time) the complexity resulting from the considered interval uncertainties on the observation matrix.

5.5 Conclusion

A new guaranteed ellipsoidal state estimation approach for multivariable linear systems with bounded perturbations and measurement noises has been proposed in this chapter. Successive improvements/extensions are elaborated in the four proposed methods.

Method 1 is applied for Linear Time Invariant (LTI) systems. In this method, the radius of the ellipsoidal set is minimized at each iteration by off-line solving an LMI problem which leads to compute a constant observer matrix gain. In *Method 2*, this gain is updated at each sample time by solving an online LMI problem. This leads to a better estimation accuracy compared to *Method 1* but with higher complexity due to the vertex enumeration when solving the LMI problem. Applying a new vector scaling technique for *Method 2*, the computation time is significantly reduced in *Method 3*, while keeping an acceptable level of the estimation accuracy.

Secondly, an extension of this *Method 3* is proposed to the case of uncer-

tain Linear Time Invariant systems with bounded perturbations and measurement noises (with interval uncertainties in both the evolution and observation matrices). This offers a good accuracy of the estimation.

Finally, this ellipsoidal state estimation method is extended to the case of uncertain Linear Time Variant (LTV) systems (*Method 4*). This method is based on the online minimization of the size of the ellipsoidal state estimation set by solving an LMI (Linear Matrix Inequality) optimization problem. The shape of the ellipsoidal set is adjusted at each time instant allowing to reduce the conservativeness in comparison to previous methods. An improvement of the accuracy of the proposed ellipsoidal estimation method has been further presented in *Improved Method 4* by adding quadratic constraints on both measurements and perturbations. This allows to reduce the bounds of the estimation domain, offering a better estimation accuracy.

In the next chapter, the proposed ellipsoidal state estimation approach is applied for fault detection and fault tolerant control purposes.

Chapter 6

Fault detection using set-membership estimation

6.1 Introduction

Fault Tolerant Control (FTC) is a new research area that makes possible the development of control laws which allow to maintain current performances close to desirable objectives even after the occurrence of faults. A generally accepted definition of a fault is that it is an intolerable deviation of at least one characteristic property or parameter of a system from its acceptable/usual/standard conditions. The determination of a fault at a certain time is referred to Fault Detection (FD). Faults are detected by developing model-based Fault Detection algorithms. It compares the behavior of the process and its model when both are fed with the same inputs. A general technique used in the literature consists in designing a controller that can adapt or reconfigure itself based on the FD information such that the system can still operate safely despite the presence of faults. A control system with this property is called FTC system. Figure 6.1 shows the architecture of a FTC system. In this figure, it can be seen that there are three parts of the system susceptible to faults: actuators, system's components and sensors. For actuator faults, the plant properties are not affected but the influence of the controller on the plant is modified. The component fault can be represented by a change of the dynamical properties of the system. The sensor fault means that the measurement readings have substantial errors. There are many types of faults. The most popular are incipient faults and abrupt faults. The incipient faults characterize a slowly developing fault while abrupt faults are modeled by a step function. In this thesis, only abrupt fault will be considered.

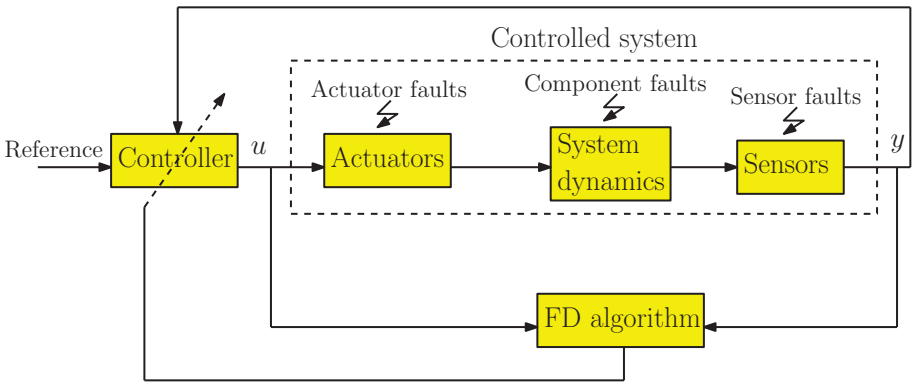

Figure 6.1: Architecture of a FTC system

Fault Tolerant Control systems can be categorized into two classes: passive FTC systems and active FTC systems. Passive FTC systems introduce fault tolerance into a control system by the use of a fixed controller that is robust to a set of anticipated faults [87], [34]. Active FTC systems differ from passive FTC systems in the sense that they can adapt online to fault information given by the FD algorithm [69]. In general, this online adaptation allows active FTC systems to achieve better performance than passive FTC systems.

Concerning Fault Detection approaches, there are also two classes: active approaches and passive approaches. The active approaches are based on generating insensitive residuals with respect to uncertainties but sensitive to faults [23], [101], [71]. The passive approaches determine if there is consistency between the model and the measurements [85]. Note that in passive approaches, set-membership estimation techniques [95], [80] are largely used for Fault Detection. Passive fault detection algorithms are applied to test the consistency [82] both in the parameter space [53], [54], [18], [90], and in the state-space [79], [97], [78], [98]. In this context, Section 6.2 proposes a first passive Fault Detection approach in state-space for linear discrete-time systems with bounded perturbations and bounded measurement noises. Based on set-membership state estimation, this method [13] checks the consistency between the model and the measurements. Only sensor faults are considered within this FD approach.

A second original approach based on the use Multiple Model (MM) systems [15] is proposed in Section 6.3. The motivation of using Multiple Model systems for Fault Detection stems from the fact that a large class of faulty situations can be modeled concomitantly (e.g. actuator, component and sensor faults), contrary to classical FD methods that are usually applied to limited

types/number of faulty situations (e.g. actuator or sensor faults). In addition, the use of Multiple linear Models represents an attractive solution for dealing with the control of non-linear systems [9]. This is motivated by the fact that non-linear systems can be modeled by Linear Parametric Varying (LPV) models [46], [91], Takagi-Sugeno fuzzy models [107], etc. A Multiple Model technique consists in the construction of a set of models that contains local models corresponding to specific fault conditions of the monitored system [73], [92].

For linear systems, the Multiple Model systems is an attractive technique for FD due to its flexible structure that allows us intuitive modeling of faults. In general, in a state-space representation, a component fault can be modeled by a modification of the evolution matrix, an actuator fault can be modeled by a change of the control matrix, and a sensor fault can be modeled by an alteration of the observation matrix. The use of Multiple Model systems allows an explicit way of considering faults and thus, recently, it has attracted significant interest [110], [109], [103], [35].

Fault Detection using Multiple Models in context of Takagi-Sugeno approach has been explored in several works [48], [70]. The authors of [47] propose a method for estimating both the weights and the state of a Multiple Model system with one common state vector. In this system, the weights are related to the activation of each individual model. However, perturbations and measurement noises are assumed to be stochastic with a given covariance representation. The fault diagnosis method presented in [74] is based on a generation of the residuals decoupled from the faults; but the residual is obtained using statistical method which sometimes makes difficult the parameters tuning. Generally, the perturbations are assumed to have a known distribution. This assumption is in many cases difficult to validate. Thus, it may be more realistic to assume that the perturbations and measurement noises are unknown but bounded. This leads to use set-membership approaches for the estimation [95], [16], [24], [39]. In this context, Section 6.3 proposes a new Fault Detection algorithm based on Multiple Models approach for linear systems with bounded perturbations. In this algorithm, FD is passively implemented by using set-membership estimation and Fault Tolerant Control is actively done by a Model Predictive Control (MPC) design. The consistency of each model with the measurements is checked at each sample time based on the ellipsoidal state estimation proposed in the previous chapter. A Min-Max Model Predictive Control is developed in order to find the optimal control and the best model to use for the system in spite of the presence of component, actuator and/or sensor faults.

6.2 Sensor fault detection using zonotopes

This section proposes a passive sensor fault detection approach [13] in state-space, based on set-membership state estimation. Note that all the previously detailed set-membership state-estimation techniques (i.e. zonotopic approaches, combined zonotopic-ellipsoidal approach, ellipsoidal approaches) can be used within this FD method. However, in order to offer a wide overview, the zonotopic estimation method described in Subsection 4.3.4 will be considered here. This estimation method based on the minimization of the P-radius of a zonotope has two steps: the prediction step and the correction step. Applying the zonotopic estimation method in the context of faulty systems does not guarantee the state estimation when a fault has occurred. In order to overcome this situation, a new fault detection algorithm based on the zonotopic state estimation is further proposed. This algorithm leads to guaranteed estimation despite the presence of sensor faults. During the presence of the faults, the idea is to use only the state estimation given by the prediction step of the estimation procedure. In the absence of faults, the two steps (prediction and correction) of the zonotopic set-membership estimation are applied. This procedure leads to guaranteed but conservative estimation. In order to overcome this inconvenient, in the context of faulty systems, a preliminary calibration of the measurements is proposed by centering the measurements relatively to the prediction zonotope. After the measurement calibration, the zonotopic P-radius minimization estimation method is applied. This allows to decrease the conservativeness of the proposed estimation technique in a faulty context and decreasing the distance to the real state, when faults are present.

Consider the following Single Output[1] Linear Time Invariant (LTI) discrete-time system with the state and measurement equations:

$$\begin{cases} x_{k+1} = Ax_k + F\omega_k \\ y_k = c^\top x_k + \sigma v_k + f_{y_k} \end{cases} \tag{6.1}$$

where $x_k \in \mathbb{R}^n$ is the state vector, $y_k \in \mathbb{R}$ is the measurement vector, $\omega_k \in \mathbb{R}^n$ is the state perturbation vector and $v_k \in \mathbb{R}$ represents the measurement noise. A, c, F and σ have the appropriate dimensions, with the assumption that the pair $(c^\top, A)$ is detectable. It is assumed that the initial state x_0 belongs to the zonotope $\mathcal{Z} = p_0 \oplus H_0\mathbf{B}^m$ and the perturbations and measurement noise are bounded by compact sets: $\omega_k \in \mathbf{B}^n$ and $v_k \in \mathbf{B}$. The scalar f_{y_k} is the sensor fault signal added to the measurement output which is equal to zero in the fault-free case and takes a non-zero value in the presence of faults.

[1] This method can be generalized for Multi-Output systems.

Using the zonotopic set-membership state estimation method, the objective is to obtain a state estimation in the presence of abrupt sensor faults.

***Remark* 6.1.** In order to keep a simple formulation, a Single Output system is considered without uncertainties and without a control input (the term Bu_k is omitted for (6.1)).

***Remark* 6.2.** The extension of this Fault Detection method is also possible to the case of uncertain systems (with interval uncertainties) by using set-membership estimation methods dedicated for uncertain systems.

First, the P-radius zonotopic state estimation for the fault free case for the system (6.1), with $f_{y_k} = 0$, is briefly reminded. In this approach, it is assumed that $x_{k-1} \in \hat{\mathcal{Z}}_{k-1} = \hat{p}_{k-1} \oplus \hat{H}_{k-1}\mathbf{B}^r$, where $\hat{\mathcal{Z}}_{k-1}$ is the zonotopic estimation at time $k-1$. The objective is to compute the zonotope $\hat{\mathcal{Z}}_k$ that contains x_k at time k. To do this, two steps are considered:

- *Prediction step*: The predicted zonotope $\bar{\mathcal{Z}}_k$ is determined as

$$\bar{\mathcal{Z}}_k = A\hat{p}_{k-1} \oplus \begin{bmatrix} A\hat{H}_{k-1} & F \end{bmatrix} \mathbf{B}^{r+n}. \tag{6.2}$$

- *Measurement*: The strip $\mathcal{S}(y_k, c, \sigma)$ is obtained using the output measurement at time k according to the following equation:

$$\mathcal{S}(y_k, c, \sigma) = \{x \in \mathbb{R}^n : |c^\top x - y_k| \leq \sigma\}. \tag{6.3}$$

- *Correction step*: The guaranteed state estimation at time k is the outer approximation of the intersection between the predicted state set $\bar{\mathcal{Z}}_k$ and the measurement strip $\mathcal{S}$, i.e. $\bar{\mathcal{Z}}_k \cap \mathcal{S}(y_k, c, \sigma)$. This outer approximation is parametrized by the vector $\lambda \in \mathbb{R}^n$, leading to the following family of zonotopes:

$$\hat{\mathcal{Z}}_k(\lambda) = \hat{p}_k(\lambda) \oplus \hat{H}_k(\lambda)\mathbf{B}^{r+n+1}, \tag{6.4}$$

with

$$\begin{cases} \hat{p}_k(\lambda) = A\hat{p}_{k-1} + \lambda\left(y_k - c^\top A\hat{p}_{k-1}\right), \\ \hat{H}_k(\lambda) = \begin{bmatrix} \left(I - \lambda c^\top\right) A\hat{H}_{k-1} & \left(I - \lambda c^\top\right) F & \sigma\lambda \end{bmatrix}. \end{cases} \tag{6.5}$$

The vector λ is then determined in order to minimize the P-radius of the zonotope $\hat{\mathcal{Z}}_k$ at each sample time. The solution is found by minimizing the scalar $\beta \in (0, 1)$ using the bisection algorithm and off-line solving the following Linear Matrix Inequality (LMI) optimization problem:

$$\max_{\tau,P,\beta,Y} \tau$$
subject to

$$\begin{cases} 0 \leq \beta < 1 \\ \frac{(1-\beta)P}{\sigma^2+const} \succeq \tau I \\ \begin{bmatrix} \beta P & 0 & 0 & A^\top P - AcY^\top \\ * & F^\top F & 0 & F^\top P - F^\top cY^\top \\ * & * & \sigma^2 & Y^\top \sigma \\ * & * & * & P \end{bmatrix} \succeq 0 \end{cases} \tag{6.6}$$

with $const = \max_{\omega \in \mathbf{B}^n} \|F\omega\|_2^2$ and $Y = P\lambda$.

This method allows to estimate the state of the system (6.1) in the fault-free case. The objective is to use a similar estimation method to detect abrupt sensor faults and try to obtain a good estimation despite the presence of these faults.

In the rest of this section, three Fault Detection algorithms [13] are proposed for abrupt sensor faults.

6.2.1 Fault Detection based on the consistency test

Model-based fault detection of dynamic processes is based on the use of the model (i.e. state equation) to check the consistency of the observed behaviour (via the measurement equation). In the case of the model (6.1), the idea is to check the consistency between the prediction zonotope ($\bar{\mathcal{Z}}_k$) and the set of measurements $\mathcal{S}(y_k, c, \sigma)$. Using the definition of the zonotope support strip and *Property* 3.6, a fault has occurred if the set $\bar{\mathcal{Z}}_k \cap \mathcal{S}(y_k, c, \sigma)$ is empty. In other words, a fault has occurred if the condition $q_u < y - \sigma$ or $q_l > y + \sigma$ given in (3.32) holds. In the fault-free case, the zonotopic estimation method presented by equations (6.4), (6.5) and (6.6) is used.

Algorithm 2 provides a general conceptual form of the fault detection strategy based on checking the consistency between the model and the measurement. The idea of this algorithm is the following. At each time instant k the prediction zonotope $\bar{\mathcal{Z}}_k$ is built according to the equation (6.2). Using the output measurement obtained from the sensor, the strip $\mathcal{S}(y_k, c, \sigma)$ is also built according to the equation (6.3). Then, consistency between the predicted zonotopic state estimation and the measurement strip is checked. If the consistency is proved, the P-radius minimization method is used to compute the intersection between the predicted zonotopic state estimation and the measurement strip according to the equations (6.5) and (6.6). Otherwise, if the intersection between the predicted zonotopic state estimation

$\bar{Z}_k$ and the measurement strip is empty according to the equation (3.32), a fault is considered to be present.

Algorithm 2. Fault detection based on the consistency test

---

1. $k \leftarrow 0$;
2. $\mathcal{Z}_0 \leftarrow p_0 \oplus H_0\mathbf{B}^m$;
3. **for** $k = 1 : N$
4. Compute the predicted zonotope $\bar{\mathcal{Z}}_k$ according to the equation (6.2). Use the output measurement y_k, i.e. the strip $\mathcal{S}(y_k, c, \sigma)$ according to equation (6.3).
5. **if** $\bar{\mathcal{Z}}_k \cap \mathcal{S}(y_k, c, \sigma) = \emptyset$
6. Indicate **fault**.
7. **else**
8. Compute the zonotope $\hat{\mathcal{Z}}_k$ that fulfills $\bar{\mathcal{Z}}_k \cap \mathcal{S}(y_k, c, \sigma)$ according to equations (6.5) and(6.6).
9. **end if**
10. $k \leftarrow k + 1$
11. **end for**.

Here N is the length of the simulation time, p_0 and H_0 denote the initial state zonotope (which is chosen sufficiently large).

***Remark* 6.3.** These sensor Fault Detection algorithms using zonotopic set-membership estimation can be generalized for Multi-Output systems by checking the consistency between a zonotope and a polytope. This polytope represents the measurement set which is formed by intersecting the different measurement strips.

The objective is now to find a solution to estimate the state of the system when the fault has occurred in the step 6 of *Algorithm* 2. Two solutions will be further discussed.

6.2.2 Fault Detection using only the prediction step

The goal is to obtain a guaranteed estimation in the presence of a fault. The idea is to improve *Algorithm* 2 when a fault has occurred. It consists in using only the prediction zonotope instead of the measurement strip and the correction zonotope if an inconsistency is detected. In the faulty situation, the measurement strip is not considered and the estimation zonotope will

not be changed at the correction step (i.e. the estimated set is considered equal to the predicted set – see Step 7 in *Algorithm* 3). If there are no faults, both the prediction and correction steps are used in *Algorithm* 3 in order to estimate the state, using equations (6.5) and (6.6).

Algorithm 3. Fault detection using only the prediction step

1. $k \leftarrow 0$;
2. $\mathcal{Z}_0 \leftarrow p_0 \oplus H_0\mathbf{B}^m$;
3. **for** $k = 1 : N$
4. Compute the predicted zonotope $\bar{\mathcal{Z}}_k$ according to the equation (6.2). Use the output measurement y_k, i.e. the strip $\mathcal{S}(y_k, c, \sigma)$ according to equation (6.3).
5. **if** $\bar{\mathcal{Z}}_k \cap \mathcal{S}(y_k, c, \sigma) = \emptyset$
6. Indicate **fault**.
7. $\hat{\mathcal{Z}}_k = \bar{\mathcal{Z}}_k$
8. **else**
9. Compute the zonotope $\hat{\mathcal{Z}}_k$ that fulfills $\bar{\mathcal{Z}}_k \cap \mathcal{S}(y_k, c, \sigma)$ according to equations (6.5) and (6.6).
10. **end if**
11. $k \leftarrow k + 1$
12. **end for**.

This gives a guaranteed state estimation but the estimation accuracy could deteriorate.

In order to increase accuracy, a calibration of the measurement is proposed in the next subsection.

6.2.3 Fault Detection based on the calibration of the measurement strip

The goal is to get a good estimation (which is closer to the real state) when a fault is detected. It consists in shifting the measurement strip $\mathcal{S}(y_k, c, \sigma)$ (e.g. the blue strip in Fig. 6.2) to the center of the predicted zonotope $\bar{\mathcal{Z}}_k$ (e.g. the red strip in Fig. 6.2). If the upper bound of the zonotope support strip q_u of the zonotope $\bar{\mathcal{Z}}_k$ satisfy the condition $q_u < y_k - \sigma$ (see the blue strip in Fig. 6.2 and the general representation of the zonotope support strip in Figure 3.7) according to the condition of inconsistency (3.32), the output measurement y_k is calibrated as follows:

$$y_k \leftarrow y_k - d_1 - \frac{d_2}{2} - \sigma = \frac{q_u + q_l}{2}, \tag{6.7}$$

where $d_1 = y_k - q_u - \sigma$ and $d_2 = q_u - q_l$. Otherwise, the condition of inconsistency concerning the lower bound of the zonotope support strip $q_l > y_k + \sigma$ (see the green strip in Fig. 6.2) holds in (3.32) hlods and the output measurement is calibrated as follows:

$$y_k \leftarrow y_k + d_3 + \frac{d_2}{2} + \sigma = \frac{q_u + q_l}{2}, \tag{6.8}$$

where $d_3 = q_l - y_k - \sigma$.

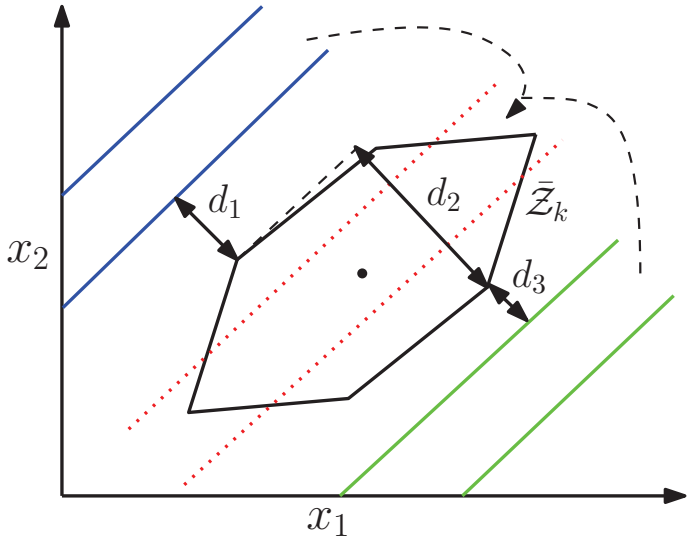

Figure 6.2: Measurement calibration

The new obtained strip is the dotted red strip (see Fig. 6.2). After this calibration, the zonotopic state estimation is computed using the P-radius minimization method. When there is no fault, the method of state estimation based on the P-radius minimization method is applied. In a faulty situation, *Algorithm* 4 provides a solution.

Algorithm 4. FD with measurement calibration

1. $k \leftarrow 0$
2. $\mathcal{Z}_0 \leftarrow p_0 \oplus H_0 \mathbf{B}^m$
3. **for** $k = 1 : N$
4. Compute the zonotope $\bar{\mathcal{Z}}_k$ according to the equation (6.2). Use the output measurement y_k, i.e. the strip $\mathcal{S}(y_k, c, \sigma)$ according to the equation (6.3)

5. **if** $\bar{\mathcal{Z}}_k \cap \mathcal{S}(y_k, c, \sigma) = \emptyset$
6. Indicate **fault**
7. **if** $(q_u < y_k - \sigma)$ or $(q_l > y_k + \sigma)$
8. $y_k \leftarrow \dfrac{q_u + q_l}{2}$
9. **end if**
10. **end if**
11. Compute the zonotope $\hat{\mathcal{Z}}_k$ that fulfills $\bar{\mathcal{Z}}_k \cap \mathcal{S}(y_k, c, \sigma)$ according to (6.4), (6.5) and (6.6)
12. $k \leftarrow k + 1$
13. **end for**

Consider that the real state estimation x_k belongs to the prediction zonotope $\bar{\mathcal{Z}}_k$ but it is outside the measurement strip (i.e. the dotted red strip in Fig. 6.2). In this case, *Algorithm* 4 does not guarantee the state estimation because the dotted red strip do not necessary cover all the predicted zonotope $\bar{\mathcal{Z}}_k$, but it still offers an estimation closer to the real state than the one obtained using *Algorithm* 3. This can be suitable for some situations encountered in control perspectives.

Example 6.1 illustrates the performance of *Algorithms* 3 and 4.

***Example* 6.1.** Consider the following LTI discrete-time system:

$$\begin{cases} x_{k+1} = \begin{bmatrix} 0.8 & 0.2 \\ -0.5 & 0.8 \end{bmatrix} x_k + \begin{bmatrix} -0.12 \\ 0.02 \end{bmatrix} \omega_k \\ \\ y_k = \begin{bmatrix} -2 & 1 \end{bmatrix} x_k + 0.2 v_k + f_{y_k} \end{cases} \tag{6.9}$$

with $\|v_k\|_\infty \leq 1$, $\|\omega_k\|_\infty \leq 1$. The initial state belongs to the box $3\mathbf{B}^2$. The order of the zonotope is limited to $m \leq 20$ (number of its segments) in order to have a fast simulation. The sensor fault f_{y_k} is introduced between sample times $k = 30$ and $k = 40$. In this example, the results obtained by (*Algorithms* 2, 3 and 4 are analyzed.

Figures 6.3 and 6.4 show the bounds of x_1 and x_2 obtained by the P-radius minimization method (blue lines). The red stars represent the real state of the system. It can be noticed that these points are not between the upper bound and the lower bound of the state estimation during the presence of faults and immediately after the sensor recovery.

Figure 6.5 shows the detection of the fault during the estimation via *Algorithm* 3. The fault occurred when the signal is equal to 1, it remains equal to 0 otherwise.

Figures 6.6 and 6.7 show the bounds of x_k obtained by *Algorithm* 3 (blue lines). The red stars represent the real state of the system. These points are between the upper and lower bounds of x_k. The reader can observe that when the fault is present (from $k = 30$ to $k = 40$), the estimated bounds are increased. This is due to the omission of the correction step in the estimation method (i.e. only the prediction step is used in *Algorithm* 3).

Figures 6.8 and 6.9 show the bounds of x_k obtained with *Algorithm* 4 (blue lines). Beside the interval time when the faut is present, similar results are obtained with *Algorithms* 3 and 4. In addition, the red stars represent the real state of the system. The distance between the upper and lower bounds obtained by *Algorithm* 4 (Figures 6.8 and 6.9) is less than the distance between the upper and lower bounds obtained by *Algorithm* 3 (Figures 6.6 and 6.7). Even if *Algorithm* 4 does not guarantee the state estimation bounds in presence of faults, the results can be less conservative compared to *Algorithm* 3. This could make *Algorithm* 4 more suitable for Fault Tolerant Control perspectives than *Algorithm* 3.

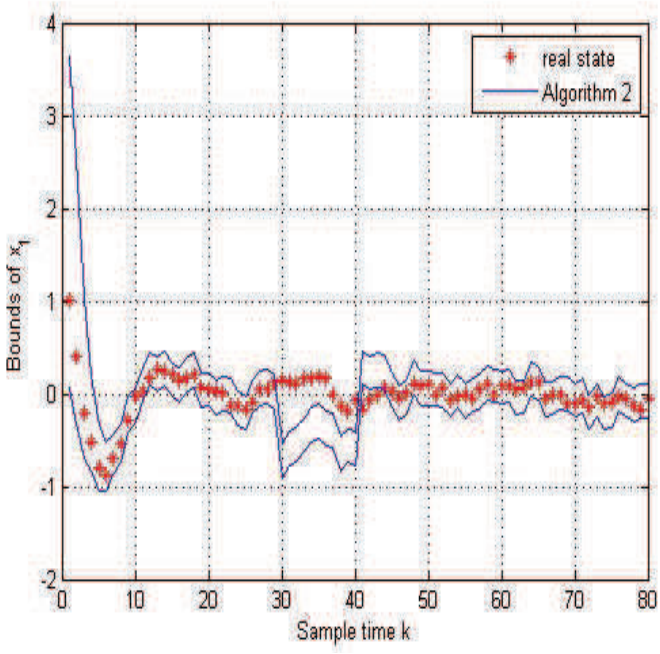

Figure 6.3: Bounds on x_1 using *Algorithm* 2

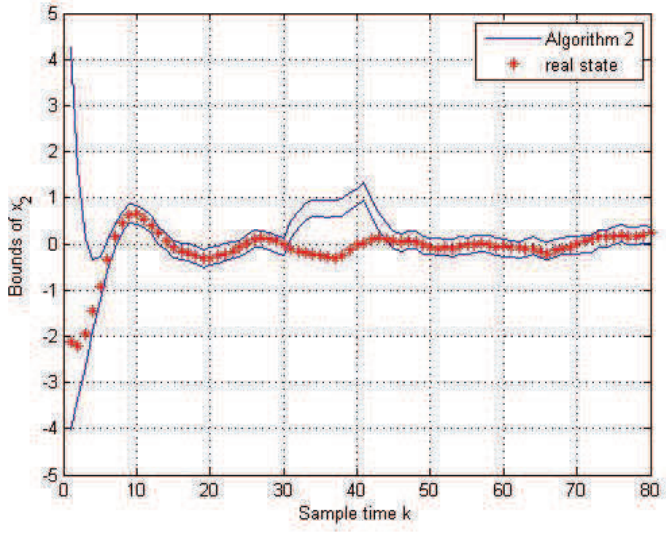

Figure 6.4: Bounds on x_2 using *Algorithm* 2

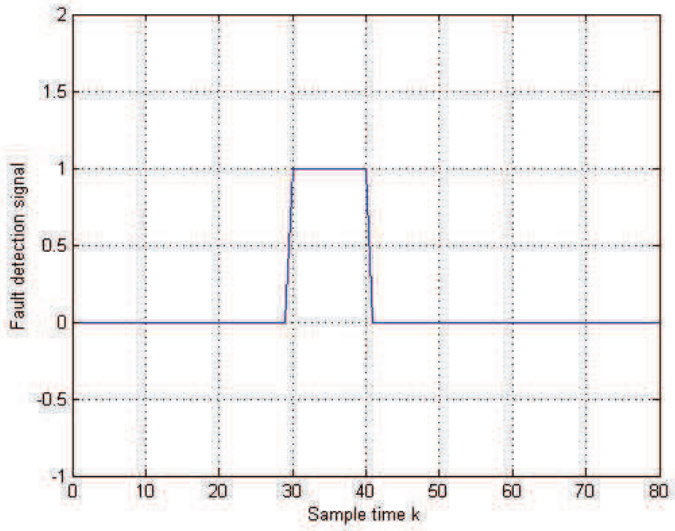

Figure 6.5: Fault detection signal using *Algorithm* 3 (step 6)

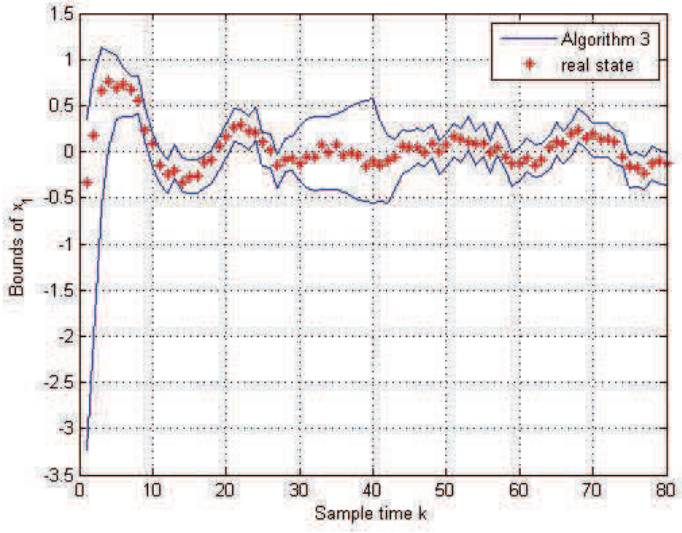

Figure 6.6: Bounds on x_1 using *Algorithm* 3

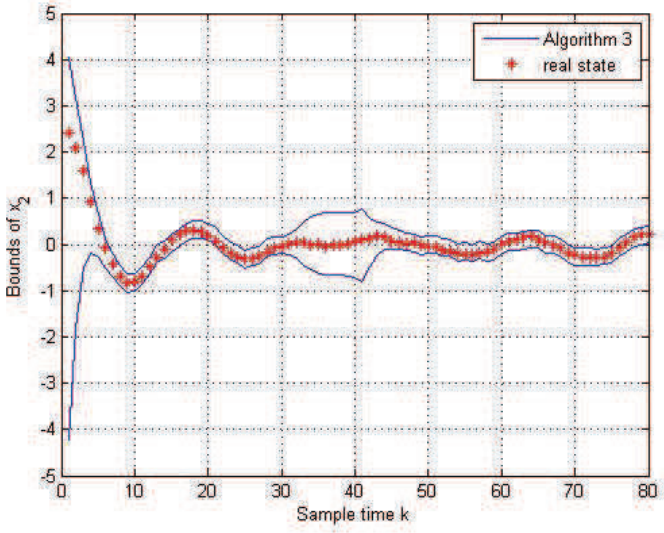

Figure 6.7: Bounds on x_2 using *Algorithm* 3

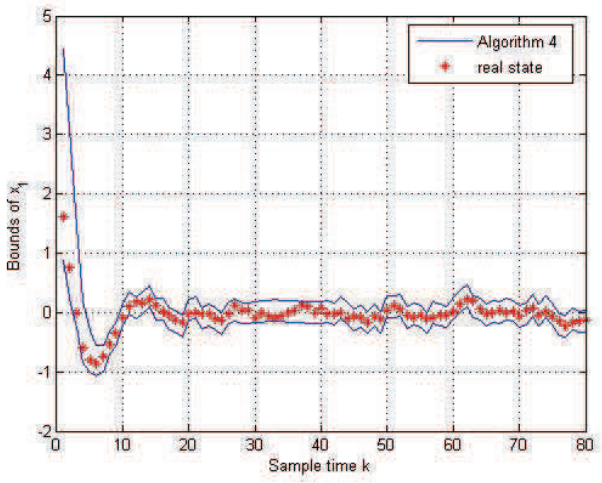

Figure 6.8: Bounds on x_1 using *Algorithm* 4

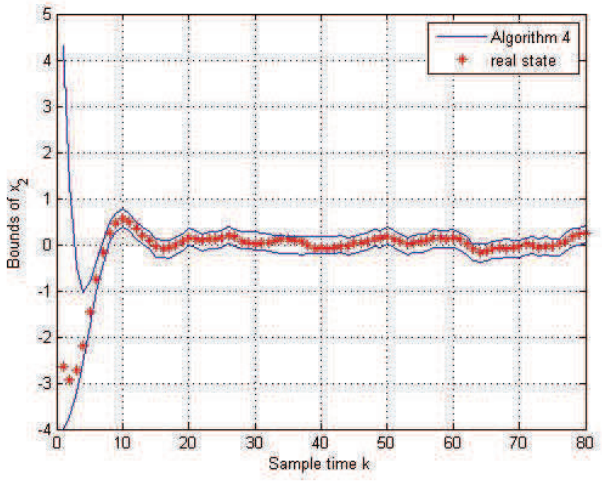

Figure 6.9: Bounds on x_2 using *Algorithm* 4

6.2.4 Fault sensitivity of the proposed algorithms

Sensitivity toward faults is an important charateristic of fault detection algorithms. The minimum abrupt fault that will be detected by the proposed algorithms for the output sensor fault f_{y_k} has to be determined.

In the following, the two cases of inconsistency expressed by equation (3.32) are considered.

- The first case is when the following equation holds:

$$q_u < y_k - \sigma. \tag{6.10}$$

From (3.30) and from (6.1), $q_u = c^\top \hat{p}_k + \|\hat{H}_k^\top c\|_1$ and $y_k = c^\top x_k + \sigma v_k + f_{y_k}$. Then, 6.10 is equivalent to:

$$c^\top \hat{p}_k + \|\hat{H}_k^\top c\|_1 \leq c^\top x_k + \sigma v_k + f_{y_k} - \sigma. \tag{6.11}$$

Assuming the worst-case with positive transition in f_{y_k} of $x_k \in \hat{\mathcal{Z}}_k(\lambda)$ and $v_k \in \mathbf{B}$ by minimizing $c^\top x_k$, i.e. $c^\top x_k = c^\top \hat{p}_k - \|\hat{H}_k^\top c\|_1$ from (3.31), and minimizing σv_k, i.e. $v_k = -1$, the condition of the magnitude of f_{y_k} is obtained as:

$$c^\top \hat{p}_k + \|\hat{H}_k^\top c\|_1 \leq c^\top \hat{p}_k - \|\hat{H}_k^\top c\|_1 - \sigma + f_{y_k} - \sigma, \tag{6.12}$$

which is equivalent to:

$$f_{y_k} \geq 2\sigma + 2\|\hat{H}_k^\top c\|_1. \tag{6.13}$$

The condition (6.13) means that the sensor fault is detected when its positive transition is greater than $2\sigma + 2\|\hat{H}_k^\top c\|_1$.

- The second case of inconsistency occurs when the following equation holds:

$$q_l > y_k + \sigma. \tag{6.14}$$

From (3.31) and from (6.1), $q_u = c^\top \hat{p}_k - \|\hat{H}_k^\top c\|_1$ and $y_k = c^\top x_k + \sigma v_k + f_{y_k}$. Then, 6.10 is equivalent to:

$$c^\top \hat{p}_k - \|\hat{H}_k^\top c\|_1 \geq c^\top x_k + \sigma v_k + f_{y_k} + \sigma. \tag{6.15}$$

Assuming the worst-case with negative transition in f_{y_k} of $x_k \in \hat{\mathcal{Z}}_k(\lambda)$ and $v_k \in \mathbf{B}$ by maximizing $c^\top x_k$, i.e. $c^\top x_k = c^\top \hat{p}_k + \|\hat{H}_k^\top c\|_1$ from (3.30), and maximizing σv_k, i.e. $v_k = 1$, the condition of the magnitude of f_{y_k} is obtained as:

$$c^\top \hat{p}_k - \|\hat{H}_k^\top c\|_1 \geq c^\top \hat{p}_k + \|\hat{H}_k^\top c\|_1 + \sigma + f_{y_k} + \sigma, \tag{6.16}$$

which is equivalent to:

$$f_{y_k} \leq -2\sigma - 2\|\hat{H}_k^\top c\|_1. \tag{6.17}$$

The condition (6.17) means that the sensor fault is detected when its negative transition is smaller than $2\sigma + 2\|\hat{H}_k^\top c\|_1$.

Summarizing these two cases, the abrupt sensor fault is detected when:

$$|f_{y_k}| \geq 2\sigma + 2\|\hat{H}_k^\top c\|_1. \tag{6.18}$$

The quantity $\|\hat{H}_k^\top c\|_1$ the sum of the semi-axes of the zonotope $\hat{\mathcal{Z}}_k$.

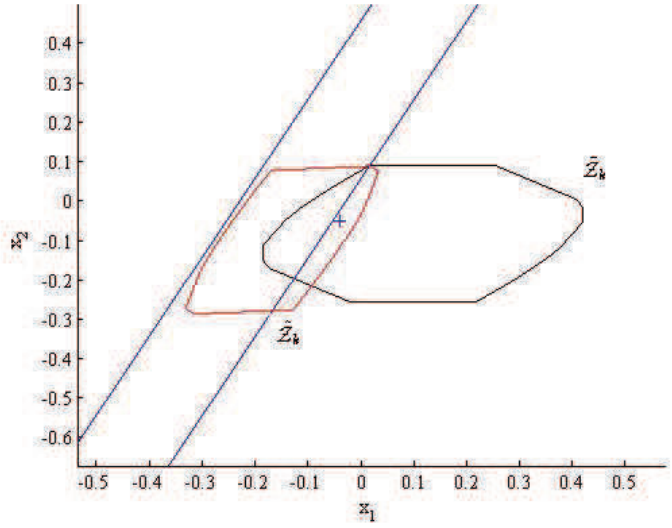

Figure 6.10: Fault detection sensitivity

An example where the abrupt fault is taken equal to 2σ is considered in Fig. 6.10. Here the fault is not detected, i.e. the intersection between the predicted black zonotope and the measurement strip (in blue) is not empty even the real state is outside the measurement strip. This figure illustrates that the red zonotopic outer approximation computed using the P-radius-based estimation method can contain the real state. Improving the sensitivity of the proposed Fault Detection algorithms will be addressed in future work.

6.3 Fault detection based on Multiple Model Systems

This section deals with a large class of faulty situations (actuator, sensor and component faults) and with a Fault Tolerant Control. A new Fault Detection using set-membership estimation approach based on Multiple Models technique is proposed. These models are constructed by referring to the original system, such that each model is adequate to one faulty mode. This

method consists first in checking the consistency between each model with the available measurements. This consistency checking is based on a guaranteed ellipsoidal set-membership state estimation presented in the previous chapter. Note that also the other set-membership estimation methods can be used. Second, the set of compatible models with the measurements is formed. In a third step, a Min-Max Model Predictive Control (MPC) [3] is developed for each compatible model ensuring the desirable performances despite the presence of faults. A quadratic criterion is minimized in order to choose:

- The best control to be applied to the original system;
- The best model for the estimation.

The novelty is the use of set-membership estimation coupled with Min-Max MPC to estimate the state of linear systems with unknown but bounded perturbations and measurement noises despite the presence of component, actuator and sensor faults.

Consider the following discrete-time LTI (Linear Time Invariant) system:

$$\begin{cases} x_{k+1} = AG_{i_c}x_k + BH_{i_a}u_k + E\omega_k \\ y_k = CI_{i_s}x_k + F\omega_k \end{cases} \tag{6.19}$$

with $A \in \mathbb{R}^{n_x \times n_x}$, $B \in \mathbb{R}^{n_x \times n_u}$, $C \in \mathbb{R}^{n_y \times n_x}$, $E \in \mathbb{R}^{n_x \times (n_x+n_y)}$, $F \in \mathbb{R}^{n_y \times (n_x+n_y)}$, $G_{i_c} \in \mathbb{R}^{n_x \times n_x}$, $H_{i_a} \in \mathbb{R}^{n_u \times n_u}$ and $I_{i_s} \in \mathbb{R}^{n_x \times n_x}$. The vector $x_k \in \mathbb{R}^{n_x}$ is the state vector of the system, $u_k \in \mathbb{R}^{n_u}$ is the input vector, and $y_k \in \mathbb{R}^{n_y}$ is the measured output vector at sample time k. The vector $\omega_k \in \mathbb{R}^{n_x+n_y}$ contains the state perturbations and the measurement perturbations (noise, offset, etc.). The perturbations are assumed to be bounded by unitary boxes $\omega_k \in \mathbf{B}^{n_x+n_y}$ for every $k \geq 0$. Consider that the initial state x_0 belongs to the ellipsoid $\mathcal{E}(P_0, \bar{x}_0, \rho_0) = \{x \in \mathbb{R}^{n_x} : (x - \bar{x}_0)^\top P_0 (x - \bar{x}_0) \leq \rho_0\}$.

The matrix G_{i_c}, with $i_c \in \mathbb{I}_c = \{0, 1, 2, \ldots, n_c\}$ and n_c denoting the number of the considered component faults, is a diagonal matrix modeling the i_c-th component mode. In a similar way, the matrix H_{i_a}, with $i_a \in \mathbb{I}_a = \{0, 1, 2, \ldots, n_a\}$ and n_a the number of considered actuator faults, is a diagonal matrix modeling the i_a-th actuator mode. The matrix I_{i_s}, with $i_s \in \mathbb{I}_s = \{0, 1, 2, \ldots, n_s\}$, where n_s denotes the number of considered sensor faults, is a diagonal matrix modeling the i_s-th sensor mode.

All diagonal entries of G_{i_c}, H_{i_a} and I_{i_s} belong to $[0, 1]$ where 0 or 1 means that the corresponding components, actuators and sensors are completely faulty or healthy, respectively. A value in the range $(0, 1)$ denotes a partial degradation of the corresponding components, actuators and sensors.

It is assumed that the pairs (AG_{i_c}, BH_{i_a}) and (AG_{i_c}, CI_{i_s}) are respectively stabilizable and detectable under all the considered modes.

***Remark* 6.4.** The system (6.19) can be rewritten in the following form:

$$\begin{cases} x_{k+1} = A(x_k + f_{x_k}) + B(u_k + f_{u_k}) + E\omega_k \\ y_k = Cx_k + F\omega_k + f_{y_k} \end{cases} \tag{6.20}$$

where f_{x_k}, f_{u_k} and f_{y_k} are respectively the component fault, actuator fault and the sensor fault. It is easy to verify this, by taking $f_{x_k} = (G_{i_c} - \mathbb{I}_{n_x})x_k$, $f_{u_k} = (H_{i_a} - \mathbb{I}_{n_u})u_k$ and $f_{y_k} = (I_{i_s} - \mathbb{I}_{n_x})x_k$.

Given an ellipsoidal estimation for x_k of the form $\mathcal{E}(P, \bar{x}_k, \rho_k)$, with P unknown and $k > 0$, the objective of this approach is to provide an ellipsoidal estimation for x_{k+1} of the form $\mathcal{E}(P, \bar{x}_{k+1}, \rho_{k+1})$ using the ellipsoidal set-membership state estimation, presented in Subsection 5.2.3 (*Method 3*) and briefly described in the next subsection, despite the presence of possible faults (on components, actuators or sensors).

The next subsection summarizes the ellipsoidal state estimation technique used for the fault-free case.

6.3.1 Ellipsoidal state estimation for the fault free case

This subsection illustrates[2] the guaranteed ellipsoidal state estimation for the system (6.19) in the fault-free case (i.e. G_{i_c}, H_{i_a} and I_{i_s} are identity matrices). In this case, the system (6.19) becomes:

$$\begin{cases} x_{k+1} = Ax_k + Bu_k + E\omega_k, \\ y_k = Cx_k + F\omega_k. \end{cases} \tag{6.21}$$

The ellipsoidal estimation method is based on the minimization of the ellipsoidal radius at each iteration by solving a Linear Matrix Inequality (LMI) problem.

Consider an initial state vector $x_0 \in \mathcal{E}(P_0, \bar{x}_0, \rho_0)$ and assume that $x_k \in \mathcal{E}(P, \bar{x}_k, \rho_k)$ at time k. If there exist a matrix $Y_k \in \mathbb{R}^{n_x \times n_y}$, a matrix $S = S^\top \succ 0$ in $\mathbb{R}^{(n_x+n_y)\times(n_x+n_y)}$ and the scalars $\rho_{k+1} > 0$ and $\beta \in (0, 1)$ for which the following LMI holds:

$$\min_{\beta, Y_k, S, \rho_{k+1}} \rho_{k+1}$$

[2]This description is used in order to permit an independent reading for each chapter.

subject to

$$\begin{cases} \begin{bmatrix} \beta P & * & * \\ PA - Y_k C & P & * \\ 0 & E^\top P - F^\top Y_k^\top & S \end{bmatrix} \succ 0, \\ \rho_{k+1} - \beta\rho_k > 0, \\ \beta < 1 \end{cases} \tag{6.22}$$

then the system state x_{k+1} at time $k+1$ is guaranteed to belong to the ellipsoid $\mathcal{E}(P, \bar{x}_{k+1}, \rho_{k+1}), \forall \omega_k \in \mathbf{B}^{n_x+n_y+n_\delta}$, with the following notations:

$$Y_k = PL_k, \tag{6.23}$$

$$\bar{x}_{k+1} = A\bar{x}_k + Bu_k + L_k(y_k - C\bar{x}_k). \tag{6.24}$$

The objective in the next subsection is twofold:

- Find the models which are compatible with the set of the measurements;
- Use this ellipsoidal estimation method to estimate the state of the system (6.19) despite the presence of faults.

6.3.2 Multiple Models Fault Detection using Min-Max MPC

The idea is to construct a set of p Multiple Models $\mathcal{M} = \{M_1, M_2, \ldots, M_p\}$ such that M_1 represents the fault-free case, i.e. $A_1 = A$, $B_1 = B$, $C_1 = C$, $E_1 = E$ and $F_1 = F$. For $i = 2, \ldots, p$, each model M_i is dedicated to one faulty mode. Note that the model M_i is defined by the matrices $A_i = AG_{i_c}$, $B_i = BH_{i_a}$, $C_i = CI_{i_s}$, $E_i = E$ and $F_i = F$, for $i = 1, \ldots, p$. A good knowledge of the system is required in order to choose the p models.

The state of the system (6.19) is estimated by each model M_i based on the ellipsoidal estimation (6.22) presented in the previous section (*Method* 3). Considering the presence of faults, the consistency between the model M_i and the measurement has to be checked at each sample time. Then, the objective is to find the models which are compatible with the set of measurements. Once this set is computed, a Min-Max Model Predictive Control is developed in order to stabilize the state x_k of the system (6.19). A quadratic criterion is minimized by using a Min Max technique in order to decide which is the best model to estimate the state of the system for the next step. Figure (6.11) summarizes the idea of this Fault Detection method based on Multiple Model and using Min Max Fault Tolerant Control. N represents the simulation horizon.

Algorithm 5 provides a general form of the Fault Detection and Fault Tolerant Control strategy based on checking consistency between the models and the measurements. The idea of this algorithm is summarized below:

- **Initialization:** (*step 1 to step 5*)

  The estimated state is initialized by the ellipsoidal set $\mathcal{E}(P_0, \bar{x}_0, \rho_0)$ in *step 2*. The estimation set for each model $M_i \in \mathcal{M}$, $i = 1, \ldots, p$, is also initialized by the same ellipsoidal set $(\mathcal{E}_i(P_0, \bar{x}_{0,i}, \rho_{0,i}) = \mathcal{E}(P_0, \bar{x}_0, \rho_0))$.

  These ellipsoids are chosen sufficiently large in order to contain the real initial state.

- **Compatible models set construction:** (*step 7 to step 18*)

  At each sample time k, the output measurement y_k in (6.19) obtained from the sensors is used to build the parametrized polytope $\mathcal{P}_{check}(C_i, y_k, F_i)$ for each model M_i, with $i = 1, \ldots, p$. This polytope corresponds to the consistent state set with the measurements y_k. The construction of the polytope $\mathcal{P}_{check}(C_i, y_k, F_i)$ is obtained from the intersection of all the n_y measurement strips (each strip is formed by one of the n_y components of the y_k). Each strip is defined by these two inequalities:

$$\begin{cases} C_{i,j}x_k \leq y_{k,j} + \|F_{i,j}\|_1 \\ -C_{i,j}x_k \leq -y_{k,j} + \|F_{i,j}\|_1 \end{cases} \tag{6.25}$$

  such that i, with $i = 1, \ldots, p$, represents the i^{th} model and j, with $j = 1, \ldots, n_y$, represents the j^{th} line of C_i, F_i and y_k.

  To construct the strip given by (6.25) for each scalar component $y_{k,j}$ of the output y_k, with $j = 1, \ldots, n_y$, the expression of $y_k = CI_{i_s}x_k + F\omega_k = C_i x_k + F_i\omega_k$ in (6.19) is used. In fact,

$$y_{k,j} = C_{i,j}x_k + F_{i,j}\omega_k, \tag{6.26}$$

  with $j = 1, \ldots, n_y$. This gives

$$C_{i,j}x_k = y_{k,j} - F_{i,j}\omega_k. \tag{6.27}$$

  Taking into account that $C_{i,j}x_k$, $y_{k,j}$ and $F_{i,j}\omega_k$ are scalars and that $F_{i,j} \in \mathbb{R}^{1\times(n_x+x_y)}$ and $\omega_k \in \mathbf{B}^{n_x+n_y}$, the scalar $C_{i,j}x_k$ can be bounded as follows:

$$y_{k,j} - \|F_{i,j}\|_1 \leq C_{i,j}x_k \leq y_{k,j} + \|F_{i,j}\|_1. \tag{6.28}$$

  This implies the inequalities of (6.25).

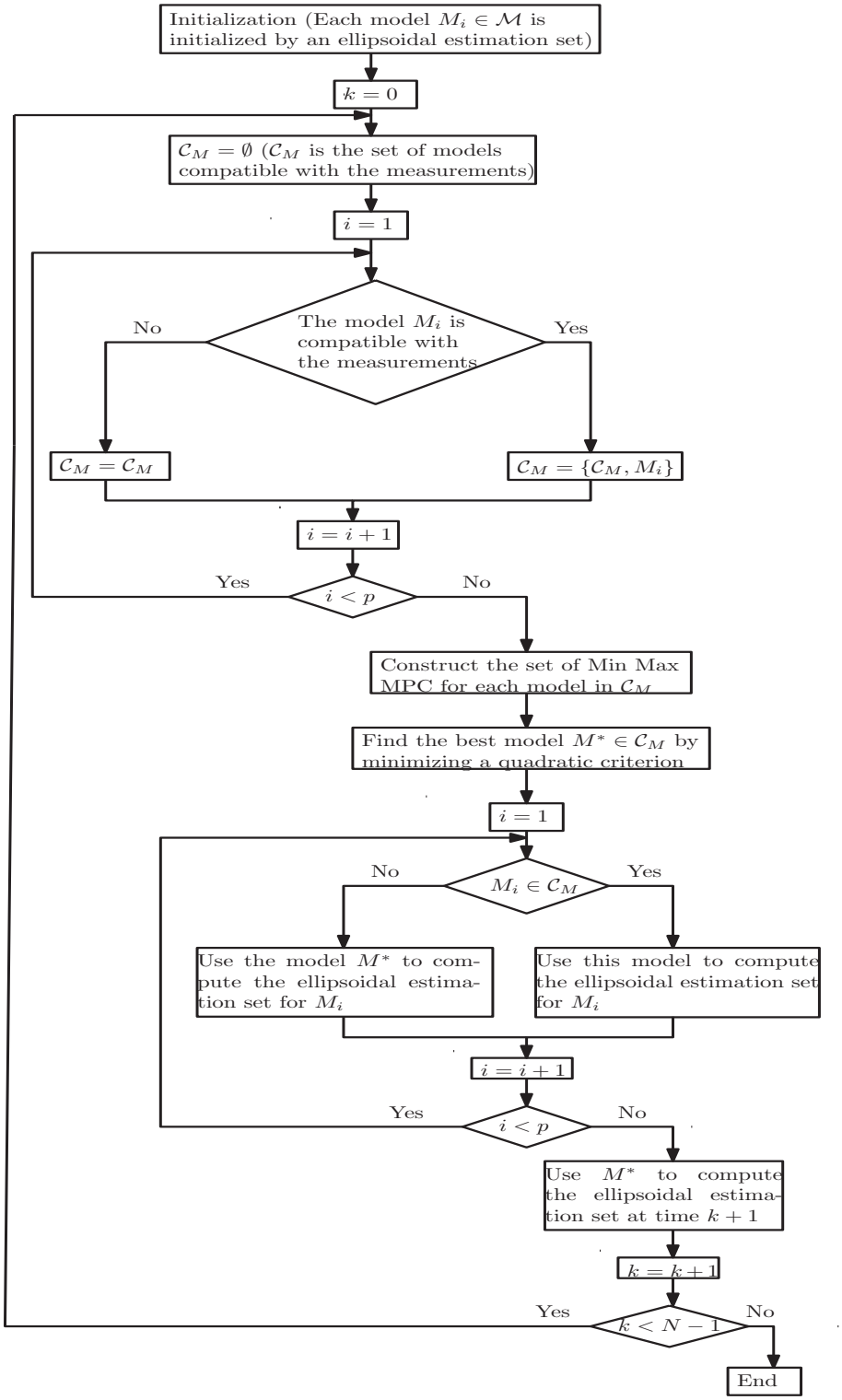

Figure 6.11: Multiple Models Fault Detection using Min-Max MPC

Then, using (6.25), the polytope $\mathcal{P}_{check}(C_i, y_k, F_i)$ is defined by the following constraints:

$$\mathcal{P}_{check}(C_i, y_k, F_i) = \{x_k \in \mathbb{R}^{n_x} : Sx_k \leq T\},$$

with the matrices $S = \begin{bmatrix} C_i \\ -C_i \end{bmatrix}$, $T = \begin{bmatrix} y_k + \mathbf{F}_i \\ -y_k + \mathbf{F}_i \end{bmatrix}$ and $\mathbf{F}_i = \begin{bmatrix} \|F_{i,1}\|_1 \\ \vdots \\ \|F_{i,n_y}\|_1 \end{bmatrix}$.

Note that $F_{i,j}$ designs the j^{th} line of the F_i matrix for the model M_i.

The consistency between the ellipsoidal estimated set $\mathcal{E}_i(P, \bar{x}_{k,i}, \rho_{k,i})$ and the polytope $\mathcal{P}_{check}(C_i, y_k, F_i)$ is verified for each model $M_i \in \mathcal{M}$. The ellipsoidal set $\mathcal{E}_i(P, \bar{x}_{k,i}, \rho_{k,i})$ represents the state estimation with the model M_i.

This consistency test (i.e. the intersection between an ellipsoid and a polytope) is solved by the following Quadratic Programming (QP) optimization problem with linear constraints:

$$\rho_k^* = \min_{x_k \in \mathcal{E}_i(P, \bar{x}_k, \rho_k)} (x_k - \bar{x}_k)^\top P (x_k - \bar{x}_k)$$
subject to
$$Sx_k \leq T. \tag{6.29}$$

If $\rho_k^* < \rho_k$, then the intersection $\mathcal{E}_i(P, \bar{x}_{k,i}, \rho_{k,i}) \cap \mathcal{P}_{check}(C_i, y_k, F_i)$ is not empty. Else, the intersection is empty $\mathcal{E}_i(P, \bar{x}_{k,i}, \rho_{k,i}) \cap \mathcal{P}_{check}(C_i, y_k, F_i) = \emptyset$.

If the consistency is proved (i.e. non-empty intersection), the model M_i is called *compatible with the measurements* and it is added to the set $\mathcal{C}_M$ containing all the compatible models with the measurements. Otherwise, the model M_i is called *incompatible with the measurements*. This process is repeated for each model M_i, with $i = 1, \ldots, p$.

Note that several models M_i of $\mathcal{M}$ can be compatible with the measurement at the same time.

- **Construction of a Min-Max Model Predictive Control for each compatible model:** (*step 19 to step 24*)

  A Min Max Model Predictive Control is developed for each model compatible with the measurement. This control can be used for stabilizing a system for example by satisfying some constraints on the state and the control. A Min Max is chosen in order to minimize a quadratic criterion for the worst-case perturbations belonging in a bounded compact set.

In order to obtain the set of controllers suitable for each model, a control sequence $\mathbf{u}_{k|k,j} = [u_{k|k,j}, u_{k+1|k,j}, \ldots, u_{k+h-1|k,j}]^\top$ is computed for each model $M_j \in \mathcal{C}_M$, with $j = 1, \ldots, s_M$ (s_M is the size of $\mathcal{C}_M$), by minimizing the following criterion:

$$\mathbf{u}_{k|k,j} = \arg \min_{\mathbf{u}_{k|k,j}} \max_{\omega_k \in \mathbf{B}^{n_x+n_y}} J_j(u_{k|k,j}, \omega_{k|k,j}, x_{k|k,j}), \tag{6.30}$$

subject to

$$x_{k+l|k} \in \mathbb{X} \text{ for } l = 1, \ldots, h$$
$$u_{k+l|k} \in \mathbb{U} \text{ for } l = 1, \ldots, h$$

where h is the prediction horizon, $x_{k+l|k}$ represents the prediction of the state for the sample time $k+l$ at the sample time k, $u_{k+l|k}$ is the control prediction for the sample time $k+l$ at the sample time k, $\omega_{k+l|k}$ is the perturbation prediction for the sample time $k+l$ at the sample time k and the cost function is defined as:

$$J_j(u_{k|k,j}, \omega_{k|k,j}, x_{k|k,j}) = \sum_{l=0}^{h-1} \left(x_{k+l+1|k,j}^\top Q x_{k+l+1|k,j}^\top + u_{k+l|k,j}^\top R u_{k+l|k,j} \right). \tag{6.31}$$

The cost function $J_j(u_{k|k,j}, \omega_{k|k,j}, x_{k|k,j})$ is maximized with respect to $\omega_{k+l|k,j} \in \mathbf{B}^{\mathbf{n_x}+\mathbf{n_y}}$ (corresponding to the worst case situation) and minimized with respect to $u_{k+l|k,j}$. The index j refers to the model $M_j \in \mathcal{C}_M$. Generally, the constraints on the state and input vectors and the choice of the weighting matrices Q and R are due to physical, safety and/or performance considerations. Then, the set of controllers $\mathcal{U}_k = \{\mathbf{u}_{k|k,1}, \ldots, \mathbf{u}_{k|k,s_M}\}$ suitable for each model $M_j \in \mathcal{C}_M$ is constructed. More details on solving the problem (6.30) are given in Appendix 1.

- **Computing the optimal control and the best model for the estimation:** (*step 25*)

  The objective is to determine the best control $\mathbf{u}_{k|k,j}^* \in \mathcal{U}_k$ for the system in faulty situation (6.19) and the best model $M_j^* = M_{k|k}^* \in \mathcal{C}_M$ to use for the estimation in case of faults. For this, the following optimization problem is solved:

$$(\mathbf{u}_{k|k}^*, M_{k|k}^*) = \arg \min_{\mathbf{u}_{k|k} \in \mathcal{U}_k} \max_{M_j \in \mathcal{C}_M} J(u_{k|k}, \omega_{k|k}, x_{k|k}), \tag{6.32}$$

with the cost function

$$J(u_{k|k}, \omega_{k|k}, x_{k|k}) = \sum_{l=0}^{h-1} \left(x_{k+l+1|k}^\top Q x_{k+l+1|k}^\top + u_{k+l|k}^\top R u_{k+l|k} \right).$$

Based on the receding horizon strategy, the control $u^*_{k|k}$ that will be applied to the system (6.19) is given by the first n_u components of the control sequence $\mathbf{u}^*_{k|k}$ as follows:

$$u^*_{k|k} = \begin{bmatrix} \mathbb{I}_{n_u} & \mathbb{O}_{n_u,(h-1)n_u} \end{bmatrix} \mathbf{u}^*_{k|k}. \tag{6.33}$$

- **Computing the estimation for each model:** (*step 26 to step 32*) Each model $M_i \in \mathcal{M}$, with $i = 1, \ldots, p$, must be fed with an ellipsoidal estimation set in order to use this estimation set to construct the set of compatible models $\mathcal{C}_M$ again at the next sample time k. It consists in computing the ellipsoidal estimated sets $\mathcal{E}_i(P, \bar{x}_{k+1,i}, \rho_{k+1,i})$ for each model $M_i \in \mathcal{M}$, for $i = 1, \ldots, p$. If the model M_i was compatible with the measurement y_k (i.e. $M_i \in \mathcal{C}_M$), then the ellipsoidal estimation set $\mathcal{E}_i(P, \bar{x}_{k+1,i}, \rho_{k+1,i})$ is computed according to (6.22) using the model M_i, the control $u^*_{k|k}$ and the measurement y_k. Otherwise, the ellipsoidal estimation set $\mathcal{E}_i(P, \bar{x}_{k+1,i}, \rho_{k+1,i})$ is computed according to (6.22) using the best model M^*_k, the control $u^*_{k|k}$ and the measurement y_k, in order to obtain a guaranteed estimation for this incompatible model with the measurement.

- **Obtained the final estimation at time** $k+1$**:** (*step 33*)

  Finally, the ellipsoidal estimation set $\mathcal{E}(P, \bar{x}_{k+1}, \rho_{k+1})$ is based on the best model M^*_k, the optimal control $u^*_{k|k}$ and y_k.

Algorithm 5. Fault Detection using Multiple Model technique

---

1. $k \leftarrow 0$;
2. $\mathcal{E}(P_0, \bar{x}_0, \rho_0) \leftarrow \{x \in \mathbb{R}^{n_x} : (x - \bar{x}_0)^\top P_0 (x - \bar{x}_0) \leq \rho_0\}$;
3. **for** $i = 1 : p$
4. $\quad \mathcal{E}_i(P_0, \bar{x}_0, \rho_0) = \mathcal{E}(P_0, \bar{x}_0, \rho_0)$;
5. **end for**
6. **for** $k = 0 : N - 1$
7. $\quad \mathcal{C}_M = \emptyset$;
8. $\quad$ Collect y_k;
9. $\quad$ **for** $i = 1 : p$
10. $\quad\quad$ Use the output measurements y_k to construct the polytope $\mathcal{P}_{check}(C_i, y_k, F_i)$;
11. $\quad\quad$ **if** $\mathcal{E}_i(P, \bar{x}_{k,i}, \rho_{k,i}) \cap \mathcal{P}_{check}(C_i, y_k, F_i) = \emptyset$
12. $\quad\quad\quad$ The model M_i is not compatible with the set of measurements;
13. $\quad\quad\quad$ $\mathcal{C}_M = \mathcal{C}_M$;
14. $\quad\quad$ **else**

15. The model M_i is compatible with the set of measurements;
16. $\mathcal{C}_M = \{\mathcal{C}_M, M_i\}$;
17. **end if**
18. **end for**
19. $s_M = \text{size}(\mathcal{C}_M)$
20. $\mathcal{U}_k = \emptyset$
21. **for** $j = 1 : s_M$
22. Compute $\mathbf{u}_{k|k,j}$ by solving the criterion (6.30);
23. $\mathcal{U}_k = \{\mathcal{U}_k, \mathbf{u}_{k|k,j}\}$;
24. **end for**
25. Compute $u^*_{k|k}$ and M^*_k using (6.32) and (6.33);
26. **for** $i = 1 : p$
27. **if** $M_i \in \mathcal{C}_\mathcal{M}$
28. Compute the ellipsoidal estimation set $\mathcal{E}_i(P, \bar{x}_{k+1,i}, \rho_{k+1,i})$ according to (6.22) using the model M_i (defined by the matrices A_i, B_i, C_i, E_i and F_i) and the control $u^*_{k|k}$;
29. **else**
30. Compute the ellipsoidal estimation set $\mathcal{E}_i(P, \bar{x}_{k+1,i}, \rho_{k+1,i})$ according to (6.22) using M^*_k and $u^*_{k|k}$;
31. **end if**
32. **end for**
33. Compute the ellipsoidal estimation set $\mathcal{E}(P, \bar{x}_{k+1}, \rho_{k+1})$ according to (6.22) using the model M^*_k;
34. $k = k + 1$;
35. **end for**.

***Remark* 6.5.** This method deals with all types of faults (i.e. actuator, component and sensor faults). A set of models is used such that each model is adequate for one faulty situation. To construct this set of models, a good knowledge of a system is required.

***Remark* 6.6.** The choice of tuning parameters, i.e. the prediction horizon (h), the weighting matrices (Q and R) and the constraints on the state ($x_{\min}$ and $x_{\max}$) and on the input ($u_{\min}$ and $u_{\max}$), is not an easy task and it depends on the desired objectives.

The following example shows the effectiveness of the *Algorithm* 5.

***Example* 6.2.** Consider the following LTI discrete-time system:

$$\begin{cases} x_{k+1} = \begin{bmatrix} 0.7 & 0.3 \\ 0.6 & 0.7 \end{bmatrix} x_k + \begin{bmatrix} 0.3 \\ 0.2 \end{bmatrix} u_k + \begin{bmatrix} 0.05 & 0 & 0 & 0 \\ 0 & 0.02 & 0 & 0 \end{bmatrix} \omega_k \\ y_k = \begin{bmatrix} -2 & 1 \\ 1 & 1 \end{bmatrix} x_k + \begin{bmatrix} 0 & 0 & 0.01 & 0 \\ 0 & 0 & 0 & 0.01 \end{bmatrix} \omega_k \end{cases} \tag{6.34}$$

with $\|\omega_k\|_\infty \leq 1$. The value of ω_k is randomly generated. The initial state belongs to the ellipsoid $\mathcal{E}(\mathbb{I}_2, [0 \;\; 0]^\top, 1)$. In this example, 4 models are considered:

- M_1 corresponds to the fault-free system, i.e. $A_1 = A$, $B_1 = B$, $C_1 = C$, $E_1 = E$ and $F_1 = F$.
- M_2 models the system with a component fault: $A_2 = \begin{bmatrix} 0.4 & 0.8 \\ 0.1 & 0.2 \end{bmatrix}$, $B_2 = B$, $C_2 = C$, $E_2 = E$ and $F_2 = F$.
- M_3 corresponds to an actuator fault, with $A_3 = A$, $B_2 = \begin{bmatrix} 0.15 \\ 0.1 \end{bmatrix}$, $C_3 = C$, $E_3 = E$ and $F_3 = F$.
- M_4 corresponds to the system having a fault in the second sensor, with $A_4 = A$, $B_4 = B$, $C_4 = \begin{bmatrix} -2 & 1 \\ 0.5 & 0.5 \end{bmatrix}$, $E_4 = E$ and $F_4 = F$. The length simulation $N = 100$. The prediction horizon is $h = 10$, the weighting matrices $Q = \begin{bmatrix} 10 & 0 \\ 0 & 10 \end{bmatrix}$ and $R = 5$. The following constraints are considered on the state $x_{\min} = \begin{bmatrix} -0.2 \\ -0.2 \end{bmatrix}$, $x_{\max} = \begin{bmatrix} 0.2 \\ 0.2 \end{bmatrix}$, and on the input $u_{\min} = -0.2$ and $u_{\max} = 0.2$.

The simulated faults are described in Table 6.1.

Table 6.1: Simulated fault scenario

Fault description	Time interval (samples)
50% fault in actuator	10 – 20
50% fault in sensor	50 – 60

Figures 6.12 and 6.13 illustrate the bounds of x_1 and x_2 after 100 iterations. The solid blue lines represent the bounds obtained by *Algorithm* 5.

The red stars represent the real state of the system (situated inside the estimated bounds). The state estimation is guaranteed despite the presence of the considered faults, however the bounds of the estimation set are larger when faults occur (compared to the fault-free time intervals).

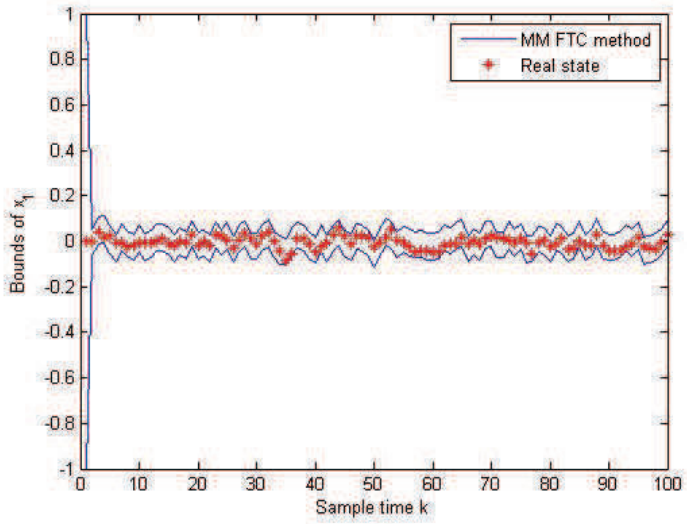

Figure 6.12: Bounds of x_1

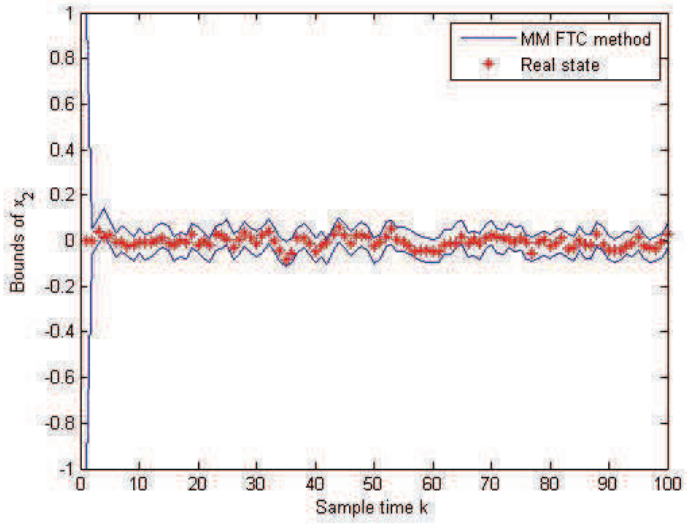

Figure 6.13: Bounds of x_2

Figure 6.14 represents the control u_k. The constraint $u_{\min} \leq u_k \leq u_{\max}$ is satisfied.

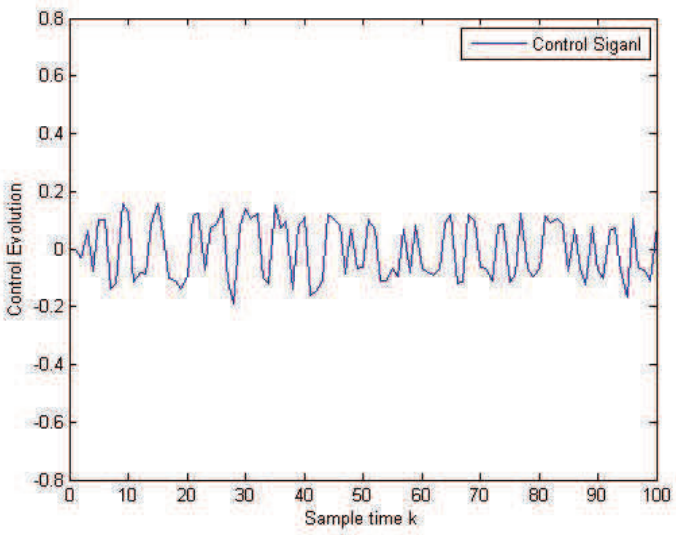

Figure 6.14: Evolution of the control u

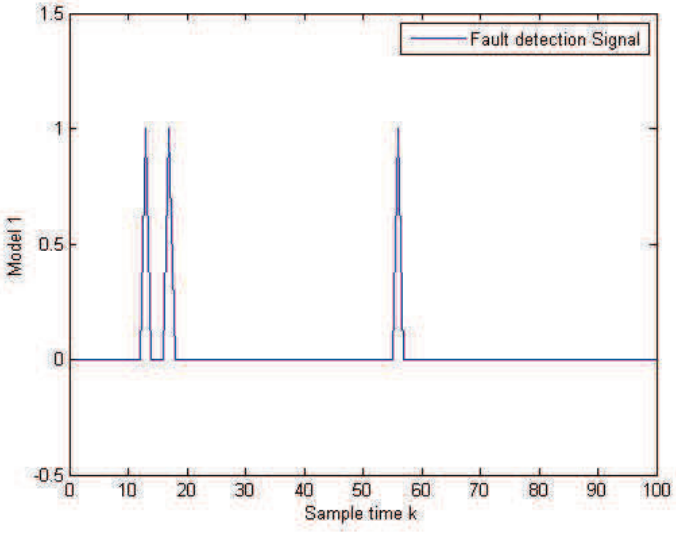

Figure 6.15: Fault signal for model M_1

Figures 6.15, 6.16, 6.17 and 6.18 represent the fault signal obtained using

the models M_1, M_2, M_3 and M_4. When the fault signal is equal to 0 (respectively 1), the model M_i is compatible (respectively incompatible) with the measurements. Effectively, the model M_1 corresponding to the fault-free case system is compatible with the measurement when there is no fault (see Figure 6.15).

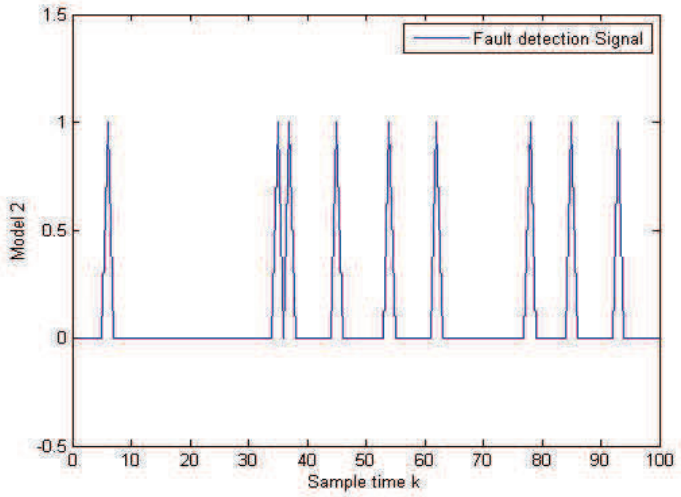

Figure 6.16: Fault signal for model M_2

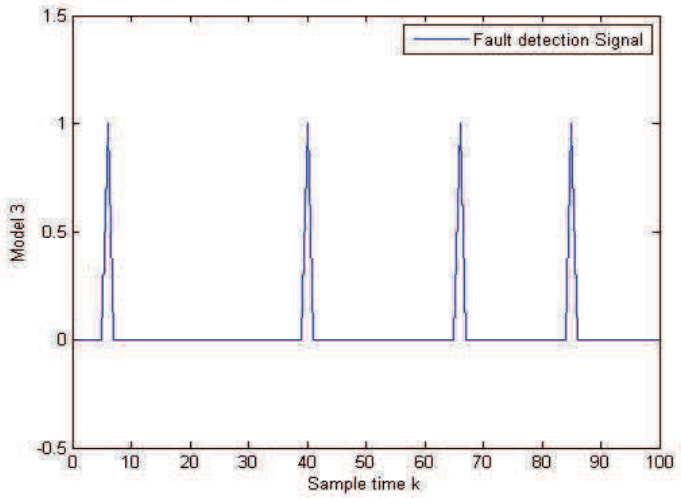

Figure 6.17: Fault signal for model M_3

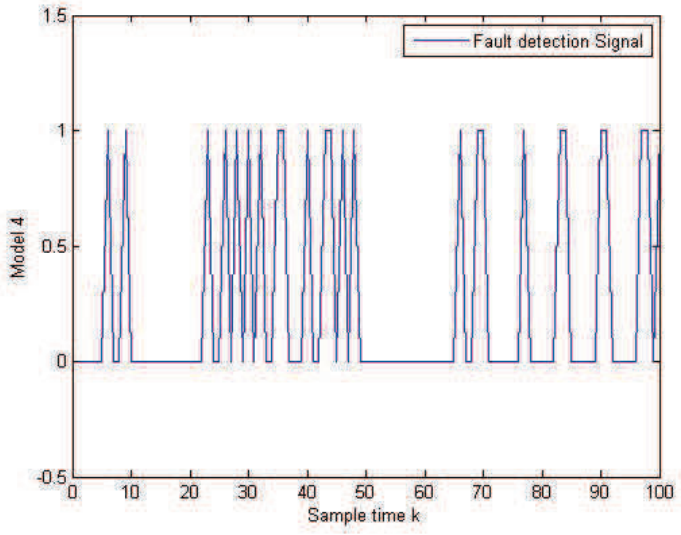

Figure 6.18: Fault signal for model M_4

Even if for the considered actuator fault (between $10-20$ samples), the models M_2, M_3 and M_4 are compatible with the measurements, the optimal model chosen by the Min-Max MPC is M_3. In a similar way, the model M_4 is found (using the proposed Min-Max MPC technique) the optimal model for the considered sensor fault. This confirms the performance of *Algorithm* 5.

6.4 Conclusion

In this chapter, Fault Detection for linear systems with bounded perturbation using set-membership estimation has been treated. Two different methodologies are proposed.

First, three sensor Fault Detection algorithms (called *Algorithms* 2, 3 and 4) based on the consistency test have been proposed. *Algorithm* 2 is used for checking the consistency between the model and the measurements. *Algorithm* 3 gives a guaranteed but conservative estimation in the presence of sensor faults. In a faulty situation, only the prediction step is used. In the fault free-case, both the prediction and correction steps are used. *Algorithm* 4 gives an estimation with reduced conservativeness when sensor faults occur by using the calibration of the measurement. This algorithm is suitable for control perspectives.

Second, a new Fault Detection algorithm (*Algorithm* 5) based on Multiple Models for linear systems with bounded perturbations and measurement noises has been proposed. These models are constructed by referring to the original system, such that each model is adequate to one faulty mode. This method consists first in checking the consistency between each model with the available measurements. The set of compatible models with the measurements is formed. A Min-Max Model Predictive Control is developed for each compatible model ensuring the desirable performances despite the presence of faults. Finally, a quadratic criterion is minimized in order to choose the best control to be applied to the original system and the best model for the estimation. The main advantage of this method consists in considering actuator, component and sensor faults in the same time.

Chapter 7

Conclusion and future directions

7.1 Conclusion

In this thesis, Fault Detection algorithms based on set-membership state estimation for linear uncertain systems with bounded perturbations and bounded measurement noises are proposed. The main contributions of this thesis are divided into three parts:

- The first part proposes an improved method which combines the good accuracy of the zonotopic set-membership state estimation and the reduced complexity of the ellipsoidal set-membership estimation.

- In the second part, a new ellipsoidal state estimation approach based on the minimization of the ellipsoidal radius is developed. Four methods have been presented in this approach. *Methods 1*, *2* and *3* are applied for LTI systems. Method 3 is extended to the case of uncertain LTI systems. Finally, *Method 4* is applied for LTV systems.

- Two Fault Detection techniques have been proposed in the third part. The fist technique allows to detect sensor faults by checking the consistency between the model and the measurements. The second technique is based on Multiple Models for linear systems with bounded perturbations and measurement noises. It deals with actuator/component/sensor faults. A Min-Max Model Predictive Control is developed in order to find the optimal control and the best model to use for the system in spite of the presence of these faults.

The first part deals with the set-membership estimation problem for uncertain linear systems with bounded perturbations and bounded measurement noises. Existing zonotopic and ellipsoidal set-membership estimation

methods are presented. For zonotopes four methods are presented: the Singular Value Decomposition-based method [27], the minimization of the zonotope segments [2], the minimization of the zonotope volume [2] and the P-radius of the zonotope. For ellipsoidal techniques, two methods are outlined: firstly, the determinant-based criterion is minimized [36] and secondly, the minimization of the trace criterion [36]. An improved method (which is the first contribution on this thesis) based on zonotopes and ellipsoids [12] is proposed. This is formulated as an optimization problem which starts with the zonotopic estimation and continues with the ellipsoidal estimation when the zonotopic estimation set is enough small (small value of the P-radius). In this way, this method takes adavantage of the accuracy of the zonotopic estimation and the reduced complexity of the ellipsoidal estimation.

A second contribution is a new guaranteed ellipsoidal state estimation. It consists in minimizing the radius of the ellipsoidal state estimation set. For this, four original methods are given. *Method 1* is applied for LTI systems with bounded perturbations and measurement noises. In this method a fixed observer gain is computed by solving a LMI problem. *Method 2* consists in computing an updated observer gain by solving a LMI optimization problem. This LMI has to be verified in all the vertices of the unitary box that contains the perturbations and measurement noises. It leads to better accuracy but with higher complexity compared to *Method 1*. *Method 3* proposes a Vector Scaling technique for the LMI problem that has to be solved in *Method 2*. It avoids the enumeration problem and it keeps a good level of accuracy with reduced complexity compared to *Method 2*. *Method 3* is also extended for the case of uncertain LTI systems. Finally, *Method 4* (which is a significant contribution of this thesis) is applied for Linear Time Variant (LTV) systems where an updated observer gain and a flexible shape of the estimated ellipsoidal set are computed. An improvement of the accuracy of the proposed ellipsoidal estimation method has been further presented in *Improved Method 4* by adding quadratic constraints on both measurements and perturbations. This allows to reduce the bounds of the estimation domain, offering a better estimation accuracy.

In third part, two Fault Detection techniques have been developed. In the first technique, three sensor Fault Detection algorithms have been proposed. The first algorithm is based on the P-radius minimization method of the zonotopic estimation method. It checks the consistency between the model and the measurements in the fault-free case. The second algorithm gives a guaranteed but conservative estimation in the presence of sensor faults by using only the prediction step. If there are no faults, all the steps (prediction, measurement, correction) are used. The last algorithm gives an estimation with reduced conservativeness using the calibration of the measurement when

sensor fault occur. A second original technique proposes a Fault Detection algorithm based on Multiple Models for linear systems with bounded perturbations and measurement noises. It deals with actuator, component and sensor faults simultaneously. In this algorithm, Fault Detection is passively implemented by using set-membership estimation and Fault Tolerant Control (FTC) is actively done by a Model Predictive Control (MPC) design. The consistency of each model with the measurements is checked at each sample time based on the ellipsoidal state estimation proposed is the second part. A Min-Max Model Predictive Control has been developed in order to find the optimal control and the best model to use for the system in spite of the presence of component/actuator/sensor faults.

7.2 Future directions

Several mid-term and long term directions are proposed below.

As stated in Example 5.4, the zonotopic estimation approach based on the minimization of the P-radius [67] is developed for systems with interval evolution matrix but with constant observation matrix. On one hand, it will be interesting to extend this method to the case of systems with interval observation matrix. On the other hand, an interesting perspective is to develop a new P-radius-based zonotopic set-membership estimation by updating the vector λ from equation (4.37) for SISO systems (or matrix Λ from equation (4.48) for MIMO systems). This leads to replace λ by λ_k (or Λ by Λ_k) at each sample time k. This will increase the accuracy of the zonotopic set-membership estimation.

Another interesting idea is to extend the proposed ellipsoidal state estimation method based on the minimization of the radius to the case of systems with time-delay, for instance by modeling the delays as an interval parametric uncertainty.

It is also possible to extend these set-membership methods (using zonotopes and ellipsoids) to the case of Piecewise Affine (PWA) systems.

It is important to extend/develop the proposed passive sensor Fault Detection algorithms for the case of Multi-Output systems and explore also the results by using ellipsoidal set-membership state estimation approaches. These sensor Fault Detection algorithms should be used also for Fault Tolerant Control purposes. Comparison with existing Fault Detection techniques will be further investigated.

A different perspective is to use a moving horizon set-membership estimation. This horizon can be used for fault monitoring and FTC purposes.

Finally, we propose to experimentally validate these methods.

Appendix 1

Min Max Model Predictive Control

This part details the development of Min-Max Model Predictive Control applied to each model M_j belonging to the compatible set $\mathcal{C}_M$. The control signal is found by minimizing the worst case (with respect to the perturbations ω_k) of a quadratic criterion (6.30). The Min-Max optimization problem (6.30) is reformulated as a quadratic programming (QP) problem. The controller is, then, computed using the ellipsoidal state estimation at the previous sample time by solving a simple QP problem.

Starting from the quadratic cost function[1]

$$J_j(u_{k,j}, \omega_k, x_{k,j}) = \sum_{l=0}^{h-1} \left(x_{k+l+1,j}^\top Q x_{k+l+1,j}^\top + u_{k+l,j}^\top R u_{k+l,j} \right), \tag{7.1}$$

the following state equations are computed for each compatible model $M_j \in \mathcal{C}_M$, with $j = 1, \ldots, s_M$:

$$\begin{cases} x_{k+1,j} &= A_j x_{k,j} + B_j u_{k,j} + E_j \omega_{k,j}, \\ \vdots & \\ x_{k+l,j} &= A_j^l x_{k,j} + A_j^{l-1} B_j u_{k,j} + A_j^{l-2} B_j u_{k+1,j} + \ldots + B_j u_{k+l-1,j} + \\ & \quad + A_j^{l-1} F_j \omega_{k,j} + A_j^{l-2} F_j \omega_{k+1,j} + \ldots + F_j \omega_{k+l-1,j}, \\ \vdots & \\ x_{k+h,j} &= A_j^h x_{k,j} + A_j^{h-1} B_j u_{k,j} + A_j^{h-2} B_j u_{k+1,j} + \ldots + B_j u_{k+h-1,j} + \\ & \quad + A_j^{h-1} F_j \omega_{k,j} + A_j^{h-2} F_j \omega_{k+1,j} + \ldots + F_j \omega_{k+h-1,j}, \end{cases}$$

with h the prediction horizon and $j = 1, \ldots, s_M$.
Denote by $\mathbf{u}_{k|k,j} = [u_{k|k,j}, u_{k+1|k,j}, \ldots, u_{k+h-1|k,j}]^\top$ and
$\boldsymbol{\omega}_{k|k,j} = [\omega_{k|k,j}, \omega_{k+1|k,j}, \ldots, \omega_{k+h-1|k,j}]^\top$ the sequences of control signals and perturbations, respectively. Then, the state equation of the model $M_j \in \mathcal{C}_M$, predicted for time $k+l+1$ at time k, can be rewritten as:

$$x_{k+l+1|k,j} = A_j^l x_{k+1|k,j} + \mathcal{A}_{l,j} B_j \mathbf{u}_{k|k,j} + \mathcal{A}_{l,j} \boldsymbol{\omega}_{k|k,j} \tag{7.2}$$

[1]Here the index $k+l|k$ is omitted and replaced by $k+l$ in order to simplify the notations.

where the $\mathcal{A}_{l,j}$ matrix is defined as:

$$\mathcal{A}_{l,j} = \begin{bmatrix} A_j^{l-1} & A_j^{l-2} & \dots & A_j^0 & \underbrace{\mathbb{O}_{n_x,n_x} & \dots & \mathbb{O}_{n_x,n_x}}_{h-j \text{ times}} \end{bmatrix}$$

.

Replacing (7.2) in (7.1) and after some manipulations, the optimization problem (6.30) becomes:

$$\mathbf{u}_{k,j} = \arg \min_{\mathbf{u}_{k|k,j} \in \mathcal{U}_k} \max_{\boldsymbol{\omega}_{k|k,j} \in \mathbf{B}^{h\times(n_x+n_y)}} f(\mathbf{u}_{k|k,j}, \boldsymbol{\omega}_{k|k,j}), \tag{7.3}$$

where $f(\mathbf{u}_{k|k,j}, \boldsymbol{\omega}_{k|k,j}) = \alpha_1 + \alpha_2\ \boldsymbol{\omega}_{k|k,j} + \alpha_3\ \mathbf{u}_{k|k,j} + \boldsymbol{\omega}_{k|k,j}^\top\ \alpha_4\ \boldsymbol{\omega}_{k|k,j} + \boldsymbol{\omega}_{k|k,j}^\top\ \alpha_5\ \mathbf{u}_{k|k,j} + \mathbf{u}_{k|k,j}^\top\ \alpha_6\ \mathbf{u}_{k|k,j}$, with

$$\begin{cases} \alpha_1 &= x_{k+1|k,j}^\top \sum_{l=0}^{h-1} {A^l}_j^\top Q A_j^l x_{k+1|k,j} \\ \alpha_2 &= 2x_{k+1|k,j}^\top \sum_{l=0}^{h-1} {A^l}_j^\top Q \mathcal{A}_{l,j} \bar{F} \\ \alpha_3 &= 2x_{k+1|k,j}^\top \sum_{l=0}^{h-1} {A^l}_j^\top Q \mathcal{A}_{l,j} \bar{B} \\ \alpha_4 &= \bar{F}^\top \sum_{l=0}^{h-1} \mathcal{A}_{l,j}^\top Q \mathcal{A}_{l,j} \bar{F} \\ \alpha_5 &= 2\bar{F}^\top \sum_{l=0}^{h-1} \mathcal{A}_{l,j}^\top Q \mathcal{A}_{l,j} \bar{B} \\ \alpha_6 &= \bar{F}^\top \sum_{l=0}^{h-1} \mathcal{A}_{l,j}^\top Q \mathcal{A}_{l,j} \bar{F} + \bar{R} \end{cases} \tag{7.4}$$

with $\bar{B} = \text{diag}(\underbrace{B, \dots, B}_{h \text{ times}})$, $\bar{F} = \text{diag}(\underbrace{F, \dots, F}_{h \text{ times}})$ and $\bar{R} = \text{diag}(\underbrace{R, \dots, R}_{h \text{ times}})$.

The function $f(\mathbf{u}_{k|k,j}, \boldsymbol{\omega}_{k|k,j})$ is quadratic with respect to $\mathbf{u}_{k|k,j}$ and $\boldsymbol{\omega}_{k|k,j}$. In [3], it is shown that the Min-Max MPC problem (7.3) is convex and it is equivalent to:

$$\mathbf{u}_{k,j} = \arg \min_{\mathbf{u}_{k|k,j} \in \mathcal{U}_k} \max_{\boldsymbol{\omega}_{k|k,j} \in \mathcal{V}_{\mathbf{B}^{h\times(n_x+n_y)}}} f(\mathbf{u}_{k|k,j}, \boldsymbol{\omega}_{k|k,j}). \tag{7.5}$$

Then, the perturbation $\boldsymbol{\omega}_{k|k,j}$ is known and consists in replacing it by all the values corresponding to the vertices $\mathcal{V}_{\mathbf{B}^{h\times(n_x+n_y)}}$. For this reason, the problem (7.5) becomes a QP problem as follows:

$$\mathbf{u}_{k,j} = \arg \min_{\mathbf{u}_{k|k,j} \in \mathcal{U}_k} \tilde{f}(\mathbf{u}_{k|k,j}), \tag{7.6}$$

such that $\tilde{f}(\mathbf{u}_{k|k,j})$ is quadratic with respect to $\mathbf{u}_{k|k,j}$. In general the constraints $x_k \in \mathbb{X}$ and $u_k \in \mathbb{U}$ are given in the following form: $x_{\min} \leq x_k \leq x_{\max}$ and $u_{\min} \leq u_k \leq u_{\max}$. Finally, the problem (6.30) to solve is a QP problem:

$\min_{\mathbf{u}_{k|k,j}} \tilde{f}(\mathbf{u}_{k|k,j})$
subject to

$$\begin{bmatrix} \mathcal{A}_{l,j}\bar{B} \\ -\mathcal{A}_{l,j}\bar{B} \\ \mathcal{I}_l \\ -\mathcal{I}_l \end{bmatrix} \mathbf{u}_{k|k,j} \prec \begin{bmatrix} b_1 \\ b_2 \\ u_{\max} \\ -u_{\min} \end{bmatrix}, \tag{7.7}$$

for $l = 0, \ldots, h-1$ with $b_1 = x_{\max} - A_j^l x_{k+1|k} - \mathcal{A}_{l,j}\bar{F}\boldsymbol{\omega}_{k|k}$ and $b_2 = -x_{\min} + A_j^l x_{k+1|k} + \mathcal{A}_{l,j}\bar{F}\boldsymbol{\omega}_{k|k}, \forall \boldsymbol{\omega}_{k|k} \in \mathcal{V}_{\mathbf{B}^{h\times(n_x+n_y)}}$ and $\mathcal{I}_l = \begin{bmatrix} \mathbb{O}_{l-1,n_u} & \mathbb{1}_{1,n_u} & \mathbb{O}_{h-l,n_u} \end{bmatrix}$.

Note that the state $x_{k|k}$ is chosen equal to the nominal state which is in this case the center of the ellipsoidal state estimation set $\bar{x}_k$.

Bibliography

[1] O. Adrot and J. M. Flaus. Trajectory Computation of Dynamic Uncertain Systems. In *Proc. of the IEEE Conference on Decision and Control*, 2003. Hawaii, USA.

[2] T. Alamo, J. M. Bravo, and E. F. Camacho. Guaranteed state estimation by zonotopes. *Automatica*, 41:1035–1043, 2005.

[3] T. Alamo, D. R. Ramirez, and D. Muñoz de la Peña. Min-Max MPC using a tractable QP problem. In *Proc. of the 49th IEEE Conference on Decision and Control, and the European Control Conference*, 2005. Seville, Spain.

[4] T. Alamo, R. Tempo, D. R. Ramírez, and E. F. Camacho. A new vertex result for robustness problems with interval matrix uncertainty. *Systems and Control Letters*, 57:474–481, 2008.

[5] A. A. Albert. An inductive proof of Descartes's rule of signs. *American Mathematical Monthly*, 50(3):178–180, 1943.

[6] M. Althoff, O. Stursberg, and M. Buss. Computing reachable sets of hybrid systems using a combination of zonotopes and polytopes. *Nonlinear Analysis: Hybrid Systems*, 4(2):233–249, 2010.

[7] J. M. Aughenbaugh and C. J. J. Paredis. Why are intervals and imprecision important in engineering design? In *Proc. of the Reliable Engineering Computing Workshop*, Savannah, USA, 2006.

[8] B. M. Ayyub and G. J. Klir. *Uncertainty modeling and analysis in engineering and the sciences*. Chapman and Hall/CRC, 2006.

[9] A. Banerjee, Y. Arkun, B. Ogunnaike, and R. Pearson. H-infinity Control of Nonlinear Processes using Multiple Linear Models. In *Proc. of European Control Conference*, Rome, Italy, 1995.

[10] A. A. Batabyal. *Dynamic and stochastic approaches to the environment and economic development*. World Scientific Publishing Company, 2008.

[11] A. Bemporad and A. Garulli. Output feedback predictive control of constrained linear systems via set-membership state estimation. *International Journal of Control*, 73(8):655–665, 2000.

[12] S. Ben Chabane, C. Stoica Maniu, T. Alamo, E. F. Camacho, and D. Dumur. Improved Set-Membership Estimation Approach based on Zonotopes and Ellipsoids. In *Proc. of European Control Conference*, Rome, Italy, 2014.

[13] S. Ben Chabane, C. Stoica Maniu, T. Alamo, E. F. Camacho, and D. Dumur. Sensor fault detection and diagnosis using zonotopic set-membership estimation. In *Mediterranean Conference on Control and Automation*, Palermo, Italy, 2014.

[14] S. Ben Chabane, C. Stoica Maniu, T. Alamo, E. F. Camacho, and D. Dumur. Ellipsoidal guaranteed state estimation for uncertain linear time-variant systems. *2nd submission to Automatica*, 2015.

[15] S. Ben Chabane, C. Stoica Maniu, E. F. Camacho, T. Alamo, and D. Dumur. A Multiple Models Approach for Fault Detection based on Set-Membership State Estimation. In *Submitted to the European Control Conference*, 2016. Aalborg, Denmark.

[16] D. P. Bertsekas and I. B. Rhodes. Recursive state estimation for a set-membership description of uncertainty. *IEEE Transactions on Automatic Control*, 16(2):117–128, 1971.

[17] F. Blanchini and S. Miani. *Set-theoretic methods in control*. Birkhauser, Boston, 2007.

[18] J. Blesa, V. Puig, and J. Saludes. Robust fault detection using polytope-based set-membership consistency test. In *Conference on Control and Fault Tolerant Systems*, Nice, France, 2010.

[19] S. Boyd, L. El Ghaoui, E. Feron, and V. Balakrishnan. *Linear Matrix Inequalities in system and control theory*. SIAM, Philadelphia, 1994.

[20] E. M. Bronstein. Approximation of convex sets by polytopes. *Journal of Mathematical Sciences*, 153(6):727–762, 2008.

[21] R. G. Brown and P. Y. C. Hwang. *Introduction to random signals and applied Kalman Filtering*. John Wiley and Sons, 1997.

[22] G. Calafiore and L. El Ghaoui. Ellipsoidal bounds for uncertain linear equations and dynamical systems. *Automatica*, 40:773–787, 2004.

[23] J. Chen and R. Patton. *Robust model-based Fault Diagnosis for dynamic systems*. Kluwer Academic Publishers, 1999.

[24] F. L. Chernousko. *State estimation for dynamic systems*. CRC Press, Boca Raton, 1994.

[25] F. L. Chernousko and D. Ya. Rokityanskii. Ellipsoidal bounds on reachable sets of dynamical systems with matrices subjected to uncertain perturbations. *Journal of Optimization Theory and Applications*, 104:1–19, 2000.

[26] L. Chisci, A. Garulli, and G. Zappa. Recursive state bounding by parallelotopes. *Automatica*, 32:1049–1055, 1996.

[27] C. Combastel. A state bounding observer based on zonotopes. In *Proc. of European Control Conference*, Cambridge, UK, 2003.

[28] C. Combastel. Observation de systèmes non linéaires appliquée à un modèle de bioréacteur. Une approche ensembliste basée sur les zonotopes. *Journal Européen des Systèmes Automatisés*, 38:933–957, 2004.

[29] C. Combastel. A state bounding observer for uncertain non-linear continuous-time systems based on zonotopes. In *Proc. of the 44th IEEE Conference on Decision and Control, and the European Control Conference*, Sevilla, Spain, 2005.

[30] C. Combastel. Zonotopes and Kalman observers: Gain optimality under distinct uncertainty paradigms and robust convergence. *Automatica*, 55:265–273, 2015.

[31] G. B. Dantzig. Fourier-motzkin elimination and its dual. Technical report, DTIC document, 1972.

[32] A. N. Daryin and A. B. Kurzhanski. Estimation of reachability sets for large-scale uncertain systems: from theory to computation. *In Proc. of 51st IEEE Conference on Decision and Control, Maui, Hawaii, USA*, pages 7401–7406, 2012.

[33] A. N. Daryin, A. B. Kurzhanski, and I. V. Vostrikov. Reachability approaches and ellipsoidal techniques for closed-loop control of oscillating systems under uncertainty. *In Proc. of 51st IEEE Conference on Decision and Control, San Diego, CA, USA*, pages 6390–6395, 2006.

[34] S. De Oca, V. Puig, M. Witczak, and L. Dziekan. Fault-tolerant control strategy for actuator faults using LPV techniques: application to a two degree of freedom helicopter. *International Journal of Applied Mathematics and Computer Science*, 37(4):161–171, 2012.

[35] G. Ducard and H. P. Geering. Efficient nonlinear actuator fault detection and isolation system for unmanned aerial vehicles. *Journal of Guidance, Control, and Dynamics*, 31(1):225–237, 2008.

[36] C. Durieu, E. Walter, and B. Polyak. Multi-input multi-output ellipsoidal state bounding. *Journal of Optimization Theory and Applications*, 111(2):273–303, 2001.

[37] D. Efimov, T. Raïssi, S. Chebotarev, and A. Zolghadri. Interval state observer for nonlinear time varying systems. *Automatica*, 49(1):200–205, 2013.

[38] E. Fogel. System identification via membership set constraints with energy constrained noise. *IEEE Transaction on Automatic Control*, AC-24:752, 1979.

[39] Eli Fogel and Y. F. Huang. On the value of information in system identification-bounded noise case. *Automatica*, 18:229–238, 1982.

[40] K. Fukuda. Cdd/cdd+ reference manual, 1999.

[41] K. Fukuda. From the zonotope construction to the Minkowski addition of convex polytopes. *Journal of Symbolic Computation*, 38(4):1261–1272, 2004.

[42] A. Garulli and A. Vicino. Set membership localization of mobile robots via angle measurement. *IEEE Transactions on Robotic and Automation*, 17(4):450 – 463, 2001.

[43] A. Girard. Reachability of uncertain linear systems using zonotopes. In *Hybrid Systems: Computation and Control*, volume 3414 of *Lecture Notes in Computer Science*, pages 291–305. Springer.

[44] P. Gritzmann and B. Sturmfels. Minkowski addition of polytopes: Computational complexity and applications to Gröbner bases. *SIAM Journal on Discrete Mathematic*, 6(2):246–269, 1993.

[45] A. Haar. *Über Lineare Ungleichungen*. 1918.

[46] R. Hallouzi, V. Verdult, R. Babuska, and M. Verhaegen. Fault detection and identification of actuator faults using linear parameter varying models. In *Proc. of the 16th Triennial World Congress IFAC*, Prague, Czech Republic, 2005.

[47] R. Hallouzi, M. Verhaegen, R. Babuska, and S. Kanev. Model weight and state estimation for Multiple Model systems applied to Fault Detection and Identification. In *Proc. of the 14th IFAC Symposium on System Identification*, Newcastle, Australia, 2006.

[48] H. Hamdi, M. Rodrigues, C. Mechmeche, and N. Benhadj Braiek. Robust Fault Detection and estimation for descriptor systems based on Multi-Models concept. *International Journal of Control, Automation, and Systems, IJCAS*, 10(6):1260–1266, 2012.

[49] E. R. Hansen. Interval arithmetic in matrix computations. *SIAM Journal on Numerical Analysis: Series B*, 2(2):308–320, 1965.

[50] D. Henrion and J. B. Lasserre. Convergent relaxations of polynomial matrix inequalities and static output feedback. *IEEE Transactions on Automatic Control*, 51(2):192 – 202, 2006.

[51] D. Henrion and J. B. Lasserre. Inner approximations for polynomial matrix inequalities and robust stability regions. Technical report, LAAS-report 11210, 2011.

[52] T. Hu and Z. Lin. Composite quadratic Lyapunov functions for constrained control systems. *IEEE Transaction on Automatic Control*, 48:440–450, 2003.

[53] A. Ingimundarson, J. M. Bravo, V. Puig, T. Alamo, and P. Guerra. Robust fault detection using zonotope-based set-membership consistency. *International journal of adaptive control and signal processing*, 23(4):311–330, 2008.

[54] A. Ingimundarson, J.M. Bravo, V. Puig, and T. Alamo. Robust fault diagnosis using parrallelotope-based set-membership consistency tests. In *Proc. of European Control Conference*, Seville, Spain, 2005.

[55] L. Jaulin, M. Kieffer, O. Didrit, and E. Walter. *Interval analysis*. Springer, 2001.

[56] M. Jouili, K. Jarray, Y. Koubaa, and M. Boussak. A Luenberger state observer for simultaneous estimation of speed and rotor resistance in sensorless indirect stator flux orientation control of induction motor drive. *International Journal of Computer Science Issues*, 8:116–125, 2011.

[57] R. E. Kalman. A new approach to linear filtering and prediction problems. *Transactions of the ASME–Journal of Basic Engineering*, 82(Series D):35–45, 1960.

[58] M. Kočvara and S. Stingl. PENNON A Code for convex nonlinear and semidefinite programming. *optimization methods and software*, 18(3):317–333, 2003.

[59] A. J. Krener. On the equivalence of control systems and the linearization of nonlinear systems. *SIAM Journal of Control*, 11:670–676, 1973.

[60] W. Kühn. Rigorously computed orbits of dynamical systems without the wrapping effect. *Computing*, 61:47–67, 1998.

[61] A. B. Kurzhanski and I. Vályi. *Ellipsoidal calculus for estimation and control*. Birkhaüser Boston, 1996.

[62] A. A. Kurzhanskiy and P. Varaiya. Ellipsoidal toolbox manual, 2006-2007.

[63] S. R. Lay. *Convex sets and their applications*. Wiley, New york, 1982.

[64] V. T. H. Le. *Commande prédictive robuste par des techniques d'observateurs à base d'ensembles zonotopiques*. PhD thesis, Supélec, France, 2012.

[65] V. T. H. Le, T. Alamo, E. F. Camacho, C. Stoica, and D. Dumur. Zonotope-based set-membership estimation for multi-output uncertain systems. In *IEEE Multiconference on Systems and Control*, Hyderabab, India, 2013.

[66] V. T. H. Le, T. Alamo, E. F. Camacho, C. Stoica, and D. Dumur. *Zonotopes: From Guaranteed State Estimation to Control*. ISTE Ltd and John Wiley & Sons, Inc., ISBN: 1-84821-589-4, 2013.

[67] V. T. H. Le, C. Stoica, T. Alamo, E. F. Camacho, and D. Dumur. Zonotopic guaranteed state estimation for uncertain systems. *Automatica*, 49(1):3418–3424, 2013.

[68] D. G. Luenberger. Observers for multivariable systems. *IEEE Transactions on Automatic Control*, 11:190 – 197, 1965.

[69] M. Mahmoud, J. Jiang, and Y. Zhang. *Active Fault Tolerant Control systems: stochastic analysis and synthesis*. Springer-Verlag, London, 2004.

[70] B. Marx, D. Koenig, and J. Ragot. Design of observers for Takagi-Sugeno nonlinear descriptor systems with unknown inputs and application to fault diagnosis. *IET Control Theory Application*, 1:1487–1495, 2007.

[71] J. Marzat, H. Piet-Lahanier, F. Damongeot, and E. Walter. Fault diagnosis for nonlinear aircraft based on control-induced redundancy. In *Conference on Control and Fault Tolerant Systems*, Nice, France, 2010.

[72] P. S. Maybeck. *Stochastic models, estimation and control*. Academic Press, 1979.

[73] P. S. Maybeck. Multiple model adaptive algorithms for detecting and compensating sensor and actuator/surface failures in aircraft flight control systems. *International Journal of Robust and Nonlinear Control*, 9(14):1051–1070, 1999.

[74] M. A. Medina, D. Theilliol, and D. Sauter. Simultaneous fault diagnosis and robust activation function estimation of linear multiple-models considering the bounded modelling uncertainty. In *Mediterranean Conference on Control and Automation*, pages 405–410, Limassol, Cyprus, 2005.

[75] H. Montgomery. Computing the volume of a zonotope. *The American Mathematicals Monthly*, 97:431, 1989.

[76] R. E. Moore. *Interval analysis*. Englewood Cliff, New Jersey: Prentice-Hall, 1966.

[77] F. Nejjari, V. Puig, S. M. Ora, and A. Sadeghzadeh. Robust fault detection for LPV systems using interval observers and zonotopes. In *Proc. of the 48th IEEE Conference on Decision and Control*, pages 1002–1007, Shanghai, P.R. China, 2009.

[78] S. Olaru, J.A. De Doná, M. M. Seron, and F. Stoican. Positive invariant sets for fault tolerant multisensor control schemes. *International Journal of Control*, 83(12):2622–2640, 2010.

[79] P. Planchon and J. Lunze. Diagnosis of linear systems with structured uncertainties based on guaranteed state observation. *International Journal of Control, Automation and Systems*, 6(3):306–319, 2008.

[80] Polyak, S. A. Nazin, C. Durieu, and E. Walter. Ellipsoidal parameter or state estimation under model uncertainty. *Automatica*, 40:1171–1179, 2004.

[81] B. Polyak, S. A. Nazin, C. Durieu, and E. Walter. Ellipsoidal estimation under model uncertainty. In *Proc. of the 15th World Congress IFAC*, Barcelona, Spain, 2002.

[82] V. Puig. Fault Diagnosis and Fault Tolerant Control using set-membership approaches: Application to real case studies. *International Journal of Applied Mathematics and Computer Science*, 20(4):619–635, 2010.

[83] V. Puig, P. Cugueró, and J. Quevedo. Worst-case estimation and simulation of uncertain discrete-time systems using zonotopes. In *Proc. of Europeen Control Conference*, Portugal, 2001.

[84] V. Puig, P. J. Cuguero, J. Quevedo, and T. Escobet. Time-invariant approach to worst-case simulation and observation of discrete-time uncertain systems. In *Proc. of the IEEE Conference on Decision and Control*, 2002. Las Vegas, USA.

[85] V. Puig, J. Quevedo, and T. Escobet. Robust fault detection approaches using interval models. In *Proc. on IFAC World Congress*, Spain, 2002.

[86] V. Puig, J. Saludes, and J. Quevedo. Worst-case simulation of discrete linear time-invariant interval dynamic systems. *Reliable Computing*, 9(4):251–290, 2003.

[87] Z. Qu, C. M. Ihlefeld, J. Yufang, and A. Saengdeejing. Robust fault-tolerant self-recovering control of nonlinear uncertain systems. *Automatica*, 39(10):1763–1771, 2003.

[88] T. Raïssi, N. Ramdani, and Y. Candau. Set membership state and parameter estimation for systems described by nonlinear differential equations. *Automatica*, 40(10):1771–1777, 2004.

[89] C. Reboulet and C. Champetier. A new method for linearizing nonlinear systems: the pseudolinearization. *International Journal of Control*, 40:631–638, 1984.

[90] V. Reppa and A. Tzes. Fault detection and diagnosis based on parameter set estimation. *IET Journal of Control Theory and Applications*, 5(1):69–83, 2011.

[91] M. Rodrigues, D. Teilliol, S. Aberkane, and D. Sauter. Fault tolerant control design for polytopic LPV systems. *International Journal of Applied Mathematics and Computer Science*, 17(1):27–37, 2007.

[92] J. Ru and X. R. Li. Variable-structure multiple-model approach to fault detection, identification, and estimation. *IEEE Transaction on Control System Technology*, 2008.

[93] C. S. Scherer and S. Weiland. Linear matrix inequalities in control, 2007.

[94] S. Schön and H. Kutterer. Using zonotopes for overestimation-free interval least-squares-some geodetic applications. *Reliable Computing Springer*, 11:137–155, 2005.

[95] F. C. Schweppe. Recursive state estimation: Unknown but bounded errors and system inputs. *IEEE Transactions on Automatic Control*, 13(1):22–28, 1968.

[96] F. Scibilia, S. Olaru, and M. Hovd. On feasible sets for MPC and their approximations. *Automatica*, 47(1):133–139, 2011.

[97] M. M. Seron and J. A. De Doná. Robust actuator fault compensation accounting for uncertainty in the fault estimation. *International Journal of Adaptive Control and Signal Processing*, DOI: 10.1002/acs.2453, 2013.

[98] M. M. Seron, J. A. De Doná, and S. Olaru. Fault tolerant control allowing sensor healthy-to-faulty and faulty-to-healthy transitions. *Automatic Control, IEEE Transactions on*, 57(7):1657–1669, 2012.

[99] P. Seymour. A note on hyperplane generation. *Journal of Combinatorial Theory, Series B*, 61(1):88–91, 1994.

[100] G. Shephard. Combinatorial properties of associated zonotopes. *Canadian Journal of Mathematics*, 26:302–321, 1974.

[101] D. Theilliol, H. Noura, and J. C. Ponsart. Fault diagnosis and accommodation of a three-tank system based on analytical redundancy. *ISA Transaction*, 41:365–382, 2002.

[102] M. Ullah and O. Wolkenhauer. *Stochastic approaches for systems biology*. Springer, 2011.

[103] V. G. Verma, R. Simmons, and S. Thrun. Real-time fault diagnosis. *IEEE Robotics and Automation Magazine*, 11(2):56–66, 2004.

[104] A. Vicino and G. Zappa. Sequential approximation of feasible parameter sets for identification with set-membership uncertainty. *IEEE Transactions on Automatic Control*, 41:774–785, 1996.

[105] E. Walter and H. Piet-Lahanier. Exact recursive polyhedral description of the feasible parameter set for bounded-error models. *IEEE Transactions on Automatic Control*, 34(8):911–915, 1989.

[106] H. S. Wistenhausen. Sets of possible states of linear systems given perturbed observations. *IEEE Transaction on Automatic Control*, 13(5):556–558, 1968.

[107] M. Witczak, L. Dziekan, V. Puig, and J. Korbicz. An integrated design strategy for fault identification and fault-tolerant control for Takagi-Sugeno fuzzy systems. In *Proc. of the 17th World Congress of the International Federation of Automatic Control*, pages 7387–7392, Seoul, Korea, 2007.

[108] Y. Yang. Controllability and observability of a class of linear, time-invariant systems with interval plants. *International Journal of Information and Systems Sciences*, 1:184–192, 2005.

[109] G. G. Yen and L. W. Ho. Online multiple-model-based fault diagnosis and accommodation. *IEEE Transactions on Industrial Electronics*, 50(2):296–312, 2003.

[110] Y. Zhang and X. R. Li. Detection and diagnosis of sensor and actuator failures using IMM estimator. *IEEE Transactions on Aerospace and Electronic Systems*, 34(4):1293–1313, 1998.

[111] G. M. Ziegler. *Lecture on polytopes*. Springer, 1995.

université PARIS-SACLAY
ÉCOLE DOCTORALE
Sciences et technologies de l'information et de la communication (STIC)

Titre : Techniques de détection de défauts à base d'estimation d'état ensembliste pour systèmes incertains

Mots clés : Estimation d'état ensembliste, détection de défauts, Inégalité Matricielle Linéaire

Résumé : Cette thèse propose une nouvelle approche de détection de défauts pour des systèmes linéaires soumis à des incertitudes par intervalles, des perturbations et des bruits de mesures bornés. Dans ce contexte, la détection de défauts est fondée sur une estimation ensembliste de l'état du système. Les contributions de cette thèse concernent trois directions principales.
La première partie propose une méthode d'estimation d'état ensembliste améliorée combinant l'estimation zonotopique (qui offre une bonne précision) et l'estimation ellipsoïdale (qui offre une complexité réduite).
Dans la deuxième partie, une nouvelle approche d'estimation d'état ellipsoïdale fondée sur la minimisation du rayon de l'ellipsoïde est développée. Dans ce cadre, des systèmes multivariables linéaires invariants dans le temps, ainsi que des systèmes linéaires variant dans le temps ont été considérés. Ces approches, résolues à l'aide de problèmes d'optimisation sous la forme d'Inégalités Matricielles Linéaires, ont été étendues au cas des systèmes soumis à des incertitudes par intervalles.
Dans la continuité des approches précédentes, deux techniques de détection de défauts ont été proposées dans la troisième partie utilisant les méthodes d'estimation ensemblistes. La première technique permet de détecter des défauts capteur en testant la cohérence entre le modèle et les mesures. La deuxième technique fondée sur les modèles multiples permet de traiter simultanément les défauts actionneur/composant/capteur. Une commande prédictive Min-Max a été développée afin de déterminer la commande optimale et le meilleur modèle à utiliser pour le système, malgré la présence des différents défauts.

Title: Fault Detection Techniques based on Set-Membership State Estimation for Uncertain Systems

Keywords: Set-membership state estimation, fault detection, Linear Matrix Inequality

Abstract: This thesis proposes a new Fault Detection approach for linear systems with interval uncertainties, bounded perturbations and bounded measurement noises. In this context, the Fault Detection is based on a set-membership state estimation of the system. The main contributions of this thesis are divided into three parts.
The first part proposes an improved method which combines the good accuracy of the zonotopic set-membership state estimation and the reduced complexity of the ellipsoidal set-membership estimation.
In the second part, a new ellipsoidal state estimation approach based on the minimization of the ellipsoidal radius is developed, leading to Linear Matrix Inequality optimization problems. In this context, both multivariable linear time-invariant systems and linear time-variant systems are considered. An extension of these approaches to systems with interval uncertainties is also proposed.
In the continuity of the previous approaches, two Fault Detection techniques have been proposed in the third part based on these set-membership estimation techniques. The first technique allows to detect sensor faults by checking the consistency between the model and the measurements. The second technique is based on Multiple Models. It deals with actuator/component/sensor faults in the same time. A Min-Max Model Predictive Control is developed in order to find the optimal control and the best model to use for the system in spite of the presence of these faults.

Université Paris-Saclay
Espace Technologique / Immeuble Discovery
Route de l'Orme aux Merisiers RD 128 / 91190 Saint-Aubin, France